UNIVERSITY OF LIVERPOOL

Catalytic conversion of biomass-derived molecules

Thesis submitted in accordance with the requirements of the University of Liverpool for the degree of Doctor in Philosophy

by

Hossein Salem S. Bayahia

October 2014

Abstract

Catalytic conversion of biomass-derived molecules

PhD thesis by Hossein Salem S. Bayahia

This study aimed to prepare, characterise and test the performance of heterogeneous catalysts in the conversion of biomass-derived molecules including deoxygenation of propionic acid in the gas phase and the Prins condensation of β-pinene with paraformaldehyde in the liquid phase. The surface area and porosity of catalysts were characterised by BET, water content and thermal stability by TGA, crystallinity by XRD and composition by ICP. The acidity of oxide catalysts was characterised using NH_3 adsorption calorimetry and FTIR of adsorbed pyridine.

High purity amorphous silicas and crystalline silicalite (MFI structure) were found to be active catalysts of the deoxygenation of propionic acid. Silicalite was prepared by the hydrothermal method. Silica and silicalite were treated with aqueous acidic (HCl) and basic (NH_3+$NH_4NO_{3\,(aq)}$ or $NH_{3\,(aq)}$) solutions in a Teflon-lined autoclave. The reaction was carried out in a fixed-bed continuous flow reactor in the gas phase at 400-500 °C. A preliminary blank reaction showed a small contribution of homogeneous catalysis at 500 °C, with 12% of propionic acid converted to form 3-pentanone. The chemical treatment did not affect silica activity; it showed only 85% selectivity with 39% conversion at 500 °C. HZSM-S zeolite (Si/Al = 180) possessing strong acid sites showed low catalytic activity at 400-500 °C and the main product was ethane. Silicalite had higher activity and selectivity of 3-pentanone than silica. Acidic treatment had little effect on catalyst activity, whereas basic treated silicalite was the most active catalyst in the deoxygenation of propionic acid at 500 °C, because silanol nests formed on the silicalite surface, acting as catalytically active sites for the reaction. Catalyst activity increased with increasing reaction temperature from 400-500 °C. Silicalite performance was stable for at least 28 h time on stream at 500 °C, with 84-92% of 3-pentanone selectivity at 93-80% conversion of acid.

Bulk Zn(II)-Cr(III) mixed oxides with a Zn/Cr atomic ratio of 1:1 – 20:1 were found to be active catalysts for the gas-phase ketonisation of carboxylic acids (acetic and propionic) to form acetone and 3-pentanone, respectively, at 300 – 400 ^oC and ambient pressure. Zn-Cr (10:1) oxide showed the best performance, significantly exceeding that of the parent oxides ZnO and Cr_2O_3. The catalytic activity was further enhanced by supporting Zn-Cr (10:1) oxide on TiO_2 and γ-Al_2O_3. With 20%Zn-Cr/Al_2O_3, ketonisation of propionic acid occurred with 97% selectivity to 3-pentanone at 99% conversion at 380 ^oC, without catalyst deactivation observed during at least 24 h time on stream. Zn-Cr oxides were characterised by BET, XRD, DRIFTS of pyridine and acetic acid adsorption and microcalorimetry of ammonia adsorption. From DRIFTS, carboxylic acid adsorbed dissociatively on Zn-Cr oxide to form a surface metal

carboxylate in bidentate bridging bonding mode. A mechanism for ketonisation of carboxylic acids via β-ketoacid intermediate route was proposed.

Metal oxides such as Nb_2O_5, Cr_2O_3, and especially a Zn(II)-Cr(III) mixed oxide were demonstrated to be highly active and recyclable heterogeneous catalysts for Prins condensation, which provides a clean, high-yielding route for the synthesis of nopol through the condensation of biorenewable β-pinene with paraformaldehyde. Zn-Cr mixed oxide with an optimum Zn/Cr atomic ratio of 1:6 gave 100% nopol selectivity at 97% β-pinene conversion, with the catalyst easily recovered and recycled. The acid properties of Nb_2O_5 and Zn-Cr mixed oxide were characterized by the diffuse reflectance IR Fourier transform spectroscopy of adsorbed pyridine and ammonia adsorption microcalorimetry. An appropriate combination of acid– base properties of Zn-Cr mixed oxide is believed to be responsible for its efficiency.

Publications and presentations

The following works have been published and presented in the United Kingdom, France and the United States of America as poster presentations or oral presentations.

Paper publications

1. Hossein Bayahia, Elena Kozhevnikova, Ivan Kozhevnikov, High catalytic activity of silicalite in gas-phase ketonisation of propionic acid, *Chem. Commun*., 2013, **49**, 3842-3844.
2. Vinicius Costa, Hossein Bayahia, Elena Kozhevnikova, Elena Gusevskaya, Ivan Kozhevnikov, High active and recyclable metal oxide catalyst for Prins condensation of bio-renewable feedstocks, *ChemCatChem.*, 2014, **6**, 2134-2139.
3. Hossein Bayahia, Elena Kozhevnikova, Ivan Kozhevnikov, Ketonisation of carboxylic acids over Zn-Cr oxide catalyst, *Applied Catalysis B: Environmental*, 2014, **165**, 253-259.

Work activities (oral and poster presentations)

1. Hossein Bayahia, Elena Kozhevnikova and Ivan Kozhevnikov, *6th Saudi Scientific International Conference (SSIC)*, University of Brunel, London, UK, 11-14th October, 2012. (**Poster**)
2. Hossein Bayahia, Elena Kozhevnikova and Ivan Kozhevnikov, *Catalytic Advances through Sustainable Technologies (CASTeach)*, Queens University, Belfast, UK, 8-11th April, 2012. (**Attendance**)

3. Hossein Bayahia, Elena Kozhevnikova and Ivan Kozhevnikov, *Postgraduate research, online poster day*, University of Liverpool, Liverpool, UK, 8-27th April, 2012. (**Poster**)
4. Hossein Bayahia, Elena Kozhevnikova and Ivan Kozhevnikov, *1st Liverpool Catalysis Symposium, Future Catalysis Challenges*, University of Liverpool, Liverpool, UK, 22nd January, 2013. (**Attendance**)
5. Hossein Bayahia, Elena Kozhevnikova and Ivan Kozhevnikov, *XIth European Congress on Catalysis (EuropaCat)*, Lyon, France, 1-6th September, 2013.(**Poster**)
6. Hossein Bayahia, Elena Kozhevnikova and Ivan Kozhevnikov, *Institution of Chemical Engineers (IChemE), Sustainable and Environmental Catalysis event*, Bath University, Bath, UK, 25-26th September, 2013. (**Poster**)
7. Hossein Bayahia, Elena Kozhevnikova and Ivan Kozhevnikov, High catalytic activity of silicalite in gas-phase ketonisation of propionic acid, *7th Saudi Students Conference (SSC)*, Edinburgh University, Edinburgh, UK, 1-2nd February, 2014. (**Oral**)
8. Hossein Bayahia, Elena Kozhevnikova and Ivan Kozhevnikov, Ketonisation of propionic acid in the gas phase over Zn-Cr oxide, *7th Saudi Students Conference (SSC)*, Edinburgh University, Edinburgh, UK, 1-2nd February, 2014. (**Oral**)
9. Hossein Bayahia, Elena Kozhevnikova and Ivan Kozhevnikov, *1st EFCATS-CNRS European Summer School on Catalyst Preparation: Fundamental Concepts and Industrial Requirements (CatPrep 2014)*, Vogüé, Ardèche, France, 18-22nd May, 2014. (**Poster**)
10. Hossein Bayahia, Vinicius Costa, Elena Kozhevnikova, Elena Gusevskaya and Ivan Kozhevnikov, High active and recyclable metal oxide catalyst for Prins condensation of bio-renewable feedstocks, *Progress & Challenges in*

Environmental Catalysis, IChemE event, Johnson Matthey Technology Centre, Reading, UK, 23-24th June, 2014. (**Poster**)

11. Hossein Bayahia, Elena Kozhevnikova and Ivan Kozhevnikov, High catalytic activity of silicalite in gas-phase ketonisation of propionic acid, *Progress & Challenges in Environmental Catalysis, IChemE event*, Johnson Matthey Technology Centre, Reading, UK, 23-24th June, 2014. (**Poster**)
12. Hossein Bayahia, Elena Kozhevnikova and Ivan Kozhevnikov, *15th International Conference on Theoretical Aspects of Catalysis (ICTAC15)*, University College London (UCL), London, 29th June – 4th July 2014. (**Poster**)
13. Hossein Bayahia, Elena Kozhevnikova and Ivan Kozhevnikov, *Postgraduate research, the University of Liverpool*, Liverpool, UK, 9th July, 2014. (**Oral**)
14. Hossein Bayahia, Elena Kozhevnikova and Ivan Kozhevnikov, *8th International Conference on Environmental Catalysis (ICEC)*, Asheville, NC, USA, 24-27th August, 2014. (**Oral**)
15. Hossein Bayahia, Vinicius Costa, Elena Kozhevnikova, Elena Gusevskaya and Ivan Kozhevnikov, High active and recyclable metal oxide catalyst for Prins condensation of bio-renewable feedstocks, *Applied Catalysis and Reaction Engineering*, Cambridge University, Cambridge, 17-18th September, 2014. (**Oral**)
16. Hossein Bayahia, Elena Kozhevnikova and Ivan Kozhevnikov, *4th Northern Sustainable Chemistry (4th NORSC)*, Huddersfield University, Huddersfield, 23rd October, 2014. (**Oral**)
17. Hossein Bayahia, Elena Kozhevnikova and Ivan Kozhevnikov, *4th RSC / SCI symposium on Challenges in Catalysis for Pharmaceuticals and Fine Chemicals*, Chemistry Centre, Royal Society of Chemistry (RSC),London, 5th November, 2014. (**Poster**)

Acknowledgements

I would first like to express my thanks to my primary supervisor, Professor Ivan Kozhevnikov, for his excellent guidance, supervision and support during my doctoral studies.

Profound thanks are due to Dr Elena Kozhevnikova for her assistance and resolution of all the technical problems during my laboratory work.

I am grateful to Vinicius Costa, PhD student at Federal Minas Gerais University, Brazil, for the collaboration project we have done together and a wonderful time I spent with him during laboratory working period for one year.

I would also like to thank the University of Liverpool for offering me the opportunity to pursue this study and to express my deep gratitude to my catalysis group, all the University of Liverpool staff and people I met and who offered useful comments, discussion and friendships around the world in conferences, workshops and interesting catalysis group meetings.

Thanks are due to all members of my family for their love and strong support, which have helped me to achieve my long-time goals.

Finally, Al-Baha University and the Saudi Cultural Bureau in London are gratefully acknowledged for their financial support and financial management.

"If we knew what it was we were doing, it would not be called research, would it?"

Albert Einstein

Abbreviations

AES	Atomic emission spectroscopy
B	Brønsted acid site
BET	Brunauer, Emmett, Teller
BJH	Barrett-Joyner-Halenda
BOC	British Oxygen Company
DRIFT	Diffuse reflectance infrared Fourier transform
DSC	Differential scanning calorimetry
ECN	Effect carbon-atom number
FID	Flame ionisation detector
FTIR	Fourier transform infrared (spectroscopy)
GC	Gas chromatography
GVL	γ-Valerolactone
HPC	Heteropoly compound
ICP	Inductively coupled plasma
IR	Infrared
L	Lewis acid site
MFI	Mordenite framework inverted
NMP	n-Methyl pyrrolidone
PF	Paraformaldehyde
REO	Rare earth oxide
SZ	Sulfated zirconia
SZF	Sulfated zinc ferrite
TEOS	Tetraethylorthosilicate
TGA	Thermogravimetric analysis
TOS	Time on stream
TPAOH	Tetrapropylammonium hydroxide
XRD	X-ray diffraction

Contents

Chapter 1

Introduction

1.1 Definition and history of catalysis

The term 'catalyst' has been defined in many ways over time.[1] Here, it can be defined as a chemical used to accelerate or otherwise affect a reaction to convert substrates to products without being consumed in the reaction. It enhances the rate of the reaction without changing its thermodynamic equilibrium. Catalysts may be solids, liquids or gases.[2] They have many industrial applications, such as in the food, chemical, pharmaceutical and petrochemical industries, which give them vital importance in the world economy. They are also environmentally significant because they facilitate the conversion of raw materials to fuels. There are many new catalytic applications, such as in green chemistry,[3-5] nanotechnology,[6, 7] fuels[8, 9] and fuel cells.[4, 10-13] More than 90% of chemicals and materials in the modern industrial economy are produced with the acid of catalysis.[1]

There are two types of catalysis, depending on the catalytic system.[14] Homogeneous catalysis occurs where catalyst and reactants are in a single phase, with no phase boundary between them, whereas in heterogeneous catalysis the catalyst and reactant phases are separated by a phase boundary. One of the most important types of catalyst is the metal oxides. Historically, gas phase oxide catalysis have been used in many reactions, such as in the petroleum and petrochemical industries.[15] Nowadays, oxides are used to promote useful reactions in many applications such as energy conversion

and storage, catalysis, sensing, adsorption and separation.[16] Table 1.1 lists some important applications of catalysis from 1939 to 2000.

Table 1.1 Historical applications of catalysis[14]

Year	Reaction/ application	Catalyst
1939-1945	Dehydrogenation	Pt- Al_2O_4 Cr_2O_3-Al_2O_3
1946-1960	Oxidation of aromatics Hydrocracking Polymerisation	V_2O_5 Ni-aluminosilicate Ziegler-Natta
1961-1970	Low pressure methanol synthesis Distillate dewaxing	Cu-ZnO-Al_2O_3 ZSM-5, mordenite
1971-1980	Automobile emission control	Pt-Rh-CeO_2, Al_2O_3
1981-1985	Carbonylation Alkylation Esterification Selective catalytic reduction	Organic Rh complex Zeolite (ZSM-5) Ion-exchange resin V-Ti, Mo, W oxides
1986-2000	Environmental control Hydration Oxidation with H_2O_2 N_2O from nitric acid by catalytic destruction	Pt-Al_2O_3 Enzyme Ti-Silicate Ti-Silicate

Metal oxides constitute a large and important class of active catalytic materials which can be classified by their behaviour as acid, basic or amphoteric. These materials are usually solid and their bulk properties rely on the interaction between the metal and the oxygen of which they consist. Table 1.2 lists some examples of the many metal oxide catalysts and their varied applications.

Table1.2 Examples of metal oxide catalysts[2]

Catalyst	Catalytic Process
$ZnCr_2O_4$, ZnO	Methanol synthesis (high pressure)
Zn Fe_2O_4	Oxidative dehydrogenation
$Cu_xZn_{1-x}Cr_2O_4$, CuO	Methanol synthesis (low pressure)
$CuCr_2O_4$, CuO	Oxidation, hydrogenation
$Cr_xAl_{2-x}O_3$	Light alkane dehydrogenation

1.2 Key reaction steps in solid porous catalysts

Figure 1.1 shows the steps in a heterogeneous catalysis reaction. It can be seen that the reaction occurs when reactant molecules or atoms bond to the surface of a solid porous catalyst. This phenomenon of adsorption is important for many processes, such as catalysis, separation, purification and chromatography. The first step, called film diffusion, involves the external transport of reactant from the bulk fluid phase (either gas or liquid) through the boundary layer to the outer surface of the catalyst granules. The second step is the internal transport of reactant through the pores to active sites on the interior surface of the granule. The reactant will then be adsorbed onto the surface, where the chemical reaction will happen. Next, the product will desorb and undergo internal transport through the pores to the external surface. The final stage is the external transport of the product through the boundary layer to the bulk fluid phase.[1, 17-19]

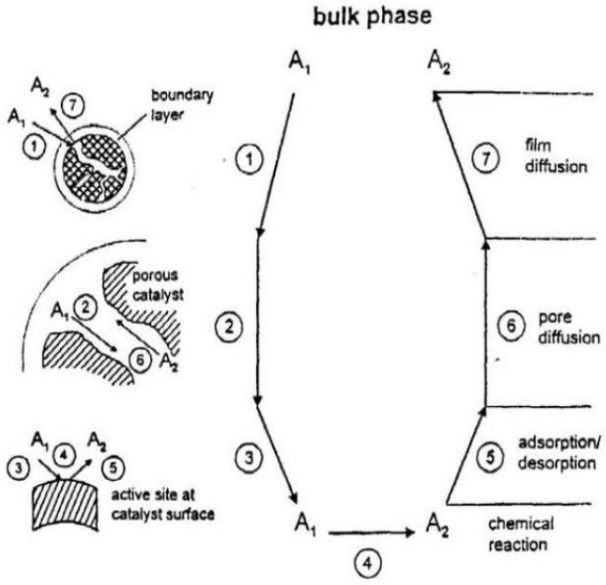

Figure 1.1 Reaction steps on a solid porous catalyst.[20]

1.3 Classification of catalysts

Catalysts can be classified according to their activity, which depends on their nature and behaviour, into three main types: redox, acid-base and polyfunctional catalysts.

Redox catalysts are used in reactions such as hydrogenation, halogenation, oxidation and dehydrogenation. They usually consist of salts, sulfides, complexes, chlorides or oxides of transition metals such as Pd, Pt, Ni and Ag. These metals present an active phase containing metal ions or metal atoms.

Acid-base catalysts include zeolites, ZnO, SiO_2-Al_2O_3, H_3PO_4/SiO_2, MgO and CaO. Their acidity and basicity are important in the activity of this large class of catalysts. They are useful in reactions such as alkylation, dehydration, cracking and isomerisation. They have active Brønsted and Lewis acid sites as well as basic sites on the catalyst surface, and an important characteristic is their ability to interact with reactants by acid-base mechanisms.[17, 21]

Polyfunctional catalysts combine the features of redox and acid-base catalysts.[22] For example, Pd supported on Zn^{II}-Cr^{III} mixed oxide acts as a polyfunctional catalyst in the one-step synthesis of methyl isobutyl ketone in the gas and liquid phases.[23] Pt/ZSM-5 has also been used as a polyfunctional catalyst for the dehydroisomerisation of n-alkanes.[24, 25]

1.4 Zn-Cr oxide catalysts

Zn-Cr mixed oxides have been well known as catalysts for many years. Their many applications include use as active and selective catalysts in reactions such as the synthesis of methanol[26-28] and higher alcohols from syngas,[29, 30] hydrogenation of secondary alcohols to ketones,[31] the synthesis of methylpyrazine using aqueous glycerol,[32] the hydrogenation of aromatic and aliphatic acids to corresponding aldehyde,[33] the dehydroisomeration of α-pinene,[34] the production of quinoline from

aniline and glycerol in the gas phase,[35] the synthesis of hydrocarbons,[36] the transformation of synthetic gas to hydrocarbons[37] and the synthesis of methyl isobutyl ketone.[23, 38]

1.4.1 Preparation of Zn-Cr oxide catalysts

The preparation of heterogeneous catalysts is a major challenge for both academia and industry.[39, 40] Zinc-chromium oxide has been prepared by several methods, including co-precipitation, where the nitrates of zinc and chromium precipitate on the addition of ammonia solution at 80 °C. The product is filtered off, washed in distilled water and dried at 110 °C. The catalyst is then calcined at different temperatures for 5 h. Pure zinc and pure chromium oxides have also been produced using the same procedure.[37] In some cases, zinc-chromium mixed oxide catalyst can be prepared by the precipitation of zinc and chromium hydroxides, which are then calcined at 550 °C for 3 h.

Zinc oxide was synthesised by adding sodium carbonate aqueous solution to zinc nitrate solution at a controlled pH of 8. The precipitate was filtered off, washed three times and dried at 100 °C for 12 h. Calcination was performed at 500 °C for 1 h in air.

Epling and co-workers[30] prepared a Zn-Cr (1:1) catalyst by dissolving their nitrates at pH 10 in a solution of KOH and K_2CO_3 at a controlled temperate of 70 °C, which was stirred for 3 h, then the precipitate was dried at 100 °C in a vacuum oven. Another method which these researchers used to synthesize zinc chromium oxides is kneading. ZnO was first obtained by calcination of zinc carbonate, then added to chromium oxide aqueous suspension. The products were kneaded together for 2 h and dried at room temperature for 24 h. The catalyst was next calcined in an oven at 100 °C for 12 h. Finally, the catalyst was dried at 500 °C for 1 h in air.

Zn-Cr oxide catalyst has also been prepared by the urea-nitrate combustion method. Zinc nitrate hexahydrate [$Zn(NO_3)_2$ $6H_2O$] and ammonium chromate [$(NH_4)_2Cr_2O_7$]

were mixed with urea. The solution of zinc nitrate and chromium nitrate was precipitated by urea at pH 9 and heated at 95-98 °C. The product was filtered off, washed three times by distilled water, and dried at 100 ^{o}C for 12 h. After that, the product was calcined at 500 °C for 1 h. This method is called catalyst precipitation from homogeneous solution.[41]

The impregnation method has been used to prepare supported oxide catalysts, including ZnO, Cr_2O_3 and other oxides. In this method, the support was impregnated with an aqueous solution of metal salts, then the sample was dried at 120 °C for 12 h. Finally, supported catalysts were calcined at 450 °C in air for 3 h.[42] Cr_2O_3 catalysts supported on alumina, silica and tin oxide were prepared by adding the support to chromium nitrate. The catalyst was dried using rotary evaporation and calcined at 700 °C.[43]

ZnCrTi supported catalyst was obtained by the impregnation method. TiO_2 was impregnated with zinc and chromium nitrates in aqueous solution. The mixture was dried at 120 °C for 5 h and the catalyst was finally calcined at 500 °C for 5 h in air. The x-ray diffraction (XRD) pattern showed the presence of TiO_2 in the catalyst. However, oxide crystalline phases did not appear.[44]

1.4.2 Properties of Zn-Cr oxides

1.4.2.1 Zn-Cr catalyst surface area and porosity

Hong and Ren[45] examined fresh Zn-Cr catalyst with a surface area of 63.2 m^2g^{-1} and reported that this decreased to 50.7 m^2g^{-1} after 100 h reaction time at 450-600 °C. The catalyst prepared by the co-precipitation method using urea showed a similar trend after calcination at 700 ^{o}C. The addition of chromium to zinc increased the surface area of the catalyst. Conversely, the surface area of K-Cr_2O_3/ZnO decreased, because potassium

induces an intrinsically lower hydrothermal stability. It was also found that the BET surface area of mixed Zn-Cr oxide was smaller than that of the pure Cr_2O_3 oxide. Adding chromium to Cu increased the surface area; however, when up to 80% of chromium was added, the surface area of the catalyst reduced compared with the pure metallic Cu catalyst. The surface area of Cr-rich Zn-Cr oxides is increased significantly by increasing the Cr content. Amorphous Cr-rich oxides have larger surface areas and pore volumes, with smaller average pore diameters than crystalline Zn-rich oxides.[23, 34]

1.4.2.2 The composition of Zn-Cr catalysts

The composition of Zn-Cr catalysts has been investigated many times.[46-50] Zn-Cr oxides with atomic ratios varying between 1:30 and 20:1 were prepared by the co-precipitation method. The catalysts were calcined at 300 °C and it was found that Zn-rich catalysts were crystalline in structure, whereas Cr-rich catalysts were amorphous. Additionally, when Zn-Cr catalysts were calcined at more than 300 °C, the XRD pattern showed them to be crystalline.[34]

Cu-Zn-Cr catalyst was used to produce H_2 from methanol. This catalyst was prepared, with low and high Cu-loading, by urea nitrate combustion. The XRD pattern showed that Zn-Cr without Cu comprised highly crystalline ZnO and a spinel-like phase. The spent catalyst was characterised using XRD and it was found that the main phases of Zn-Cr had not changed during the reaction. However, a small increase was observed in the ZnO pattern.[45]

Simard *et al.*[37] and Bradford *et.al.*[51] observed that when the Cr/Zn ratio was increased from 0.5 to 15 (calcined at 350 °C) and from 0 to 1.9 (calcined at 700 °C) respectively, the content of the ZnO phase decreased and $ZnCr_2O_4$ increased. A further increase in the chromium content resulted in the appearance of a Cr_2O_3 crystalline phase and a concomitant decrease in $ZnCr_2O_4$ content.

Zn-Cr (1:10) oxide catalysts have been characterised by XRD. It was found that the catalyst was amorphous after calcination at 300 °C and crystalline after calcination at 350 °C. The crystalline oxide presented both Cr_2O_3 and $ZnCr_2O_4$ phases.[38]

Errani *et al.*[28] found that Zn-Cr oxide with Zn/Cr > 1:1 was crystalline and that ZnO phases were present, whereas with Zn/Cr ratios ≤ 1:1 it had only one spinel-type phase.

1.4.2.3 Acidity of Zn-Cr catalysts

In heterogeneous catalysis, catalyst acidity plays significant role in the activity and selectivity of the reaction. A range of techniques including IR spectroscopy can be used to determine the acidity of catalysts and characterise the effects of the nature of acid sites on their behaviour. The relative number of Brønsted and Lewis acid sites can be determined by FTIR-pyridine adsorption in the 1540-1450 cm^{-1} region.[23, 34, 52, 53] Differential scanning calorimetry (DSC) is another technique used to determine the strength and the number of acid sites by ammonia adsorption.[23, 54]

The acidity of Zn-Cr oxides was studied. The total number of acid sites was determined by ammonia adsorption at 100 °C at the gas/solid interfaces. The results showed that increasing the chromium content increased the acid strength of catalysts. In addition, the Brønsted and Lewis sites of the catalyst were measured by FTIR-pyridine spectroscopy. It was found that only Zn-Cr (1:30) had Brønsted acid sites, in contrast to the same catalyst with different zinc-chromium ratios.[23, 34]

1.5 Zeolite catalysts

Zeolites are aluminosilicates with a highly ordered crystalline structure. Cavities of a definite size are formed in a rigid, three-dimensional network composed of SiO_4 and AlO_4 tetrahedra. The lattice contains cavities of varying diameters, depending on the type of zeolite.[55] Zeolites have specific properties which make them unique among

solid catalysts, such as high surface area, the molecular dimensions of the pores, high adsorption capacity, partitioning of reactant and products, the possibility of modulating the electronic properties of the active sites and the possibility of pre-activating molecules in the pores by using strong electric fields and molecular confinement.[56]

Various methods are used to design the unique framework structures which make zeolites very important heterogeneous catalysts for the chemical and petrochemical industries, the estimated size of the global catalyst market being 15 to 20 billion US dollars. Their importance for the global economy arises not from a high specific surface area, but because they provide shape/size selectivity in catalytic reactions.[57, 58]

Shape and size selectivity have been important in many catalytic processes for decades and zeolites therefore remain vital materials for new structures and applications in industry. Zeolite catalysts are able to select reactants, products and intermediate compounds according to shape and size, because of the pores and channels which are fundamental to zeolite structure.[59] The various types of zeolites have different channel openings, thus varying the accessibility to organic molecule. Zeolite catalysts present three types of shape selectivity, affecting reactants, products and transition states, respectively.

In the shape selectivity of reactants, only those molecules of reactant smaller than the opening size can access the zeolite cages, allowing the reaction to happen inside the cavities. When the product is able to pass through the zeolite channels in order to exit from the cages, this is referred to as product shape selectivity.[22]

Zeolites have pore sizes in the range of 3-10 Å. The IUPAC classification divides the most common industrial zeolites into the mordenite framework inverted (MFI), A and FAU types.[60] The difference between two common MFI-type zeolites, silicalite-1 and

ZSM-5, is that ZSM-5 has Si/Al ratio 10-200, while silicalite has little or no aluminium content.[61]

1.5.1 Silicalite

Silicalite is a pure siliceous zeolite with the MFI crystal structure (Figures 1.2 and 1.3).[62] The structure of silicalite consists of three-dimensional pore system similar to ZSM-5.[63] Its surface is almost completely internal and formed almost entirely by Si–O–Si bonds. Silicalite can be organophilic, inert and hydrophobic,[64] because it has low charge concentration centres. The structure of silicalite has been investigated by both X-ray and ^{29}Si NMR spectroscopy.[63] It has been used as a catalyst and selective adsorbent in Industrial applications such as petroleum and petrochemicals. Silicalite exhibits selective sorption of organic molecules in comparison with the aluminosilicate materials.[63] It has no Brønsted acid sites and is normally synthesised in basic media by the hydrothermal process.[65]

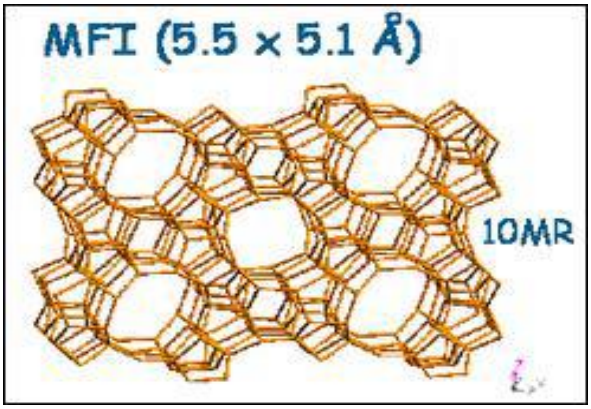

Figure 1.2 MFI zeolite structure.[66]

The MFI surface can be divided in two parts, the internal and external. The internal one is made by the wall of channels. The external surface accounts for a small percentage of

the total surface of zeolite. Nevertheless, it has been found that catalytic performance of silicalite is affected by its external surface.[67]

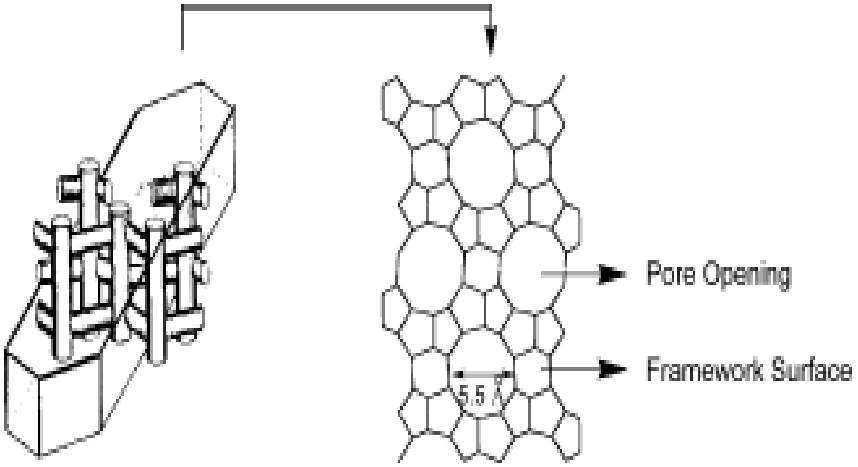

(a) (b)

Figure 1.3 a) MFI zeolite and its channel structures, [63, 66-68] b) external surface.[67]

1.5.1.1 Preparation and modification of silicalite

The procedure of silicalite preparation is discussed widely in the literature.[68-71] A mixture of tetraethylorthosilicate (TEOS), ethanol and tetrapropylammonium hydroxide (TPAOH) in aqueous solution were hydrothermally heated to 105 °C for 96 h, then the silicalite product was washed in distilled water, dried and finally calcined in air.[68] Alternatively, Fickel *et al.*[69] used different sources of silica: fumed silica, TEOS and Ludox As-40 in an aqueous solution of TPAOH, at a temperature range of 100-150 °C.

Silicalite can be hydrothermally modified using various basic or acidic solutions. The type of solution and its concentration will affect the number of silanol sites that are created on the catalyst surface. It has been reported that basic treatment produces a silicalite containing a large number of silanol nests, giving it interesting catalytic properties and commercial uses, including the production of ε-caprolactam by the

Beckmann rearrangement of cyclohexanone oxime,[62, 68, 69, 72] paraffin separation,[73] and the ketonisation of carboxylic acids.[70, 74]

1.5.1.2 Characterisation of silicalite

Silicalite has a typical XRD pattern, as reported in the literature,[65, 68, 72, 75] which indicates that the purity and crystallinity of silicalite depend on the temperature of calcination.[69] The results show that silicalite comprises orthorhombic or monoclinic unit cells which can be identified by XRD in the range of 24.5° at the 2θ angle.[68, 72] If a single peak is observed the unit cell is orthorhombic, whereas if there are two peaks the unit cell is monoclinic. The unit cell can be changed from monoclinic to orthorhombic depending on the calcination temperature,[72] synthesis and modification of zeolites.[68]

The IR spectrum of silicalite has been studied to distinguish silanol families and to determine the number of silanol groups on the catalyst. The type of silanol groups depends on the modification solution, the concentration of the solution and the calcination temperature. It has been reported that modification by acidic and basic solutions improved the catalytic performance of the silicalite because of strong adsorption in the 3500 cm^{-1} band of the IR spectrum. This band is attributed to silanol nest groups, which provide favourable sites for the ketonisation of propionic acid at 500 °C in the gas phase[70] described in this thesis (Chapter 4) and the Beckmann rearrangement of cyclohexanone oxime to ε-caprolactam.[68]

Both terminal and H-bonded silanol groups on silicalite materials indicate the presence of weak Brønsted acid sites. When the strength of these sites was measured by TPD-NH_3, the results showed low total acidity. However, a sample of silicalite calcined at 450 °C and modified by basic solution showed higher total acidity.[72]

Calorimetry and gravimetry have been used to calculate the heat of adsorption (ΔH_{ads}) of linear alcohols such as methanol and 1-propanol on silicalite, which was found to be –(90-100) kJ/mol.[65]

The surface area and porosity of silicalites have been measured and discussed in many articles.[21, 65, 71] Bayahia *et al.*[70] (Chapter 4) measured the surface area of fresh untreated, basic treated and spent treated silicalite catalysts. The surface area of the untreated and basic treated samples was higher than that of the treated silicalite. Varying the sources of silica in the preparation of silicalite affected the surface area and pore volume of the catalyst. TEOS silicalite showed higher microporosity than that of silicalite from other sources such as fumed silica.[69]

1.6 Biofuel as alternative to petroleum based fuel

Oil is the world's primary source of energy and chemicals with a current demand of about 12 million tonnes per day (84 million barrels a day) with a projection to increase to 16 million tonnes per day (116 million barrels a day) by 2030. While 30% of the global oil consumption accounts for transportation fuels at present, it is strikingly expected to increase to 60% by 2030.[76]

Renewable biofuels are needed to displace petroleum derived transportation fuels, which contribute to global warming and are of limited availability. Biodiesel and bioethanol are the two potential renewable fuels that have attracted the most attention. However, biodiesel and bioethanol produced from agricultural crops using existing methods cannot sustainably replace fossil-based transportation fuels. In general, increased demand for biofuels has caused the prices of agricultural commodities used as feedstocks and other competing crops to increase because of the direct impact of biofuels production on agricultural commodities and markets, with implications for food

prices and allocations of rural agricultural land. There is an alternative, however, which is biodiesel from microalgae. This biodiesel seems to be the only renewable biofuel that has the potential to completely displace petroleum-derived transport fuels without adversely affecting supply of food and other crop products. Most productive oil crops, such as oil palm, do not come close to microalgae in being able to sustainably provide the necessary amounts of biodiesel. Similarly, bioethanol from sugarcane is no match for microalgal biodiesel.[77]

First generation biodiesel is currently the most common biofuel in Europe. It remains in the political and economic arena and is playing a part in the biofuels expanding process as the awareness of alternative fuel spreads among the general public. In 2007, 19 biodiesel plants started operations or were under construction/planning in the new EU member states. Relatively large plants can be found in Lithuania, Poland and Romania, with capacities of 100,000 tonnes/year.[76]

Europe has been involved in direct production of liquid fuels from biomass for over two decades. Prior to 1989, the only European plant was a conventional slow pyrolysis demonstration plant of 500 kg/h operating in Italy for liquid and char production to yield approximately 25% of each. Also Bio-Alternative in Switzerland was operating a fixed bed carbonisation pilot plant fed with wood and waste for charcoal production yielding 20% of secondary liquids as a by-product. Tests carried out on combustion of these oils served to foster interest in direct production of liquids from biomass in atmospheric processes. This also revealed a poor liquid quality and low product yields. In 1993, a 200 kg/h fast pyrolysis pilot plant based on the University of Waterloo (Canada) process was launched in Spain by Union Fenosa. In 1991 – 1992, Egemin (Belgium) designed and operated a 200 kg/h capacity entrained down bio-oil pilot plant. ENEL purchased a 15 t/d Ensyn RTP3 pilot plant to produce bio-oils for testing which

was installed in Italy in 1996. The inclusion of fast pyrolysis in the 4th Non Fossil Fuel Obligation (NFFO) tranche in the UK in 1996 served to strengthen awareness of this technology and boosted interest in it Europe.[78]

In North America a number of commercial and demonstration plants for fast pyrolysis have been operating at a scale of up to 2000 kg/h. Ensyn (Canada) are marketing commercial fast pyrolysis plants of up to 10 t/h throughput. Two plants of around 1 t/h capacity are operated in the USA for food edditives production which is still the only commercial application for fast pyrolysis. Castle Capital have acquired the Continuous Ablative Reaction (CAR) process and were operating a 1-2 t/h plant in Canada until 1996. The second generation 1360 kg/h Interchem demonstration plant in Kansas is based on the NREL vortex ablative pyrolysis process.[78]

The UK currently has a total biofuel production capacity of over 1,500 million litres per year. Figure 1.4 shows the larger scale commercial biofuel plants in the UK, indicating both operational and planned plants. Bioethanol projects have been slower to develop with the UK's first bioethanol plant being commissioned by British Sugar in 2007. This plant remained the UK's only bioethanol plant for three years until had been complemented by two very large bioethanol plants (Ensus in 2010 and Vivergo in 2013), significantly increasing the overall bioethanol capacity in the UK, with a third plant (Vireol) planned for 2016. Therefore, bioethanol capacity represents the larger share in the UK biofuel industry.[79]

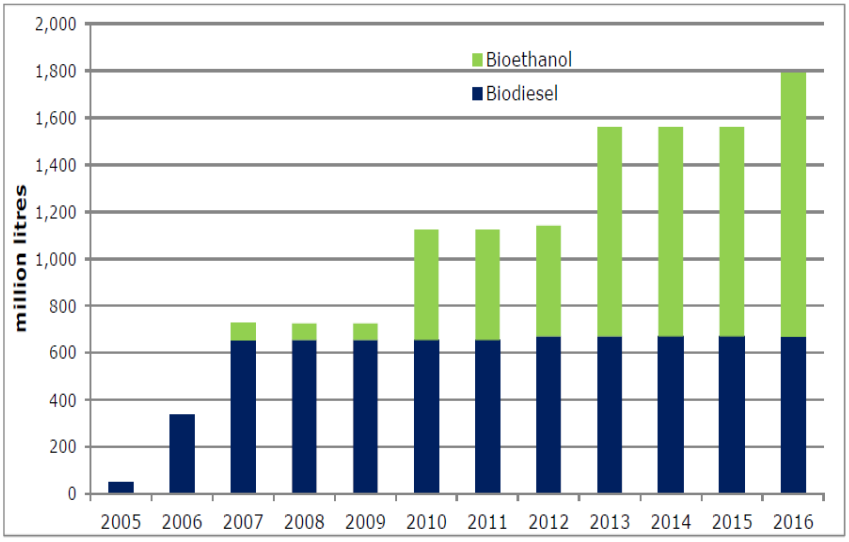

Figure 1.4 Commercial-scale bioethanol and biodiesel production in the United Kingdom.[79]

Several biodiesel initiatives were planned in the UK in recent years, but did not result in actual projects. These include a 255 million litre plant in South West England proposed by ABS Biodiesel running on virgin and waste oils and a 204 million litre plant in North Tyneside proposed by Goes on Green running on yellow grease (both planned for 2011). UK bioethanol production has also been significantly lower than production capacity since 2009, particularly in 2011 and 2012 when utilisation was only 6% and 17% respectively.[79]

1.7 Deoxygenation of biomass-derived molecules

Biomass is a renewable feedstock with a significant role in the economy.[80] It is a source of fuels and other useful chemicals,[81, 82] representing an important strategy in the replacement of fossil fuels.[83] It can be transformed into these chemicals by removing oxygen or C-C coupling.[81, 84, 85] The energy provided by raw biomass has been estimated as reaching 150-450 Ej/year in 2030, when 20% of transportation fuels and

25% of chemicals will be extracted from biomass. Plant biomass is currently the main renewable source of carbon for chemicals and fuels. Biomass-derived carbon can be used in producing a variety of biofuels and bio-based products, depending on soil quality, climate and precipitation.[86]

Biomass can be converted in various ways, such as by thermochemical and catalytic processes.[82, 87] The reactions of biomass conversion have been reported as facilitated by many types of catalysts, including zeolites and metal oxides.[81, 84, 88] Carboxylic acid is a common intermediate in biomass conversion. In this case, two molecules of acid can be condensed into a linear molecule of ketone via ketonisation, which involves carbon dioxide and water as by-products.[8, 89]

1.7.1 Deoxygenation of carboxylic acids

Carboxylic acids are readily available from natural resources and attractive as renewable raw materials for the production of value-added chemicals and bio-fuel components.[8, 90] For fuel applications, carboxylic acids require reduction in their oxygen content, i.e., deoxygenation. Therefore, much recent research has addressed the deoxygenation of carboxylic acids using heterogeneous catalysis.[91, 92]

1.7.1.1 Ketonisation of carboxylic acids

The reaction of two carboxylic acid molecules to produce a molecule of ketone, carbon dioxide and water as co-products is called ketonisation.[93-96] Ketonisation of carboxylic acids (Equation 1.1) is widely used as a clean method for the synthesis of ketones.[97] It allows for partial deoxygenation of carboxylic acids, accompanied by the upgrading of their carbon backbone.

$$\mathbf{2\ RCOOH \longrightarrow R_2CO + CO_2 + H_2O} \qquad (1.1)$$

Ketonisation is catalysed by many basic and acidic metal oxide and mixed-oxide catalysts in the temperature range of 300-500 °C,[33, 89, 95, 97-100] but the nature of catalytically active sites is not yet clear. It is generally thought that basic sites are favourable for ketonisation.[97] However, heteropoly acid $H_3PW_{12}O_{40}$ and CsPW catalysts were used in the investigation of propionic acid in the gas phase.[101]

When the reaction is used to obtain a symmetric ketone, it is called homo-ketonisation, whereas when asymmetrical ketone is obtained from carboxylic acid, this is called cross-ketonisation. This reaction plays a role in the conversion of biomass by removing carboxylic groups and it is an upgrading step which increases the length of the carbon chain. It has been reported that the rate of cross-ketonisation is greater by a factor of two than that of homo-ketonisation. Figure 1.5 depicts both the homo-ketonisation and cross-ketonisation reactions. The reactivity of ketonisation decreases with increasing acid chain length.[102]

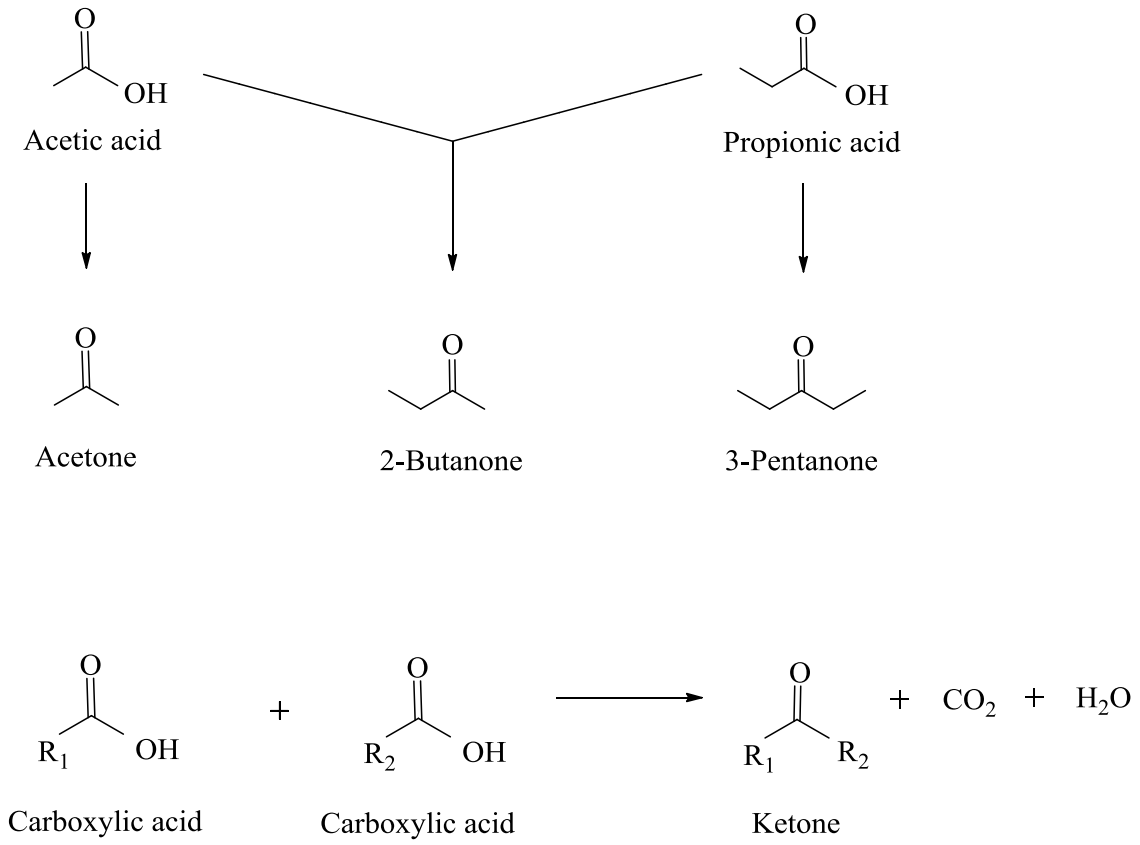

Figure 1.5 Homo-ketonisation and cross-ketonisation.[103]

The ketonisation of carboxylic acids has been known since 1858, when it was used to produce acetone by decomposing calcium acetate.[94, 104] The solid catalysts were used in the ketonisation of acetic acid as a direct reaction.[95] Recently, ketonisation has been catalysed by many basic and acidic metal oxides, mixed-oxides[33, 95, 97] and zeolites,[70, 105] because it has promising applications in the conversion of biomass to produce and upgrade bio-oil[89, 96, 102, 104] and in other industrial uses.[94]

It has been reported that amphoteric oxides seem to have better activity than pure acidic and basic oxides.[95, 106-108] Among the oxides that have been used in the ketonisation of carboxylic acids are CeO_2,[109, 110] MnO_2,[94] Cr_2O_3,[111-113] ZrO_2, PbO_2, BiO_3,[111] ZnO,[114] TiO_2,[115] SiO_2,[70] mesoporous base catalysts (CM-HMS and CM-MCM-

41),[95] MgO,[116] Nd_2O_3[93] and Al_2O_3.[114, 117] It was also found that Mn_2O_3-CeO_2 and ZrO_2-CeO_2 achieved high activity at 350-450 °C.[118] Uranium, thallium and 32 other chemical elements oxides have been tested in the ketonisation of propionic acid in the gas phase. Some of them were highly active catalysts.[119] However, ketonisation mechanisms are still under discussion.[93] It has also been found zeolite was active catalyst in the ketonisation reaction.[70, 74]

1.7.1.1.1 Ketonisation catalysts

1.7.1.1.1.1 Ketonisation of carboxylic acid over metal oxides

A variety of basic, acidic and amphoteric metal oxides have been tested in the ketonisation of carboxylic acids under different conditions. The ketonisation of acetic acid catalysed by different metal oxides supported on silica[42, 94] is shown in Table 1.3.

Table 1.3 Activity of 10 wt% MO_x/SiO_2 catalysts in ketonisation of acetic acid[42, 94]

Catalyst	Yield of acetone (%)	
	648 K	673 K
B_2O_3	2	3
MoO_3	4	5
WO_3	6	5
P_2O_5	10	12
V_2O_5	9	21
Bi_2O_3	11	18
NiO	31	
Al_2O_3	15	37
CuO	29	39
ZnO	19	33
PbO	36	76
Cr_2O_3	48	39
Fe_2O_3	66	59
CoO	50	63
MgO	53	59
Nd_2O_3	22	61
La_2O_3	50	87
MnO_2	72	96
CdO	76	94
CeO_2	96	97

It has been found that amphoteric metal oxides such as MnO_2, TiO_2 and CeO_2 have better activity in the ketonisation of carboxylic acids than pure acidic or basic oxides. They showed very good activity and selectivity in ketonisation reactions.

The ketonisation of carboxylic acids over oxides is determined by some important properties including the interaction of carboxylic acid with the catalyst, the redox properties, dopants and pre-treatment of catalysts which have been studied both theoretically and experimentally. Carboxylic acids are adsorbed onto the surface of the catalyst to produce surface carboxylate and hydroxyl groups associated with one or two metal oxygen atoms in the different coordination structures.[120, 121]

The acid-base properties have a significant effect on activity in the ketonisation of carboxylic acids, because the surface cations/anions are exposed to coordination vacancies. Many different techniques can be used to characterise the acidity and basicity of catalysts, such as FTIR-pyridine spectroscopy, NH_3 adsorption and TPD of CO_2.[94]

The basic sites of CeO_2, MgO and ZrO_2 have been studied by CO_2 adsorption. The density of basic sites was calculated so that these catalysts could be compared. CeO_2 had a higher basic site density than ZrO_2 and MgO, whereas MgO had the strongest basic sites.[122]

Transition metals such as Co and Pd were added to CeO_2 to study the effects on the gas phase ketonisation of acetic acid. The results showed that the activity in ketonisation was enhanced by both Co and Pd addition.[106] When ZrO_2 was added to CeO_2, this enhanced the ketonisation activity, because it increased the number of Lewis acid sites and oxygen vacancies.[94]

Likewise, the ketonisation of carboxylic acids using CeO_2 and MnO_2 supported on Al_2O_3, TiO_2 and SiO_2 was examined. The support was found to affect the activity of ketonisation Al_2O_3 and TiO_2 significantly increased the catalytic activity in comparison

with SiO_2, because of the incorporation of the acid function of the support with the basic sites of the supported oxides.[42]

Benaissa *et al.*[99] tested $H_4[PMo_{11}VO_{40}]$ and its caesium salts as catalysts of the hydrogenation and ketonisation of hexanoic acid to the corresponding aldehydes, ketones and other products at 350 °C and 1 bar H_2 pressure in the vapour phase. $H_4[PMo_{11}VO_{40}]$ and its Cs salt achieved higher thermal stability in the reaction. Selectivity to 6-undecanone increased up to 71-76% by increasing the Cs content of the catalysts. After the reaction, the heteropoly compounds (HPCs) decomposed to their oxides, which were more active in the hydrogenation of hexanoic acid than the HPCs. MoO_2 gave 95% conversion with 75% selectivity of hexanal.

The ketonisation of acetic acid by copper oxide, iron oxide and tin oxide has been studied. The addition of platinum to the catalyst had no effect on the selectivity of acetone except in the case of manganese oxide, indicating that the strength of the M-O bond played a role. Acetone was the main by-product with pure oxides, where increasing the amount of oxides increased the amount of acetaldehyde.[111]

Deoxygenation of propionic acid on metal-loaded heteropoly acid in the gas phase was studied in N_2 and H_2. All catalysts were active in the ketonisation of propionic acid from 250 to 300 °C. However, HPW and its caesium salt were active in decarbonylation and decarboxylation in H_2 at 400 °C. Using Pd/SiO_2 and Pt/SiO_2 in H_2 achieved 100% of ethene selectivity. Other main routes of deoxygenation of propionic acid to corresponding aldehyde and alcohol were studied using Cu, Cu/CsPW and Cu/SiO_2.[101]

The gas-phase ketonisation of acetic, propionic and butyric acid on chromium-zinc-manganese catalyst in the range 330-400 °C in the presence of water was studied. At 325 °C the yield was 96% of acetone, 95% of diethyl ketone and 92% of dipropyl ketone. Reducing the amount of water affected the reactant mixture positively. At a

ratio of 1:0.5 acetic acid to water, acetone selectivity reached 98% at 100% conversion of acetic acid at 375 °C.[123]

Pestman and co-workers[117] tested the oxides of iron, vanadium, zirconium and titanium. At low temperatures, only acetone formed on TiO_2, but at high temperatures acetaldehyde also formed. In this reaction, the selectivity of products depended on the presence of α- hydrogen atoms. Ketene might be an intermediate for ketone formation, as suggested in the literature.[124] At shorter contact times, ketene was formed, while at longer contact times, more ketone was formed, which indicates that ketene is an intermediate in the conversion of acetic acid to acetone.

The ketonisation of a variety of carboxylic acids was studied over 10 and 20 wt% of metal oxide catalysts supported on SiO_2, Al_2O_3 and TiO_2 in the range of 300-450 ^oC. At temperatures lower than 325 ^oC, all catalysts formed acetone from acetic acid, while increasing the temperature increased the acetone yield. CeO_2/SiO_2 at 10 wt% showed a higher acetone yield at 375 ^oC than all other supported oxide catalysts in the series, while CeO_2/Al_2O_3 at 20 wt% exhibited the highest activity at 350 ^oC in the synthesis of 3-pentanone from propionic acid.[42]

The ketonisation of heptanoic acid over a series of catalysts was tested. Manganese, cerium and zirconium oxides at 20 wt% were supported by Al_2O_3, SiO_2 and TiO_2. Pure silica was less active in the reaction than Al_2O_3 and TiO_2. Increasing the reaction temperature increased conversion, but selectivity decreased. MnO_2/Al_2O_3 at 20 wt% showed the highest activity at 400 ^oC, giving a 95% yield of 7-tridecanone. The catalysts showed good long-term stability at 400 ^oC.[125]

The ketonisation of carboxylic acids was unselective when red mud bauxite was used. However, the reduction of red mud produced an active catalyst for the ketonisation of carboxylic (propionic, butyric, iso-pentanoic and n-pentanoic) acids at

365 °C under H_2 flow in the liquid phase. The recycled catalyst was active without loss of activity.[126]

The ketonisation of propionic acids to form 3-pentanone and the cross-ketonisation of various carboxylic acids were studied on CeO_2 modified with Mn, Mg, Al, Ni, Fe and Zr at 300-425 °C. It was found that CeO_2-Mn_2O_3 was the most active catalyst in the ketonisation of propionic acid to form 3-pentanone. In the ketonisation of propionic acid with another linear carboxylic acid on CeO_2-Mn_2O_3 at 375 °C, the reactivity was slightly decreased because of the increase in the chain length. In addition, branched acids were less reactive because steric hindrance and the lack of α-hydrogen decrease the reactivity to ketonisation of acid by either homo- or cross-ketonisation.[98]

Martinez *et al.*[115] synthesised TiO_2-functionalized silica monoliths by hydrolysis of titanium isopropoxide on the silica surface. The steady-state reaction of acetic acid to form acetone was studied between 533 and 680 °C. The catalyst was very selective for the ketonisation of acetic acid. At these temperatures two reactions were observed, forming coke and acetone. Acetone selectivity was not improved by shortening contact time.

Kobune and co-workers[127] investigated several reactions over CeO_2 and the effect of calcination of the catalysts on the activity. Calcination affected the particle size of the catalysts and it was found that the ketonisation of propionic acid increased as particle size increased. Propionic acid was ketonised over cerium oxide at 350 °C with different particle sizes and the main product was found to be 3-pentanone with > 99% of selectivity at 50% conversion of propionic acid.

The ketonisation of pentanoic acid using a bifunctional metal/acid catalyst was tested. A yield of 70% of 5-nonanone was produced from γ-valerolactone (GVL) in a

single bed on Pd/ Nb_2O_5. The yield increased to 90% of 5-nonanone by using a double bed reactor over Pd/ Nb_2O_5 + $Ce_{0.5}Zr_{0.5}O_2$ at 325 and 425 °C.[128]

This work involved multiple reaction steps to produce the ketone. The aim was to convert cellulose to diesel and gasoline fuels as a cascade strategy for the deoxygenation of biomass. The first step was the deconstruction of cellulose in an aqueous solution of H_2SO_4, which yielded a mixture of levulinic acid and formic acid. The second step was to produce GVL over Ru/C at 423 K, which was upgraded to 90% of 5-nonanone. Pd/Nb_2O_5 + $Ce_{0.5}Zr_{0.5}O_2$ was chosen because it provided good hydrothermal stability as well as much stronger acidity for producing GVL.[129]

The citrate method was used to create active centres of MnO_x/CeO_x on mesoporous silica (HMS and MCM-41). Ten mol% of MnO_x in CeO_2 enhanced the ketonisation activity to form 3-pentanone from propionic acid. A high selectivity of > 98% was achieved at 73% conversion of propionic acid over CM-MCM-41 at 410 °C. However, under the same conditions, the combined ketonisation of propionic acid and butyric acid achieved only 38 and 14% conversion respectively.[95]

The ketonisation of acetic acid in the liquid phase was tested at low temperatures typically needed for this reaction. The impregnation method was used to prepare a new and efficient catalyst of Ru/TiO_2/C. The catalyst was calcined in air, reduced in H_2 and tested at 180 °C using water and organic solvents such as n-hexane and n-methyl pyrrolidone (NMP). It exhibited high selectivity and activity in ketonisation in organic solvents.[130]

A ceria–zirconia catalyst was tested in the ketonisation of hexanoic[89] and pentanoic acids.[131] The ketonisation of hexanoic acid was studied in the presence of 2-butanone and 1-pentanol. The reaction of ketonisation was less rapid than esterification at low temperatures, which is consistent with the activation energies of ketonisation and

esterification. The adsorption of acid on the catalyst surface is an important step in the reaction. It was found that the ketonisation of ester did not happen directly, but that the ester was first hydrolysed by water, followed by the ketonisation of the acid. This means that the direct ketonisation of the ester did not take place in this system. Kinetic studies show that the ketonisation activation energy is higher than the activation energy of esterification, 132 and 40 kJ/mol respectively.[89]

A series of fourteen rare earth oxides (REOs) including Pr_6O_{11}, Nd_2O_3, CeO_2 and La_2O_3 was investigated in the gas phase ketonisation of acetic acid at 350 °C. Acetone selectivity was > 99.9% with 38-80% conversion of acetic acid. Pr_6O_{11} gave 80% acetone yield. The reaction involves two main steps, producing MO(AcO) (M= La, Pr, and Nd), acetone and carbon dioxide by surface decomposition of $M_2O(AcO)$, followed by the reaction of MO(AcO) with acetic acid to produce water.[93]

Many current environmental problems arise from activities such as the disposal of biomass waste by burning or burial in the ground. To protect the environment from these problems, it is necessary to find new and efficient methods of processing biomass waste, such as hydrothermal modification. Livestock manure in the form of liquid slurry can thus be converted to useful chemicals such as ketone. Funai *et al.*[132] reported that acetone was produced from biomass waste over ZrO_2-FeO_x, Fe_2O_3 and ZrO_2/FeO_x at 300-500 ^oC. When zirconia was added to iron oxide, catalyst activity was enhanced. ZrO_2/FeO_x produced a large amount of CO_2 rather than acetone, compared to ZrO_2-FeO_x, because the reaction depended on the dispersion of ZrO_2 on FeO_x. This reaction was affected by temperature and acetone concentration. Acetone yields increased with increasing temperature up to 450 °C, but at 500 °C the yield decreased, so that the optimal temperature for the reaction was 450 °C. It was also found that when the

concentration of acetic acid in the slurry was increased, the concentration of acetone increased as well.

$Ni/\gamma Al_2O_3$ with different loadings of Ni was used to catalyse the steam reforming of acetic acid at different temperatures. Conversion of acetic acid decreased with increased Ni loading, because the cracking reaction took place, rather than the ketonisation of acetic acid to form acetone. Thermogravimetric analysis (TGA) showed that the lowest coking and highest activity were at 12 wt% Ni loading.[133]

The ketonisation of carboxylic acids to produce biorenewable fuel needs high temperatures to remove oxygen or acidity from the initial materials. Controlling catalyst calcination temperature ensures that the ketonisation reaction occurs at lower temperatures. The calcination temperature affects the crystallinity and oxidation state of oxide catalysts. For example, cerium oxide was used as a catalyst in the ketonisation of acetic acid at 230 °C. Calcination of the catalyst at higher temperatures increased the rate of ketonisation of acetic acid at low temperatures, based on the surface area.[107]

Liquid phase ketonisation reaction at a moderate temperature is a challenge. This reaction has been found very limited up to date. Using metal oxides in the liquid phase, ketonisation of carboxylic acids showed very low activity due to the blocking of active sites and competitive adsorption in the presence of high concentration of water.[134]

1.7.1.1.1.2 Ketonisation of carboxylic acid over zeolite

H-T zeolite was used in the gas phase ketonisation of mixtures of acetic, propionic and butyric acids. It was found that the reactivity of propionic acid increased in the presence of acetic acid rather than butyric acid, because of the synergetic effect of the mixture of acids. Shape selectivity and affected the activity of the ketonisation of acids. H-T zeolite was found to be appropriate for obtaining 3-hexanone from a mixture of propionic and

butyric acids.[105] It was also observed that the surface acidity of the H-T zeolite catalyst influenced the ketonisation of butyric acid. There were different pathways, leading to the formation of a symmetrical ketone, 4-heptanone, and butyric anhydride, depending on the zeolite active sites.[94, 105]

The ketonisation of carboxylic acids over acidic zeolites may take one of the following routes: the formation of carboxylates on the zeolite surface, the coupling of acyl and adsorbed carboxylic acid, or adsorbed anhydrides decomposing to form ketones.[94]

1.7.1.1.2 Ketonisation mechanism

The reaction mechanism of ketonisation and the properties of catalysts are still largely unknown, although many mechanisms have been offered during the past 30 years.[135] It is important to know the balance between bulk and surface ketonisation. For bulk ketonisation, it is important to have suitable oxides to decompose the carboxylate salts. Surface ketonisation can occur by means of various surface intermediates, as discussed in the following subsections.[94]

1.7.1.1.2.1 Ketonisation over metal oxides

The mechanism of ketonisation varies according to which metal oxide catalysts are used in the reaction.[107, 111] While these catalytic mechanisms are still debated,[107] it is clear that there are significant differences between bulk ketonisation, which occurs via the decomposition of carboxylate salts, and surface ketonisation, which involves α-hydrogen, β-ketoacid intermediates, acyl carbonium ions, adsorbed carboxylate and acid anhydrides.[94]

In the α-hydrogen ketonisation mechanism, carboxylic acid has hydrogen bonded in the α-carbon position relative to the acid carbonyl group. However, if two species are coupled on the surface via α-hydrogen to form intermediates and later decompose to carbon dioxide and water, this is called the β-ketoacid intermediate mechanism.

In the ketene mechanism, depicted in Figure 1.6, the carboxylate forms first, then reacts with ketene intermediates to obtain ketones,[94, 115] as suggested in reports. [94, 106, 136]

Another possible mechanism is the production of cyclic ketones from acid anhydride as an intermediate by loss of CO_2. The ketonisation of carboxylic acids to form ketones relies on α-hydrogen atoms in the acids. For example, the self-ketonisation of propionic acid is 10 times faster than the ketonisation of 2,2-dimethylpropionic acid, because 2,2-dimethylpropionic acid has less α-hydrogen and steric hindrance appears to reduce its reactivity.

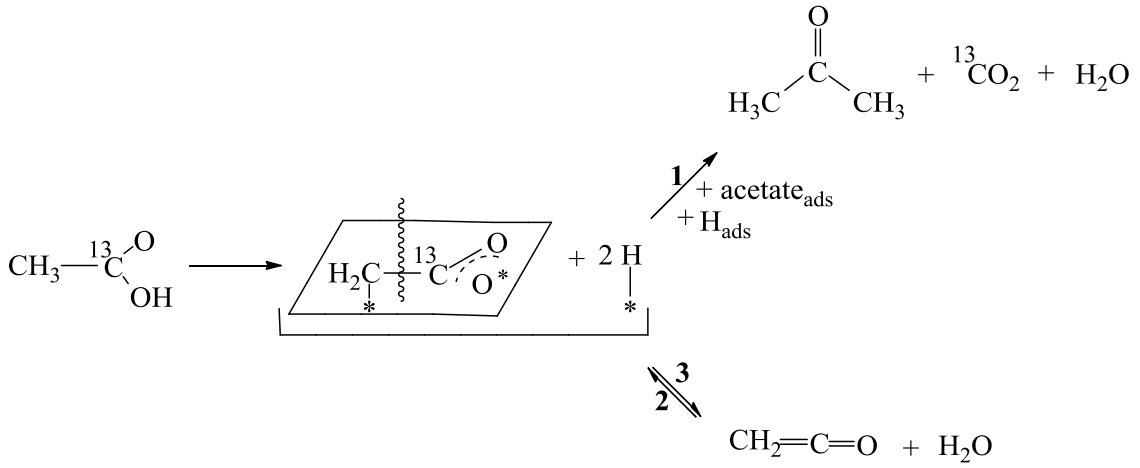

Figure 1.6 Ketonisation of carboxylic acid by the ketene mechanism.[111]

1.7.1.1.2.2 Ketonisation over zeolites

The mechanism of ketonisation over zeolites is detailed in a few reports, which mention different pathways. It has been found that acidic protons encourage the formation of

acyl rather than carboxylate species on the zeolite surface. It has been suggested that ketonisation occurs by nucleophilic attack of the acylium ions by the carboxylates.[94]

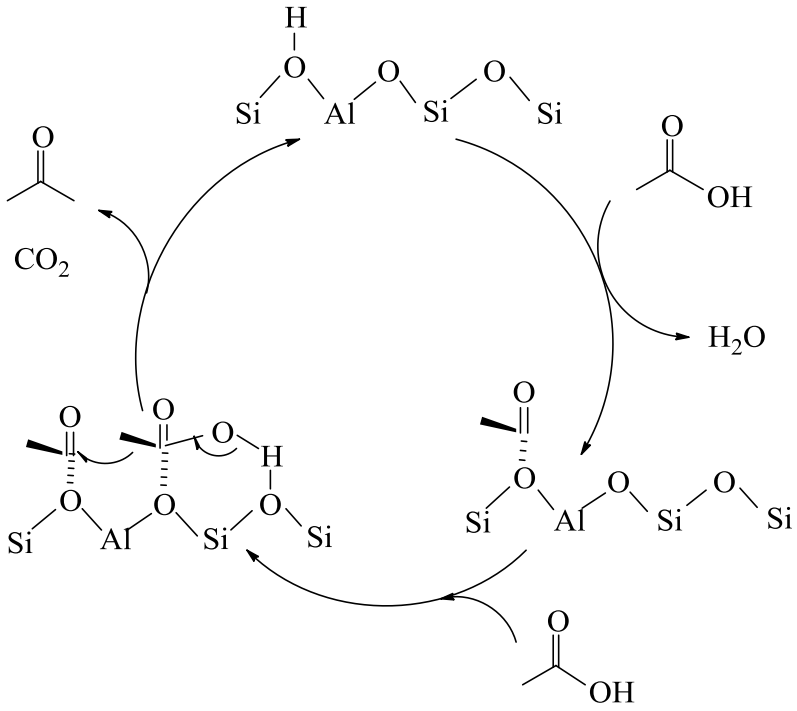

Figure 1.7 The route of ketonisation of acetic acid to form acetone over zeolites.[94]

1.7.1.1.3 Implications of ketonisation

Ketonisation plays a key role in the upgrading of biofuels. One of its most important applications is producing fuel-grade products from biomass sources of lignocellulose and triglycerides.

Pyrolysis and hydrolysis can be used to produce fuels and other chemicals from some short-chain carboxylic (acetic and propionic) acids derived from biomass, where ketonisation is significantly promising. It was found that short-chain acids gave 10% yields of bio-oil. It is easy to couple ketones with other products of bio-oil by aldol condensation or other processes such as alkylation to produce longer chains in the fuel range.[137, 138] Thus, ketonisation is a promising reaction and research in this field has

increased in recent years. One application of ketonisation is catalytic fast pyrolysis. In this strategy, it has been reported that HZSM-5 is the most typical catalyst and that it is in direct contact with biomass in the temperature range of 400-600 °C.

Acetone is the product of the ketonisation of acetic acid, using either basic or acid catalysts, and the molecular weight of this product can be increased by coupling itself via aldol condensation, or it can couple with other chemicals such as furan to give longer carbon chains. Acetone can also be converted to isopropanol, which can be dehydrated to form olefins and thence diesel and other liquid hydrocarbon automotive fuels.[94]

1.8 Nopol synthesis by Prins condensation

Nopol[139] [2-(7,7 dimethyl-4-bicyclo[3.1.1] het-3-enyl ethanol][140] ($C_{11}H_{18}O$) is an active bicyclic primary alcohol which is useful for the synthesis of agricultural and household chemicals and products[141, 142] such as pesticides,[143] perfume soaps,[144, 145] polishes,[146] detergents and fragrances.[147, 148]

Prins condensation of β-pinene and paraformaldehyde has been used to produce nopol[149] and is a significant and well known carbon-carbon coupling reaction in the synthesis of organic materials, producing different compounds depending on the reaction conditions. To obtain nopol, several methods have been used:[144, 150] a homogeneous acid catalysed reaction using $ZnCl_2$ at 115-120 °C,[141, 146] or autoclaving a mixture of β-pinene and paraformaldehyde for several hours at 150-230 °C,[146] or mixing β-pinene with paraformaldehyde in acetic acid at 120 °C to produce nopyl acetate which is then saponified to nopol.[151, 152] Homogeneous systems, which are traditional in nopol synthesis, suffer from unwanted side products and low yields of nopol.[147] Current studies of the heterogeneous catalysis of Prins condensation are directed towards

improving nopol yields. Additional advantages are that the catalyst is easy to recover and it is reusable and has low energy requirements, because it can be regenerated by washing with suitable solvents instead of requiring thermal treatment.[141] Heterogeneous catalysis of Prins condensation also shows higher activity and less substrate toxicity.[144]

1.8.1 Prins condensation catalysts

Terpenoids are one of the most important groups of inexpensive renewable raw materials for the perfumery, food and pharmaceutical industries. The chemical nature of the numerous components of essential oils is relatively simple. However, the arrangements that the carbon skeletons can assume and the changing positions of certain groups make possible the synthesis of a very large number of odoriferous substances, each having individual qualities. A small change in the structure of a carbonic terpene alters the characteristic profile of the molecule, giving different flavour and aroma from those of the initial terpene.

Acid-catalyzed transformations are a promising route for obtaining a range of fragrant compounds with wide applicability from biomass. Among these are the isomerization of various compounds,[153] the esterification and hydration of terpenes in the liquid phase,[154] and condensation.

Homogeneous and several heterogeneous catalytic systems have been reported for nopol synthesis via the Prins reaction of β-pinene and paraformaldehyde.[155] Nopol was synthesised under anhydrous conditions using $ZnCl_2$ as a homogeneous catalyst or in acetic acid to produce nopyl acetate which is hydrolysed to nopol.[140] Heterogeneous catalytic reactions have been demonstrated using various materials including Sn-MCM-41,[156] Sn-kenyaite, Fe-Zn double cyanide, mesoporous iron phosphate,[148] $SnCl_4$ grafted

on MCM-41 silicate,[149] Al-MCM-41, Sn-SBA-15,[140, 156] SZF catalyst,[144] $ZnCl_2$,[145] Zn-Al-MCM-41,[157] Zr-SBA-15[146] and zeolite.[140]

The range of important products that can be obtained by Prins condensation has stimulated increasing interest in developing different catalysts and modifying them for use in this system. Given this interest and the practical importance of nopol, we chose to study its production from β-pinene and paraformaldehyde, screening the use of catalysts such as metal oxides (e.g. Nb_2O_5 and Cr_2O_3) and the readily available Zn(II)-Cr(III) mixed metal oxides (Zn-Cr in different proportions), in order to identify the best material for this reaction. To our knowledge, little research has so far been reported on the use of metal oxides as catalysts for the Prins reaction.

1.8.2 Parameters affecting Prins condensation to produce nopol

1.8.2.1 The effect of temperature

Many studies have investigated the effect of temperature on nopol yields.[146, 150, 158] Wang and co-workers studied nopol production by Prins condensation in the liquid phase, catalysed by a series of zeolites.[158] Prior to use, the catalyst was dried at 80 °C overnight. Typically, 0.05 g of catalyst in 5 mL of toluene was mixed with 1:2 mol ratio of β-pinene/paraformaldehyde and the reaction was carried out at 70-90 °C. NaITQ2 mesopores zeolite catalyst showed 60% conversion and 87% nopol selectivity at 80 °C, while activity was lower at lower temperatures and selectivity was reduced at higher temperatures than 80 °C. At 70 °C the catalyst showed 46% conversion of β-pinene, while at 90 °C, the conversion increased to 90% but nopol selectivity dropped to 10%, and at 70° C conversion was only 46%. However, it was found that the reaction temperature did not practically affect the Prins reaction when MIL-100(Cr) was used as a catalyst.[150]

Opanasenko *et al.*[140] found that the reaction was more strongly affected by temperature than by the nature of solvent used. The yield of nopol and initial rate of Prins condensation increased significantly over FeBTC and MIL-53(Al) with p-xylene as solvent instead of acetonitrile at 120 °C. At 80 °C, the effect was smaller, however.

Increasing the temperature from 25 to 90 °C increased nopol selectivity when Zn-Al-MCM-41 was used. The highest conversion and selectivity were recorded at 90 °C, while increasing the temperature above 90 °C reduced both conversion of β-pinene and selectivity of nopol due to product isomerisation.[157]

1.8.2.2 The effect of solvent

Different solvents have been used in the production of nopol from β-pinene and paraformaldehyde in the liquid phase. The choice of solvent such as acetonitrile, ethanol, toluene, p-xylene, dodecane, methanol, ethyl acetate, hexane or dichloromethane strongly affected the reaction. The yield of nopol increased in parallel with the solvent polarity, indicating its importance in the reaction. Non-polar solvents showed a very low conversion of β-pinene on SZF catalyst when all other parameters were constant. In contrast, non-polar-aprotic solvents such as hexane, ethyl acetate and toluene improved the conversion of β-pinene as well as nopol selectivity. Toluene was found to be the best solvent in this study giving 88% Nopol selectivity at 70% conversion.[144]

The amount of solvent influenced the Prins reaction to produce nopol catalysed by Sn-SBA-15. The amount of toluene was varied from 5 mL to 15 mL. At 9 ml of toluene, the conversion of β-pinene was 99.3% and the selectivity of nopol was 95.4%. When the amount of solvent was reduced to 5 mL, catalyst activity decreased to 55.4%, probably because the paraformaldehyde did not dissolve completely and therefore

reacted less with β-pinene. Conversely, increasing the amount of solvent up to 15 mL affected neither conversion nor selectivity.[156]

1.8.2.3 The effect of substrate ratio

The effect of β-pinene/PF ratio was studied in the presence of Sn-SAB-15 in toluene solvent at 90 °C. It was found that the conversion of β-pinene decreased at a 1:1 β-pinene/PF ratio, whereas both conversion and selectivity increased at a 2:1 ratio.[159] The same effect was noted when Sn-ken-A catalyst was used at 90 °C: 0.5:1 mmol ratio of β-pinene/PF gave 44% nopol yield, which decreased to 25% with a 2:1 mmol ratio.[149]

1.8.2.4 The effect of catalyst amount

Many studies have found that yields of nopol increase as the amount of catalyst is increased.[145, 148] Jadhav *et al.*[144] used from 2.5 to 3.4 wt% of catalyst with a 1:3 ratio of β-pinene/PF in toluene at 95 °C and report that the conversion of β-pinene increased as the amount of catalyst increased, 2.5 wt% of catalyst gave 56% of β-pinene conversion and with 3.4 wt% the conversion was 75%, while selectivity of nopol remained unchanged.

1.8.2.5 The effect of catalyst calcination temperature

The Prins condensation reaction to obtain nopol is affected by the catalyst calcination temperature. It has been noted that β-pinene conversion decreased as the calcination temperature increased. In this case, sulfated zirconia (SZ) was calcined at 650, 750 and 850 °C in air at atmospheric pressure. The catalyst calcined at 650 °C showed the highest conversion of β-pinene (98%), compared with only 8% conversion when the catalyst was calcined at 850 °C and reaction conditions were unchanged.[151] The explanation is that the SZ catalyst is most active in its tetragonal phase, which is predominant at lower temperatures, rather than in its monoclinic form.[160]

1.8.3 Catalysts for Prins condensation

Prins condensation was carried out with β-pinene and paraformaldehyde at 90 °C using tin (II) hydroxychloride and toluene as solvent. In this reaction, Sn(OH)Cl achieved 99% of nopol selectivity at 98% conversion, while SnO and SnO_2 showed lower activity under the same conditions. $Sn(OH)Cl_2$ was prepared by co-precipitation and characterised by techniques such as FTIR, XRD, ^{1}H MAS NMR, TG-DTA, SEM, BET surface area and porosity. FTIR-pyridine showed that Sn(OH)Cl had a very large number of Brønsted acid sites on the catalyst surface compared with SnO and SnO_2. The acidity of Sn(OH)Cl was also confirmed by ^{1}H MAS NMR. The catalyst was efficient and had good recyclability, maintaining activity for at least three cycles.[147]

Opanasenko *et al.*[150] investigated some metal organic frameworks over zeolite in the Prins condensation of β-pinene and paraformaldehyde in the liquid phase at 80-120 °C under atmospheric pressure.[140] MIL-100(Fe) was the most active catalyst, giving 82% nopol yield in the presence of acetonitrile as solvent. However, at 120 °C, the yield of nopol increased to 87% with p-xylene as solvent. The researchers found that the β-pinene/catalyst ratio affected nopol yield, which also increased as solvent polarity increased. The catalysts were used at least three times without any observed loss in activity.

Do and co-workers[146] studied mesoporous catalyst Zr-SBA-15 platelets with 4-8 nm pore size distribution as a catalyst for Prins condensation of β-pinene and paraformaldehyde in the liquid phase. The reaction conditions were 0.5 g of catalyst, 1 mmol of β-pinene, 2 mmol of paraformaldehyde and 5 ml of toluene as solvent at 80-110 °C. The catalyst was characterised by N_2 adsorption, TGA analysis, SEM and TPD ammonia. The results showed that the catalyst had strong Lewis sites and weak Brønsted acidity, which affected its activity and selectivity. Zr-SBA-15 showed 100%

nopol selectivity in 6 h reaction time. H-beta catalyst was also tested in the reaction and found to have only 4% nopol selectivity, because this catalyst has too strong Brønsted acidity. Therefore, Zr-SBA-15 has excellent selectivity probably because of an appropriate combination of Lewis and Brønsted sites on its surface. The used catalyst was regenerated by solvent washing and a hydrothermal H_2O_2 wash at 40 °C, after which it had 100% nopol selectivity at > 95% conversion.

Extra-large pore UTL zeolite, large-pore aluminosilicate zeolite beta and metal-organic-framework $Cu_3(BETC)_2$ and Fe(BTC) were tested in the Prins reaction to produce nopol. X-ray diffraction and N_2 (-196 °C) adsorption were used to determine the crystallinity, porosity and surface area of the catalysts, while pyridine adsorption and FTIR spectroscopy were used to determine properties such as the concentration of Lewis and Brønsted acid sites. The Prins reaction was carried out in the liquid phase with 0.2 g of catalyst at 80 °C. Typically, 4 mmol of β-pinene and 8 mmol of paraformaldehyde were added to 0.4 g of internal standard (mesitylene) and 10 ml of acetonitrile as solvent. $Cu_3(BETC)_2$ was the catalyst with the greatest surface area (1500 m^2g^{-1}), while Fe(BTC) had a surface area of 1060 m^2g^{-1} and contained a larger number of accessible active sites within MOF at the appropriate strength.[155]

Jadhav *et al.*[151] studied nanosized sulfated zinc ferrite (SZF) to catalyse the synthesis of nopol from β-pinene and paraformaldehyde. Zinc ferrite was prepared by simple co-precipitation, then sulphated by impregnating it with ammonium sulfate. The resulting catalyst was calcined at 470 °C, then characterised by techniques such as FTIR-pyridine and ammonia TPD to measure the acid sites. The catalyst was pre-treated at 200 °C for 1 h, then the reaction was carried out in the liquid phase for 12 h. Five mmol of β-pinene and 15 mmol of paraformaldehyde were added to 4 ml of toluene solvent and 0.14 g of catalyst, then refluxed at 95 °C. The catalyst showed good activity and

selectivity, converting 70% β-pinene with 88% nopol selectivity. It is reported that increasing the reaction temperature to 110 °C improved conversion, but the selectivity decreased to 57%. The catalyst was recycled four times and no significant loss in the performance was observed.

Sn-MCM-41 was characterised by BET, XPS and H_2-TPR and tested for nopol synthesis from β-pinene and paraformaldehyde by Prins condensation. The reaction was affected by various parameters. It was found that increasing catalyst concentration increased the rate of conversion but reduced the selectivity. The catalyst showed 95% selectivity of nopol after 6 h using ethyl acetate as solvent instead of toluene. The catalyst was regenerated twice by washing with acetone.[161]

Yadav *et al.*[145] prepared $ZnCl_2$-impregnated montmorillonite and tested it in the Prins reaction to obtain nopol. Prior to use, the catalyst was heated at 120 °C for 2 h. The reaction was affected by catalyst amount, reaction time, reaction temperature, β-pinene/ PF molar ratio and the type and amount of solvent. It was found that using acetonitrile gave a better conversion compared with toluene, because the polarity of the solvent affected the activity of the catalyst. The reaction was run at temperatures ranging from 60 to 100 °C. At 80 °C, with a 1:2 molar ratio of β-pinene/PF and 0.1 g of catalyst, there was 75% β-pinene conversion. This fell to 64% when the temperature was increased to 100 °C. Under the same conditions, the amount of catalyst was increased to 0.4 g and conversion was observed to increase from 75% to 90% with the same selectivity (97%).

Finally, mesoporous $FePO_4$ was used in the Prins condensation of β-pinene and paraformaldehyde in the liquid phase to produce nopol. The catalyst was found to be active, environmentally benign and without toxic constituents. Acetonitrile was used as solvent under different conditions of temperature and amount of catalyst: temperature was varied in the range of 30-80 °C, with 0.01-1 g of catalyst. The ratio of β-pinene to

paraformaldehyde and reaction time were also studied. Under optimised conditions (5 mmol of β-pinene, 10 mmol of PF, 10 mL of acetonitrile and 1 g of catalyst at 80 °C) nopol yield reached 100% after 4 h and was stable for at least 6 h. The catalyst was reused five times and showed no loss in activity or nopol selectivity.[148]

1.8.4 Mechanism of Prins condensation

The mechanism proposal for Prins reaction over sulfated zirconia is illustrated in Figure 1.8. It is proposed that reactant molecules are first adsorbed and coordinated to the Zr centre of the catalyst, then hydrogen is removed by the neighbouring oxygen and finally a C-C bond is formed. If the catalyst has a combined strong Lewis site and week Brønsted acid site, the catalyst becomes active in Prins condensation[151]. If, however, the catalyst has a very strong Brønsted acid site, the reaction tends to produce some isomers such as limonene and camphene.[146]

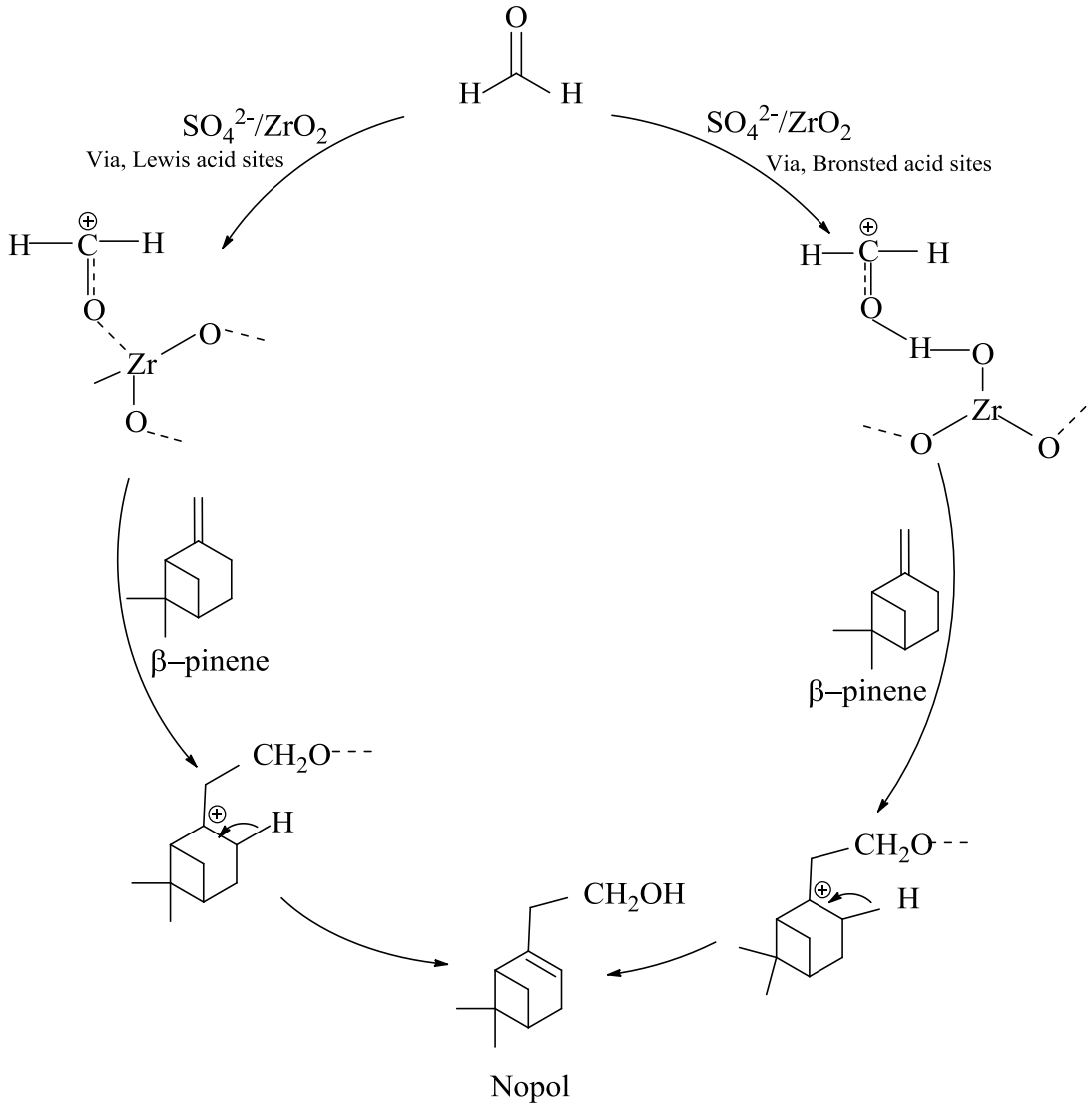

Figure 1.8 Proposed reaction mechanism for Prins condensation of β-pinene with paraformaldehyde over sulfated zirconia catalysts.[151]

Alternatively, as Figure 1.9 shows in the case of the SZF-470 catalyst, it is proposed that paraformaldehyde interacts with Zn^{2+} on the catalyst surface to produce carbocations, which react with β-pinene, then nopol is formed by allylic transfer.[144]

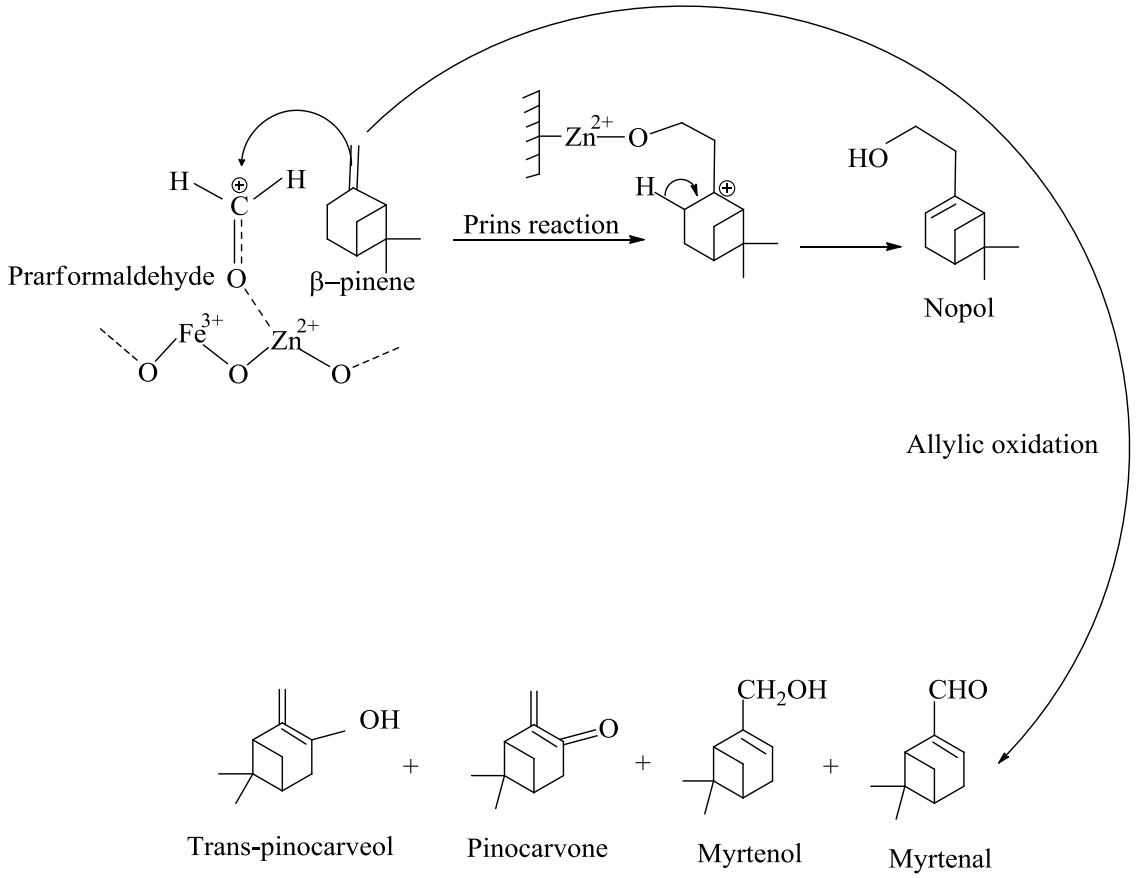

Figure 1.9 Proposed mechanism of Prins condensation for nopol synthesis over SZF-470 catalyst.[144]

Yadav *et al.*[145] proposed the pathway of Prins condensation reaction as shown in Figure 1.10. First, the formaldehyde interacted with the $ZnCl_2$ catalyst acid site and then the carbocation intermediate (A) formed followed by attacked β-pinene to form intermediate (B). Finally, the intermediate (B) decomposed and then nopol produced.

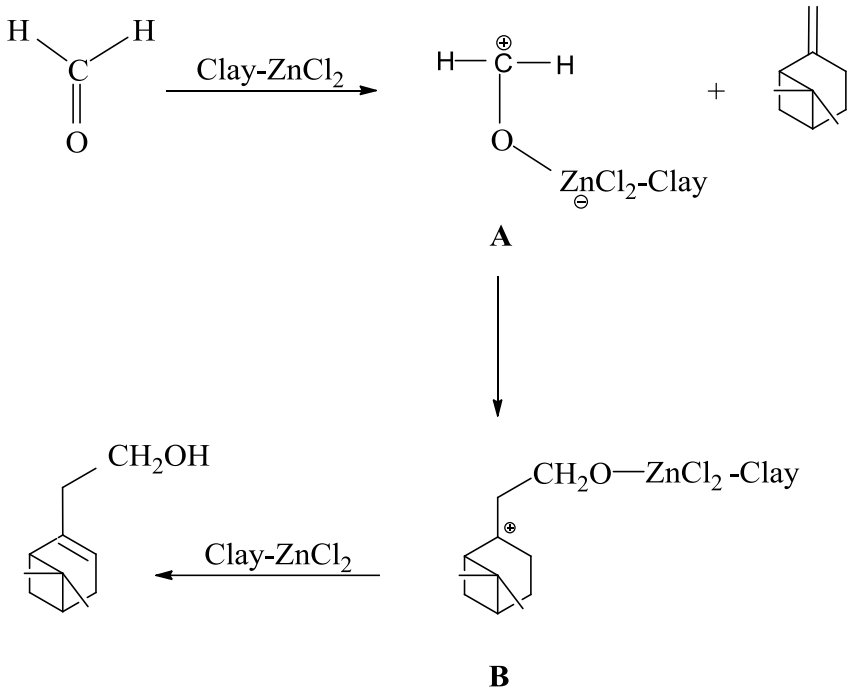

Figure 1.10 Proposed Prins condensation reaction pathway.[145]

1.9 Objectives and thesis organisation

Ketones are widely used in many applications, such as solvents, chemicals, household materials, fragrances and medicines, so their synthesis is very important. To date, research into the ketonisation of carboxylic acids on oxides catalysts has been carried out mainly on cerium oxide, titanium oxide and zirconium oxide. In this study, we examine the gas phase ketonisation of propionic and acetic acids over Zn-Cr oxides and silicalite.

Another target of this study is Prins condensation catalysed by metal oxides. It is expected to provide a clean, high-yielding route for the synthesis of nopol by the condensation of bio-renewable β-pinene with paraformaldehyde.

The catalysts are characterised both chemically and physically using various techniques, including nitrogen adsorption for their texture and IR spectroscopy and DRIFTS to detect adsorbed pyridine and to determine active Brønsted and Lewis acid sites and the silanol groups which are formed on the catalyst surface. Other techniques used are XRD, for structural properties, inductively coupled plasma (ICP) atomic emission spectroscopy, elemental analysis (C, H analysis) and microcalorimetry.

Chapter 1 provides a general introduction to catalysis, its definition and history, and outlines the steps of heterogeneous catalysis. The preparation of Zn-Cr oxides and their properties are discussed. Recent literature on the ketonisation of carboxylic acids and the Prins condensation reaction is also reviewed.

Chapter 2 begins the experimental part of the thesis, describing some methods used in preparing the silicalite, zinc chromium and niobium oxide catalysts. All of the techniques used to characterise the catalysts used in this study are also explained in detail.

The results of catalyst characterisation techniques are then presented in detail in **Chapter 3**. It is important to elucidate the properties that correspond to the performance of catalysts in the ketonisation of carboxylic acids in the gas phase.

Chapter 4 reports an investigation of the catalytic activity of silica, silicalite and their modifications, in the ketonisation of propionic acid in the gas phase. The effects on this reaction of modifications to the silica and silicalite, temperature and reaction times are presented.

Chapter 5 reports an investigation of the catalytic performance of ZnO, Cr_2O_3, Zn-Cr oxides and Zn-Cr (10:1) supported catalysts in the gas-phase ketonisation of acetic and propionic acids.

Chapter 6 reports experiments on the production of nopol by liquid phase Prins condensation over zinc and chromium oxide, zinc-chromium mixed oxide and niobium oxide catalysts. The effects of varying parameters such as type of solvent, amount of catalyst, substrates concentration, reaction temperature and reaction time are described.

Finally, **Chapter 7** draws conclusions regarding the findings of the reaction studies and the characterisation of all catalysts used in this work.

1.10 References

1. G. Ertl, H. Knözinger and J. Weitkamp, *Handbook of heterogeneous catalysis*, VCH, 1997.
2. O. Deutschmann, H. Knözinger, K. Kochloefl and T. Turek, in *Ullmann's Encyclopedia of Industrial Chemistry*, Wiley-VCH Verlag GmbH & Co. KGaA, Editon edn., 2009.
3. P. T. Anastas, M. M. Kirchhoff and T. C. Williamson, *Applied Catalysis A: General*, 2001, **221**, 3-13.
4. G. Centi and S. Perathoner, *Catalysis Today*, 2003, **77**, 287-297.
5. R. A. Sheldon, I. W. C. E. Arends and U. Hanefeld, in *Green Chemistry and Catalysis*, Wiley-VCH Verlag GmbH & Co. KGaA, Editon edn., 2007, pp. 1-47.
6. J. Pyun, *Angewandte Chemie International Edition*, 2011, **50**, 46-48.
7. S. Chaturvedi, P. N. Dave and N. K. Shah, *Journal of Saudi Chemical Society*, 2012, **16**, 307-325.
8. E. L. Kunkes, D. A. Simonetti, R. M. West, J. C. Serrano-Ruiz, C. A. Gärtner and J. A. Dumesic, *Science*, 2008, **322**, 417-421.
9. S. Furuta, H. Matsuhashi and K. Arata, *Catalysis Communications*, 2004, **5**, 721-723.
10. S. Ha, R. Larsen and R. I. Masel, *Journal of Power Sources*, 2005, **144**, 28-34.
11. S. Park, J. M. Vohs and R. J. Gorte, *Nature*, 2000, **404**, 265-267.
12. T. R. Ralph and M. P. Hogarth, *Platinum Metals Review*, 2002, **46**, 117-135.
13. H. Liu, C. Song, L. Zhang, J. Zhang, H. Wang and D. P. Wilkinson, *Journal of Power Sources*, 2006, **155**, 95-110.
14. H. Knözinger and K. Kochloefl, in *Ullmann's Encyclopedia of Industrial Chemistry*, Wiley-VCH Verlag GmbH & Co. KGaA, Editon edn., 2000.

15. J. N. Armor, *Applied Catalysis A: General*, 2001, **222**, 407-426.

16. Y. Ren, Z. Ma and P. G. Bruce, *Chemical Society Reviews*, 2012, **41**, 4909-4927.

17. G. C. Bond, *Heterogeneous catalysis: principles and applications*, Clarendon Press, 1974.

18. J. W. Niemantsverdriet, in *Spectroscopy in Catalysis*, Wiley-VCH Verlag GmbH & Co. KGaA, Editon edn., 2007, pp. 1-10.

19. G. Ertl, *Angewandte Chemie International Edition in English*, 1990, **29**, 1219-1227.

20. R. Klaewkla, M. Arend and W. F. Hoelderich, *de Mass Transfer-Advanced Aspects, Germany, InTech*, 2011, 668-684.

21. C.-C. Chang, A. R. Teixeira, C. Li, P. J. Dauenhauer and W. Fan, *Langmuir*, 2013, **29**, 13943-13950.

22. F. Cavani and F. Trifiró, *Catalysis Today*, 1997, **34**, 269-279.

23. F. Al-Wadaani, E. F. Kozhevnikova and I. V. Kozhevnikov, *Journal of Catalysis*, 2008, **257**, 199-205.

24. G. D. Pirngruber, K. Seshan and J. A. Lercher, *Journal of Catalysis*, 1999, **186**, 188-200.

25. X. Li and E. Iglesia, *Journal of Catalysis*, 2008, **255**, 134-137.

26. M. C. Molstad and B. F. Dodge, *Industrial & Engineering Chemistry*, 1935, **27**, 134-140.

27. H. H. Storch, *The Journal of Physical Chemistry*, 1927, **32**, 1743-1747.

28. E. Errani, F. Trifiro, A. Vaccari, M. Richter and G. Del Piero, *Catalysis Letters*, 1989, **3**, 65-72.

29. E. Tronconi, N. Ferlazzo, P. Forzatti and I. Pasquon, *Industrial and Engineering Chemistry Research*, 1987, **26**, 2122-2129.

30. W. S. Epling, G. B. Hoflund and D. M. Minahan, *Journal of Catalysis*, 1998, **175**, 175-184.

31. D. Gulková and M. Kraus, *Journal of Molecular Catalysis*, 1994, **87**, 47-55.

32. R. Sarkari, C. Anjaneyulu, V. Krishna, R. Kishore, M. Sudhakar and A. Venugopal, *Catalysis Communications*, 2011, **12**, 1067-1070.

33. T. Yokoyama and N. Yamagata, *Applied Catalysis A: General*, 2001, **221**, 227-239.

34. F. Al-Wadaani, E. F. Kozhevnikova and I. V. Kozhevnikov, *Applied Catalysis A: General*, 2009, **363**, 153-156.

35. B. M. Reddy and I. Ganesh, *Journal of Molecular Catalysis A: Chemical*, 2000, **151**, 289-293.

36. R. A. Comelli and N. S. Figoli, *Industrial and Engineering Chemistry Research*, 1993, **32**, 2474-2477.

37. F. Simard, U. A. Sedran, J. Sepúlveda, N. S. Fígoli and H. I. de Lasa, *Applied Catalysis A, General*, 1995, **125**, 81-98.

38. E. F. Kozhevnikova and I. V. Kozhevnikov, *Journal of Catalysis*, 2006, **238**, 286-292.

39. J. B.-S. Juan, V. C. Raghunath and S. Bala, in *Novel Materials for Catalysis and Fuels Processing*, American Chemical Society, Editon edn., 2013, vol. 1132, pp. 3-68.

40. 1st European Summer School on Catalysis Preparation: *Fundamental concepts and industrial requirements*, France, 2014.

41. M. Ohta, Y. Ikeda and A. Igarashi, *Applied Catalysis A: General*, 2004, **266**, 229-233.

42. M. Gliński, J. Kijeński and A. Jakubowski, *Applied Catalysis A, General*, 1995, **128**, 209-217.

43. T. Yokoyama and N. Fujita, *Applied Catalysis A: General*, 2004, **276**, 179-185.

44. R. Grabowski, B. Grzybowska, K. Samson, J. Słoczyński and K. Weisło, *Reaction Kinetics and Catalysis Letters*, 1996, **57**, 127-132.

45. X. Hong and S. Ren, *International Journal of Hydrogen Energy*, 2008, **33**, 700-708.

46. N. Liu, Z. Yuan, C. Wang, S. Wang, C. Zhang and S. Wang, *Fuel Processing Technology*, 2008, **89**, 574-581.

47. A. Patil, C. Dighavkar, R. Borse, S. Patil and R. Khadayate, *Journal of Electron Devices*, 2012, **15**, 1274-1281.

48. P. Bharali, R. Saikia, R. K. Boruah and R. L. Goswamee, *Journal of Thermal and Analysis Calorimetry*, 2004, **78**, 831-838.

49. M. del Arco, V. Rives, R. Trujillano and P. Malet, *Journal of Materials Chemistry*, 1996, **6**, 1419-1428.

50. S. Naidu, A. Banerjee, N. Ganguli and S. Sen, *Journal of The Research Institute for Catalysis Hokkaido University*, 1974, **21**, 172-186.

51. M. C. J. Bradford, M. V. Konduru and D. X. Fuentes, *Fuel Processing Technology*, 2003, **83**, 11-25.

52. M. I. Zaki, M. A. Hasan and L. Pasupulety, *Langmuir*, 2001, **17**, 768-774.

53. A. M. Alsalme, P. V. Wiper, Y. Z. Khimyak, E. F. Kozhevnikova and I. V. Kozhevnikov, *Journal of Catalysis*, 2010, **276**, 181-189.

54. J. H. Ferrasse and D. Lecomte, *Chemical Engineering Science*, 2004, **59**, 1365-1376.

55. J. Cejka, H. van Bekkum, A. Corma and F. Schueth, *Introduction to Zeolite Molecular Sieves*, Elsevier Science, 2007.

56. A. Corma, *Journal of Catalysis*, 2003, **216**, 298-312.

57. B. Yilmaz, U. Muller, M. Feyen, H. Zhang, F.-S. Xiao, T. De Baerdemaeker, B. Tijsebaert, P. Jacobs, D. De Vos, W. Zhang, X. Bao, H. Imai, T. Tatsumi and H. Gies, *Chemical Communications*, 2012, **48**, 11549-11551.

58. B. Yilmaz, U. Muller, B. Tijsebaert, D. D. Vos, B. Xie, F.-S. Xiao, H. Gies, W. Zhang, X. Bao, H. Imai and T. Tatsumi, *Chemical Communications*, 2011, **47**, 1812-1814.

59. B. Yilmaz and U. Müller, *Topics in Catalysis*, 2009, **52**, 888-895.

60. K. J. Balkus, M. E. Kinsel and L. L. Washmon, Google Patents, Editon edn., 2002.

61. C. N. Satterfield, *Heterogeneous Catalysis in Industrial Practice*, Krieger Publishing Company, 1996.

62. S. Bordiga, P. Ugliengo, A. Damin, C. Lamberti, G. Spoto, A. Zecchina, G. Spanò, R. Buzzoni, L. Dalloro and F. Rivetti, *Topics in Catalysis*, 2001, **15**, 43-52.

63. C. Tsiao, D. R. Corbin, V. Durante, D. Walker and C. Dybowski, *The Journal of Physical Chemistry*, 1990, **94**, 4195-4198.

64. S. Bordiga, I. Roggero, P. Ugliengo, A. Zecchina, V. Bolis, G. Artioli, R. Buzzoni, G. Marra, F. Rivetti, G. Spano and C. Lamberti, *Journal of the Chemical Society, Dalton Transactions*, 2000, 3921-3929.

65. E. E. Mallon, M. Y. Jeon, M. Navarro, A. Bhan and M. Tsapatsis, *Langmuir*, 2013, **29**, 6546-6555.

66. C. Anderson, Nina Bass, and Amanda Clark, Worcester Polytechnic Institute, Project number: CHE-RWT-1189, 2011.

67. Z. Liu, M. F. Ottaviani, L. Abrams, X. Lei and N. J. Turro, *The Journal of Physical Chemistry A*, 2004, **108**, 8040-8047.

68. G. P. Heitmann, G. Dahlhoff and W. F. Hölderich, *Journal of Catalysis*, 1999, **186**, 12-19.

69. D. W. Fickel, A. M. Shough, D. J. Doren and R. F. Lobo, *Microporous and Mesoporous Materials*, 2010, **129**, 156-163.

70. H. Bayahia, E. Kozhevnikova and I. Kozhevnikov, *Chemical Communications*, 2013, **49**, 3842-3844.

71. A. Petushkov, J. Intra, J. B. Graham, S. C. Larsen and A. K. Salem, *Chemical Research in Toxicology*, 2009, **22**, 1359-1368.

72. L. Forni, G. Fornasari, G. Giordano, C. Lucarelli, A. Katovic, F. Trifiro, C. Perri and J. B. Nagy, *Physical Chemistry Chemical Physics*, 2004, **6**, 1842-1847.

73. F. Akhtar, L. Andersson, S. Ogunwumi, N. Hedin and L. Bergström, *Journal of the European Ceramic Society*, 2014, **34**, 1643-1666.

74. T. C. Keller, E. G. Rodrigues, eacute, rez, Ram, iacute, J. rez, T. C. Keller, E. G. Rodrigues, eacute, R. rez, iacute and J. rez, *ChemSusChem*, 2014, **7**, 1729-1738.

75. D. Pugh, E. Newton, A. Naik, S. Hailes and I. Parkin, *Journal of Materials Chemistry A*, 2014, **2**, 4758-4764.

76. R. Luque, L. Herrero-Davila, J. M. Campelo, J. H. Clark, J. M. Hidalgo, D. Luna, J. M. Marinas and A. A. Romero, *Energy & Environmental Science*, 2008, **1**, 542-564.

77. Y. Chisti, *Trends in biotechnology*, 2008, **26**, 126-131.

78. A. V. Bridgwater and G. V. C. Peacocke, *Renewable and Sustainable Energy Reviews*, 2000, **4**, 1-73.

79. Sacha Alberici, Gemma Toop, ECOFYS, 2013, 1-33.

80. A. Pandey, C. Larroche, S. C. Ricke, C. G. Dussap and E. Gnansounou, *Biofuels: Alternative Feedstocks and Conversion Processes*, Elsevier Science, 2011.

81. J. C. Serrano-Ruiz, R. M. West and J. A. Dumesic, *Annual review of chemical and biomolecular engineering*, 2010, **1**, 79-100.

82. D. Mohan, C. U. Pittman and P. H. Steele, *Energy and Fuels*, 2006, **20**, 848-889.

83. W. Wang, M. Niu, Y. Hou, W. Wu, Z. Liu, Q. Liu, S. Ren and K. N. Marsh, *Green Chemistry*, 2014, **16**, 2614-2618.

84. L. Chen, Y. Zhu, H. Zheng, C. Zhang and Y. Li, *Applied Catalysis A: General*, 2012, **411–412**, 95-104.

85. R. Weingarten, G. A. Tompsett, W. C. Conner Jr and G. W. Huber, *Journal of Catalysis*, 2011, **279**, 174-182.

86. G. W. Huber, S. Iborra and A. Corma, *Chemical Reviews*, 2006, **106**, 4044-4098.

87. T. P. Vispute, H. Zhang, A. Sanna, R. Xiao and G. W. Huber, *Science*, 2010, **330**, 1222-1227.

88. H. Zhang, Y.-T. Cheng, T. P. Vispute, R. Xiao and G. W. Huber, *Energy & Environmental Science*, 2011, **4**, 2297-2307.

89. C. A. Gaertner, J. C. Serrano-Ruiz, D. J. Braden and J. A. Dumesic, *Journal of Catalysis*, 2009, **266**, 71-78.

90. A. Corma Canos, S. Iborra and A. Velty, *Chemical Reviews*, 2007, **107**, 2411-2502.

91. H. Bernas, K. Eränen, I. Simakova, A. R. Leino, K. Kordás, J. Myllyoja, P. Mäki-Arvela, T. Salmi and D. Y. Murzin, *Fuel*, 2010, **89**, 2033-2039.

92. M. Arend, T. Nonnen, W. F. Hoelderich, J. Fischer and J. Groos, *Applied Catalysis A: General*, 2011, **399**, 198-204.

93. Y. Yamada, M. Segawa, F. Sato, T. Kojima and S. Sato, *Journal of Molecular Catalysis A: Chemical*, 2011, **346**, 79-86.

94. T. N. Pham, T. Sooknoi, S. P. Crossley and D. E. Resasco, *ACS Catalysis*, 2013, **3**, 2456-2473.

95. A. D. Murkute, J. E. Jackson and D. J. Miller, *Journal of Catalysis*, 2011, **278**, 189-199.

96. T. Pham, D. Shi and D. Resasco, *Topics in Catalysis*, 2013, 1-9.

97. M. Renz, *European Journal of Organic Chemistry*, 2005, 979-988.

98. O. Nagashima, S. Sato, R. Takahashi and T. Sodesawa, *Journal of Molecular Catalysis A: Chemical*, 2005, **227**, 231-239.

99. H. Benaissa, P. N. Davey, E. F. Kozhevnikova and I. V. Kozhevnikov, *Applied Catalysis A: General*, 2008, **351**, 88-92.

100. H. Benaissa, P. N. Davey, Y. Z. Khimyak and I. V. Kozhevnikov, *Journal of Catalysis*, 2008, **253**, 244-252.

101. M. A. Alotaibi, E. F. Kozhevnikova and I. V. Kozhevnikov, *Applied Catalysis A: General*, 2012, **447-448**, 32-40.

102. C. A. Gaertner, J. C. Serrano-Ruiz, D. J. Braden and J. A. Dumesic, *Industrial and Engineering Chemistry Research*, 2010, **49**, 6027-6033.

103. D. Mansur, T. Yoshikawa, K. Norinaga, J.-i. Hayashi, T. Tago and T. Masuda, *Fuel*, 2013, **103**, 130-134.

104. R. W. Snell and B. H. Shanks, *ACS Catalysis*, 2014, **4**, 512-518.

105. J. A. Martens, M. Wydoodt, P. Espeel and P. A. Jacobs, Editon edn., 1993, vol. 78, pp. 527-534.

106. K. M. Dooley, A. K. Bhat, C. P. Plaisance and A. D. Roy, *Applied Catalysis A: General*, 2007, **320**, 122-133.

107. R. W. Snell and B. H. Shanks, *ACS Catalysis*, 2013, **3**, 783-789.

108. R. W. Snell, S. H. Hakim, J. A. Dumesic and B. H. Shanks, *Applied Catalysis A: General*, 2013, **464-465**, 288-295.

109. S. D. Randery, J. S. Warren and K. M. Dooley, *Applied Catalysis A: General*, 2002, **226**, 265-280.

110. L. Vivier and D. Duprez, *ChemSusChem*, 2010, **3**, 654-678.

111. R. Pestman, R. M. Koster, A. van Duijne, J. A. Z. Pieterse and V. Ponec, *Journal of Catalysis*, 1997, **168**, 265-272.

112. J. C. Kuriacose and R. Swaminathan, *Journal of Catalysis*, 1969, **14**, 348-354.

113. M. Gliński, W. Szymański and D. Łomot, *Applied Catalysis A: General*, 2005, **281**, 107-113.

114. R. Pestman, R. M. Koster, J. A. Z. Pieterse and V. Ponec, *Journal of Catalysis*, 1997, **168**, 255-264.

115. R. Martinez, M. C. Huff and M. A. Barteau, *Journal of Catalysis*, 2004, **222**, 404-409.

116. G. A. H. Mekhemer, S. A. Halawy, M. A. Mohamed and M. I. Zaki, *Journal of Catalysis*, 2005, **230**, 109-122.

117. R. Pestman, A. van Duijne, J. A. Z. Pieterse and V. Ponec, *Journal of Molecular Catalysis. A, Chemical*, 1995, **103**, 175-180.

118. C. Liu, A. Karim, V. Lebarbier, D. Mei and Y. Wang, *Topics in Catalysis*, 2013, **56**, 1782-1789.

119. M. Gliński, G. Zalewski, E. Burno and A. Jerzak, *Applied Catalysis A: General*, 2014, **470**, 278-284.

120. A. G. Thomas and K. L. Syres, *Chemical Society Reviews*, 2012, **41**, 4207-4217.

121. H. Onishi, T. Aruga, C. Egawa and Y. Iwasawa, *Surface Science*, 1988, **193**, 33-46.

122. D. Martin and D. Duprez, *Journal of Molecular Catalysis A: Chemical*, 1997, **118**, 113-128.

123. W. Stonkus, J. Yuskovets, L. Leite, M. Fleisher, K. Edolfa, I. Liepina, A. Mishnev and A. Shmidlers, *Russian Journal of General Chemistry*, 2011, **81**, 1523-1528.

124. E. J. Grootendorst, R. Pestman, R. M. Koster and V. Ponec, *Journal of Catalysis*, 1994, **148**, 261-269.

125. M. Gliński and J. Kijeński, *Applied Catalysis A: General*, 2000, **190**, 87-91.

126. E. Karimi, I. F. Teixeira, L. P. Ribeiro, A. Gomez, R. M. Lago, G. Penner, S. W. Kycia and M. Schlaf, *Catalysis Today*, 2012, **190**, 73-88.

127. M. Kobune, S. Sato and R. Takahashi, *Journal of Molecular Catalysis A: Chemical*, 2008, **279**, 10-19.

128. J. C. Serrano-Ruiz, A. Pineda, A. M. Balu, R. Luque, J. M. Campelo, A. A. Romero and J. M. Ramos-Fernández, *Catalysis Today*, 2012, **195**, 162-168.

129. J. C. Serrano-Ruiz, D. J. Braden, R. M. West and J. A. Dumesic, *Applied Catalysis B: Environmental*, 2010, **100**, 184-189.

130. T. N. Pham, D. Shi, T. Sooknoi and D. E. Resasco, *Journal of Catalysis*, 2012, **295**, 169-178.

131. A. A. Shutilov, M. N. Simonov, Y. A. Zaytseva, G. A. Zenkovets and I. L. Simakova, *Kinetics and Catalysis*, 2013, **54**, 184-192.

132. S. Funai, T. Tago and T. Masuda, *Catalysis Today*, 2011, **164**, 443-446.

133. L. An, C. Dong, Y. Yang, J. Zhang and L. He, *Renewable Energy*, 2011, **36**, 930-935.

134. T. N. Pham, D. Shi and D. E. Resasco, *Applied Catalysis B: Environmental*, 2014, **145**, 10-23.

135. R. W. Snell and B. H. Shanks, *Applied Catalysis A: General*, 2013, **451**, 86-93.

136. T. S. Hendren and K. M. Dooley, *Catalysis Today*, 2003, **85**, 333-351.

137. P. Zapata, J. Faria, M. Pilar Ruiz and D. Resasco, *Topics in Catalysis*, 2012, **55**, 38-52.

138. L. Nie and D. E. Resasco, *Applied Catalysis A: General*, 2012, **447–448**, 14-21.

139. *Food and Cosmetics Toxicology*, 1979, **17, Supplement**, 879.

140. M. Opanasenko, A. Dhakshinamoorthy, Y. K. Hwang, J.-S. Chang, H. Garcia and J. Cejka, *Chemsuschem*, 2013, **6**, 865-871.

141. A. L. Villa, L. F. Correa and E. A. Alarcón, *Chemical Engineering Journal*, 2013, **215–216**, 500-507.

142. V. V. Costa, H. Bayahia, E. F. Kozhevnikova, E. V. Gusevskaya and I. V. Kozhevnikov, *ChemCatChem*, 2014, **6**, 2134-2139.

143. M. V. Patil, M. K. Yadav and R. V. Jasra, *Journal of Molecular Catalysis A: Chemical*, 2007, **273**, 39-47.

144. S. V. Jadhav, K. M. Jinka and H. C. Bajaj, *Catalysis Today*, 2012, **198**, 98-105.

145. M. K. Yadav and R. V. Jasra, *Catalysis Communications*, 2006, **7**, 889-895.

146. D. M. Do, S. Jaenicke and G. K. Chuah, *Catalysis Science and Technology*, 2012, **2**, 1417-1424.

147. V. S. Marakatti, G. V. Shanbhag and A. B. Halgeri, *RSC Advances*, 2013, **3**, 10795-10800.

148. U. R. Pillai and E. Sahle-Demessie, *Chemical Communications*, 2004, **10**, 826-827.

149. A. L. Villa De P, E. Alarcón and C. Montes De C, *Catalysis Today*, 2005, **107-108**, 942-948.

150. M. Opanasenko, A. Dhakshinamoorthy, Y. K. Hwang, J. S. Chang, H. Garcia and J. Čejka, *ChemSusChem*, 2013, **6**, 865-871.

151. S. V. Jadhav, K. M. Jinka and H. C. Bajaj, *Applied Catalysis A: General*, 2010, **390**, 158-165.

152. J. P. Bain, *Journal of the American Chemical Society*, 1946, **68**, 638-641.

153. K. A. Da Silva Rocha, J. L. Hoehne and E. V. Gusevskaya, *Chemistry - A European Journal*, 2008, **14**, 6166-6172.

154. V. V. Costa, K. A. Da Silva Rocha, L. F. De Sousa, P. A. Robles-Dutenhefner and E. V. Gusevskaya, *Journal of Molecular Catalysis A: Chemical*, 2011, **345**, 69-74.

155. M. Shamzhy, M. Opanasenko, O. Shvets and J. Cejka, *Frontiers in Chemistry*, 2013, **1**.

156. M. Selvaraj and Y. Choe, *Applied Catalysis A: General*, 2010, **373**, 186-191.

157. M. Selvaraj and S. Kawi, *Journal of Molecular Catalysis A: Chemical*, 2006, **246**, 218-222.

158. J. Wang, S. Jaenicke, G. K. Chuah, W. Hua, Y. Yue and Z. Gao, *Catalysis Communications*, 2011, **12**, 1131-1135.

159. M. Selvaraj, P. K. Sinha, M. Selvaraj and P. K. Sinha, *New Journal of Chemistry*, 2010, **34**, 1921-1929.

160. B. M. Reddy and M. K. Patil, *Chemical reviews*, 2009, **109**, 2185-2208.

161. E. A. Alarcón, L. Correa, C. Montes and A. L. Villa, *Microporous and Mesoporous Materials*, 2010, **136**, 59-67.

Chapter 2

Experimental

2.1 Introduction

This chapter describes the experimental processes that were followed in this study of the ketonisation of carboxylic acids using various solid heterogeneous catalysts. Silicalite was prepared and modified by treatment with acid and base aqueous solutions. Pure zinc and chromium oxides and zinc chromium mixed oxides in different ratios were also prepared. Mixed oxide catalysts supported on Al_2O_3, SiO_2 and TiO_2 were prepared and used in the deoxygenation of propionic and acetic acid in the gas phase. In addition, niobium oxide was prepared and calcined at different temperatures. This catalyst was used to produce nopol from β-pinene by the Prins reaction in the liquid phase. All of the catalysts were characterised by means of various techniques to determine properties such as their thermal stability, water content, surface area, porosity, crystallinity and acidity. FTIR-pyridine and ammonia adsorption, carbon and hydrogen analysis, and inductively coupled plasma atomic emission spectroscopy analysis were used to determine their elemental composition and impurities. The chapter also describes in detail a variety of reaction procedures and conditions for the gas phase deoxygenation of carboxylic acids and the liquid phase Prins condensation reaction, as well as GC calibration of the substrates and products obtained. Finally, the calculation of activation energy based on the conversion of carboxylic acids over Zn-Cr mixed oxide catalyst is detailed.

2.2 Chemicals and solvents

All chemicals and solvents used in the preparation of catalysts, reaction testing and calibration were purchased from Aldrich® unless stated otherwise and used as supplied without further purification. A number of amorphous silicas were purchased from Aldrich, Degussa, BDH and Grace. Most of these silicas were high purity powdered materials employed as catalyst supports and stationary phases in chromatography. Aerosil-300 was supplied by Degussa. Also tested were Grace Silica Catalyst Supports (grades 3 to 6) from Grace Catalysts & Carriers. The reactants used were propionic acid (99.0%), 3-pentanone (>99.0%), isopropanol (99.5%), acetic acid (99%) and acetone (99%). Dodecane (>99.0%) was used as a standard and 1,2-dichloroethane as a solvent for gas chromatography (GC). TEOS, TPAOH, $Zn(NO_3)_2.6H_2O$, $Cr(NO_3)_3.9H_2O$, $Cu(NO_3)_2.3H_2O$, ammonia solution (>30%), ethanol (99.9%), $NbCl_5$ (99%) and $ZrOCl_2.8H_2O$ (98.0%) were used in preparing the catalysts. SiO_2, γ-Al_2O_3 and TiO_2 (>98.0%) were used as catalyst supports (Aerosil 300, Titanoxid P25 and Aluminiumoxid C from Degussa). NH_4-ZSM-5 (Si/Al = 180) was obtained from Zeolyst International as a commercial catalyst. Decane (99%) was used as a standard for GC for nopol synthesis in the liquid phase. β-pinene (99%), paraformaldehyde (powder, 95%), nopol and acetonitrile were used in this reaction. All gases were supplied by the British Oxygen Company (BOC). Liquid nitrogen used in the BET and FTIR equipment was available at the Department of Chemistry, University of Liverpool.

2.3 Catalyst preparation

2.3.1 Preparation of silicalite

The literature describes several different procedures for the preparation of silicalite.[1-5] Here, the synthesis of crystalline silicalite was carried out according to Heitmann *et al.*[6] First, 5 g of TEOS, 10.70 g ethanol and 11.20 ml aqueous solution (10 wt%) of TPAOH were charged into a Teflon-lined autoclave and the mixture was stirred thoroughly for 2 h without heating. The autoclave was then heated to 105 °C under autogenous pressure with stirring for 96 h. The powder was next washed with distilled water, filtered off, then dried at 110 °C for 16 h. Finally, the catalyst was calcined at 550 °C for 12 h in air, ground into a powder and sieved to a particle size of 45-180 μm.

2.3.1.1 Silica and silicalite modification

Both silica and silicalite were chemically modified via acid and basic procedures.[6] For modification by acid, 5 g of silicalite was mixed with 100 g of 0.1 or 0.01 M of hydrochloric acid (HCl) aqueous solution and the mixture was stirred for 24 h at 100 °C with reflux cooling. For basic modifications, 5 g of catalyst was mixed with 3.7 M of aqueous ammonia ($NH_{3(aq)}$) and 0.7 M of ammonium nitrate ($NH_4NO_{3(aq)}$) in a ratio of 1:3. For further research and comparison, the catalyst was modified by 3.7 M of ammonia only. In both basic and acidic solutions, the mixture was stirred and heated at 90 °C in Teflon-lined autoclave for 1 h under autogenous pressure. Finally, the catalysts were filtered through a Buchner funnel, washed several times with distilled water and dried in an oven for 4 h at 110 °C.

2.3.2 Preparation of ZnO, Cr_2O_3 and Zn-Cr mixed oxide catalysts

Chromium oxide, zinc oxide and a series of Zn–Cr mixed oxides with Zn/Cr atomic ratios of 1:1, 1:6, 10:1, 20:1 and 30:1 were prepared by co-precipitation of Zn^{II} and Cr^{III}

hydroxides.[7-9] The co-precipitation was carried out by adding 10 wt% aqueous ammonia dropwise to a stirred aqueous solution of a mixture of Zn^{II} + Cr^{III} nitrates ([Zn^{II}] + [Cr^{III}] = 0.2 M) at 70 ºC until pH = 7 was achieved, followed by aging the slurry for 3 h at 70 ºC, as reported in the literature.[8, 9] The precipitates were filtered off and washed with distilled water until ammonia-free. The catalyst was dried in air at 110 ºC overnight and finally calcined under nitrogen flow for 5 h at 300 ºC. The oxides were ground into a powder to particle sizes of 45-180 μm. For further study, the catalyst was calcined at a higher temperature in nitrogen for 5 h.

2.3.3 Preparation of Zn-Cr oxide supported catalysts

The Zn-Cr (10:1) and (1:6) catalysts were supported on Al_2O_3, TiO_2 and SiO_2. These were prepared by co-impregnation[10-12] of Zn(II) and Cr(II) nitrate onto the supports. In this method the metal nitrates were dissolved separately in a minimum amount of distilled water, then poured onto the supports. The water was removed by rotary evaporation at 50 ºC and drying completed in the oven at 110 ºC overnight under air at atmospheric pressure. Prior to use, the catalysts were calcined at 400 ºC from 2 to 5 h in air to decompose the metal nitrates to metal oxides.

2.3.4 Preparation of Nb_2O_5

Niobium oxide was prepared as described in several articles.[13, 14] In our work, $NbCl_5$ powder (5.0 g, 18.5 mmol) was dissolved in 10 ml of absolute ethanol. These amounts were then added dropwise into 200 ml of 0.3 M ammonia aqueous solution at room temperature to precipitate niobium hydrous oxide. The precipitate was stirred for 2 h, then filtered and washed many times with distilled water until chloride free. The product was dried in an oven at 100 ºC for 3 h and calcined at 110, 200, 300 and 500 ºC in air.

2.4 Catalyst characterisation techniques

2.4.1 Surface area and pore size analysis

There is a variety of reasons for measuring surface area, pore volume and pore size distribution in heterogeneous catalysts; their reactivity, conversion, selectivity and stability depend on these parameters. Depending on preparation methods and according to the IUPAC classification, the pore size of solid materials is divided into three groups:[15-20]

Micropores < 2 nm and ultramicropores < 0.7 nm

Mesopores between 2 and 50 nm

Macropores > 50 nm.

Heterogeneous catalysts commonly have a total surface area from 1 to 1000 $m^2 g^{-1}$ and an external surface area of 0.1-10 $m^2 g^{-1}$.[20] In comparison, the total surface area of porous solid materials is much higher than the external surface area, because of the contribution of the porous cavity walls. Several techniques have been used to measure catalyst porosity, based on the physical adsorption of a gas on the solid material.

Nitrogen adsorption at boiling temperature (-196 °C)[21-24] is a technique widely used to determine total surface area, pore volume and pore size distribution.[19, 20] The total surface area and porosity of catalysts were measured by using Brunauer-Emmett-Teller (BET) method,[25] which was developed in the 1940s.[20, 26] Catalyst surface area and pore texture can be calculated from the following BET equation:

$$\frac{\mathbf{P}}{\mathbf{V(P_o - P)}} = \frac{\mathbf{1}}{\mathbf{V_m C}} + \frac{\mathbf{C-1}}{\mathbf{V_m C}} \times \frac{\mathbf{P}}{\mathbf{P_o}} \qquad (2.1)$$

In this equation, P is the equilibrium pressure, P_o is the saturation pressure at the test temperature of 77 K, V is the gas volume adsorbed at pressure P, V_m is the volume of

gas adsorbed on the monolayer and C is the BET constant. In this equation, P/P_o should be between 0.05 and 0.35.[16] Plotting $P/(V \times (P_o-P))$ versus P/P_o, gives a straight line with the slope $(C-1)/(V_m \times C)$ and intercept $1/(V_m \times C)$. Therefore, V_m can be calculated and used to determine the surface area, as shown in equation 2.2.

$$A_s = \sigma V_m N_A / V_o \qquad (2.2)$$

where σ is the area covered by nitrogen molecule, N_A is Avogadro's number = 6.023×10^{23} $mole^{-1}$ and V_o is the nitrogen molar volume = 22.414 $l.mol^{-1}$.

Mesoporous volume and mesopore size of the catalysts was calculated using the Barrett-Joyner-Halenda (BJH) method,[27] which is based on the Kelvin equation and describes mesoporous adsorption-capillary condensation.[20] In this case, capillary condensation occurs when $P/P_o > 0.4$ and when the pressure increases, the thickness of the adsorbed layer on the pore walls and the capillary condensation in the pores also increase, as given by the Kelvin equation:

$$\ln\left(\frac{P}{P_0}\right) = \frac{-(2\gamma w_m Cos\theta)}{RTr_c} \qquad (2.3)$$

where r_c is the radius of pores, γ is the surface tension of liquid, w_m is the molar volume and θ denotes the contact angle. The contribution of the thickness of the adsorbed film to the total adsorption and the pore volume can be calculated. From these values and assuming a particular pore geometry, the core volume is transformed into the pore volume and the core size into the pore size.

The t-plot method, developed by de Boer et al,[28] can be used to distinguish between the external surface area and the microporous surface area. Figure 2.1 depicts examples of the t-plots for non-porous, microporous and mesoporous solids.

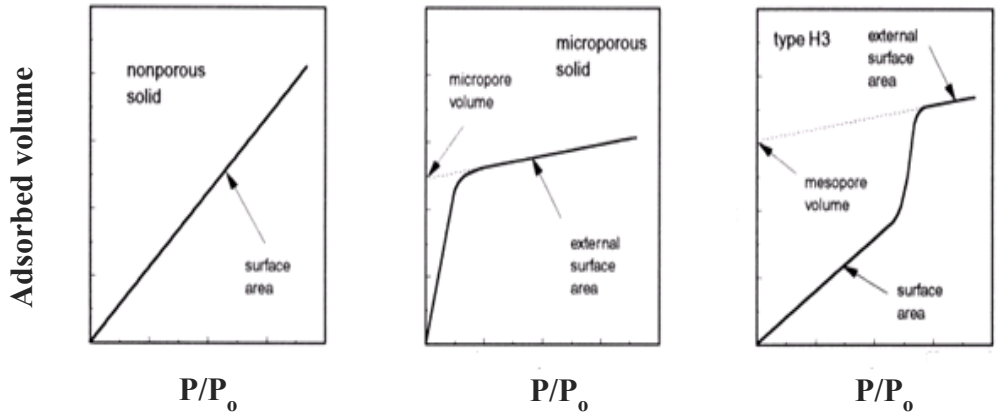

Figure 2.1 The t-plot shapes of N_2 adsorption for non-porous, microporous and mesoporous materials.[20]

Characterisation of silicalite (unmodified and modified), bulk and supported oxide catalysts used in this study was carried out on a Micromeritics adsorption apparatus model ASAP, which was available in our lab. Typically, 150-200 mg of sample was degassed under vacuum for 1 h at 150 °C in the furnace to dry the catalyst, then cooled under a dry nitrogen atmosphere. The catalyst was next evacuated at 250 °C until the pressure reached 8 μmHg, which usually took 2-3 h. The sample was allowed to cool to room temperature and gas pressure was allowed to reach equilibrium before subsequent dosing. After a series of successful nitrogen doses (≈55), analysis was performed in order to obtain sufficient information to plot an adsorption isotherm. Figure 2.2 shows the Micromeritics ASAP 2000 analyser which was used to measure the surface area and porosity of the catalysts.

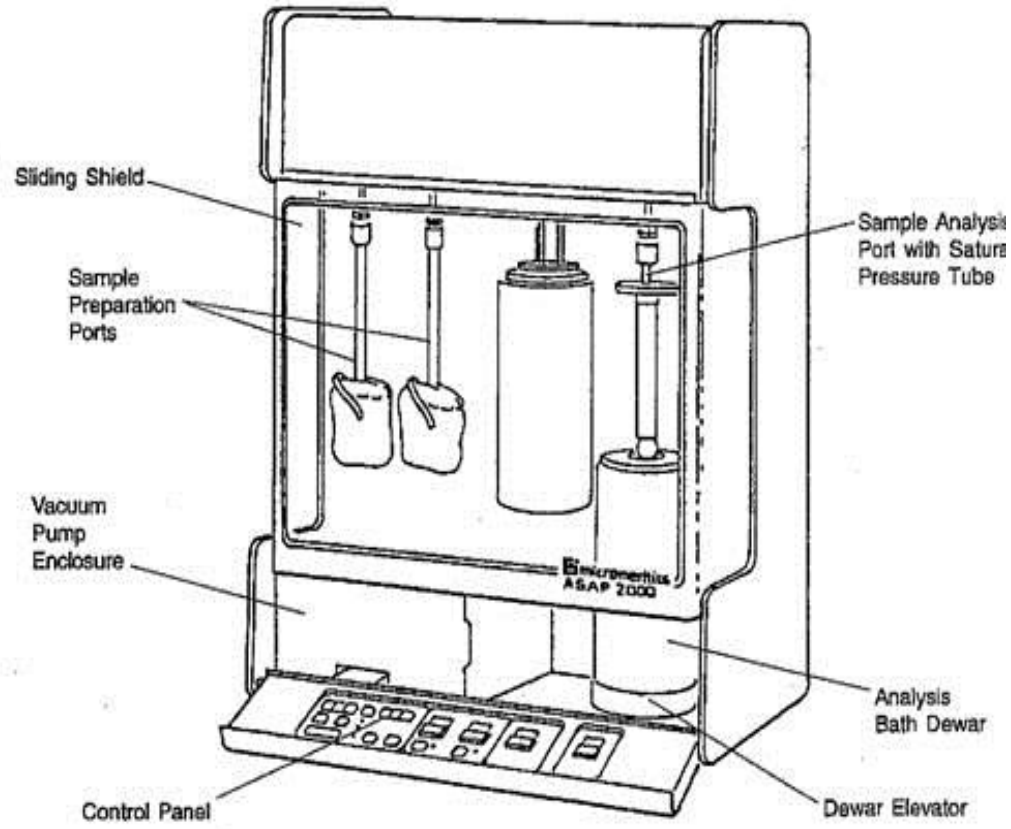

Figure 2.2 Schematic of the Micromeritics ASAP 2000 instrument from the official brochure.[29]

2.4.2 C, H, N analysis

Determination of elements such as carbon, hydrogen, nitrogen and sulfur in organic compounds is one of the most important chemical applications.[30] Typically, a milligram-sized sample was weighed, placed in the reactor and heated from room temperature to 1273 K under flowing helium gas, which was then temporarily enriched with pure oxygen, causing flash combustion to occur. The combustion quantities were obtained by passing the mixtures of gases to the GC detector. To allow further study of catalyst deactivation by coke formation and the effect of carbonaceous deposits on catalyst performance, combustion analysis was used to measure the C and H content of

some spent catalysts. Carbonaceous deposits on the surface of a catalyst can reduce its activity. Coke, which is always formed on the catalyst surface during hydrotreatment, can be soft or hard.[31] In this work, the amount of coke was measured for all spent catalysts which were tested for a long time; for example, silicalite was tested for at least 28 h time on stream in the deoxygenation of propionic acid in the gas phase. There was some reduction in catalytic activity with time of reaction. Moreover, C and H analysis was performed for supported mixed metal oxide catalysts used in the deoxygenation of carboxylic acids. The results were important, because they gave important information about catalyst deactivation. The reduction of catalyst activity or selectivity can be explained by the deposition of coke on the surface. The results of C and H analysis are given in section 3.8. Catalyst coke was measured using the Thermo Flash EA 1112 series analyser in the Department of Chemistry at Liverpool University.

2.4.3 Fourier transform infrared (FTIR) spectroscopy

Fourier transform infrared (FTIR) spectroscopy has many applications in chemistry, such as obtaining structural framework information,[30, 32-34] measuring stability and investigating the presence of Lewis (L) and Brønsted (B) active sites on the surface of catalysts. The L or B nature of acid sites can be determined by FTIR of adsorbed pyridine, as mentioned in several published articles.[8, 35-37]

The region of bending and stretching vibration of infrared absorption lies between 400 and 4000 cm^{-1} in the bonds of molecules. The intensity of absorption depends on the strength and chemical environment of the bonds, so information about the structure of a molecule can be obtained from the particular frequencies at which absorption occurs.

Diffuse reflectance infrared Fourier transform (DRIFT) spectroscopy measures the infrared radiation which is reflected from the sample across the spectral region. The

reflectance intensity is plotted against wave number (λ). This can be shown in both absorption and transmission mode as a resulting spectrum. In this technique, mirrors are used to focus diffusely scattered light (Figure 2.3), which is then sent to a detector. Powder samples are particularly suitable for use in this technique.

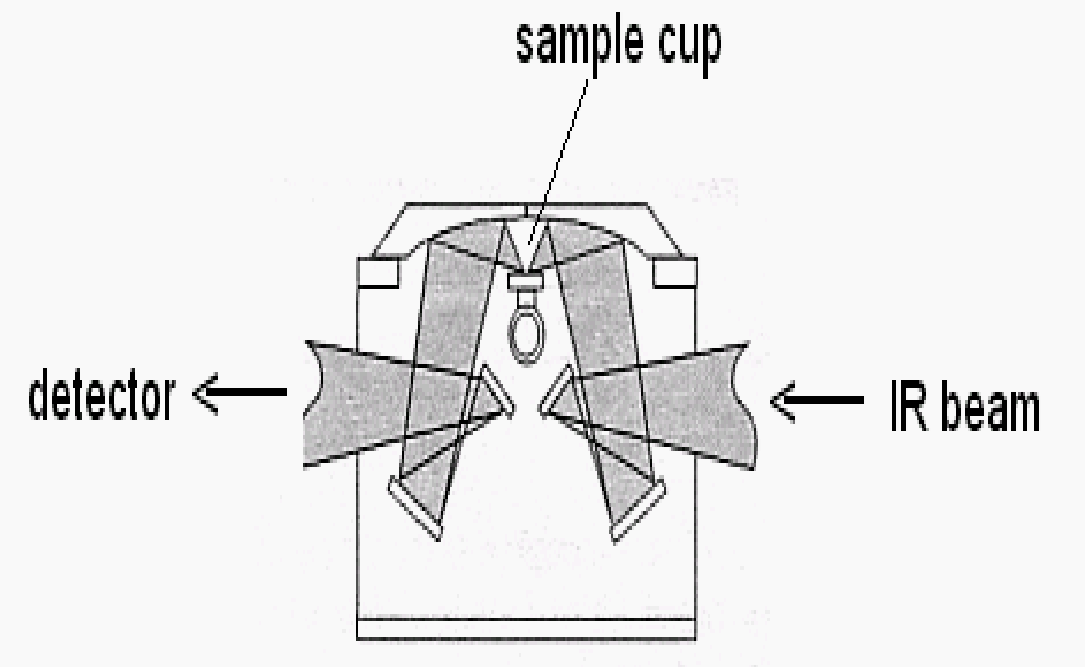

Figure 2.3 Schematic of the diffuse reflectance accessory.

Silica and silicalite catalysts were used in this study, the fingerprint region of the spectrum (3100-4000 cm^{-1}) being used to investigate the silanol groups as active sites on the surface of fresh catalysts. Before FTIR analysis, the catalyst was pretreated at 300-500 °C for 1 h in N_2 gas flow, under the same conditions as for the deoxygenation of propionic acid. Next, 5 mg of catalyst was mixed with 45 mg dry KBr powder[38] and the mixture was thoroughly ground to create a diffusely scattering matrix that would reduce adsorption and thus increase the throughput of the beam to enhance the resolution of the analysis. Characterisation of silica (Aersil-300) and silicalite catalysts

by DRIFT spectroscopy revealed significant differences and gave important information regarding the active sites in the ketonisation of propionic acid at temperatures of 400-550 °C.

Pyridine adsorptions on DRIFT spectra were obtained for pure zinc and chromium oxides, their mixtures and niobium oxide catalysts used in the ketonisation of acetic and propionic acids and in Prins condensation to form nopol. Catalyst samples were diluted to 10 wt% with KBr powder, pretreated at 150 °C/0.01 kPa for 1 h under vacuum to remove physisorption water, then cooled at room temperature under a dry N_2 atmosphere. The minimum amount of pyridine was next dropped onto each sample. The samples were exposed to pyridine for 1 h then the samples with pyridine were degassed again at 150 °C for 1 h under vacuum to remove the physisorbed pyridine. Finally, the samples were analysed and the B and L acid sites were determined in the regions of 1540 and 1450 cm^{-1} respectively.[8, 35, 39]

For this purpose, DRIFT spectra were recorded on a Nicolet NEXUS FTIR spectrometer at room temperature and ambient pressure under dry N_2 atmosphere using powdered catalyst mixtures with KBr. This equipment is available in our lab.

2.4.4 Inductively coupled plasma atomic emission (ICP-AE) spectroscopy

Most elements in the sample were present at low concentrations, in the part per billion range, which can be determined using plasma as an excitation source, since plasma, created by heating a gas such as argon at temperatures higher than 6000 K, has a high proportion of electrons and ions. This technique can detect a great number of elements in wide range of concentrations.[32] The inductively coupled plasma atomic emission spectroscopy **(**ICP-AES) apparatus consists of three concentric tubes, usually made of

silica, as shown in Figure 2.4. These are the outer tube, the inner tube and the central tube, which together comprise the ICP torch.

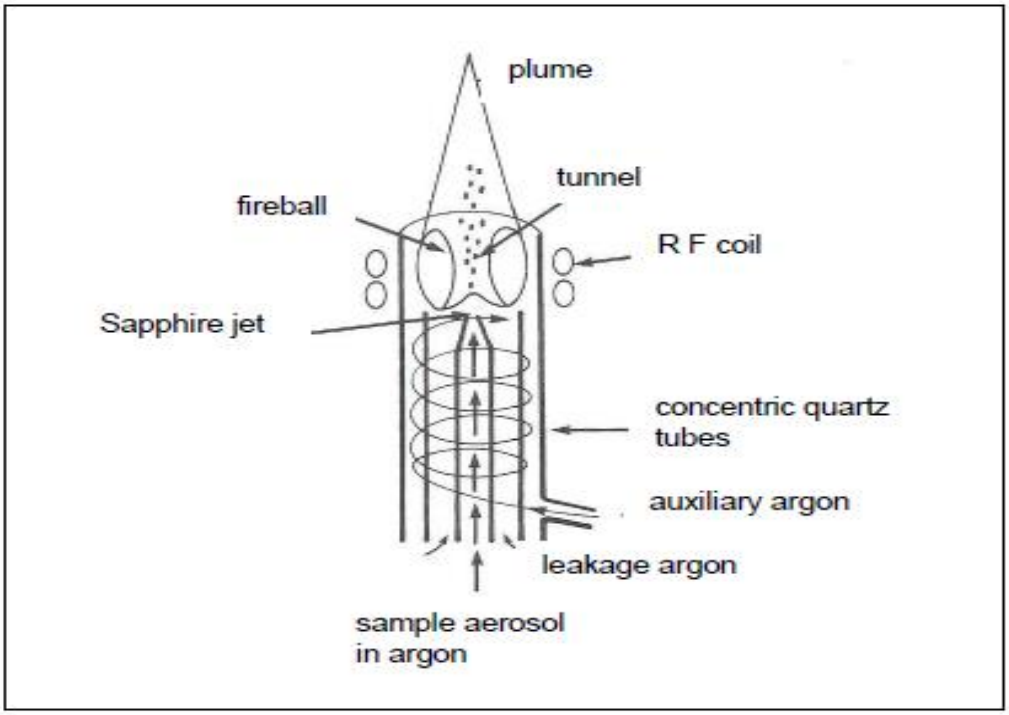

Figure 2.4 An ICP torch.

Before analysis, a 20 mg sample of catalyst is dissolved in an appropriate solution. In this case, it was dissolved in an aqua regia solution $(HNO_3 + HCl)_{(aq)}$ and gently heated at 30 °C for some time. The solution then was diluted to 100 ml using distilled water in a standard flask and 5 ml of this solution was submitted for analysis. The ICP-AES was performed by G. Miller within the Department of Chemistry, University of Liverpool, using a Spectro Ciros emission spectrometer.

2.4.5 Powder X-ray diffraction (XRD)

Powder XRD is an analytical technique which provides useful information about sample structures and phases, developed by Peter Debye, Paul Scherrer and Albert Hull.[40] It is commonly used to determine the crystalline phase of materials. Each pure solid material has fingerprint of x-ray intensity and the powder diffraction method is suitable to characterise the crystalline phase. X-ray wavelengths are equivalent to the spaces between atoms in crystals, so x-rays pass through these materials to give characteristic diffraction patterns. This occurs when a fraction of the particles of crystalline material in the catalysts are orientated at the correct angle to the crystal plane, thus obeying Bragg's law (equation (2.4):

$$2d \sin \theta = n \lambda \qquad (2.4)$$

In this equation, n is the order of reflection, λ is the incident x-ray wavelength, d is the lattice planar spacing and θ is the diffraction angle.

Here, we used XRD to study crystal structures and matched them with authentic materials, because it was very helpful to compare our silicalite samples with authentic ones. The technique is also important when active groups are formed on the surface of catalysts. Typically, the powdered sample was placed on a sample holder and exposed to x-radiation at room temperature by transmission or reflection methods. The sample was ground to a fine powder and a suitable disk was used for analysis. The pattern was recorded in the range of 2θ between 10 and 80° on a Bruker D8 Advance diffractometer in Bragg-Brentano geometry equipped with a Ge monochromator giving Cu Kα radiation (λ = 0.154 nm), which is available in the Department of Chemistry at Liverpool University.

2.4.6 Differential scanning calorimetry (DSC)

Figure 2.5 shows a SETARAM TG-DSC 111 differential scanning calorimeter. Thermogravimetric DSC is an analytical technique most commonly used for catalyst characterisation.[41] It is important for determining acid or basic properties such as the number of acid sites and their strength. Physical and chemical transformations of catalysts such as crystallisation, phase changes, sublimation, adsorption, desorption, decomposition, oxidation, reduction, surface reactivity and calcination can be studied.[42] Typically, the ammonia pulse chemisorption method[41] is used, which was used here to determine the acid sites of the catalysts.

The DSC is designed around two open refractory tubes, crossing a heating furnace. A detection unit placed between the tubes is designed according to the Calvet principle. The sample cell is placed in the furnace and connected to the balance and the reference sample is placed on the other side of the furnace, as Figure 2.5 shows. The gas flow system is equipped with a pressure regulator.

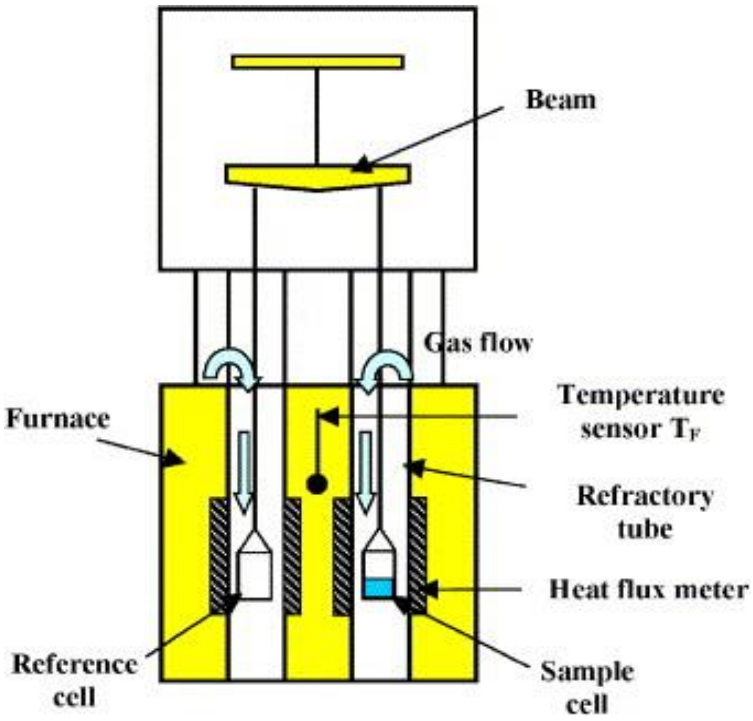

Figure 2.5 TG-DSC schematic cross section.[43]

In this project, a 100 mg catalyst sample was pre-treated at 380 °C for 1 h with a temperature ramp rate of 5 °C min^{-1} under N_2 gas at a flow rate of 30 ml min^{-1} to eliminate water molecules. The programmed temperature was reduced to 150 °C and held for about 2 h until the sample weight stabilised. The analysis was then started by pulsing ammonia consecutively, with N_2 as the carrier gas. After injection, sufficient time (30 min) was allowed for ammonia adsorption to be completed and equilibrium to be reached. The weight gained and the corresponding heat of ammonia adsorption were recorded.

2.4.7 Microcalorimetry

Calvet calorimetry is one of the most important techniques for measuring thermal phenomena in chemical reactions. In this study, a Setaram C80 heat flux Calvet type

microcalorimeter was used to measure the heat of adsorption of ammonia and carbon dioxide on mixed oxide catalysts. Each sample was pre-treated at 200 °C then set up in the microcalorimeter and it usually took 90 minutes to stabilize before analysis began.

The setup consisted of two stainless steel cells, one for the sample and another for reference, both located in the calorimetric block, (Figure 2.6).

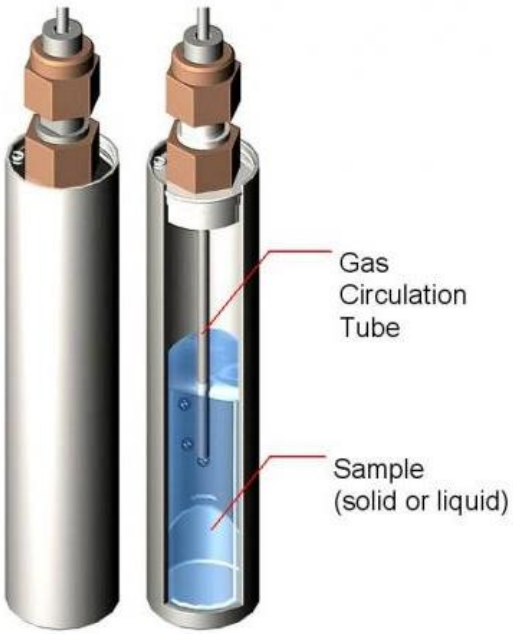

Figure 2.6 Setaram C80 gas circulation cell.[44]

Each fresh catalyst oxide sample (500-1000 mg) was pre-treated at 200 °C under vacuum for 1 h and cooled at room temperature. The analysis was then performed in the isothermal mode of operation at 150 °C for 90 minutes under dry nitrogen atmosphere and ammonia was injected every 30 minutes. The heat of ammonia adsorption was calculated as per mole of ammonia uptake.

2.4.8 Thermogravimetric analysis (TGA)

The principle of TGA relies on changes in the weight of a sample as the temperature increases. Weight may change as a result of chemical or physical reactions, such as loss of water or other volatile components, or the decomposition temperature being reached. The measurement of water content can help in the preparation of catalysts, because the quantity of some hydrated salts, such as chromium and zinc nitrates, must be accurately determined when preparing metal oxide catalysts. A TGA instrument is equipped with a sensitive balance and sample container placed inside a furnace under gas flow of nitrogen or air. A derivative thermogravimetric curve shows the point at which weight is lost, as Figure 2.7 shows. TGA is a useful technique for many purposes, such as studying the thermal stability of a solid sample or determining its water content.

TGA of a 20-50 mg sample was carried out on a Perkin-Elmer TGA 7 instrument available in our lab, under nitrogen flow at a heating rate of 20 ºC min^{-1} to raise the temperature from room temperature to 700 ºC. Figure 2.8 shows a Perkin Elmer thermogravimetric analyser.

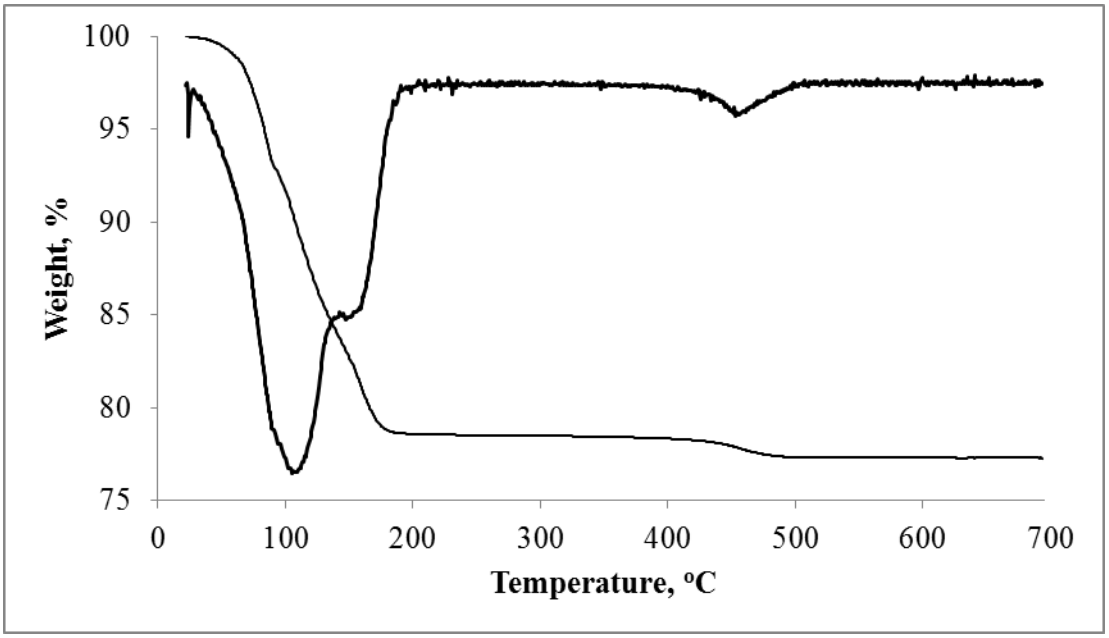

Figure 2.7 TG for fresh Co-Mo/Al_2O_3 catalyst (heating rate: 20 ºC/min).

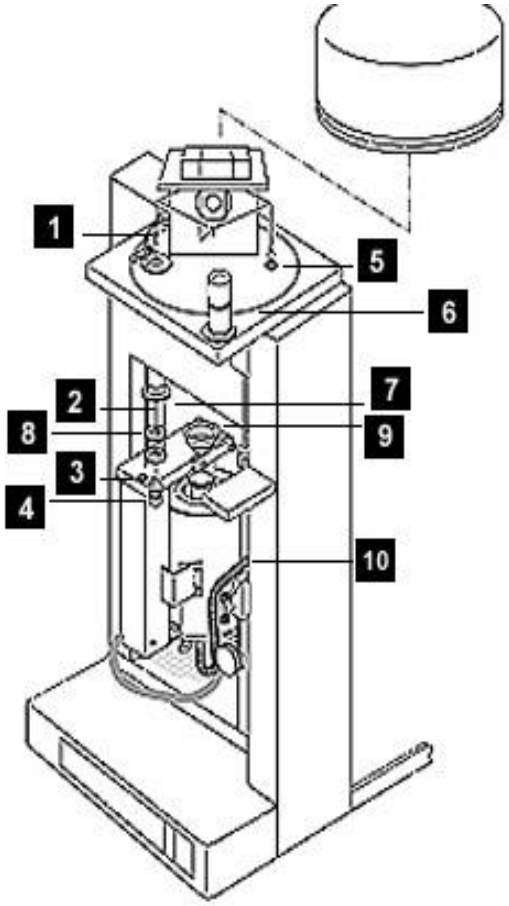

Key

1) Quartz hangdown wire link
2) Platinum hangdown wire kit
3) Platinum stirrup kit
4) Platinum sample pan kit
5) Balance tare weight
6) O-ring
7) Extension tube
8) Sample thermocouple
9) Furnace
10) Flexible Teflon ™ tubing.

Figure 2.8 Perkin Elmer TGA 7 instrument.

2.5 Catalyst testing

2.5.1 Product analysis

In both gas and liquid phase catalytic reactions, gas chromatography was used to separate and quantitatively analyse products. However, the temperature and pressure used in GC analysis differ between products in the gas and liquid phases. Here, we used three different columns: one to analyse gas phase products in the deoxygenation of carboxylic acids, the second to analyse the light gas by-product and the third to analyse liquid phase samples in the Prins condensation reaction to produce nopol. Because of

the importance of this part, the GC conditions, the response factors (R_f) and the calculation of the conversion and selectivity of products are explained here in detail.

2.5.1.1 Gas chromatography (GC)

GC is an extremely important analytical technique for the detection, identification and quantitation of trace substances in the fields of chemistry, biology and medicine. In this case, the mixture of volatile compounds was transported in a gas stream with an inert carrier gas (N_2, He, Ar or H_2),[45, 46] passing as a mobile phase through the GC column at different speeds, depending on their boiling points and solubility. Figure 2.9 shows the setup of a typical GC, while Figure 2.10 shows the GC setup for this study.

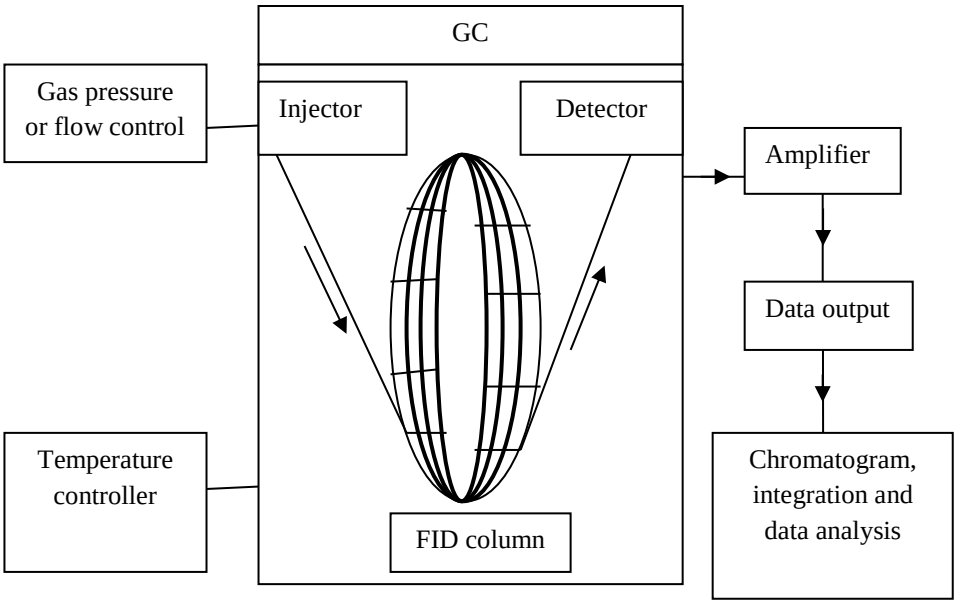

Figure 2.9 Schematic diagram of a typical GC.

Figure 2.10 Varian 3800 gas chromatograph with Varian Star Software equipped with ZB-WAX capillary column and a flame ionization detector.

In order to analyse the sample, the compounds were measured as they emerged from the column using a flame ionisation detector (FID), as shown the Figure 2.11. This widely used type of detector is highly sensitive and responsive to most organic compounds. The effluent from the column was mixed with hydrogen and air and burnt at a small metal jet to form ions in proportion to the concentration of ions derived from the solutes. The electrical conductivity of the flame and the current were measured to determine these proportions.

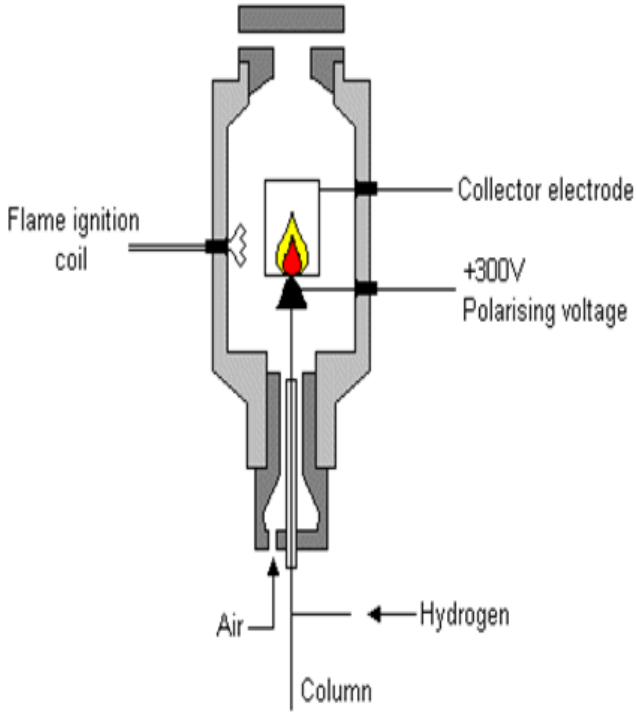

Figure 2.11 Flame ionisation detector.[47]

The column was fitted with an injection port at one end and a detector at the other. A split/splitless injector was used to introduce the samples into the column, which was always maintained above the evaporation temperature of the sample. The samples were introduced using a standard microlitre syringe through a septum into the vaporizing chamber. This type of injector, as illustrated in Figure 2.12, comprises a heated chamber containing a glass liner into which the sample is injected through the injection septum. The chamber is heated independently of the chromatographic oven. The injected sample vaporizes rapidly to form a mixture of carrier gas, solvent vapour and vaporized solutes. A portion of this vapour mixture passes into the column, while a greater volume leaves through the split valve outlet.

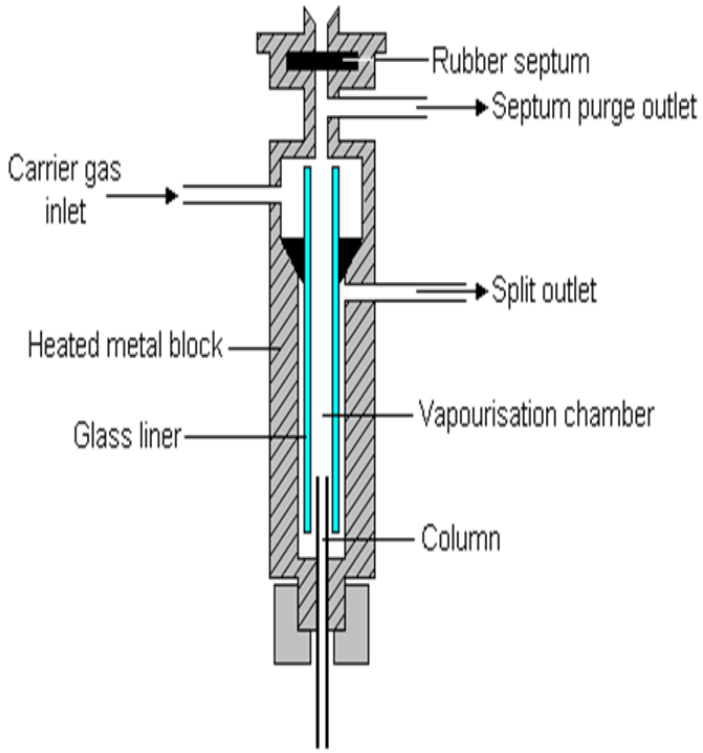

Figure 2.12 Split/splitless vaporising injector.[47]

2.5.1.2 Product calibration

Several different methods may be used to calibrate GC products, the most common being the internal and external standard. A known concentration of a standard compound, which should be very close to the compound under analysis, is added to the mixture of analyte and solvent. The ratios of peak areas of compounds depend on their concentrations, not on the amount injected, and the concentration of the amount injected can be calculated using the following equation:

$$M/M_o = R_f \times S/S_o \qquad (2.5)$$

M/M_o is the molar ratio of the compound being analysed to that of the standard, plotted against S/S_o, which is the ratio of the area counts of compound and standard. R_f is the calibration factor or response factor, obtained from the calibration.

The molecular weights, boiling points, retention times and calibration factors for all components used in the deoxygenation of carboxylic acids are given in Table 2.1.

Table 2.1 Molecular weights, boiling points, GC retention times and calibration factors for all compounds involved in the gas-phase deoxygenation of propionic, acetic and pentanoic acids using Varian 3800 ZB-WAX capillary column.

Compound	M wt (g/mol)	Boiling points (°C)	Retention time (min)	Calibration factor[a]	Calibration factor[b]
Light gas			0.60-0.65		
Propionic acid	74.08	141	7.40	1	-
3-Pentanone	86.13	100	1.74	1.27	-
Propionic anhydride	130.14	167	6.16	1	-
2-propanol	60.09	82.5	1.28	1.31	-
Acetone	58.10	56	0.93	1.10	1.51
Acetic acid	60.05	118	6.78	-	1
Pentanoic acid	102.13	186-187	8.73	1[c]	-
5-Nonanone	142.24	186-187	5.86	1.29[c]	-

[a] Calibration factor relative to propionic acid.

[b] Calibration factor relative to acetic acid.

[c] Calibration factor relative to pentanoic acid.

Table 2.2 Molecular weights, boiling points, GC retention times and calibration factors for the light gases involved in the gas-phase deoxygenation of propionic, acetic and pentanoic acids using Varian 3800 GC-Gas Pro capillary column.[a]

Compound	M wt (g/mol)	Boiling points (°C)	Retention time (min)	Effect carbon number	Calibration factor
Methane	16.04	-164	4.40	1.0	1.0
Ethane	30.07	-89	4.70	2.0	0.50
Ethene	28.05	-103	4.77	1.9	0.53
Propene	42.08	-47	5.85	2.9	0.34

[a] Column B; calibration factors were estimated using the effective carbon-atom number.[48]

Figures 2.13 to 2.20 show the calibrations relative to the response factors for all of the substrates used in this study and the products obtained.

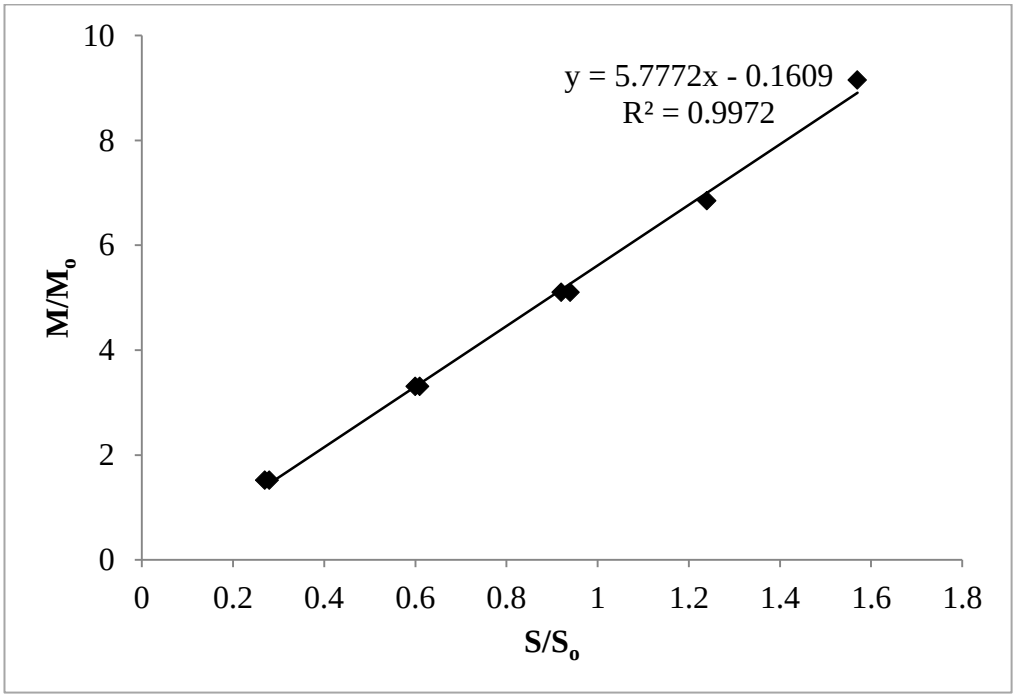

Figure 2.13 Calibration for propionic acid with dodecane as standard.

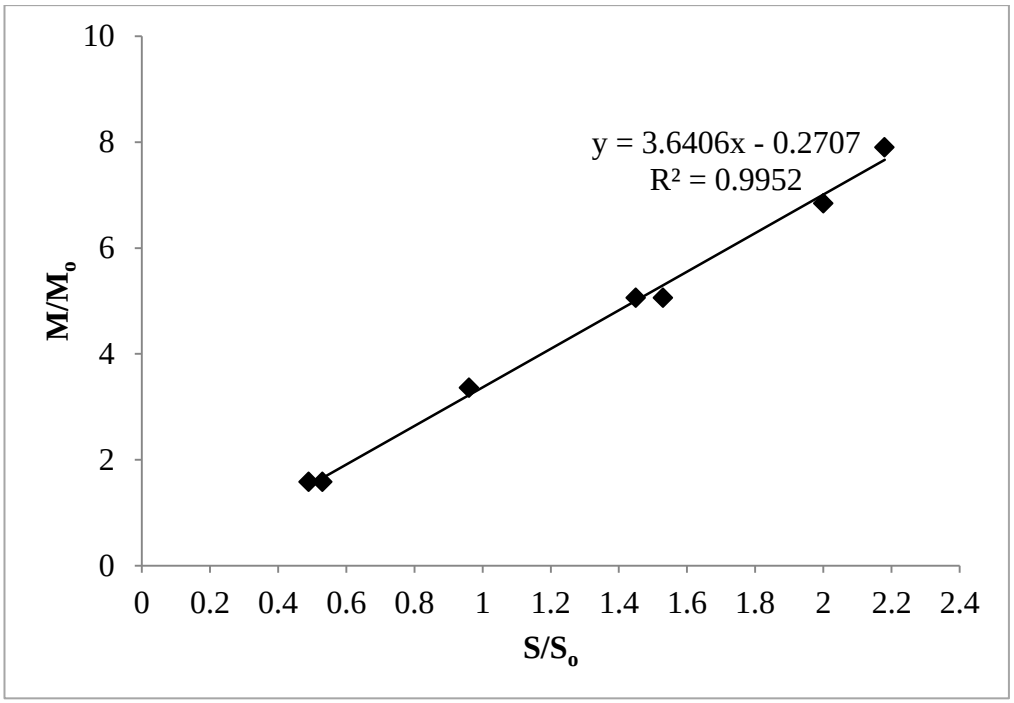

Figure 2.14 Calibration for 3-pentanone with dodecane as standard.

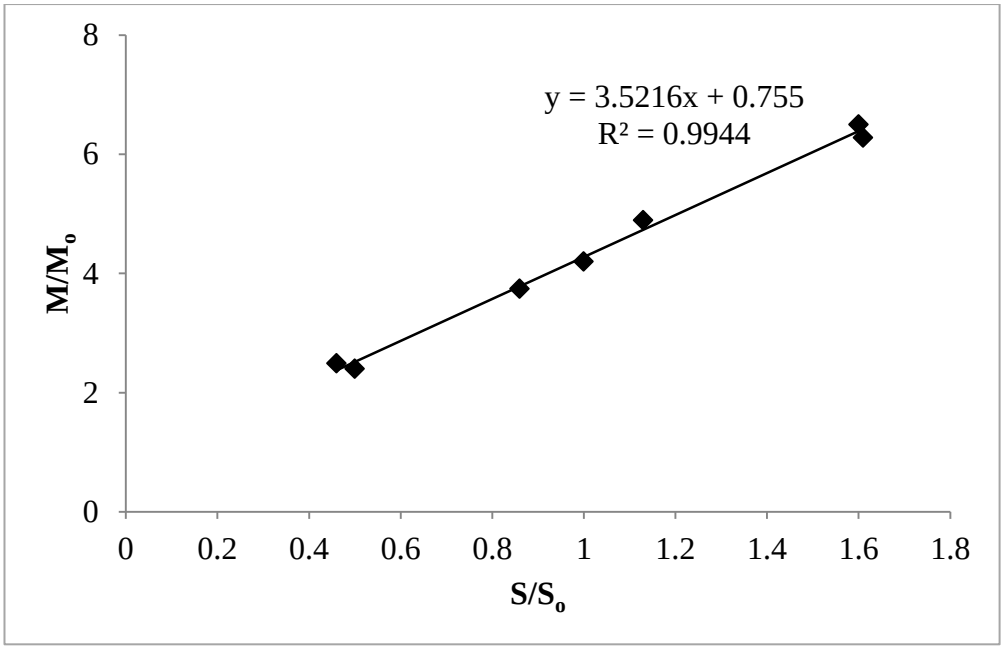

Figure 2.15 Calibration for propionic anhydride with dodecane as standard.

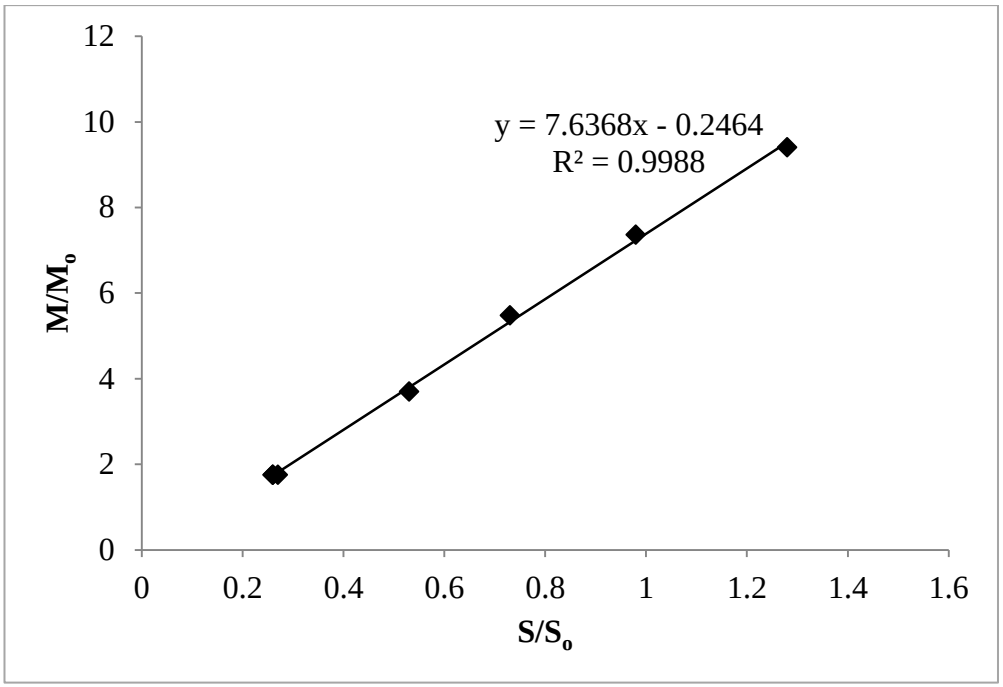

Figure 2.16 Calibration for 2-propanol with dodecane as standard.

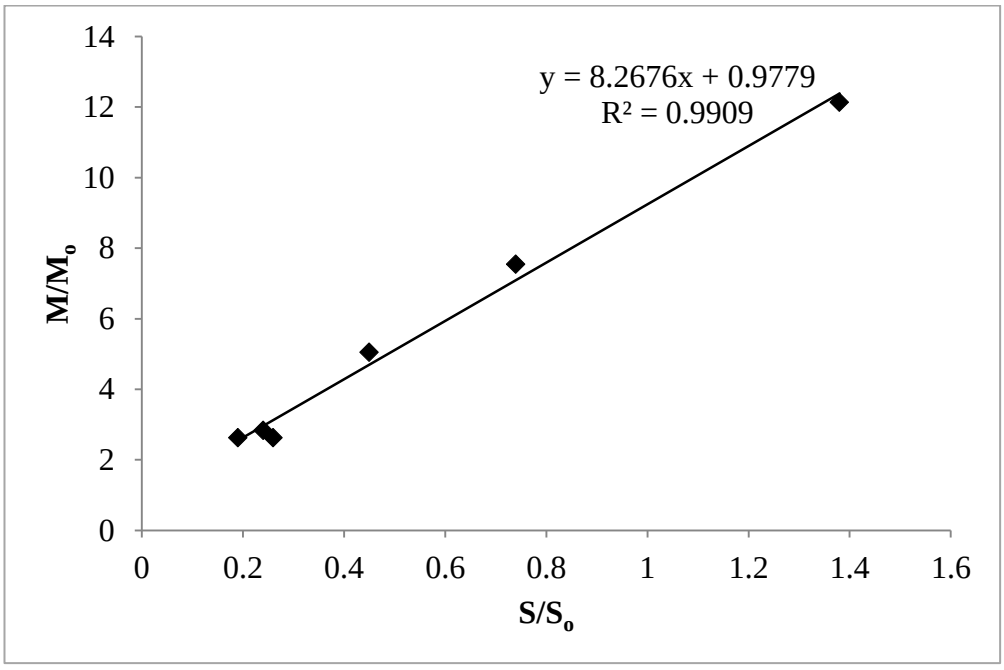

Figure 2.17 Calibration for acetic acid with dodecane as standard.

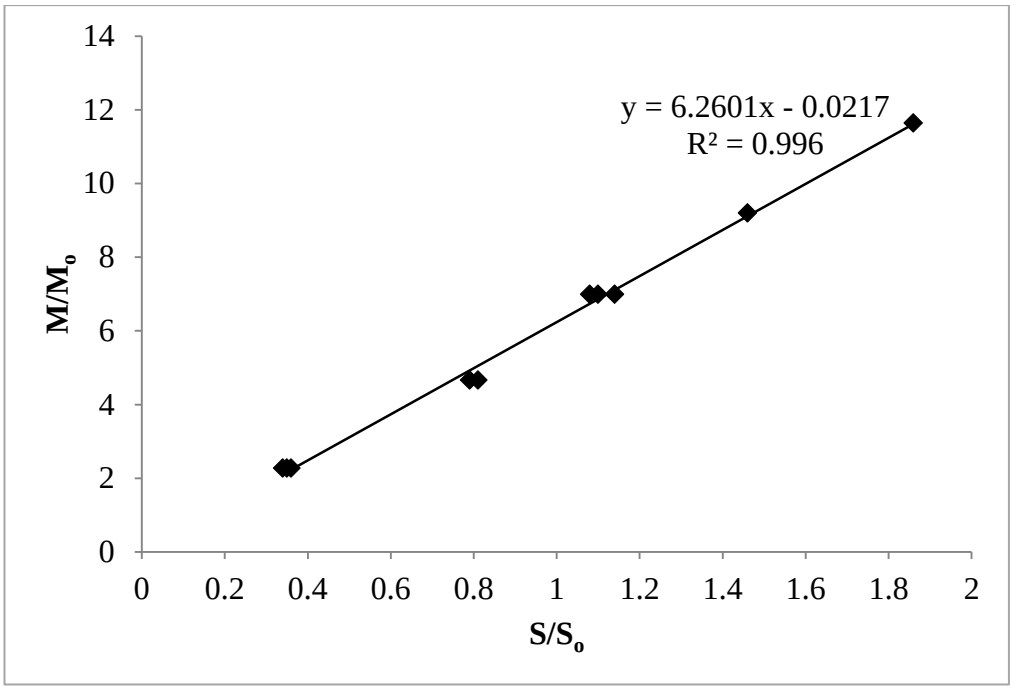

Figure 2.18 Calibration for acetone with dodecane as standard.

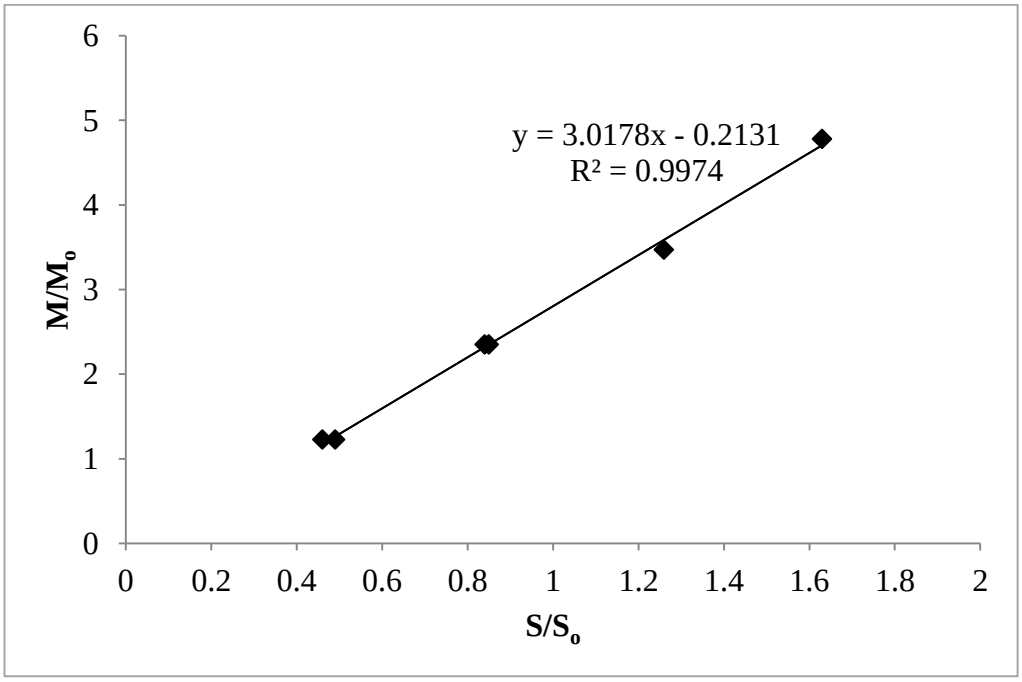

Figure 2.19 Calibration for pentanoic acid with dodecane as standard.

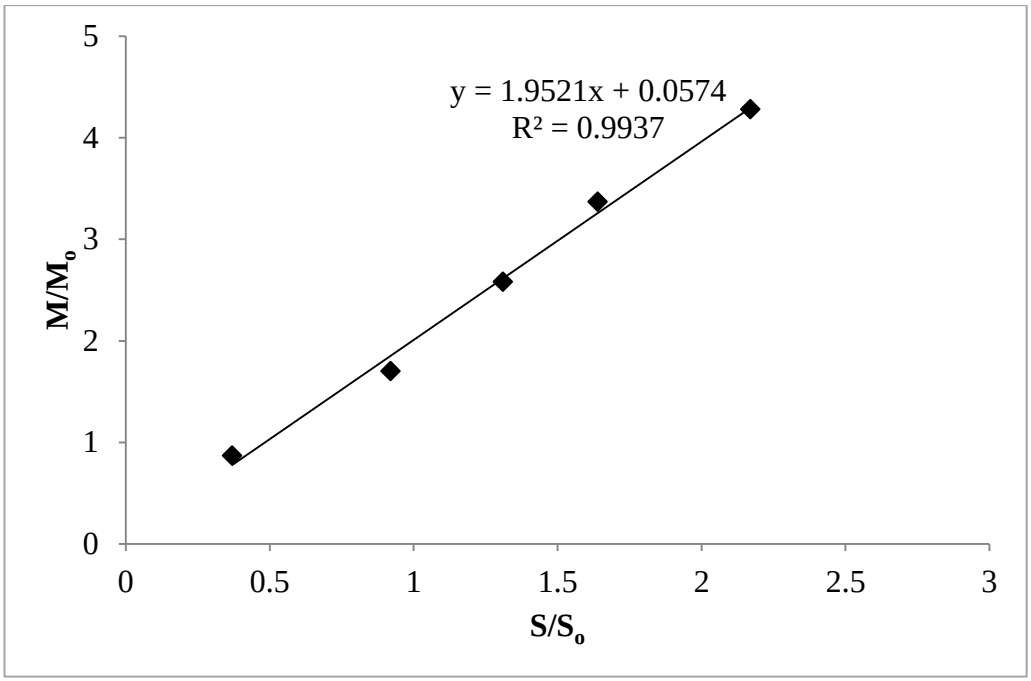

Figure 2.20 Calibration for 5-nonanone with dodecane as standard.

Typical traces for the gas phase deoxygenation of carboxylic acids are given in Figures 2.21 to 2.23, while column detector temperatures and pressure conditions are given in Figures 2.24 to 2.27.

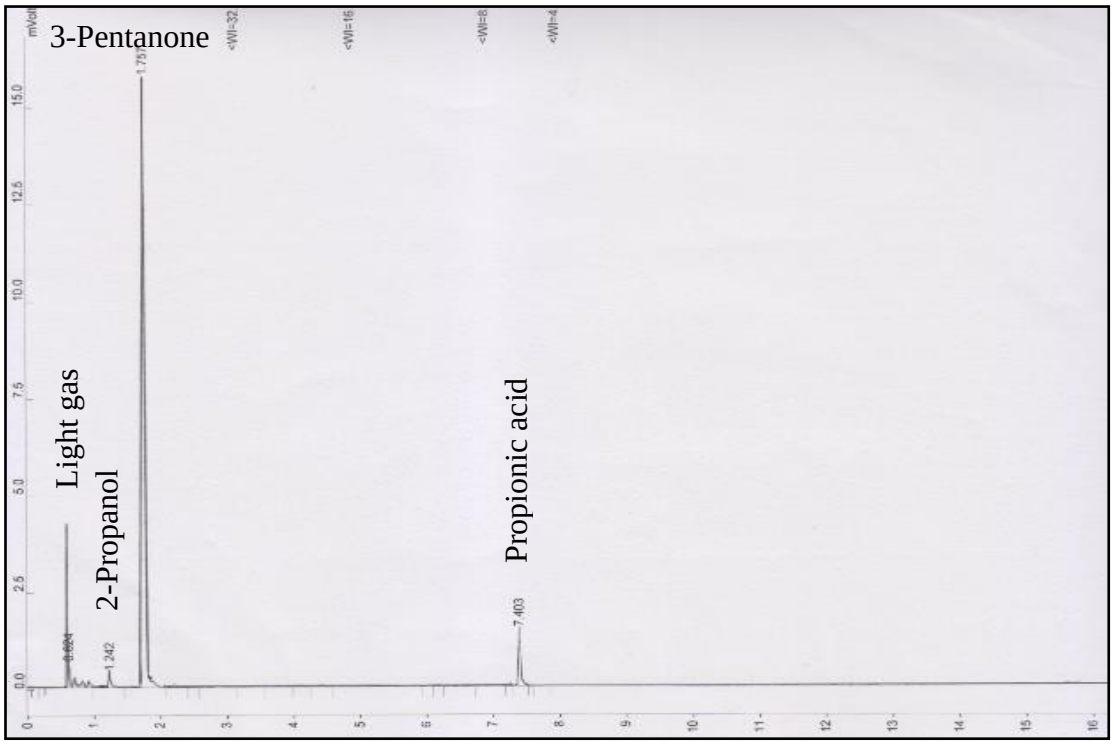

Figure 2.21 GC traces for deoxygenation of propionic acid in the gas phase over 0.2 g of silicalite modified by 0.7 M $NH_4NO_{3(aq)}$ + 3.7 M $NH_{3(aq)}$ at 500 °C and 20 ml min^{-1} N_2.

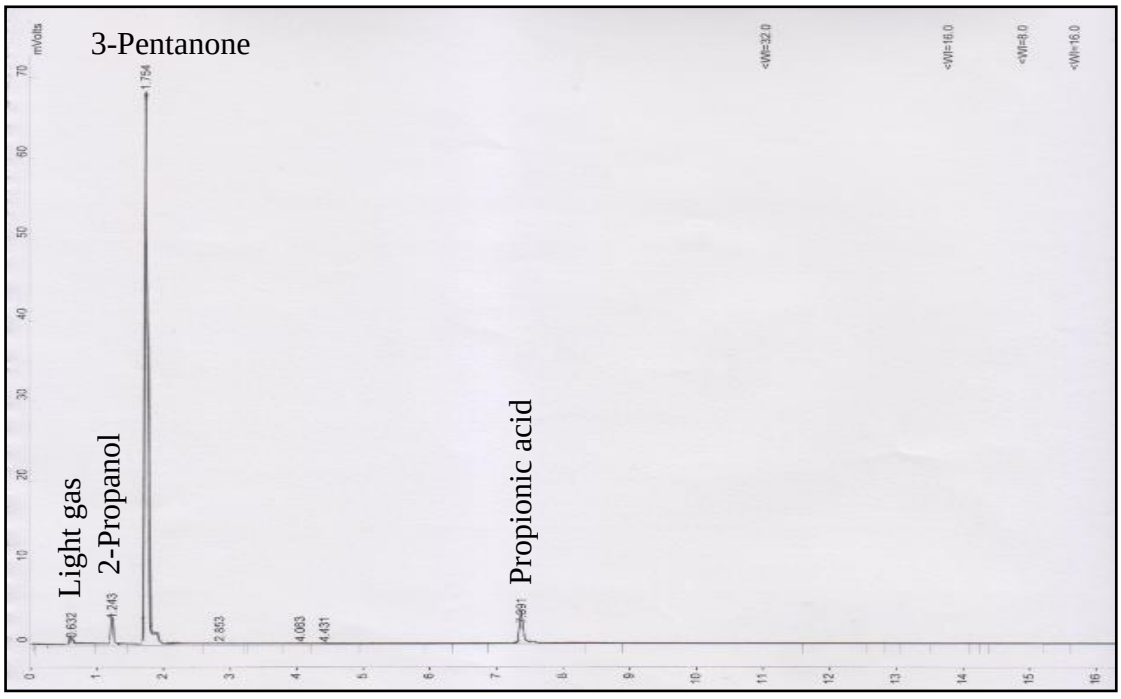

Figure 2.22 GC traces for deoxygenation of propionic acid in the gas phase over 0.2 g of Zn-Cr (10:1) at 380 °C and 20 ml min^{-1} N_2.

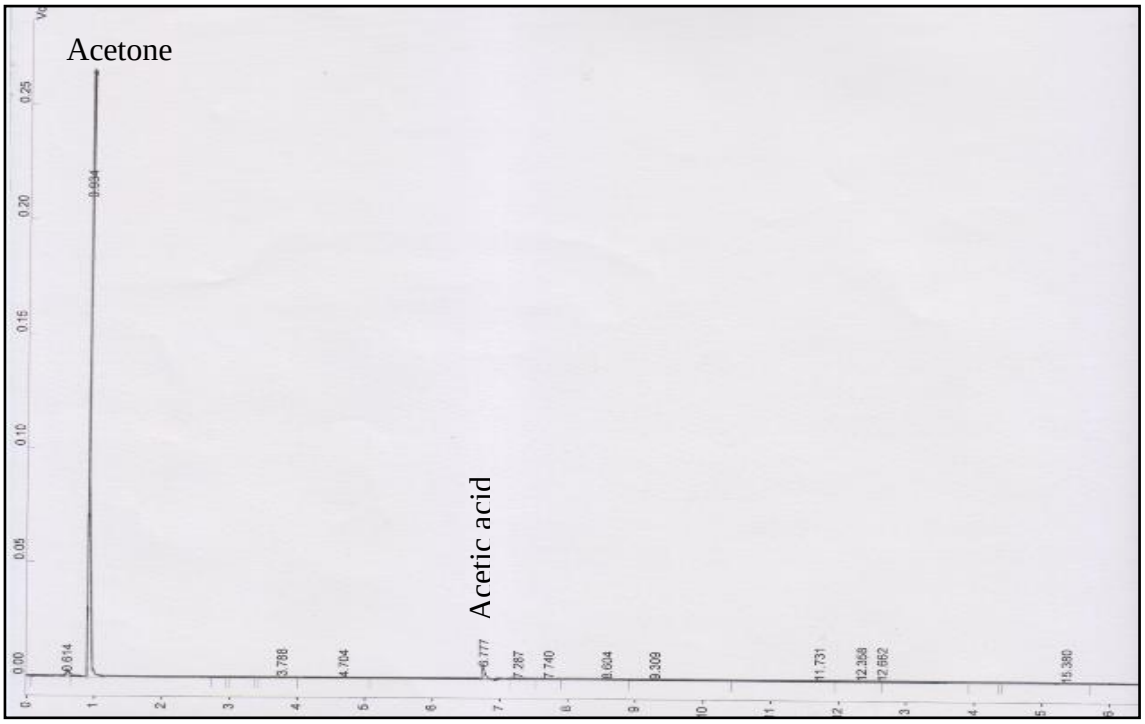

Figure 2.23 GC traces for deoxygenation of acetic acid in the gas phase over 0.2 g of Zn-Cr (10:1) at 350 °C and 20 ml min^{-1} N_2.

.

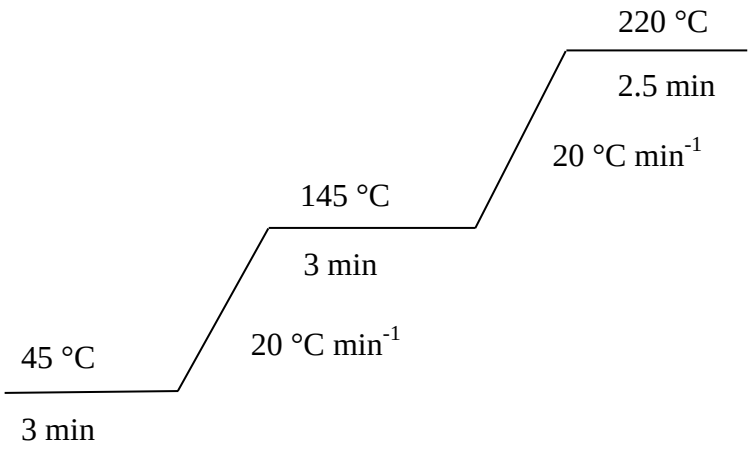

Injector spilt ratio = 12, temperature = 300 °C

FID temperature = 300 °C

Figure 2.24 Varian 3800 ZB-WAX capillary column temperature programme and injector and detector conditions used in the deoxygenation of carboxylic acids.

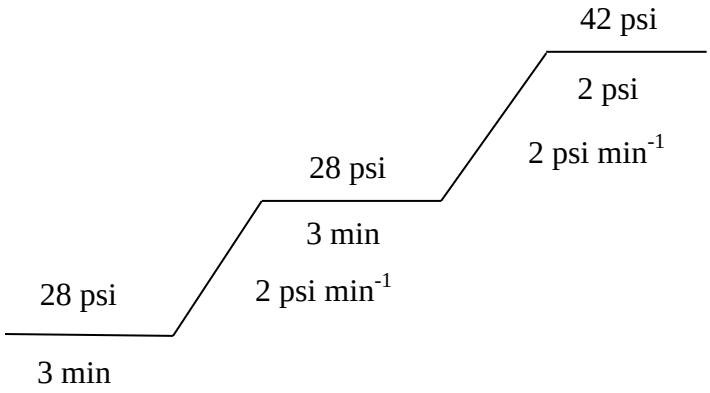

Figure 2.25 Varian 3800 ZB-WAX capillary column pressure programme and injector and detector conditions used in the deoxygenation of carboxylic acids.

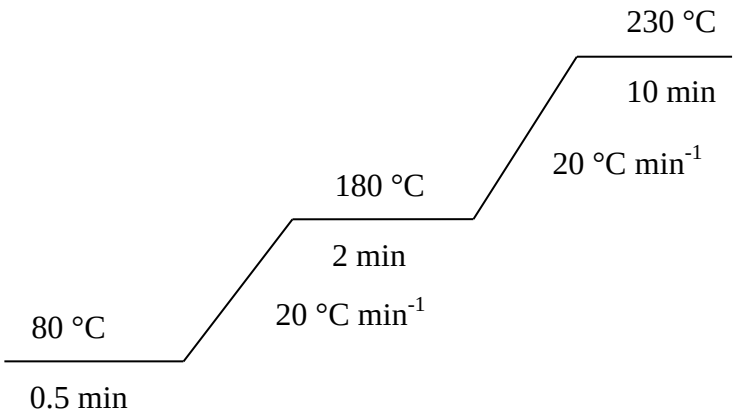

Figure 2.26 Varian 3800 GC-Gas Pro capillary column temperature programme and injector and detector conditions used in the deoxygenation of carboxylic acids.

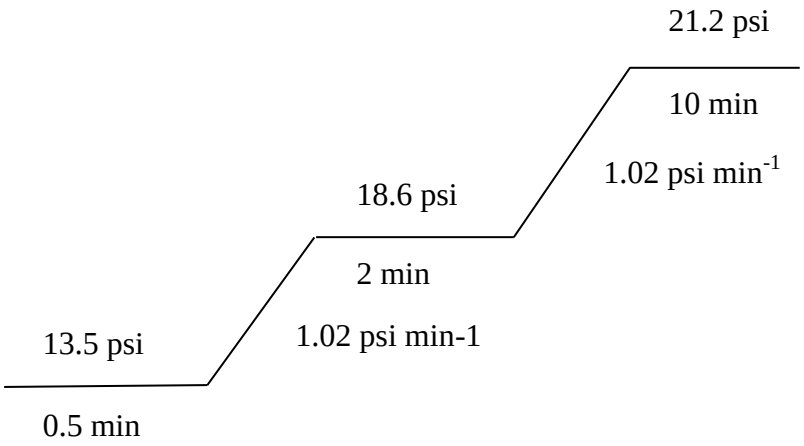

Figure 2.27 Varian 3800 GC-Gas Pro capillary column pressure programme and injector and detector conditions used in the deoxygenation of carboxylic acids.

For the liquid phase synthesis of nopol by the Prins reaction, molecular weights, boiling points, retention times and calibration factors for all components are given in Table 2.3.

Table 2.3 Molecular weights, boiling points, GC retention times and calibration factors for all compounds involved in the liquid phase condensation of β-pinene to produce nopol.

Compound	M wt (g/mol)	Boiling point (°C)	Retention time (min)	Calibration factor
β- pinene	164-166	136	4.61	1.4
Nopol	166	230-240	7.91	1.8
Dodecane	170	216	7.27	1.0

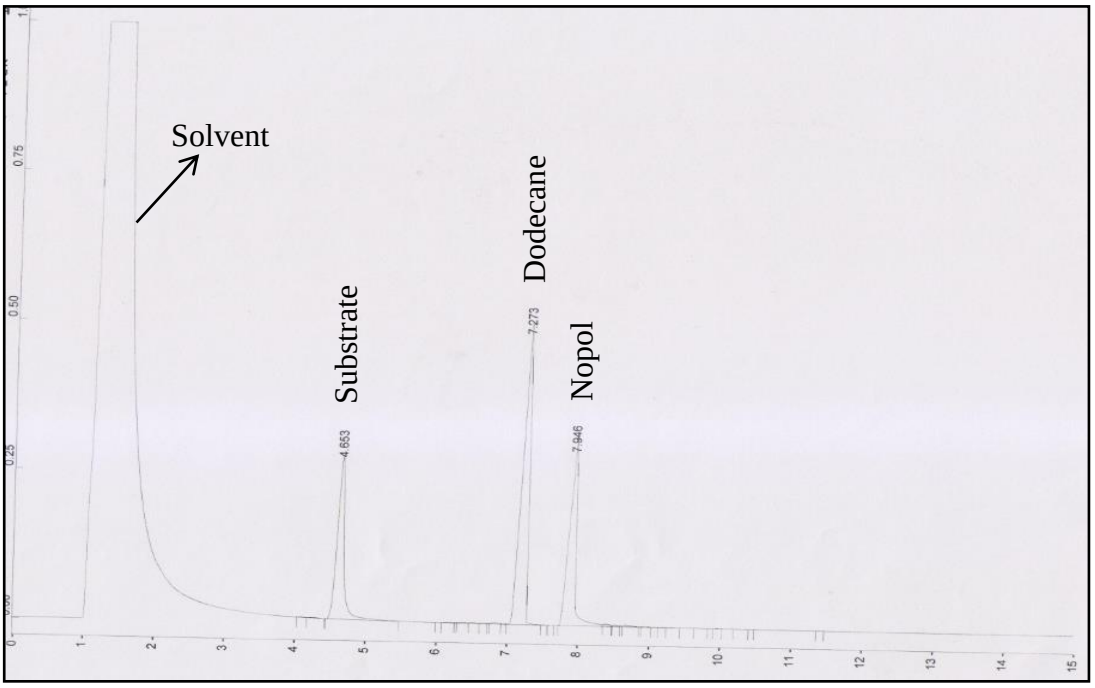

Figure 2.28 GC traces for liquid phase synthesis of nopol by Prins reaction over Zn-Cr (1:6), 0.1 g of catalyst, 80 °C, 5 ml of acetonitrile and 30 ml of paraformaldehyde with 5 mmol of β-pinene and 6 h time on stream.

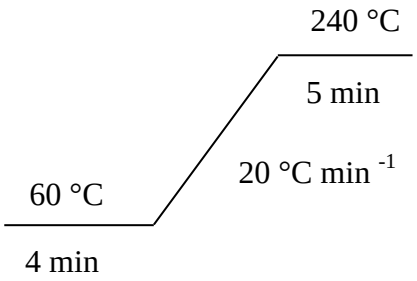

Injector spilt ratio = 11, temperature = 160 °C

FID temperature = 250 °C

Figure 2.29 Varian Star 3400 CX instrument with a 30 m x 0.25 mm x 0.25 μm ZB-1701 capillary column and FID, and injector and detector conditions used in the Prins condensation of β-pinine to nopol.

2.5.1.2.1 Gas phase reaction

The gas-phase ketonisation of propionic acid was performed in flowing N_2 at 300-550 °C under atmospheric pressure in a downflow quartz fixed-bed reactor (9 mm ID) with online GC analysis (Varian 3800 instrument with 30 m x 0.32 mm x 0.5 μm Zebron ZB-WAX capillary column and FID). The diagram of the reactor setup used in the gas-phase ketonisation reaction is shown in Figure 2.30. For more accurate analysis of C_1-C_5 hydrocarbon products, a 60 m x 0.32 mm GC-Gas Pro capillary column was used, which allowed for full separation of these hydrocarbons. The temperature in the reactor was controlled by a Eurotherm controller using a thermocouple placed at the top of the catalyst bed. Propionic acid was fed by passing the carrier gas flow controlled by a Brooks mass flow controller through a stainless steel saturator, which held liquid propionic acid at an appropriate temperature to maintain the chosen reactant concentration. The downstream gas lines and valves were heated to 180 °C to prevent substrate and product condensation. The reactor was packed with 0.2 g catalyst powder of 45-180 μm particle size. Typically, the reaction was carried out at a propionic acid concentration of 2 vol% and an N_2 flow rate of 20 ml min^{-1} (contact time W/F = 4.0 h g mol^{-1}, where W is the catalyst weight (g) and F the total molar flow rate (mol h^{-1})). Prior to reaction, the catalysts were heated at the reaction temperature in N_2 flow for 1 h. Once the reaction had started, the downstream gas flow was analysed by the on-line GC to obtain reactant conversion and product selectivity. The selectivity is defined as moles of product formed per one mole of propionic acid converted and quoted in mole per cent (mol %). On the other hand, CO and CO_2 were not quantified and not included in the reaction selectivity.

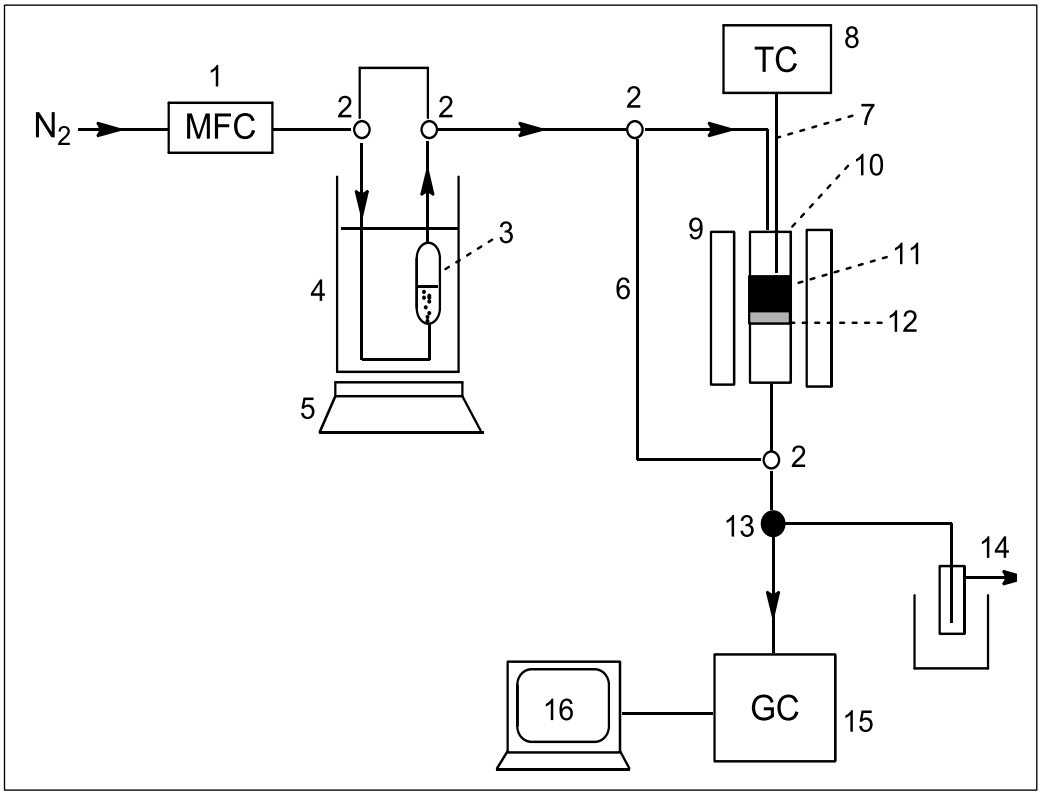

Figure 2.30 Diagram for a continuous flow fixed-bed reactor for ketonisation of carboxylic acids in the gas phase.

Key

(1) Brooks mass flow controller.
(2) 3-way valve.
(3) Saturator containing liquid substrate.
(4) Temperature-controlled water bath.
(5) Stirring hotplate.
(6) Bypass.
(7) Thermocouple.
(8) Eurotherm temperature controller.
(9) Furnace.
(10) Quartz tubular reactor.
(11) Catalyst bed.
(12) Glass wool.
(13) Valco multiposition sampling valve.
(14) Product trap.
(15) Online Varian gas chromatograph.
(16) Computer.

2.5.1.2.2 Liquid phase reaction

Prins condensation was carried out in a glass reactor equipped with a magnetic stirrer and a reflux condenser. Figure 2.31 shows the equipment setup for the liquid phase synthesis of nopol by Prins condensation reaction. In a typical run, the reactor was charged with β-pinene (5 mmol), paraformaldehyde (10-30 mmol HCHO), acetonitrile solvent (5-10 ml) and a catalyst (100-500 mg) and placed in an oil bath heated to 80 °C. The reaction was followed by GC (Varian Star 3400 CX with a 30 m x 0.25 mm x 0.25 µm ZB-1701 capillary column and an FID) by taking aliquots of the reaction mixture at appropriate time intervals and using dodecane as a GC standard. The product nopol was identified by GC using a standard nopol sample from Sigma-Aldrich. The mass balance, defined as nopol yield/β-pinene conversion, was 1.00±0.04, i.e. complete within 96%. After reaction with Zn-Cr (1:6), pure nopol was isolated as colourless oil. The isolation procedure comprised filtration of the catalyst from the reaction mixture, rotary evaporation of acetonitrile solvent, extraction of the product from oily residue with hexane, followed by column chromatography separation of nopol using silica gel as stationary phase and hexane as the mobile phase. Unreacted paraformaldehyde could be recovered from the residue and recycled.

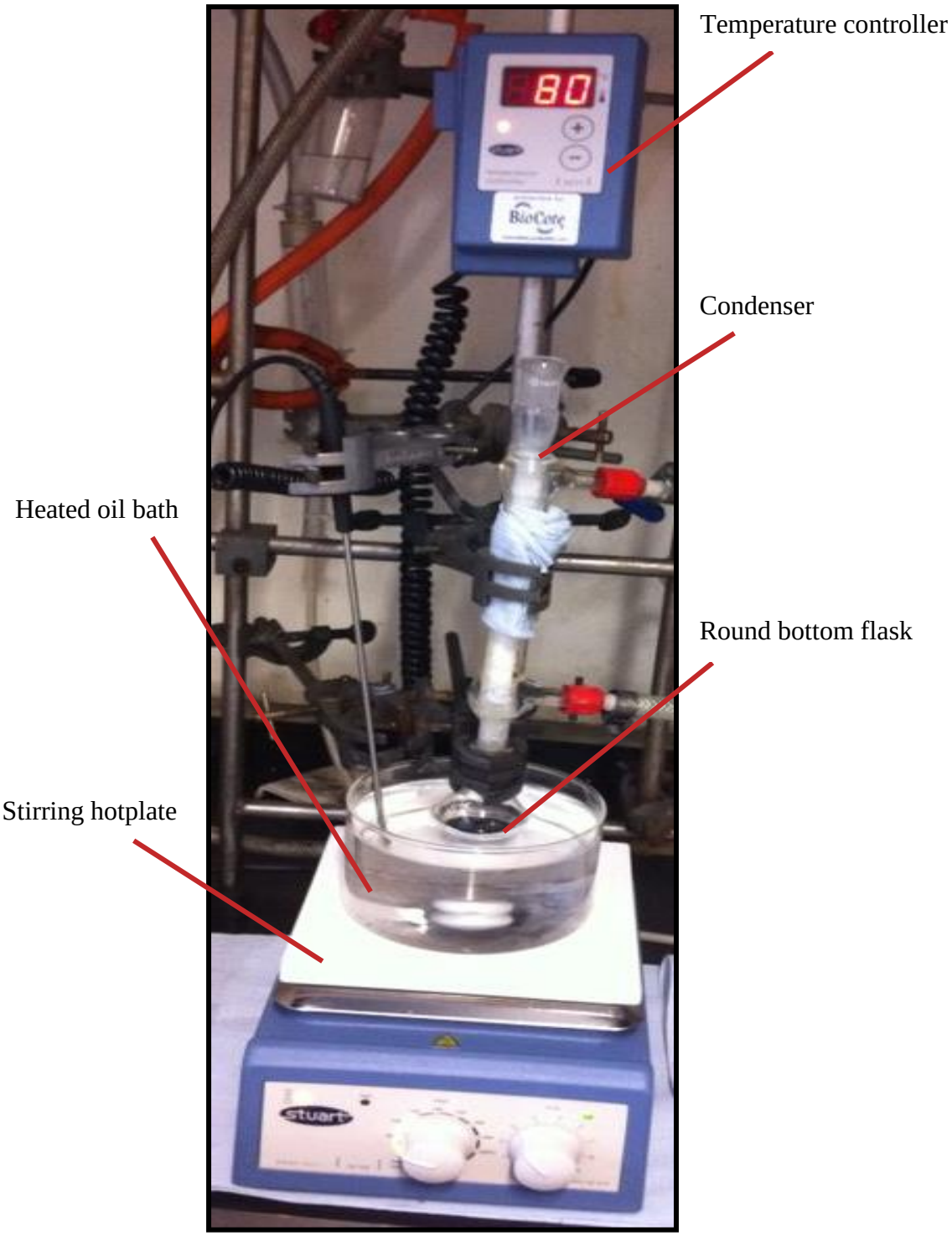

Figure 2.31 Equipment setup for liquid phase synthesis of nopol by Prins reaction.

2.6 Calculation of reaction results

2.6.1 Gas phase

In the gas phase acid ketonisation processes, the total conversion, the yield for each individual product and the selectivity of product were calculated by using equations 2.5, 2.6 and 2.7.[49] Here, the values for moles of product formed per mole of substrate converted are quoted in mol %.

$$\text{Acid conversion (\%)} = \frac{\text{Moles of acid reacted}}{\text{Moles of acid fed}} \times 100 \qquad (2.5)$$

$$\text{Product yield (\%)} = \frac{\text{Moles of acid converted to product}}{\text{Moles of acid fed}} \times 100 \qquad (2.6)$$

$$\text{Product selectivity (\%)} = \frac{\text{Product yield}}{\text{Acid conversion}} \times 100 \qquad (2.7)$$

2.6.2 Liquid phase

In the liquid phase reaction, conversion, yield and selectivity of nopol were calculated as in the following equations.

$$\text{Conversion (\%)} = \frac{\text{Moles of β-pinene converted}}{\text{Moles of β-pinene fed}} \times 100 \qquad (2.8)$$

$$\text{Yield of nopol (\%)} = \frac{\text{Moles of nopol formed}}{\text{Moles of β-pinene fed}} \times 100 \qquad (2.9)$$

$$\text{Selectivity of nopol (\%)} = \frac{\text{yield of nopol}}{\text{conversion of β-pinene}} \times 100 \qquad (2.10)$$

2.6.3 Activation energy of ketonisation of carboxylic acids

The reaction activation energy, E_a, of the ketonisation of carboxylic acids was measured under differential conditions at an acid conversion < 10%. The Zn-Cr (10:1) catalyst was diluted with silica, using 0.16 g of Aerosil-300 to 0.04 g of catalyst. Under differential conditions (conversion <10%), the reaction rate becomes approximately linearly proportional to the change in conversion. Therefore, the activation energy can be calculated directly from the incremental change in conversion.[50] The activation energy was calculated using the Arrhenius equation (Equations 2.11 and 2.12).

$$k = Ae^{\frac{-E_a}{RT}} \qquad (2.11)$$

$$\ln(k) = \frac{-E_a}{R} \times \frac{1}{T} + \ln(A) \qquad (2.12)$$

Here, k is the reaction rate constant, A is the pre-exponential factor, E_a is the activation energy, R is the gas constant and T is the absolute temperature. A plot of ln(*conversion*) against 1/T gives a straight line, from which the activation energy can be determined under differential conditions, acid conversion can be used instead of rate constant. Thus, when the conversion log was plotted against the inverse of the temperature (K) and a straight line drawn through the plots, the gradient of this line represented $-E_a/R$, from which the activation energy could be deduced.[29] In this study, the activation energy for the deoxygenation of propionic acid in gas phase over Zn-Cr (10:1) is presented in Chapter 5, section 5.4.

2.7 References

1. D. W. Fickel, A. M. Shough, D. J. Doren and R. F. Lobo, *Microporous and Mesoporous Materials*, 2010, **129**, 156-163.
2. M. K. Naskar, D. Kundu and M. Chatterjee, *Bulletin of Materials Science*, 2009, **32**, 537-541.
3. L. Forni, G. Fornasari, G. Giordano, C. Lucarelli, A. Katovic, F. Trifiro, C. Perri and J. B. Nagy, *Physical Chemistry Chemical Physics*, 2004, **6**, 1842-1847.
4. Z. Liu, M. F. Ottaviani, L. Abrams, X. Lei and N. J. Turro, *The Journal of Physical Chemistry A*, 2004, **108**, 8040-8047.
5. E. E. Mallon, M. Y. Jeon, M. Navarro, A. Bhan and M. Tsapatsis, *Langmuir*, 2013, **29**, 6546-6555.
6. G. P. Heitmann, G. Dahlhoff and W. F. Hölderich, *Journal of Catalysis*, 1999, **186**, 12-19.
7. L. Vayssieres and A. Manthiram, *Journal of Physical Chemistry B*, 2003, **107**, 2623-2625.
8. F. Al-Wadaani, E. F. Kozhevnikova and I. V. Kozhevnikov, *Journal of Catalysis*, 2008, **257**, 199-205.
9. E. F. Kozhevnikova and I. V. Kozhevnikov, *Journal of Catalysis*, 2006, **238**, 286-292.
10. M. Gliński and J. Kijeński, *Applied Catalysis A: General*, 2000, **190**, 87-91.
11. M. Gliński, J. Kijeński and A. Jakubowski, *Applied Catalysis A, General*, 1995, **128**, 209-217.
12. J. A. Perdigon-Melon, A. Gervasini and A. Auroux, *Journal of Catalysis*, 2005, **234**, 421-430.

13. N. Uekawa, T. Kudo, F. Mori, Y. J. Wu and K. Kakegawa, *Journal of Colloid and Interface Science*, 2003, **264**, 378-384.

14. M. Paulis, M. Martın, D. Soria, A. Dıaz, J. Odriozola and M. Montes, *Applied Catalysis A: General*, 1999, **180**, 411-420.

15. K. Parida and J. Das, *Journal of Molecular Catalysis A: Chemical*, 2000, **151**, 185-192.

16. G. C. Bond, *Heterogeneous catalysis: principles and applications*, Clarendon Press, 1974.

17. G. C. Bond, *Journal of Chemical Technology & Biotechnology*, 1998, **73**, 444-444.

18. K. Kaneko, *Journal of Membrane Science*, 1994, **96**, 59-89.

19. G. Rothenberg, *Catalysis: Concepts and Green Applications, Wiley-VCH, Weinheim*, 2008.

20. G. Leofanti, M. Padovan, G. Tozzola and B. Venturelli, *Catalysis Today*, 1998, **41**, 207-219.

21. Y. Yamada, M. Segawa, F. Sato, T. Kojima and S. Sato, *Journal of Molecular Catalysis A: Chemical*, 2011, **346**, 79-86.

22. M. Kobune, S. Sato and R. Takahashi, *Journal of Molecular Catalysis A: Chemical*, 2008, **279**, 10-19.

23. A. D. Murkute, J. E. Jackson and D. J. Miller, *Journal of Catalysis*, 2011, **278**, 189-199.

24. L. Chen, Y. Zhu, H. Zheng, C. Zhang and Y. Li, *Applied Catalysis A: General*, 2012, **411–412**, 95-104.

25. S. Brunauer, P. H. Emmett and E. Teller, *Journal of the American Chemical Society*, 1938, **60**, 309-319.

26. C. B. G. Atteard, *Oxford University Press, Oxford*, 1998.

27. E. P. Barrett, L. G. Joyner and P. P. Halenda, *Journal of the American Chemical Society*, 1951, **73**, 373-380.

28. B. C. Lippens and J. H. de Boer, *Journal of Catalysis*, 1965, **4**, 319-323.

29. Robert Hetterley, *Ph.D Thesis*, Department of Chemistry, University of Liverpool, UK, 2008.

30. J. Mendham, R. C. Denney J.D. Barnes, M.J.K Thomas, Vogel's Textbook of Quantitative Chemical Analysis, *Preston Education Ltd*, 2000.

31. E. Furimsky, *Industrial & Engineering Chemistry Product Research and Development*, 1979, **18**, 206-207.

32. F. W. Fifield, D. Kealy, *Principles and practice of analytical chemistry*, (5^{th} ed) Blackwell Science Ltd, 2000.

33. G. Schwedt, *The Essential Guide to Analytical Chemistry John Wiley and Sons, Chichester, England*, 1997.

34. L.M. Harwood, C. J. Moody, J.M. Percy, *Experimental Organic Chemistry: Standard and Microscale, Blackwell Science*, 2001.

35. A. M. Alsalme, P. V. Wiper, Y. Z. Khimyak, E. F. Kozhevnikova and I. V. Kozhevnikov, *Journal of Catalysis*, 2010, **276**, 181-189.

36. T. Pham, D. Shi and D. Resasco, *Topics in Catalysis*, 2014, **57**, 706-714.

37. V. V. Costa, H. Bayahia, E. F. Kozhevnikova, E. V. Gusevskaya and I. V. Kozhevnikov, *ChemCatChem*, 2014, **6**, 2134-2139.

38. M. A. Alotaibi, E. F. Kozhevnikova and I. V. Kozhevnikov, *Applied Catalysis A: General*, 2012, **447-448**, 32-40.

39. F. Al-Wadaani, E. F. Kozhevnikova and I. V. Kozhevnikov, *Applied Catalysis A: General*, 2009, **363**, 153-156.

40. P. W. Atkins, *Physical Chemistry, Oxford University Press*, 1998.

41. F. Lefebvre, F. X. Liu-Cai and A. Auroux, *Journal of Materials Chemistry*, 1994, **4**, 125-131.

42. P. Gill, T. T. Moghadam and B. Ranjbar, *Journal of biomolecular techniques: JBT*, 2010, **21**, 167.

43. J. H. Ferrasse and D. Lecomte, *Chemical Engineering Science*, 2004, **59**, 1365-1376.

44. http://www.setaram.com/C80-Cells.htm.

45. G. Schomburg, *Journal of Chromatography A*, 1995, **703**, 309-325.

46. R. J. Bartram and P. Froehlich, *LC GC Magazine-North America-Solutions forSeparation Scientists*, 2011, **63**, 58.

47. http://teaching.shu.ac.uk/hwb/chemistry/tutorials/chrom/gaschrm.htm.

48. L.G. Robert, F. B. E.ugene, *Modern Practice of Gas Chromatography*, 4th ed., Wiley-Interscience, 2004.

49. A. Alhanash, E. F. Kozhevnikova and I. V. Kozhevnikov, *Applied Catalysis A: General*, 2010, **378**, 11-18.

50. S. Vyazovkin, *Thermochimica Acta*, 1994, **236**, 1-13.

Chapter 3

Catalyst characterisation

3.1 Introduction

In this chapter, catalyst characterisation results are presented and discussed. A wide range of catalyst characterisation techniques were used for bulk and surface analysis. Catalyst texture features such as surface area, porosity and pore size were measured using the BET technique. Catalyst stability and temperature evolution were measured by TGA, while XRD was used to measure crystallinity and phase composition. Finally, the nature and strength of acid sites were investigated using methods such as infrared (IR) spectroscopy of pyridine adsorption, chemisorption, DSC and microcalorimetry.

3.2 Surface area and porosity studies

3.2.1 Introduction

The measurement of physisorption of nitrogen at 77 K provides very useful data from which information about a catalyst's surface area and porosity can be obtained. For the characterisation of catalyst texture, the volume of N_2 adsorbed is plotted against its relative pressure to generate the N_2 adsorption isotherm. According to the IUPAC classification, there are six types of adsorption isotherm, depending on the porous texture of individual solid materials.[1-5] Four such isotherms are commonly exhibited by real surfaces in catalyst characterisation,[5] as Figure 3.1 shows. Types I, II, IV and VI isotherms are representative of microporous, macroporous, mesoporous and uniform

ultramicroporous solids respectively. Types II and IV are discussed in detail because they are applicable to the catalysts prepared in this study.

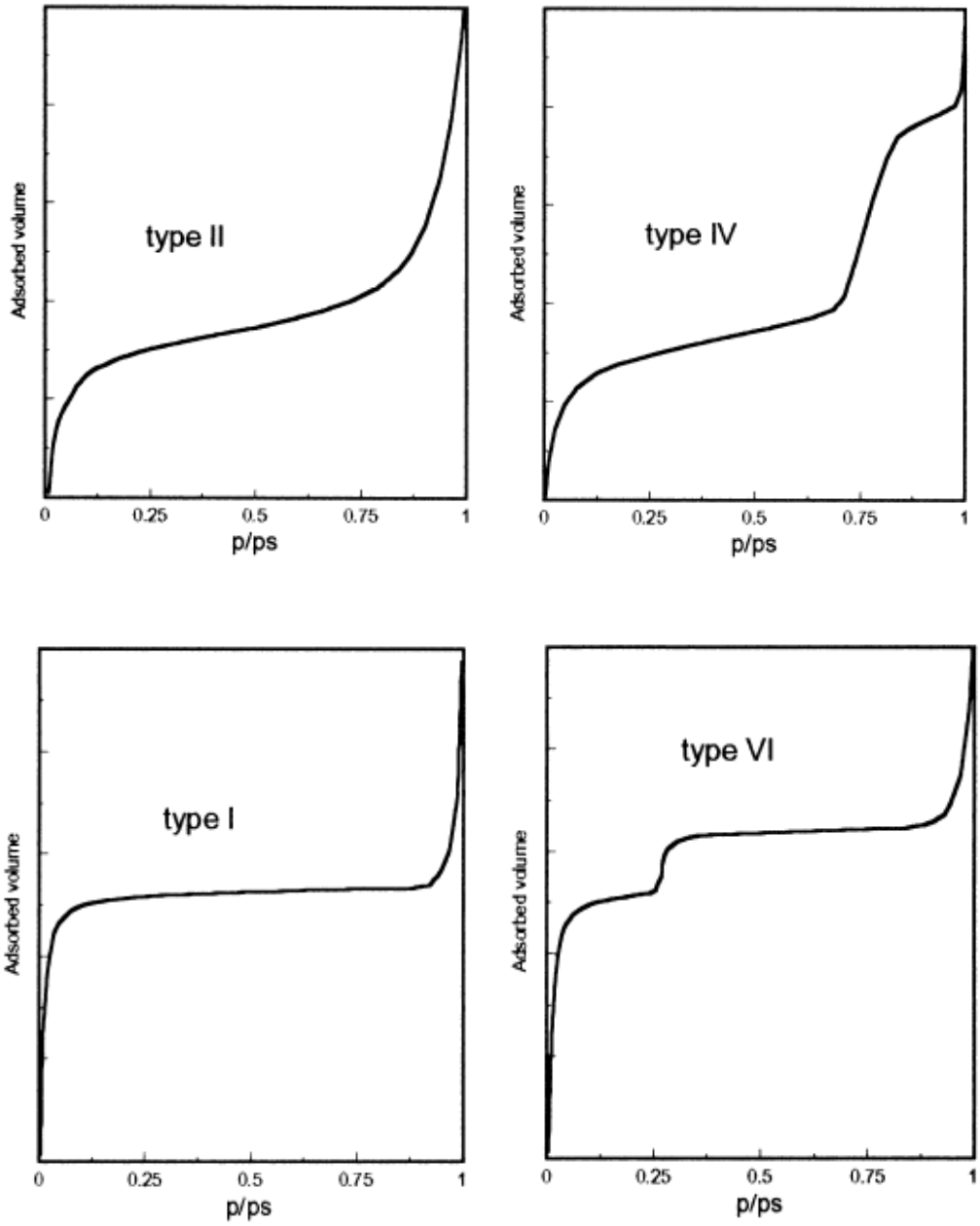

Figure 3.1 The four types of adsorption isotherm found in N_2 adsorption.[5]

In macroporous solids (Type II), the formation of the adsorption monolayer is the main process at low relative pressure, whilst the formation of adsorption multilayers

occurs at high relative pressure. The adsorbate thickness increases with time until the condensation pressure is reached. A strong interaction between adsorbate and adsorbent causes the pressure of the first monolayer formation to be lower. However, the formation of the adsorption monolayer and multilayer processes always overlap.

In mesoporous solids (Type IV), the same formation process with regard to the adsorption monolayer occurs at low relative pressures, while at high relative pressures the formation of adsorption multilayers occurs until condensation takes place, giving a sharp increase in the observed volume of the adsorption gas physisorbed. The larger the mesopores present in the material, the higher the relative pressure at which this process occurs. Adsorption continues as mesopores are filled. Many common catalysts belong to this class of solids.

When the adsorbate reaches saturation, desorption takes place by evaporating the adsorbate from the solid surface and pores. However, in mesoporous solids, this process takes place at lower pressures than in macroporous solids, giving rise to capillary condensation and to a hysteresis loop. Figure 3.2 shows the four hysteresis types that have been recognized in terms of the IUPAC classification.[5]

Types H1 and H2 hysteresis isotherms occur respectively when the sample pores are uniform and non-uniform in size, and are formed when the solid materials consist of particles crossed by closely cylindrical channels or made by aggregates (consolidated) or agglomerates (unconsolidated) that are spheroidal in shape. These hystereses are due to a different size of pore bodies (e.g. ink-bottle shaped pores) and pore mouths or to a different behaviour in terms of adsorption and desorption in near-cylindrical pores. Many common mesoporous catalysts exhibit Type H1 and H2 hysteresis adsorption isotherms.[5]

Types H3 and H4 hysteresis occur when the sample pores are uniform (H4) or non-uniform (H3) in size, and are produced with solid materials consisting of aggregates or agglomerate particles forming slit-shaped pores (plates or edged particles analogous to cubes). These hystereses are due to differences in adsorption and desorption behaviour. Active carbon and zeolites are typical examples of catalysts that generate these types of hysteresis isotherms. Furthermore, when solid materials possess blind cylindrical, cone-shaped and wedge-shaped pores, no hysteresis isotherm will be formed. However, due to the usual irregular catalyst pores, only solids with a much reduced hysteresis loop will be observed.

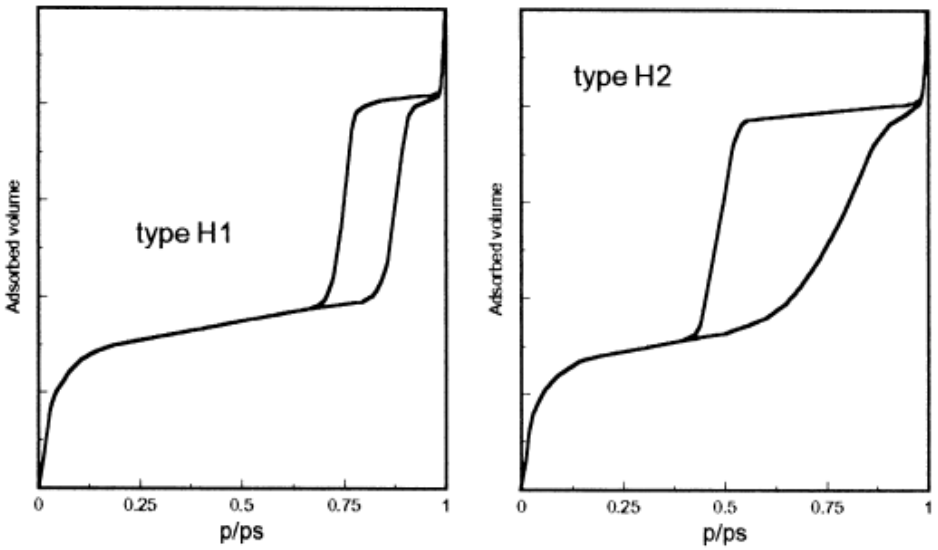

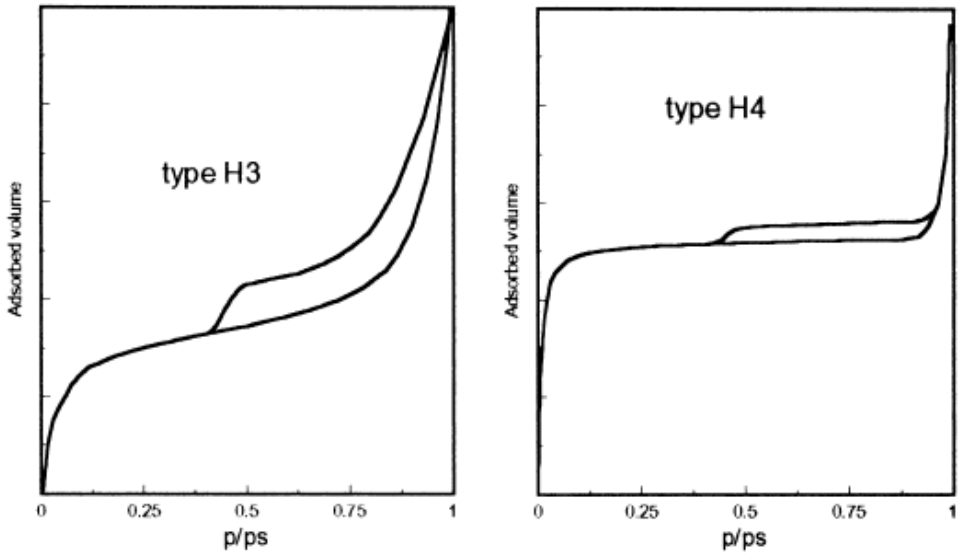

Figure 3.2 The four hysteresis shapes usually observed with N_2 adsorption.[5]

The total surface area of the catalysts prepared here was calculated using the BET method,[6] while pore size distribution and total pore volumes were determined using the BJH method.[7] The general procedure for the measurement of surface area and porosity is described in detail in section 2.4.1. The results of the BET surface areas and the porosities of all the catalysts used in this project are discussed in detail. Zn-Cr oxide catalysts vary in surface area, depending on the catalyst composition (amorphous or crystalline) and on the preparation method, while the calcination temperature may also affect surface area measurements.[8-15] For niobium oxide catalysts, the surface area depends on the calcination temperature, so differences can clearly be seen between those calcined at low temperatures and others calcined at high temperatures, as shown in section 3.2.4.

3.2.2 Surface area and porosity of silicalite

The surface area and porosity of silicalites have been discussed by several authors.[16-23] Table 3.1 summarises textural features (surface area, pore diameter and pore volume) of the amorphous silica and silicalite fresh and spent catalysts used in this study, measured by the BET method and N_2 adsorption isotherms. Prior to BET analysis, all the catalysts were degassed for 30 minutes at 90 °C under slow vacuum, followed by degassing for at least 4 h under fast vacuum.

Table 3.1 Catalyst characterisation

Catalyst	S_{BET}[a] ($m^2\ g^{-1}$)	Pore volume[b] ($cm^3\ g^{-1}$)	Pore size[c] (Å)
Aerosil-300[d]	296	1.15	156
Silicalite	379	0.23	24
Silicalite modified by $NH_{3(aq)}/NH_4NO_3$	364	0.23	26
Silicalite modified by $NH_{3(aq)}/NH_4NO_3$[e]	333	0.19	23

[a] BET surface area.

[b] Single point total pore volume.

[c] Average BET pore diameter.

[d] Aerosil-300 was wetted to form a gel then oven dried at 110°C and ground to a powder of 45-180 μm particle size.

[e] Spent catalyst after 28 h reaction at 500 °C.

Table 3.1 shows that the fresh unmodified silicalite catalyst had a surface area of 379 $m^2\ g^{-1}$, while the value for the basic modified one was 364 $m^2\ g^{-1}$. The pore sizes of the unmodified and basic modified silicalites were 24 and 26 Å respectively. It can be concluded that the texture of silicalite was not changed by the chemical treatment applied. However, the values of surface area and pore size for spent catalyst after the ketonisation of propionic acid at 500 °C, 1 bar for 28 h time on stream (TOS) and

20 ml min^{-1} of N_2 were 333 $m^2 g^{-1}$ and 23 Å respectively. The results also show that the surface area decreased slightly when catalysts were spent. This occurs because of coke deposited on the catalyst surface, which amounted to 6.6 wt% as determined by C, H, N analysis.[23] Coke can be removed by aerobic gasification at 450-500 °C, allowing full recovery of catalyst activity. The amount of coke can be measured using the thermogravimetric (TG)-FTIR method, whereby gases from a sample placed in the furnace are transferred to the flow cell of an FTIR spectrometer by purge gas. The IR intensity of CO_2 gas, for example, is measured as a time function and a chromatogram displayed. The integration of the chromatogram of the sample is compared to a standard sample, allowing calculation of the amount of coke deposition on the catalyst.[24]

Figures 3.3, 3.4 and 3.5 display N_2 adsorption/desorption isotherms for fresh and spent silicalite catalysts. The fresh unmodified silicalite exhibited a reversible isotherm typical of microporous materials with small mesoporous. The isotherm for the fresh sample modified with $NH_{3(aq)}$ + $NH_4NO_{3(aq)}$ shown in Figure 3.4 is slightly different from that of the unmodified silicalite, with a hysteresis at a lower P/P_o of 0.1-0.3, results which are in agreement with a previous report.[22] This may be explained by the formation of framework defects (silanol nests) on the silicalite catalyst. The spent modified catalyst (Figure 3.5) behaved similarly, with minor differences from the fresh sample, probably caused by coking, as mentioned above.

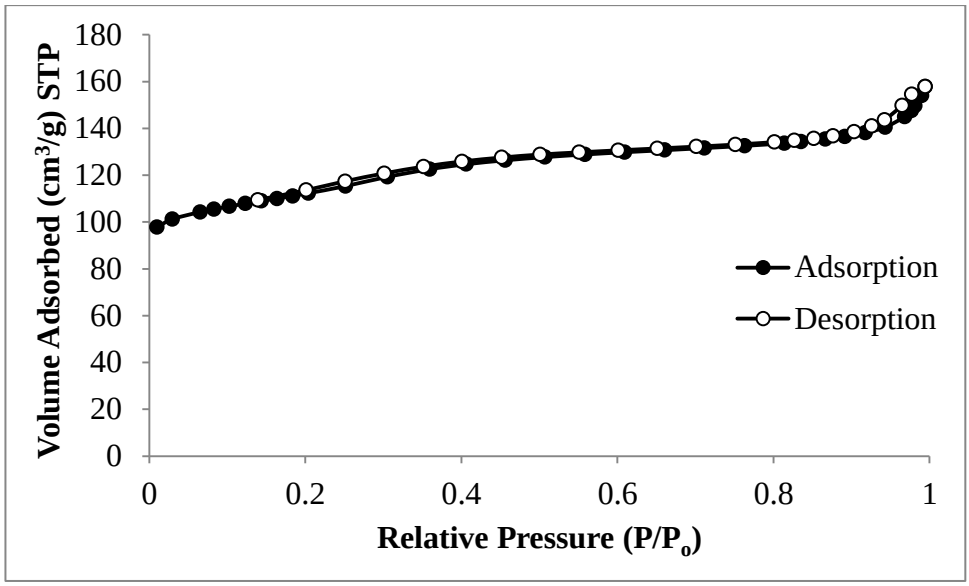

Figure 3.3 Nitrogen adsorption and desorption isotherms for fresh unmodified silicalite.

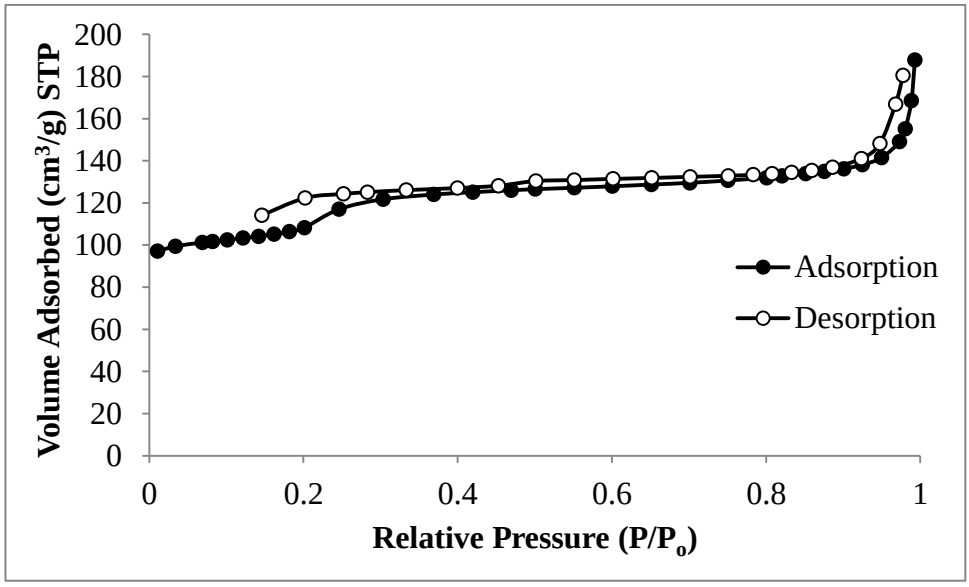

Figure 3.4 Nitrogen adsorption and desorption isotherms for fresh silicalite modified with $NH_{3(aq)}$ + NH_4NO_3.

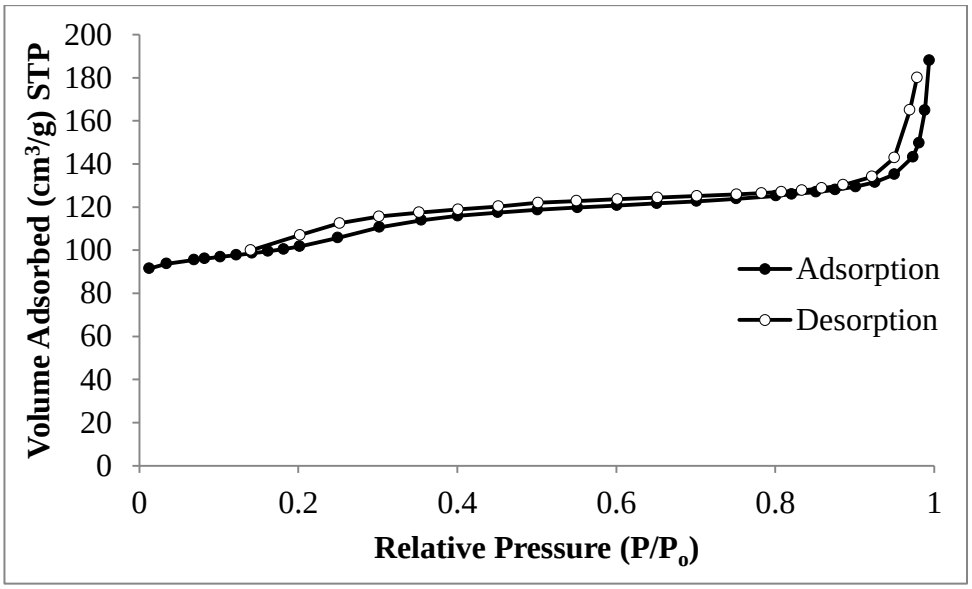

Figure 3.5 Nitrogen adsorption and desorption isotherms for spent silicalite catalyst modified with $NH_{3(aq)}$ + NH_4NO_3 (after reaction at 500 °C, 28 h TOS).

Figure 3.6 shows the mesopore size distribution of fresh unmodified and fresh modified silicalite catalysts, derived from BJH analysis of the desorption isotherm. The isotherm of basic modified silicalite shows a sharp peak at about 30 Å diameter and another broader peak at 50 Å, while that of the unmodified silicalite has a smaller peak at 25 Å.

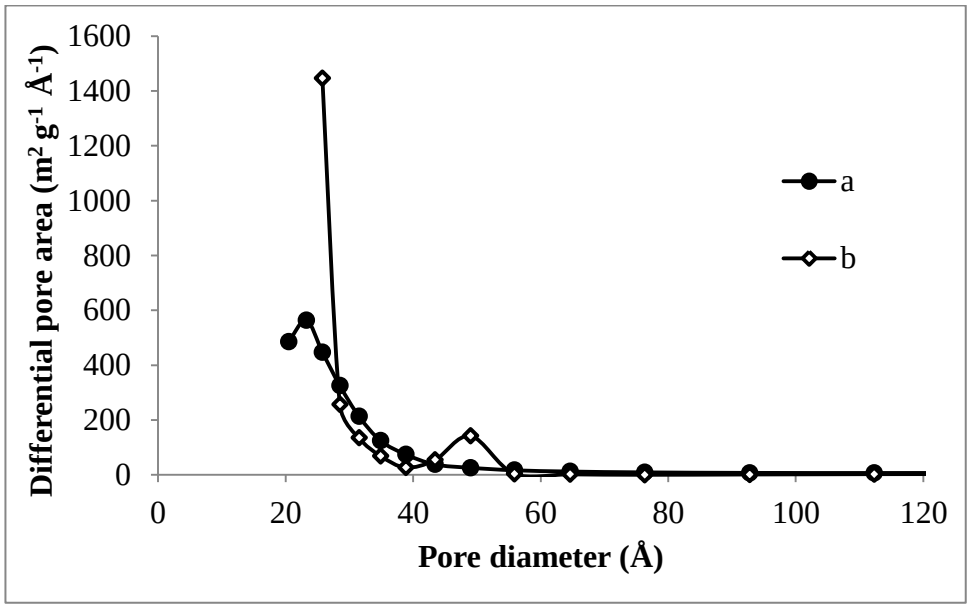

Figure 3.6 Pore size distribution for fresh silicalite catalyst: a) unmodified, b) basic modified by 3.7 M $NH_{3(aq)}$ + 0.7 M $NH_4NO_{3\ (aq)}$.

3.2.3 Surface area and porosity of Zn-Cr oxide catalysts

3.2.3.1 Surface area and porosity for bulk Zn-Cr oxide catalysts

Surface areas, pore diameters and pore volumes from the N_2 physisorption isotherms for the catalysts containing bulk and supported zinc and chromium oxides are presented in Table 3.2, while the BET isotherms and pore size distributions for the Cr_2O_3, ZnO and Zn-Cr mixed oxide catalysts used in this study are presented in Figures 3.7 to 3.12. It can be seen that the surface area of the Cr-rich oxides increased significantly as Cr content increased.[13, 25]

Table 3.2 BET results for zinc, chromium and Zn-Cr mixed oxides

Catalyst[a]	S_{BET}[b] ($m^2\ g^{-1}$)	Pore volume[c] ($cm^3\ g^{-1}$)	Pore size[d] (Å)
Cr_2O_3	243	0.26	42
Zn-Cr (1:6)	230	0.32	55
Zn-Cr (1:1)	136	0.11	32
Zn-Cr (3:1)	101	0.10	56
Zn-Cr (10:1)	43	0.10	90
Zn-Cr (20:1)	13	0.03	87
Zn-Cr (30:1)	10	0.02	86
ZnO	12	0.03	98

[a] Bulk oxides calcined at 300 ^oC under N_2 for 5 h.

[b] BET surface area.

[c] Single point total pore volume.

[d] Average BET pore diameter.

The amorphous Cr-rich oxides had larger surface areas (136-243 m^2g^{-1}) and pore volumes (0.11-0.32 $cm^3\ g^{-1}$) but smaller average pore diameters (32-42 Å) than the crystalline Zn-rich oxides (10-43 $m^2\ g^{-1}$, 0.03-0.1 $cm^3\ g^{-1}$, and 86-98 Å). Some changes

in physical properties were found to depend on the atomic ratio of zinc to chromium in the catalysts. In addition, the calcination temperature of the catalysts may have affected their surface area and pore volume. Previously, Simard *et al.*[12] have reported that calcination conditions affected surface area and pore volume of Zn-Cr catalysts: the pores became smaller as the calcination temperature increased from 300 to 500 °C.

It was also found that increasing the temperature in the range of 450-900 °C affected the surface area of fresh and spent ceria catalysts used in the ketonisation of acetic acid: the surface area decreased from 88 $m^2 g^{-1}$ for catalyst calcined at 450 °C to 1.7 $m^2 g^{-1}$ when calcined at 900 °C. For spent catalysts, the surface area decreased from 88 m^2g^{-1} to 28 m^2g^{-1} for catalysts calcined at 450 °C and tested at 230 °C, but at 290 °C reaction temperature the surface area decreased to 2 m^2g^{-1}.[16]

The nitrogen adsorption-desorption isotherm for bulk Zn-Cr (10:1) oxide catalyst is shown in Figure 3.9. A Type IV isotherm was observed for the crystalline Zn-rich catalyst with a wider pore. This type of isotherm is characteristic of mesoporous materials (between 2 to 50 nm pore diameter).[4, 5] This result is in agreement with that of a previous study.[26] However, a small hysteresis loop (type H3) with a non-uniform slit-shaped pore distribution was also observed. A Type IV isotherm was observed for the amorphous Cr-rich catalyst. This type of isotherm is indicative of a mesoporous material (2 nm < pore diameter < 50 nm).[5] This result is also in agreement with the previous study.[26] This isotherm has a Type H2 hysteresis loop and there is also an indication of the presence of narrow (2-50 nm) mesopores of non-uniform shape. This indicates the presence of mesoporous solids.[4, 5] These results are again in agreement with previous studies.[27, 28]

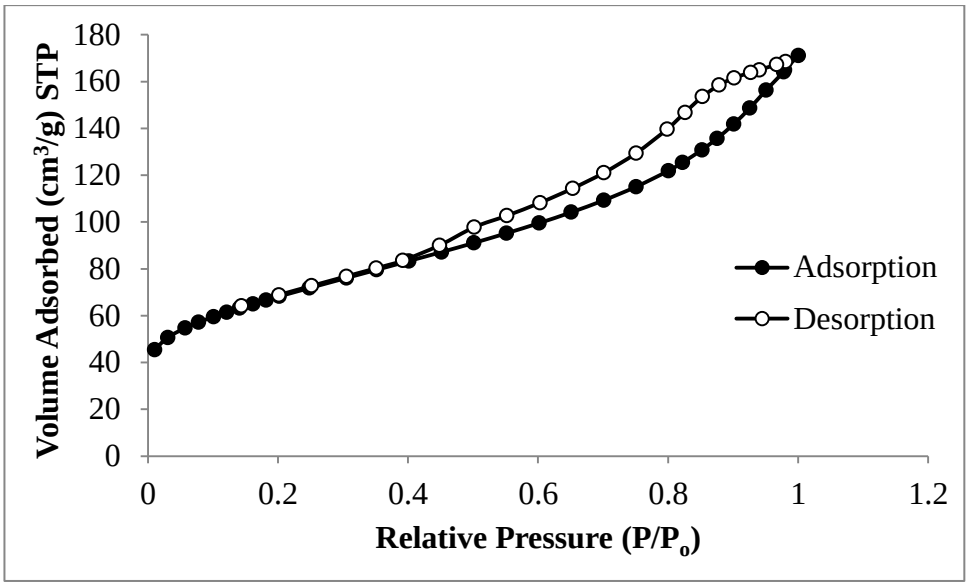

Figure 3.7 Nitrogen adsorption and desorption isotherms for Cr_2O_3 fresh catalyst.

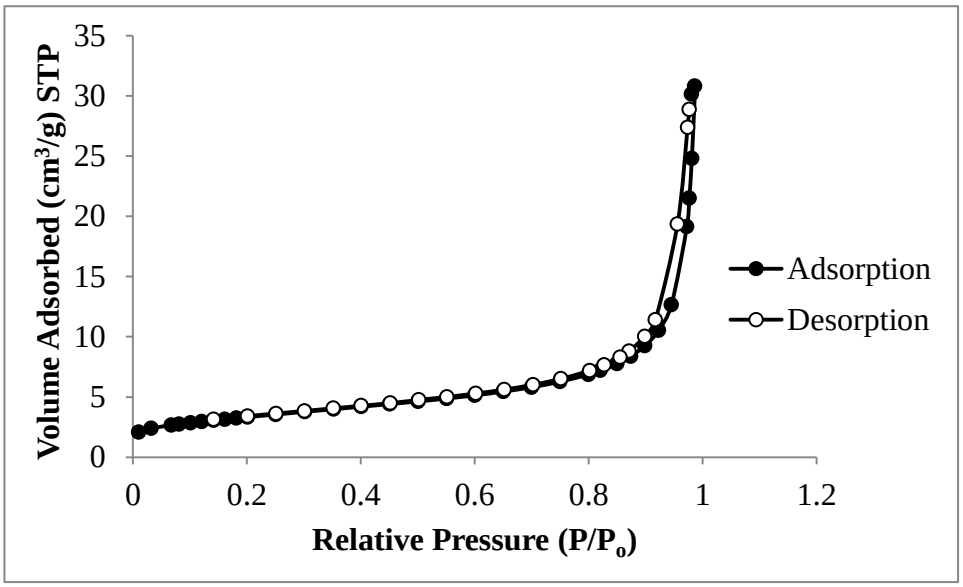

Figure 3.8 Nitrogen adsorption and desorption isotherms for fresh ZnO catalyst.

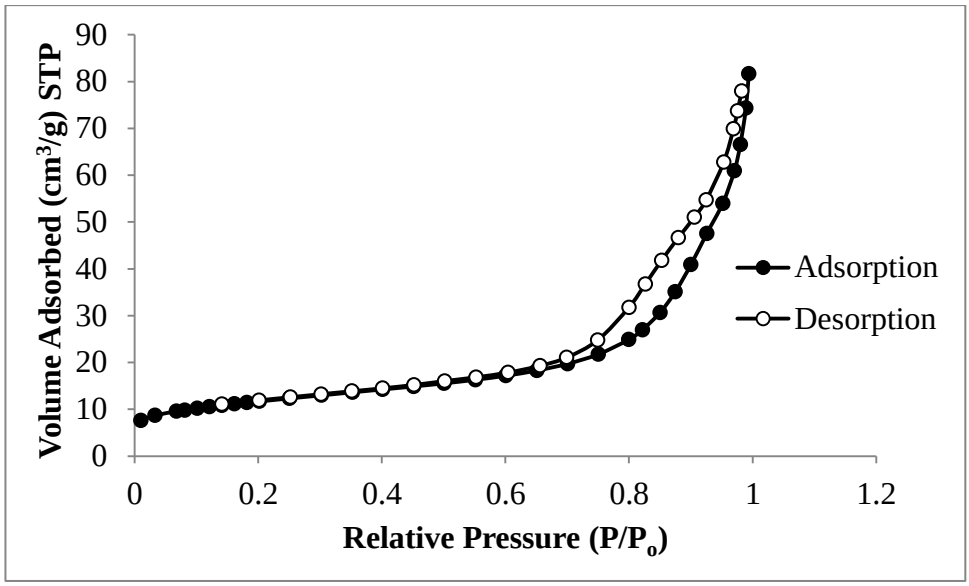

Figure 3.9 Nitrogen adsorption and desorption isotherms for fresh Zn-Cr (10:1) catalyst.

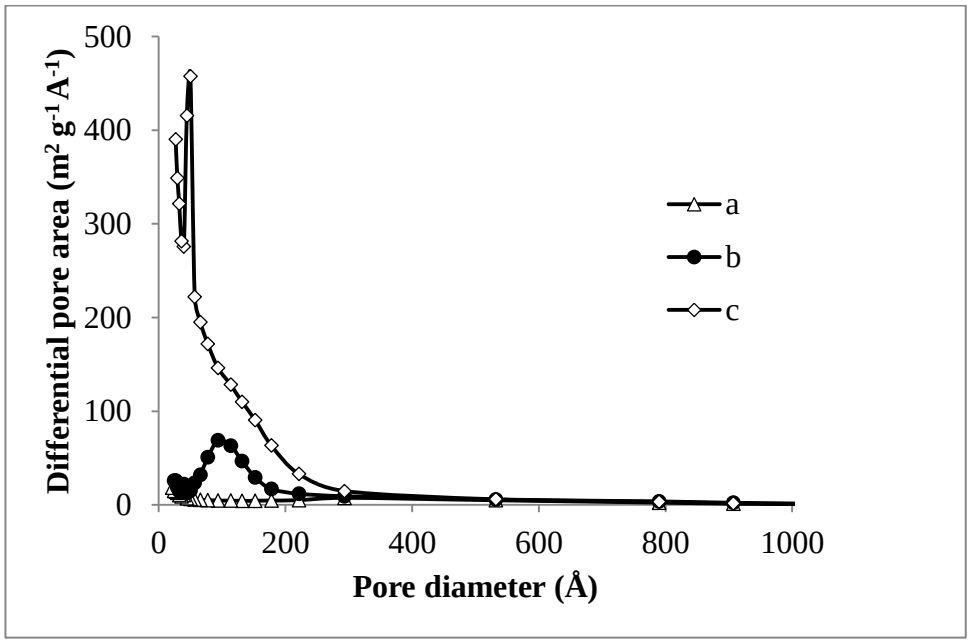

Figure 3.10 Pore size distribution for fresh catalysts calcined at 300 °C for 5 h in nitrogen: a) ZnO, b) Zn-Cr (10:1), c) Cr_2O_3.

Figure 3.11 displays the N_2 adsorption-desorption isotherms for the fresh Zn-Cr (1:6) mixed oxide catalyst used in the liquid phase Prins condensation reaction. This Zn-Cr catalyst, which had the optimum atomic ratio, i.e. it showed the best catalytic

performance in nopol synthesis, had a surface area of 230 $m^2 g^{-1}$, a pore volume of 0.32 $cm^3 g^{-1}$ and an average pore diameter of 55 Å.[29]

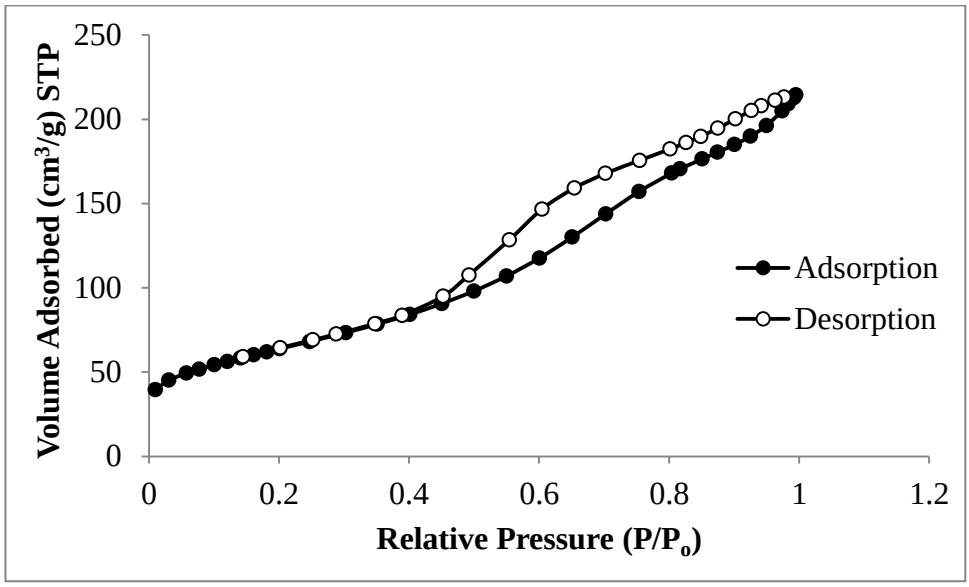

Figure 3.11 Nitrogen adsorption and desorption isotherms for Zn-Cr (1:6) fresh catalyst.

The Type II isotherm in Figure 3.11 is characteristic of a mesoporous material, as is the sharp peak at about 55 Å in Figure 3.12. In addition, the isotherm has a Type H1 hysteresis loop. On the other hand, the Zn-Cr (1:6)/SiO_2 catalyst demonstrated a narrow pore size distribution peaking at a pore diameter of 35 Å, with another broader peak at ≈250 Å from silica (Figure 3.12).

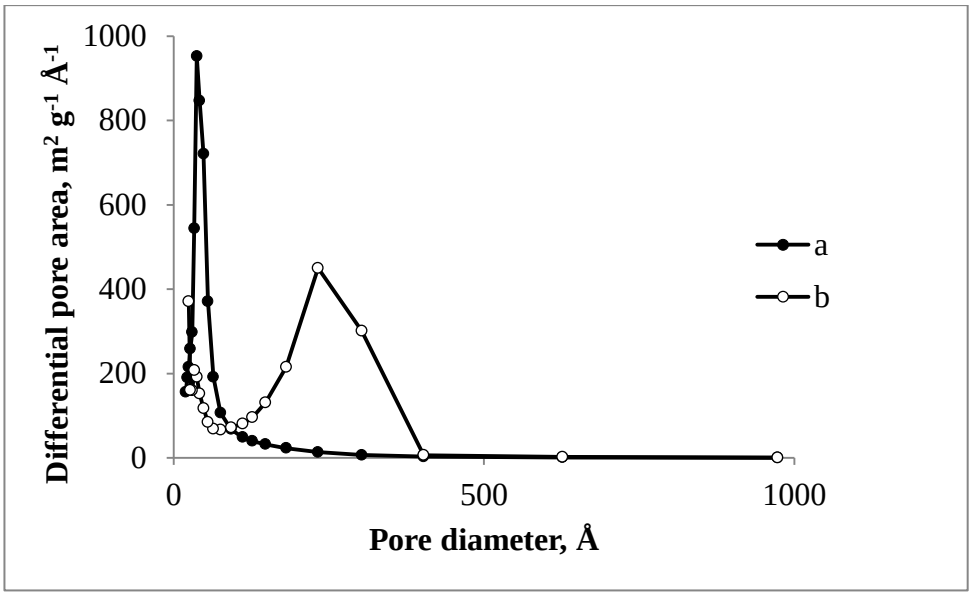

Figure 3.12 Pore size distribution for a) Zn-Cr (1:6) b) Zn-Cr(1:6)/SiO_2. Both catalysts were fresh.

3.2.3.2 Surface area and porosity for supported Zn-Cr oxide catalysts

Table 3.3 summarises the BET results for all Zn-Cr oxide supported catalysts, while the N_2 adsorption–desorption isotherms for Zn-Cr (10:1) catalysts supported on Al_2O_3, SiO_2 and TiO_2 are shown in Figures 3.13-3.15. The isotherms for catalysts supported on silica are of Type II.[30] For other supported catalysts, Zn-Cr (10:1) supported on alumina and titanium oxide had isotherms closer to Type IV.[31] Previously, an Mg/Al(4:1) oxide catalyst was found to have an adsorption-desorption isotherm near to the Type IV classification.[19] The surface area of supported catalysts increased in the order of 20% Zn-Cr/SiO_2 > 20% Zn-Cr/Al_2O_3 > 20% Zn-Cr/TiO_2, at 156, 81 and 45 m^2 g^{-1} respectively, while the bulk Zn-Cr (10:1) catalyst had the smallest surface area (43 m^2 g^{-1}) of all supported catalysts. These results are in agreement with previous reports.[30, 32]

Table 3.3 BET for supported Zn-Cr mixed oxides

Catalyst[a]	Calcination Temp (ºC)	S_{BET}[b] ($m^2 g^{-1}$)	Pore vol[c] ($cm^3 g^{-1}$)	Pore size[d] (Å)
Zn-Cr(1:6)/SiO_2	300	209	0.86	164
20% Zn-Cr(10:1)/SiO_2	400	156	0.60	153
20% Zn-Cr(10:1)/Al_2O_3	400	81	0.39	195
20% Zn-Cr(10:1)/TiO_2	400	45	0.11	102

[a] Fresh supported catalyst calcined at 400 °C under air for 2 h.

[b] BET surface area.

[c] Single point total pore volume.

[d] Average BET pore diameter.

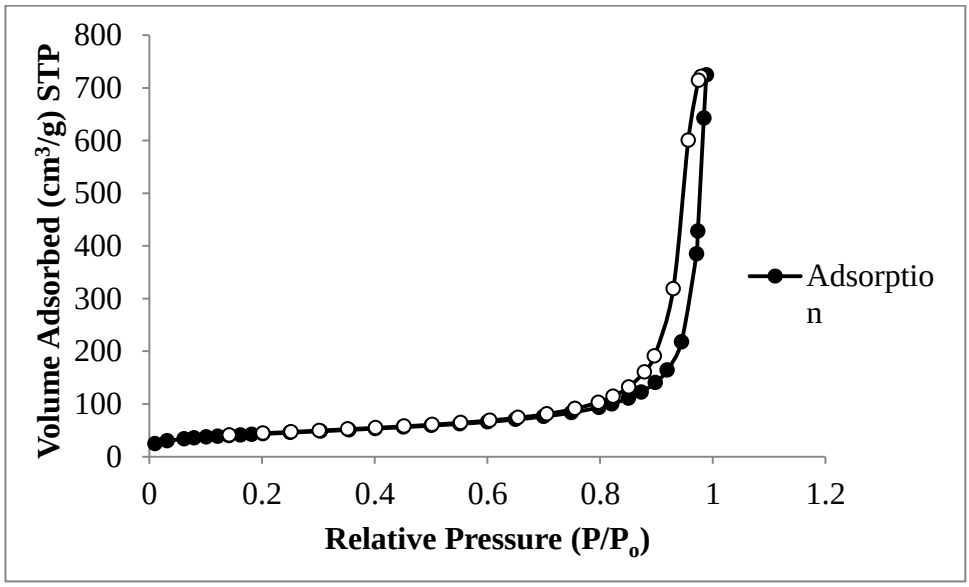

Figure 3.13 Nitrogen adsorption and desorption isotherms for 20% Zn-Cr (10:1)/SiO_2 fresh catalyst.

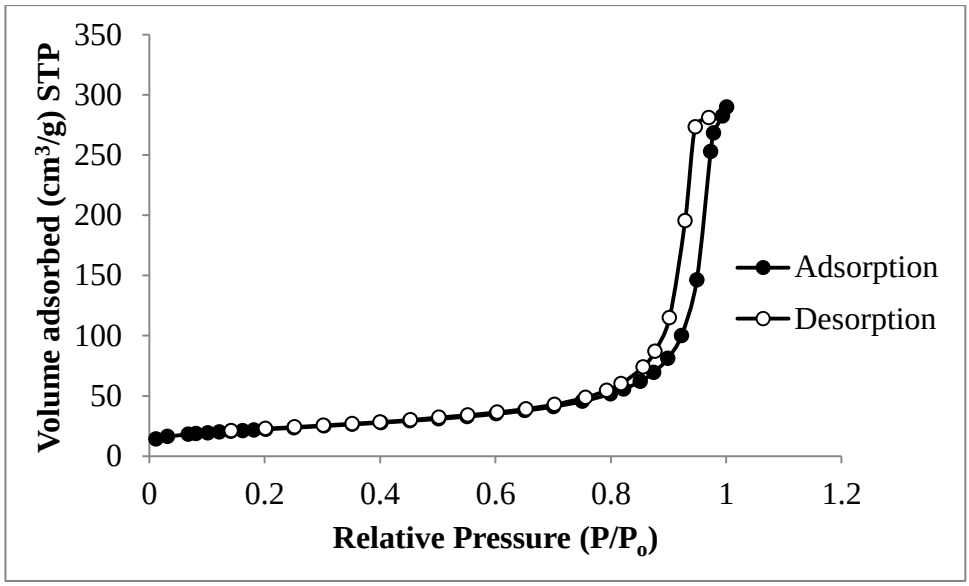

Figure 3.14 Nitrogen adsorption and desorption isotherms for 20%Zn-Cr (10:1)/Al_2O_3 fresh catalyst.

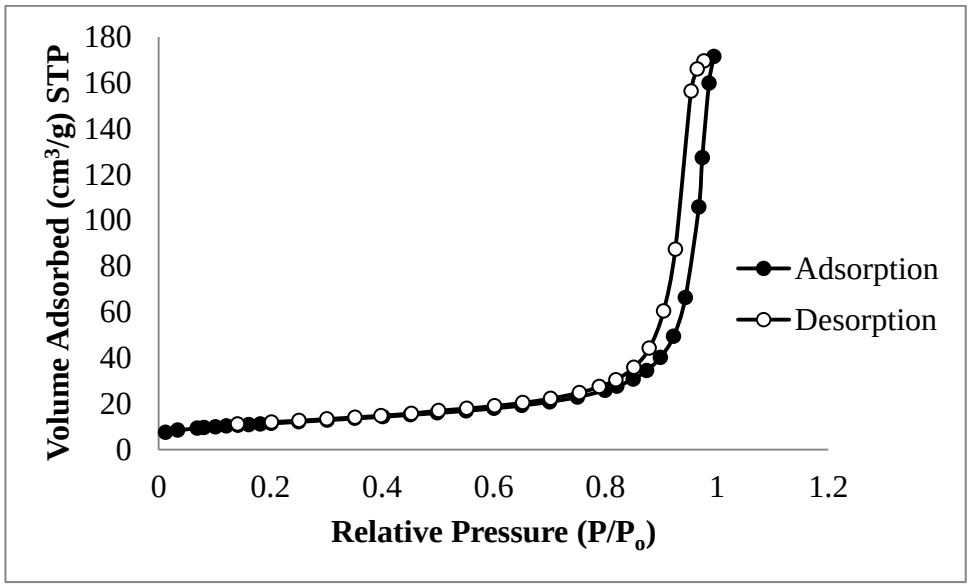

Figure 3.15 Nitrogen adsorption and desorption isotherms for 20% Zn-Cr (10:1)/TiO_2 fresh catalyst.

3.2.4 Surface area and porosity of niobium oxide

This subsection discusses in detail the results of N_2 adsorption studies on bulk hydrated niobium oxide, which was found to have a higher surface area at low calcination

temperature than at higher calcination temperatures, in agreement with a report by Paulis *et al.*[33] In this case, a reduction in surface area was clearly observed at 500 °C, accompanied by a significant loss in catalyst acidity after calcination from 110-500 °C, which is discussed further in section 3.7.1.

Figures 3.16 to 3.19 show the BET adsorption-desorption isotherms for Nb_2O_5 catalysts, of Type IV, which is characteristic of mesoporous materials. The H2 hysteresis loop indicates non-uniform size and/or mesoporous shape. Increasing the calcination temperature led to a decrease in surface area and pore volume of niobium oxides.[34, 35] Catalyst calcined at 110 °C had a surface area of 243 $m^2 g^{-1}$, whereas a 500 °C calcination temperature gave only 90 m^2g^{-1} surface area with Type IV adsorption isotherm and H2 hysteresis loop, indicating mesoporosity. The catalyst calcined at 110 °C showed a narrower pore size distribution compared with calcination at 500 °C. Table 3.4 summarises results for the texture (surface area, pore diameter and pore volume) from N_2 adsorption isotherms for the niobium oxide catalysts used in the Prins condensation reaction to produce nopol.

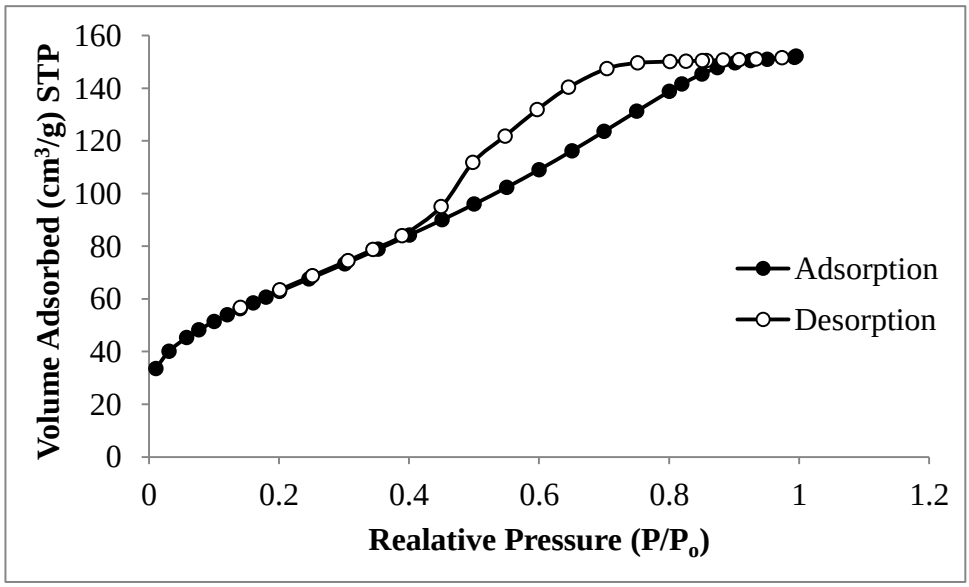

Figure 3.16 Nitrogen adsorption and desorption isotherms of fresh Nb_2O_5 catalyst calcined at 110 °C.

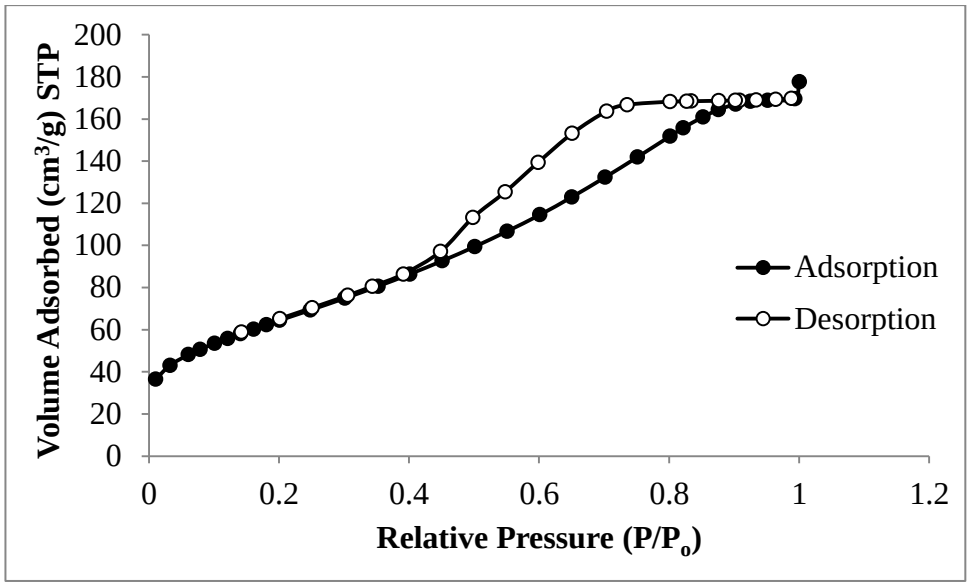

Figure 3.17 Nitrogen adsorption and desorption isotherms of fresh Nb_2O_5 catalyst calcined at 200 °C.

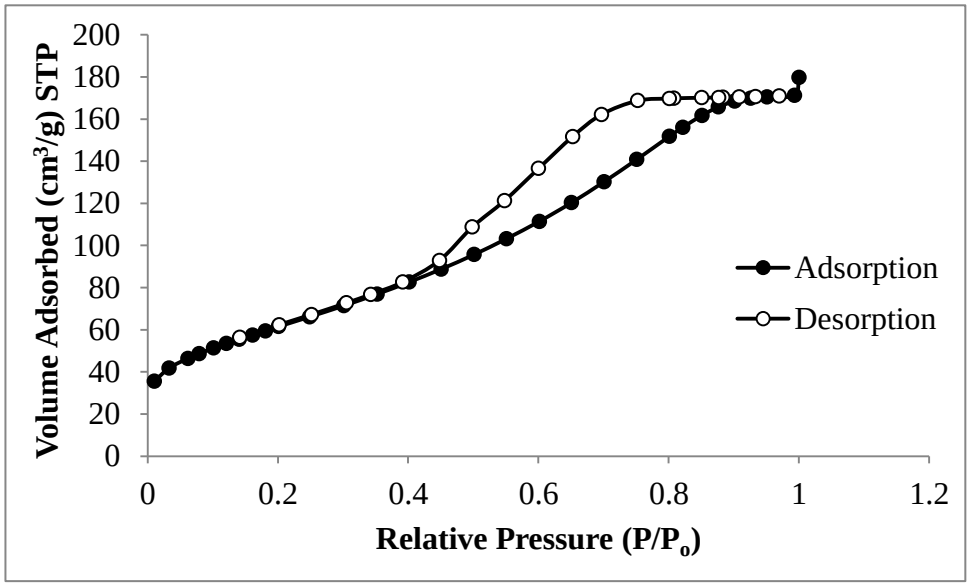

Figure 3.18 Nitrogen adsorption and desorption isotherms of fresh Nb_2O_5 catalyst calcined at 300 °C.

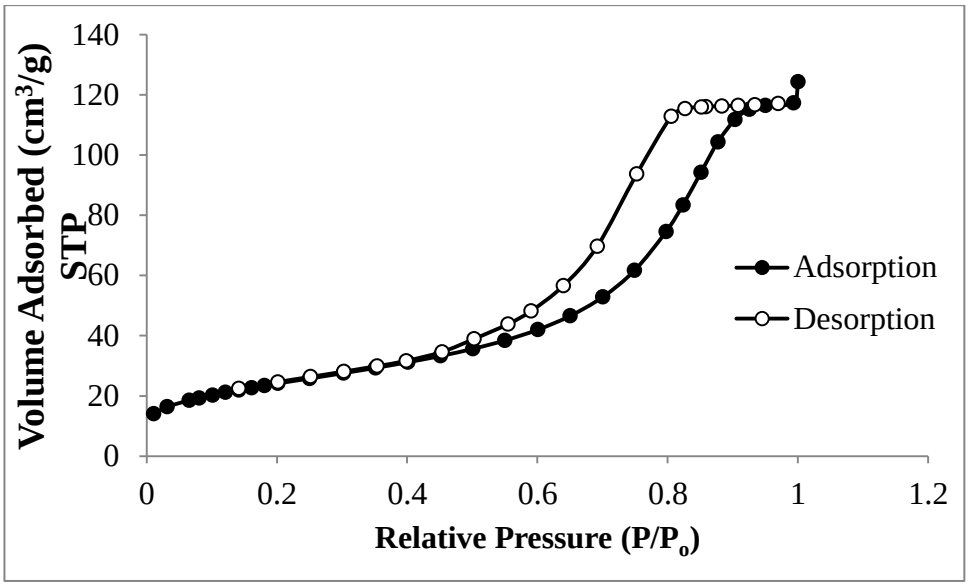

Figure 3.19 Nitrogen adsorption and desorption isotherms Nb_2O_5 fresh catalyst calcined at 500 °C.

Table 3.4 BET values for niobium oxide catalysts

Catalyst[a]	Calcination Temperature [°C]	S_{BET}[b] ($m^2\ g^{-1}$)	Pore volume[c] ($cm^3\ g^{-1}$)	Pore size[d] (Å)
Nb_2O_5	110	243	0.25	41
Nb_2O_5	200	238	0.27	45
Nb_2O_5	300	226	0.27	47
Nb_2O_5	400	172	0.16	38
Nb_2O_5	500	90	0.18	82

[a] Calcined at 110-500 °C under air for 3 h and ground to 45-180 μm particle size.

[b] BET surface area.

[c] Single point total pore volume.

[d] Average BET pore diameter.

The pore size distribution profiles obtained from the desorption branch using the classical BJH method indicated that all niobium oxide catalysts, calcined at different temperatures, were of mesoporous diameter. There was a sharp peak at about 35-39 Å,

as Figure 3.20 shows. In addition, it was found that the pore size distribution for niobium oxide calcined at 500 °C was larger, at about 80 Å, than the value of 39 Å for the catalyst calcined at 110 °C.

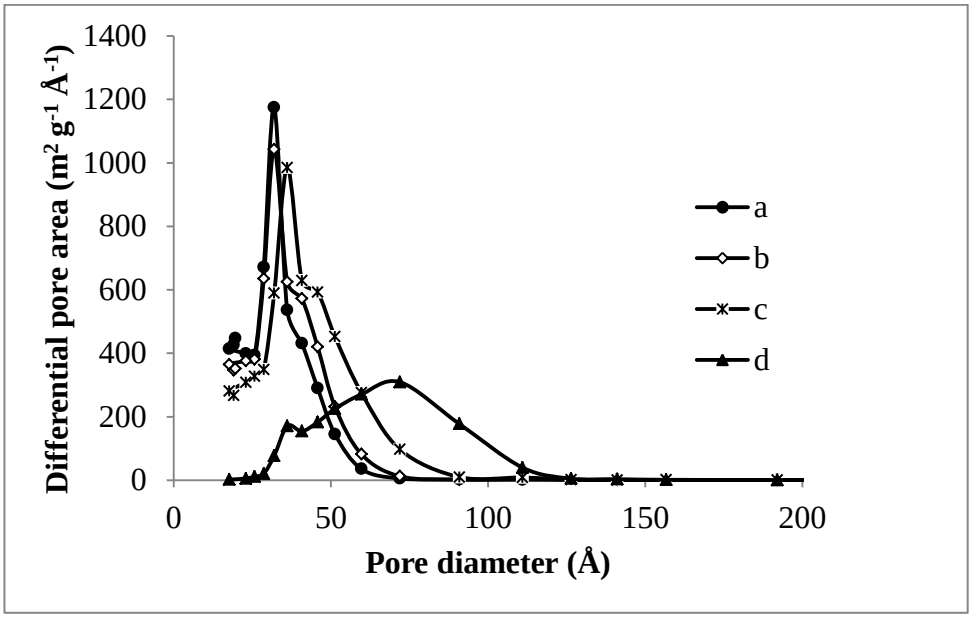

Figure 3.20 Pore size distribution for niobium oxide (Nb_2O_5) calcined at a) 110 °C, b) 200 °C, c) 300 °C, d) 500 °C.

3.3 Thermogravimetric analysis

3.3.1 TGA of amorphous silica and crystalline silicalite

TGA was used for several purposes, including determining the water content of the catalysts, and observing the loss of mass at different temperatures, which increased up to a range of 600-700 °C, and measuring the thermal stability of the catalysts. TGA results for silicalite and silica are shown in Figures 3.21 and 3.22 respectively. These experiments were carried out at a heating rate of 20 ml min^{-1} in N_2 flow, using 20-30 mg of silicalite catalyst calcined at 550 °C for 5 h in atmospheric air. Thermal analysis revealed about 2.1% of weight loss at 100 °C, corresponding to the removal of

physisorbed water from the silicalite, while from 100 °C to 450 °C, there was a 1.4% mass loss. From 450 °C to 700 °C, a further loss of 0.3% mass was observed, due to the decomposition of the catalyst, making a total loss of 3.8%.[36] The mass losses of silica were much greater than those of the silicalite: 6.5% at 100 °C, 1.3% at 450 °C and 0.3% at 700 °C, making a total final mass loss of 8.1%. Since the largest change in weight occurred around 100 °C, it was determined that it was a result of water desorption from the catalyst.

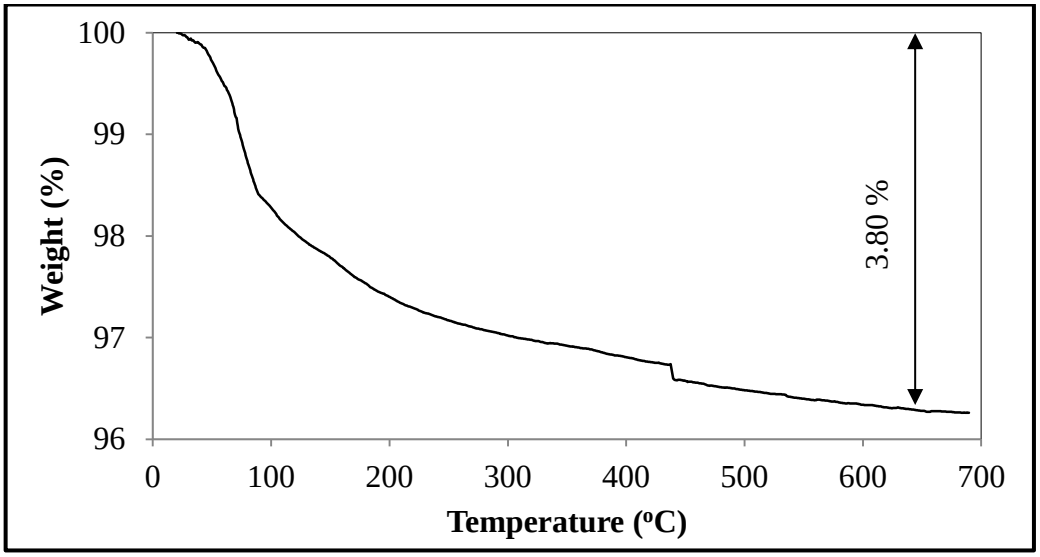

Figure 3.21 TGA of fresh unmodified silicalite calcined at 550 °C for 5 h under air.

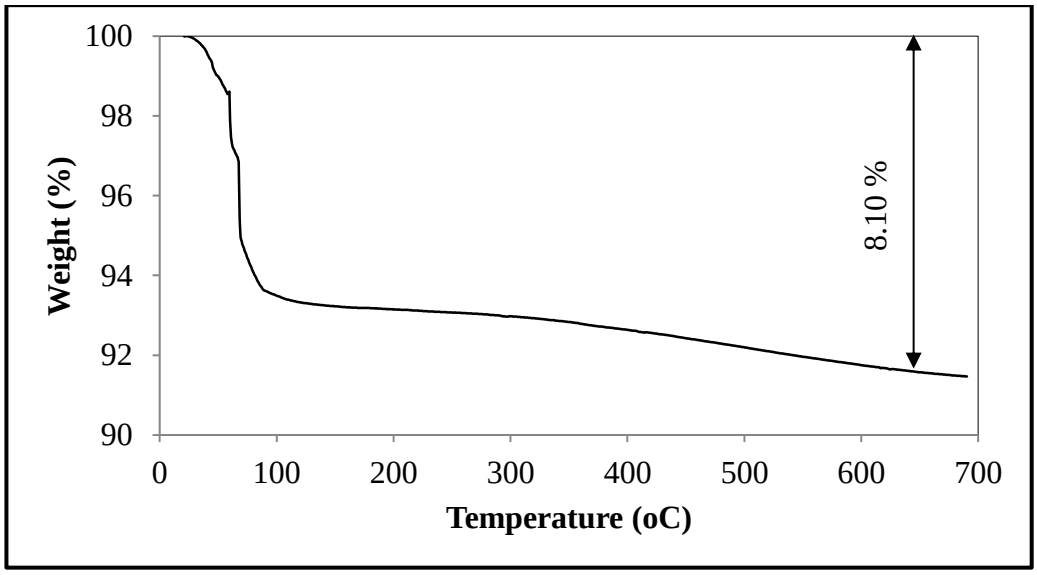

Figure 3.22 TGA of fresh silica (Aerosil-300) under air.

3. Inductively coupled plasma atomic emission spectroscopy

ICP-AES was used to measure trace impurities in the silica used as a catalyst in this study. Silica samples were dissolved in an aqua regia solution, i.e. a mixture of $HNO_{3(aq)}$ and $HCl_{(aq)}$. The results of ICP elemental analysis showed only traces of aluminium, iron, zinc and magnesium. ICP analysis was used to measure catalyst leaching in the liquid phase condensation of β-pinene to produce nopol. After the reaction, the catalyst was filtered off, then washed many times in acetonitrile (the solvent used in the reaction) to remove any nopol product adsorbed on the catalyst surface. A small amount of the resulting solution (5 ml) was analysed by ICP-AES to measure the amount of leaching, which was found to be negligible (0.003% loss of Cr and 0.07% of Zn in the filtrate). As the nopol yield was found to fall from 93% to 75 % in four consecutive runs, this amount of catalyst leaching was probably caused by loss of catalyst during filtration.

3.5 Powder X-ray diffraction

The zeolite (silicalite and HZSM-5), Cr_2O_3, ZnO and Zn-Cr mixed oxide catalysts were subjected to powder XRD tests, using the experimental procedure described in Section 2.4.5, to determine their phase composition.

3.5.1 Powder X-ray diffraction of zeolites

The XRD patterns for our unmodified and modified silicalite samples, calcined at 550 °C under air for 5 h, matched those of the authentic materials (Figure 3.23). The XRD patterns show that all samples were pure and crystalline, with peaks in the region of 2θ / 22.5-25.0º, these results being in agreement with the literature.[37] It was found that the treatment did not affect the catalyst structure.

The catalysts were crystalline and the results show that the silicalite material was pure. In addition, the silicalite catalyst did not change upon treatment with base or acid, which indicates that the crystal structure of the silicalite was not affected by the chemical modification. Base-treated samples (b) and (c), however, showed small broad humps centred at a 2θ of 15°, which may be attributed to amorphous silica formed upon generating silanol nests by base treatment (Scheme 3.1). Therefore, the XRD results are consistent with the formation of silanol nests upon base treatment of silicalite as scheme 3.1 shows.

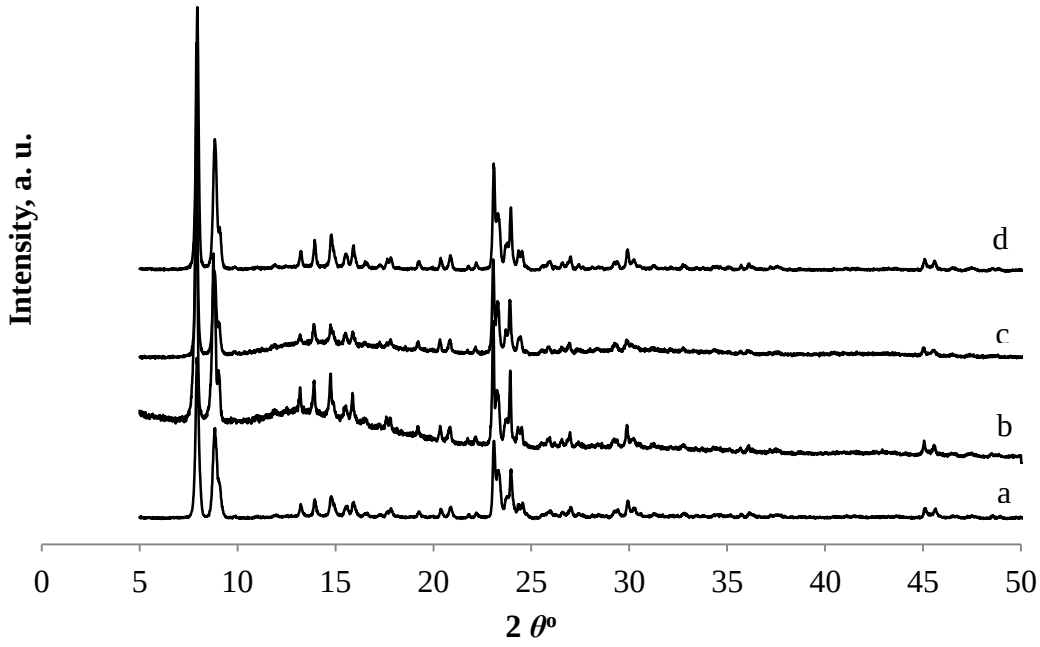

Figure 3.23 XRD patterns for silicalite: (a) unmodified; (b)-(d) modified by: (b) 3.7 M $NH_{3(aq)}$ + 0.7 M NH_4NO_3, (c) 3.7 M $NH_{3(aq)}$ and (d) 0.1 M HCl.

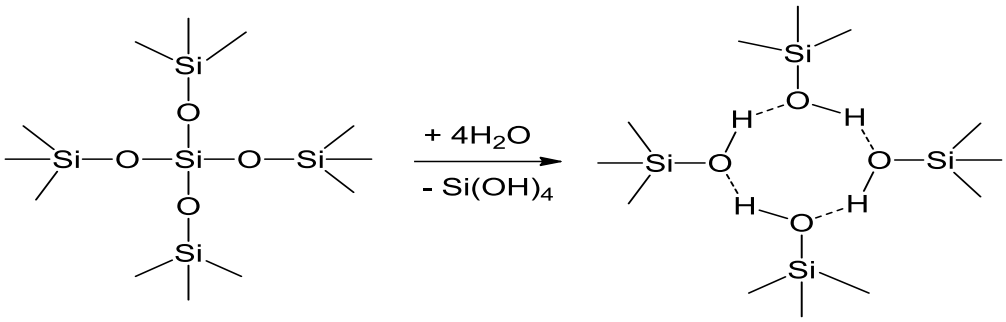

Scheme 3.1 Formation of a silanol nest.

3.5.2 Powder X-ray diffraction of Zn-Cr oxides

Figure 3.24 shows XRD patterns for Cr_2O_3, ZnO and Zn-Cr mixed oxide catalysts with Zn/Cr atomic ratios of 1:6, 1:1, 10:1, 20:1 and 30:1. These catalysts were prepared by coprecipitation of Zn^{II} and Cr^{III} hydroxides, followed by calcination at 300 °C under nitrogen for 5 h. The results show that ZnO and Zn-rich oxides with molar ratios of Zn/Cr = 10:1 – 30:1 were crystalline. XRD peaks at 2θ = 31.8°, 34.4°, 36.3°, 47.6°, 56.6°, 62.9°, 68.0° and 69.1° may be attributed to the ZnO phase.

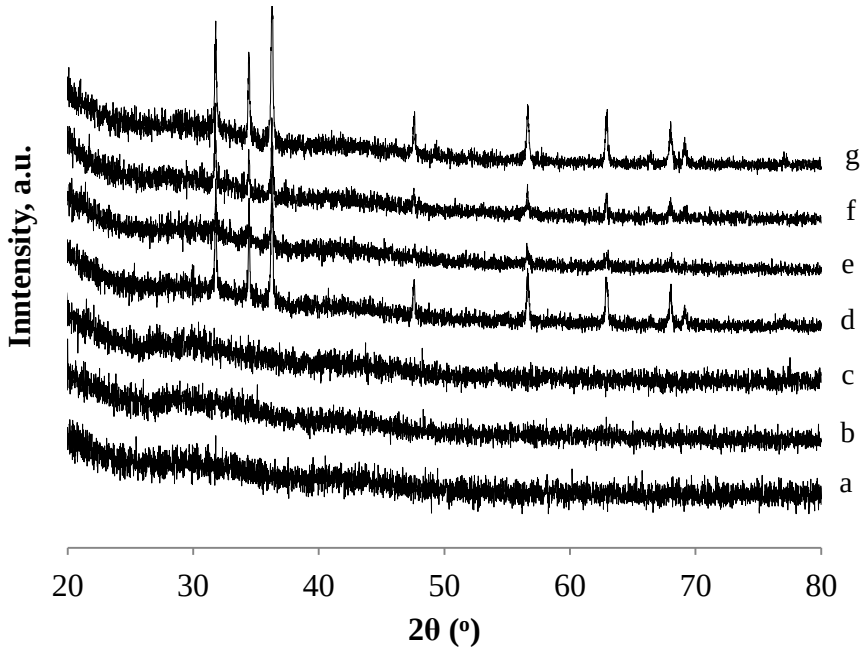

Figure 3.24 XRD patterns of fresh catalysts calcined at 330 °C under N_2 for 5 h: a) Cr_2O_3, b) Zn-Cr (1:6) c) Zn-Cr (1:1), d) Zn-Cr (10:1), e) Zn-Cr (20:1), f) Zn-Cr (30:1), g) ZnO.

In contrast, chromium oxide and Cr-rich oxides (Zn/Cr = 1:6 and 1:1) were amorphous. XRD results showed no crystalline ZnO, due to the high chromium content of these oxides. Previously, Wang *et al.*[38] in Cr-rich oxides, did not observe Cr_2O_3 in the XRD spectrum, indicating that Cr_2O_3 was completely dispersed and existed in the amorphous phase. The same results with regard to XRD measurements for Zn-Cr (1:10) oxide were reported by Kozhevnikova *et al*,[13] who found that it was amorphous after calcination at 300 °C and crystalline after calcination at 350 °C. Crystalline Zn-Cr (1:10) oxide was found to have a smaller surface area and a lower catalytic activity in MIBK synthesis than amorphous Zn-Cr (1:10).

It has been found that Zn-Cr oxides can be amorphous or crystalline, depending on the calcination temperature and Zn/Cr atomic ratio. Zn-rich oxides are crystalline, exhibiting a ZnO wurtzite phase. The oxides calcined at >350 ºC also exhibit Cr_2O_3 and $ZnCr_2O_4$ spinel crystalline phases, the relative amounts of which depend on the Zn/Cr atomic ratio. From the XRD analysis (Figure 3.24), ZnO exhibited the wurtzite phase (JCPDS file No. 36-1451). Zn-Cr (10:1) oxide calcined at 330 ^oC also exhibited wurtzite pattern, with the same crystallite size. This indicates that Zn^{2+} ions had similar location in both ZnO and Zn-Cr (10:1) oxide. In addition to the wurtzite phase, oxides calcined at >350 °C also exhibited Cr_2O_3 and $ZnCr_2O_4$ spinel crystalline phases, the relative amounts of which depended on the Zn/Cr atomic ratio. When Zn-Cr (1:6) oxide was calcined at 330 °C it became amorphous (Figure 3.24). However, after calcination at 400 °C in N_2 for 5 h it exhibited the pattern of a Cr_2O_3 phase, with a little $ZnCr_2O_4$ spinel also present (Figure 3.25). From the XRD pattern of Zn-Cr oxides, Simard *et al.*[12] and Bradford *et al.*[15] have both observed that when the Cr/Zn ratio was increased from 0.5 to 15 (calcined at 350 °C) and from 0 to 1.9 (calcined at 700 °C) respectively, the content of ZnO decreased and $ZnCr_2O_4$ increased.

$ZnCr_2O_4$ crystalline phase was not observed in the XRD patterns after calcination at 300°C, indicating that the formation of $ZnCr_2O_4$ depends on the calcination temperature and on the ratio between Zn and Cr, as well as on the way the catalyst is prepared.[12-15, 28, 38, 39]

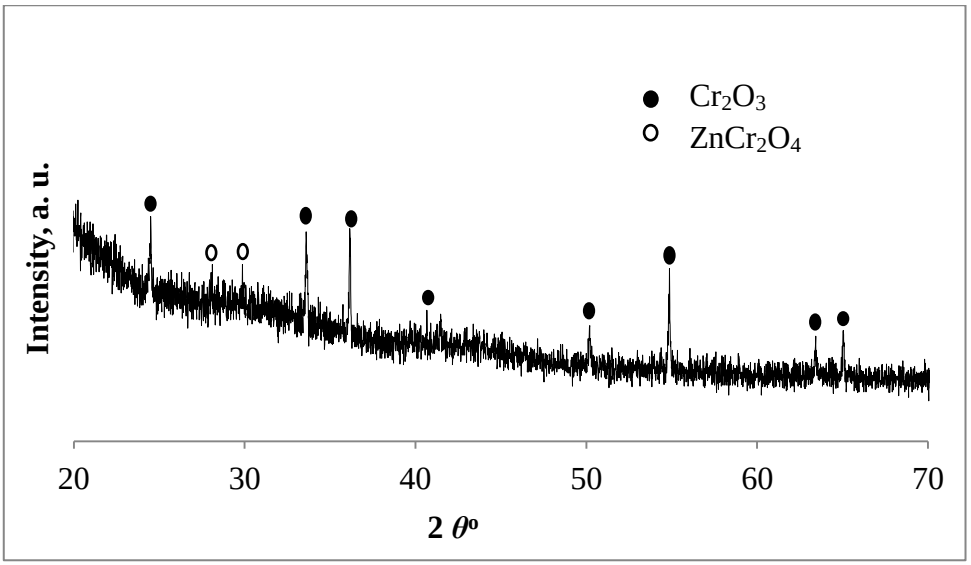

Figure 3.25 XRD pattern for fresh Zn-Cr (1:6), calcined at 400 °C under N_2 for 5 h.

Figures 3.26 and 3.27 show the powder XRD patterns for the bulk Zn-Cr (10:1) oxide and 20%Zn-Cr(10:1)/Al_2O_3 supported catalyst calcined at the optimum reaction temperature of 380 ^oC. Both exhibit the clear pattern of wutzite ZnO crystal phase (JCPDS file No. 36-1451). The crystallite average diameter, as estimated from the Scherrer equation using the peaks at 31.8, 34.4 and 36.3^o, is 52±6 nm for the bulk Zn-Cr (10:1) and 37±1 for the 20%Zn-Cr(10:1)/Al_2O_3. This indicates a higher dispersion of ZnO in the supported catalyst compared to the bulk one.

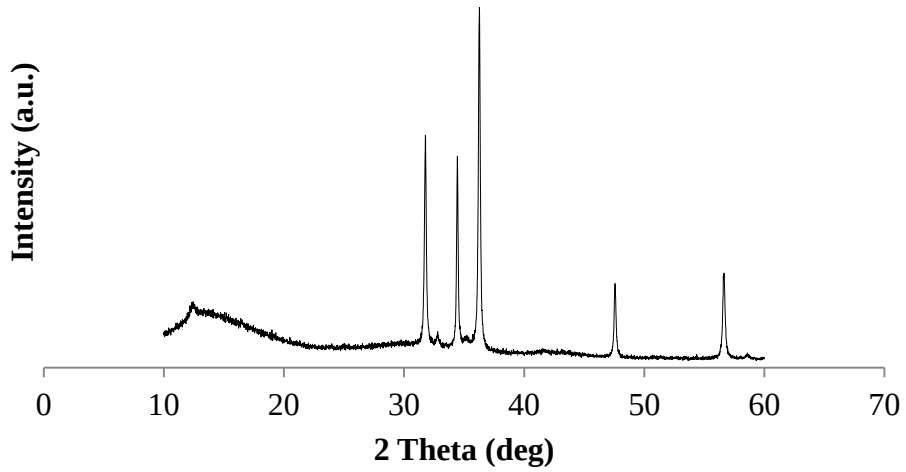

Figure 3.26 XRD pattern for Zn-Cr (10:1) calcined at 380 ^{o}C under N_2 for 5 h.

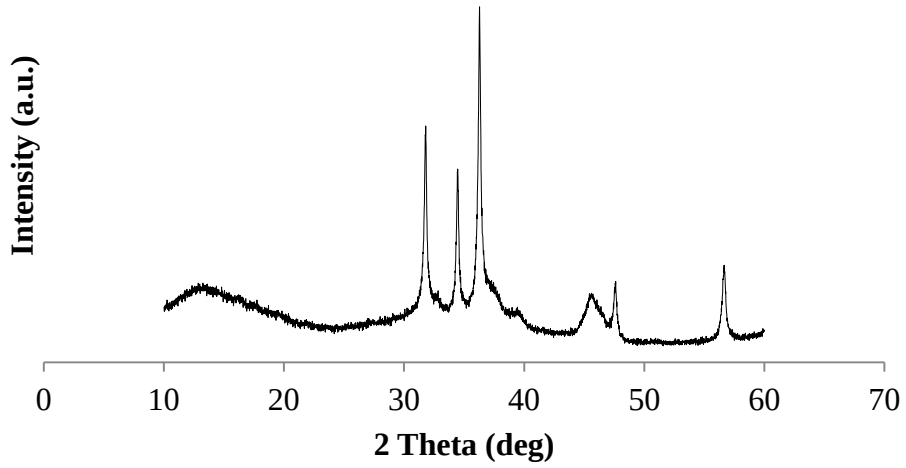

Figure 3.27 XRD pattern for 20%Zn-Cr (10:1)/Al_2O_3 calcined at 380 ^{o}C under air for 5 h.

3.6 Diffuse Reflectance Infrared Fourier Transform (DRIFT) spectroscopy

3.6.1 DRIFT spectroscopy for zeolites

DRIFT spectra were recorded at room temperature and ambient pressure under dry N_2 using powdered catalyst mixtures with KBr. The catalysts were pretreated at 300-500

°C for 1 h in N_2 flow, as for the ketonisation reaction. Characterisation of the silicalite catalysts by DRIFT spectroscopy revealed significant differences and gave important information regarding active sites in the ketonisation reaction. Figure 3.28 shows the DRIFT spectra of our Aerosil 300 and silicalite samples in the region of OH stretching modes of silanol (SiOH) groups. These spectra are in agreement with those reported in the literature.[22] The sharp peak at 3744 cm^{-1} is attributed to the free terminal silanol groups located on external and internal surfaces. The broader band around 3680 cm^{-1} is attributed to the hydrogen-bonded vicinal silanols.

The very broad band in the 3600-3100 cm^{-1} region is generally ascribed to silanol nests, which consist of a number of silanol groups interacting through extended hydrogen bonding. Such nests occur at silicon vacancies (defects) created by removing a tetrahedral Si atom from the framework and termination of the four loose oxygen atoms by hydrogen atoms (Scheme 3.1). DFT (density functional theory) analysis shows that the OH groups in silanol nests, due to the extended H-bonding, possess enhanced acidity compared to that for an isolated silanol group. This effect leads to increased reactivity of silanol nests, as documented for the Beckmann rearrangement of cyclohexanone oxime over defect-free silicalite.[22] As can be seen from the band in the 3600-3100 cm^{-1} region (Figure 3.28), our base-modified silicalite samples had much higher density of silanol nests than the unmodified silicalite (c). This is in agreement with the literature,[22] which reports the formation of silanol nests in silicalite upon base treatment.

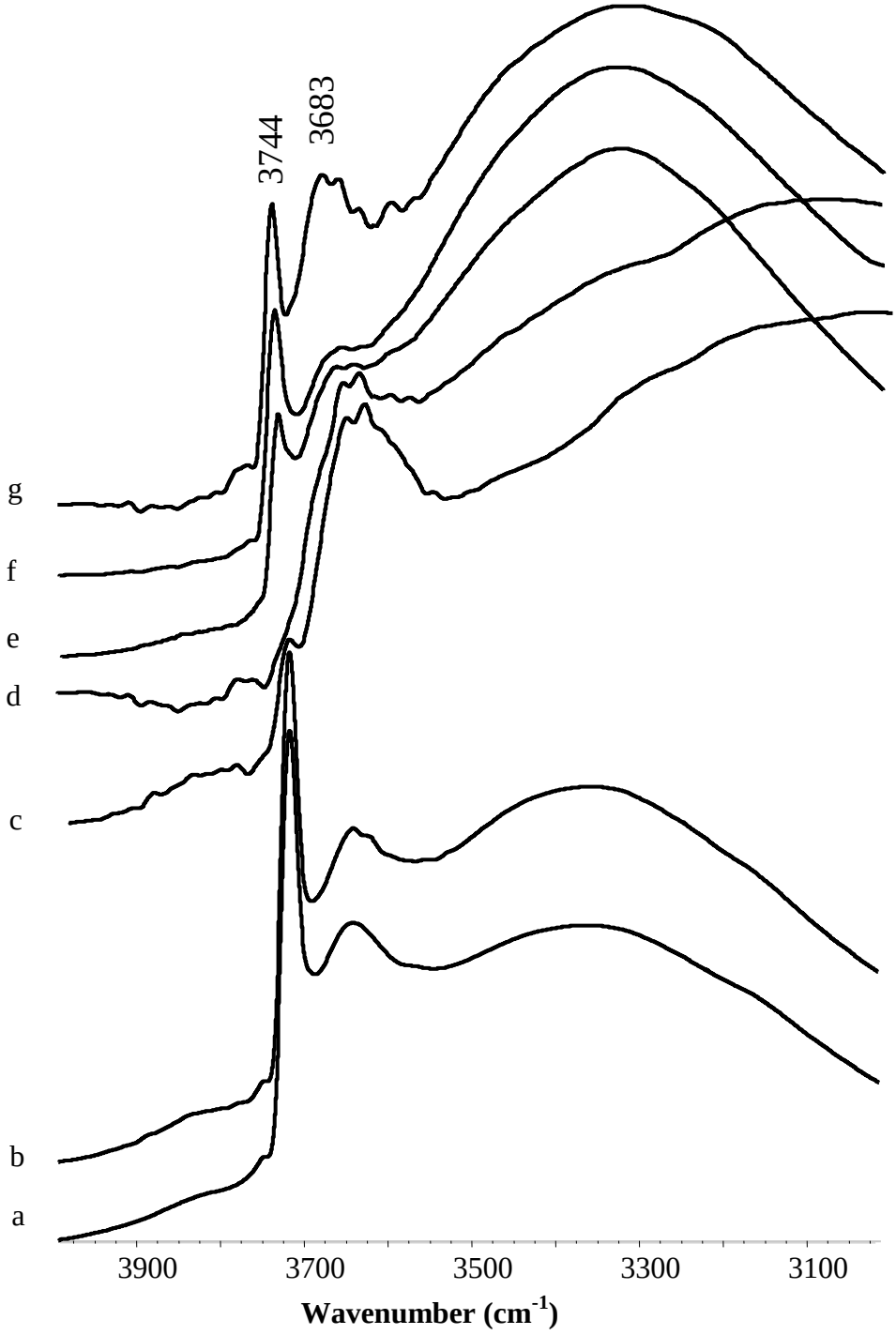

Figure 3.28 DRIFT spectra of Aerosil-300 [(a) and (b)] and silicalite [c-g]. Aerosil-300: (a) unmodified and (b) modified with 3.7 M $NH_{3(aq)}$ + 0.7 M $NH_4NO_{3(aq)}$, both pre-treated at 500 °C in N_2 for 1 h. Silicalite unmodified, pre-treated in N_2 for 1 h at: (c) 400 °C and (d) 500 °C; silicalite modified with 3.7 M $NH_{3(aq)}$ + 0.7 M $NH_4NO_{3(aq)}$, pre-treated in N_2 for 1 h at: (e) 300 °C, (f) 400 °C, (g) 500 °C.

Therefore, our DRIFT data indicate that silanol nests may be the active sites responsible for the high selectivity of the base-modified silicalite in propionic acid ketonisation. It should be noted that the density of silanol nests decreases upon heating above 500 °C, due to dehydration of the silanol groups. This may be the reason for the lower efficiency of the unmodified silicalite. The results will be presented in Table 4.3 in Chapter 4, section 4.3.3, which had been calcined at 550°C for 12 h in the final step of its preparation. As mentioned in Chapter 2, DRIFT spectra were taken on a Nicolet NEXUS FTIR spectrometer using powdered catalyst mixtures with KBr. The catalysts were pretreated at 300-500 °C for 1 h in N_2 flow, as they were pretreated for the ketonisation reaction. The DRIFT spectra were recorded at room temperature and ambient pressure under dry N_2.

3.7 Acidity studies and measurements

Various techniques were used to study the acidity of catalysts used in this work. The strength of catalyst acid sites was determined by ammonia adsorption,[40, 41] while the nature of acid sites (Brønsted or Lewis) was determined by FTIR-pyridine adsorption.[40, 42] Experimental procedures are detailed in Chapter 2, section 2.4.3.

3.7.1 FTIR study of pyridine adsorption

Surface acidity characterisation is fundamental to understanding the reaction mechanisms in heterogeneous catalysis. In this case, the adsorption of pyridine as a base on the acidic surface of the catalyst offers a powerful method for the characterisation of catalyst acidity.

The B or L nature of acid sites and their relative amounts in Zn-Cr oxide and niobium oxide catalysts was determined by the DRIFT spectroscopy of adsorbed

pyridine from the characteristic infrared bands at 1540 and 1450 cm^{-1} respectively.[25] Since these bands have approximately equal extinction coefficients,[25] the ratio of their integral intensities gives directly the B/L ratio of acid site densities.

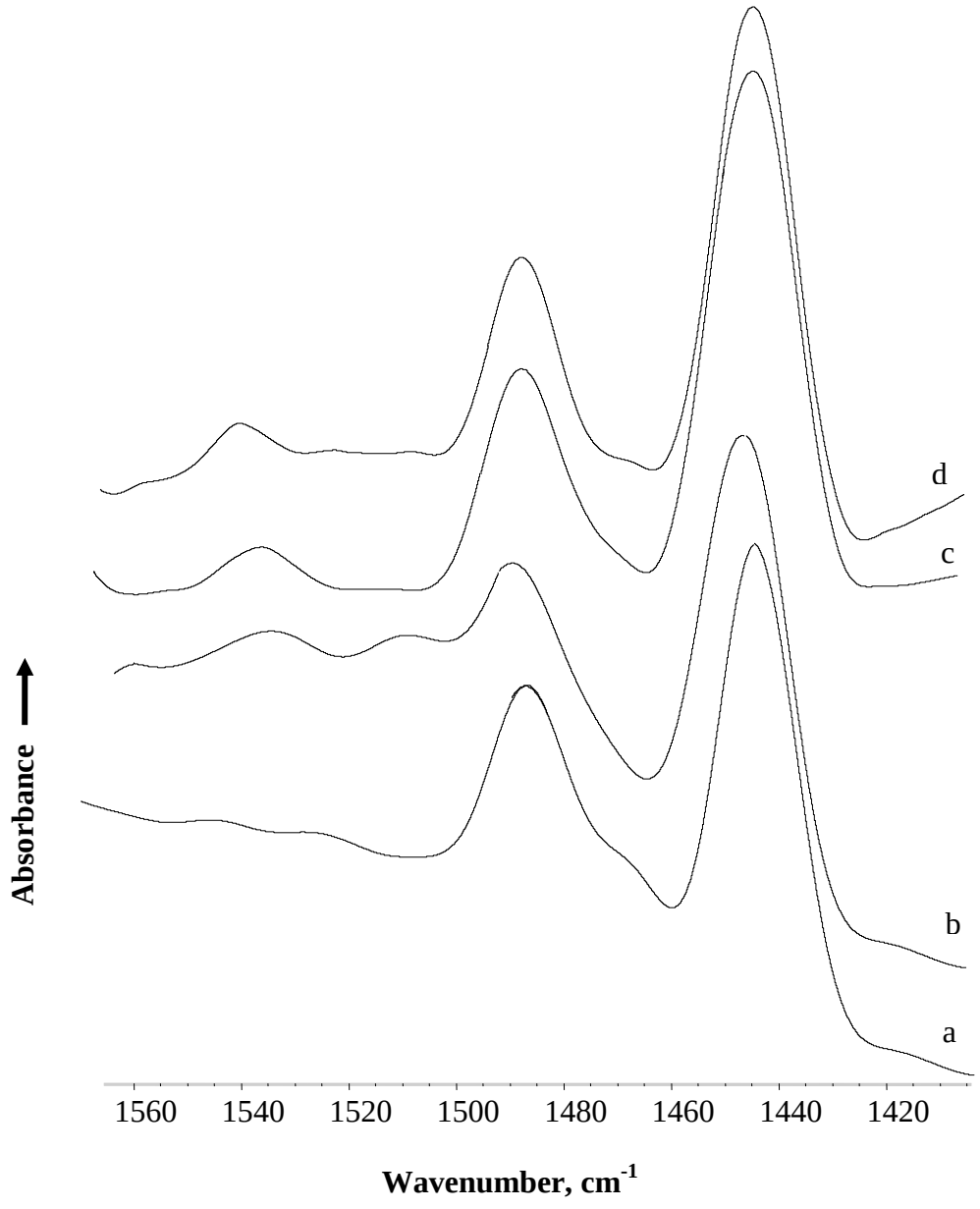

Figure 3.29 DRIFT spectra of adsorbed pyridine on a) ZnO, b) Zn-Cr (10:1), c) Zn-Cr (1:6), d) Cr_2O_3.

Zn-Cr (1:6) mixed oxide, as well as its parent ZnO and Cr_2O_3 oxides, had predominantly Lewis acid sites, as evidenced from the strong adsorption band at 1450 cm^{-1} in their spectra (Figure 3.29). Zn-Cr (1:6) and Cr_2O_3 also had Brønsted acid sites, as indicated by the band at 1540 cm^{-1}, with an approximate B/L ratio of 0.1 in these oxides. ZnO, however, had no Brønsted acid sites of sufficient strength to protonate pyridine. Alwadaani *et al*.[25, 40] reported that only Zn-Cr (1:30) mixed oxide, with the largest Cr content, had Brønsted acid sites of such strength.

Table 3.5 Brønsted (B) versus Lewis (L) acidity of catalysts from DRIFTS of adsorbed pyridine on catalysts which were calcined at 300 °C for 5 h under N_2 flow.

Catalyst	B/L[a]
Cr_2O_3	0.07
Zn-Cr (10:1)	0.07
ZnO	-

[a] Ratio of intensities (integrals of peak areas) of DRIFT peaks at 1540 and 1450 cm^{-1}.

In contrast to Zn-Cr oxide, Nb_2O_5 has been found to possess significant Brønsted acidity.[41] Figure 3.30 shows the FTIR-pyridine adsorption spectra of niobium oxides at calcination temperatures from 110-300 °C. The sharp pyridine absorption peaks at around 1450 cm^{-1} are indicative of Lewis acid sites. Pyridine molecules bonded to Brønsted acid as pyridinium ions sites are absorbed at 1540 cm^{-1}. The peak which can be seen at 1490 cm^{-1}, between the B and L peaks, is a combined band originating from pyridine bonded to both Brønsted and Lewis acid sites.[42]

Table 3.5 shows the B/L ratios derived from the spectra in Figure 3.30.

Table 3.5 Brønsted (B) versus Lewis (L) acidity of catalysts from DRIFT spectra of adsorbed pyridine

Catalyst	Calcination temperature (°C)	B/L[a]
Nb_2O_5	200	0.22
Nb_2O_5	300	0.10

[a] Ratio of intensities (integrals of peak areas) of DRIFT peaks at 1540 and 1450 cm^{-1}.

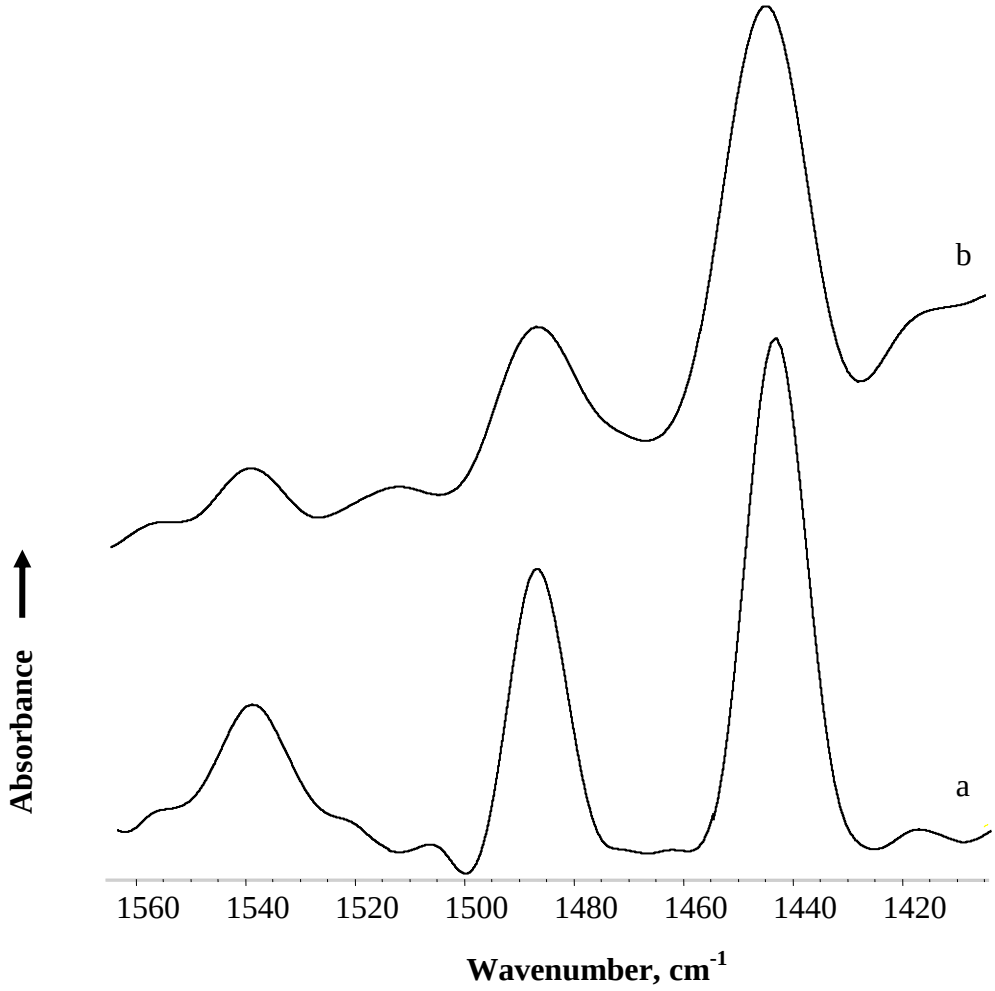

Figure 3.30 DRIFT spectra of adsorbed pyridine on Nb_2O_5, calcined at a) 200 °C, b) 300 °C.

3.7.2 Pulse ammonia adsorption analysis

Adsorption calorimetry can generally be used to determine the number and strength of acid sites. In this case, this technique was used to obtain the strength of Brønsted or Lewis acid sites, because many properties of catalysts are directly related to their acidity. For example, It has been reported that the reaction of fluid cracking on zeolites such as ZSM-5 was controlled by the Al/Si ratio and also by catalyst acidity.[43]

3.7.2.1 Pulse ammonia adsorption analysis for Zn-Cr oxides

The acid strength of catalysts was measured by ammonia adsorption microcalorimetry in terms of the differential enthalpy of ammonia adsorption at zero coverage (ΔH). This technique does not discriminate Brønsted from Lewis acidity, but provides a measure of total acid strength. The acid strength of Zn-Cr oxides, possessing mainly Lewis acidity, increased significantly as Cr content increased, with ΔH values varying from -127 to -193 kJ mol^{-1}, which mostly represents the strength of Lewis acid sites in Zn-Cr oxides.[40] Therefore, given the different nature of acidity in Zn-Cr oxide and Nb_2O_5 catalysts, it is not possible to quantitatively characterise the strength of each type of acid site in these catalysts by ammonia adsorption microcalorimetry. The results are summarised in Table 3.6.

Table 3.6 Acid properties of catalysts

Catalyst[a]	Acid site type[b]	ΔH (kJ mol^{-1})[c]
Cr_2O_3	B + L	-193[d]
Zn-Cr (1:6)	B + L	-170[d]
Zn-Cr (10:1)	B + L	-150
ZnO	L	-127[d]

[a] Catalyst pretreatment: Cr_2O_3 and Zn-Cr (1:6) were calcined at 300 °C in N_2 for 5 h. [b] B and L acid sites from DRIFT spectra of adsorbed pyridine. [c] Initial enthalpy of NH_3 adsorption at zero adsorption coverage. [d] Estimated from literature.[40]

3.7.2.2 Pulse ammonia adsorption analysis for niobium oxide catalyst*

Nb_2O_5 calcined at 110-300 °C was found to possess Brønsted and Lewis acidity, exhibiting ΔH values in the range of -115 to -129 kJ mol^{-1}. The acid strength of niobia predictably increased as the calcination temperature increased.

In this study, it was found that niobium oxide and Zn-Cr oxides differed in the nature of their acidity, making it impossible to quantitatively characterise the strength of each type of acid site in these catalysts by ammonia adsorption microcalorimetry. The results for the acidity of niobium oxide catalysts are presented in Figures 3.31-3.33 and summarised in Table 3.7. It has been reported that increasing the niobium oxide calcination temperature above 500 °C reduced the acidity of the resulting catalysts.[33] This can be explained by the transformation of protonic sites to Lewis sites with the elimination of water. The loss of acidity can probably be attributed to the change from amorphous to crystalline structure.[33] This can be explained by the transformation of protonic sites to Lewis sites with the elimination of water. The loss of acidity can probably be attributed to the change from amorphous to crystalline structure.[44, 45]

Table 3.7 Acid properties of catalysts

Catalyst[a]	Acid site type[b]	ΔH (kJ mol^{-1})[c]
Nb_2O_5 (110 °C)	B + L[41]	-115
Nb_2O_5 (200 °C)	B + L[41]	-123
Nb_2O_5 (300 °C)	B + L[41]	-129

[a] Nb_2O_5 at 110-300 °C in air for 3 h. [b] B and L acid sites from DRIFT spectra of adsorbed pyridine. [c] Initial enthalpy of NH_3 adsorption at zero adsorption coverage.

---

* Studied in collaboration with Vinicius V. Costa, Federal Minas Gerais University, Brazil.

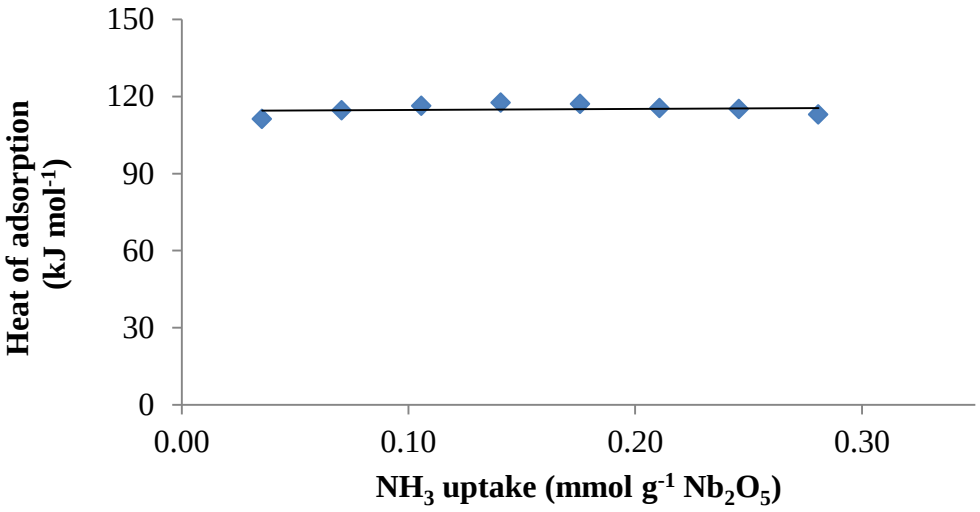

Figure 3.31 Plot of enthalpy of NH_3 adsorption versus NH_3 uptake for Nb_2O_5 calcined at 110 °C.

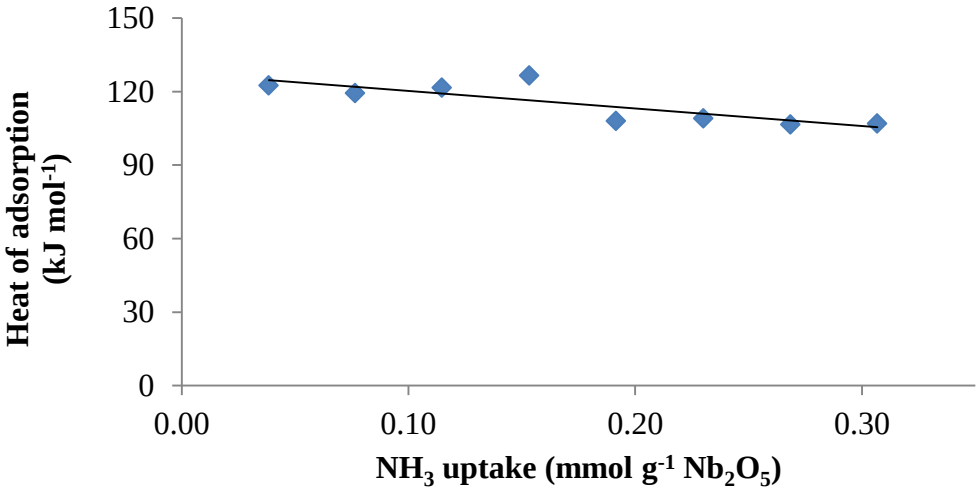

Figure 3.32 Plot of enthalpy of NH_3 adsorption versus NH_3 uptake for Nb_2O_5 calcined at 200 °C.

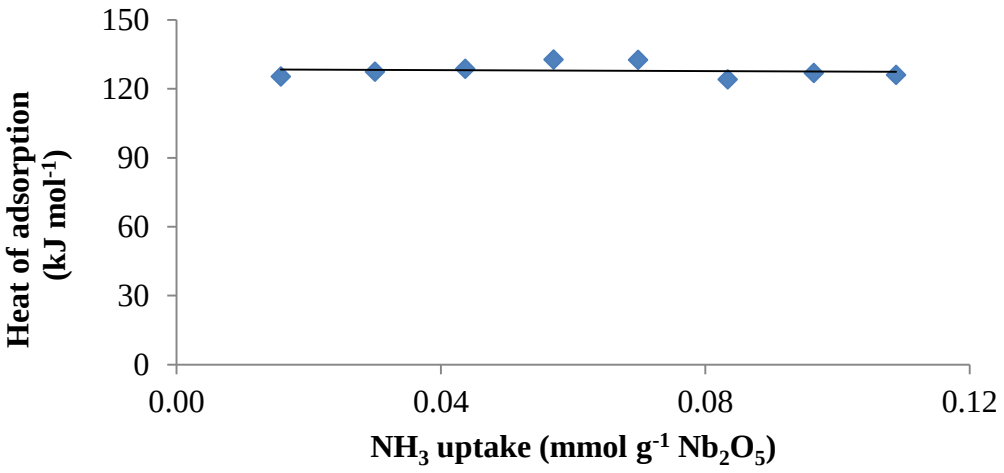

Figure 3.33 Plot of enthalpy of NH_3 adsorption versus NH_3 uptake for Nb_2O_5 calcined at 300 °C.

3.8 C, H, N analysis

To examine catalyst stability over longer time on stream, the silicalite was tested for at least 28 h TOS (time on stream) using 0.2 g of catalyst, 500 ^oC and 20 mL min^{-1} N_2 flow rate. While the Zn-Cr oxide and Al_2O_3 supported catalysts were tested at 380 ^oC, and 20 mL min^{-1} N_2 flow rate for 18 and 24 h TOS respectively. Table 3.8 shows the total amount of carbon deposits in the spent catalysts used in the gas phase ketonisation of propionic acid using C and H combustion analysis.

Table 3.8 C and H combustion analysis for spent catalysts used in the gas phase deoxygenation of propionic acid

Catalyst	C (%)	H (%)
Silicalite chemically treated by $NH_{3(aq)}/NH_4NO_3$ [a]	6.60	0.94
Zn-Cr (10:1) [b]	4.10	0.67

[a] After 28 h reaction at 500 °C.

[b] After 18 h reaction at 380 °C.

3.9 Conclusion

This chapter has addressed in detail the catalyst texture, XRD and FTIR spectroscopy, and the acidity of catalyst used in the ketonisation of carboxylic acids. First, the catalysts were characterised using N_2 physisorption. The specific surface area, pore diameter and pore volume were calculated for silicalite, zinc-chromium oxides and for niobium oxide catalysts, which were calcined at different temperatures. It was found that the texture of zeolite catalysts was not affected by chemical treatment, as their surface area, pore diameter and pore volume remained largely unchanged. The surface area was, however, positively affected by the Cr/Zn ratio in Zn-Cr catalyst, while the pore size decreased as the ratio increased. XRD measurements showed that silicalite was crystalline, while the crystallinity of zinc chromium oxides depended on their chromium and zinc content. Increasing the amount of chromium made the catalyst more amorphous, while those with high zinc content were crystalline.

The nature of acid sites was measured using DRIFT spectroscopy of pyridine adsorption. It was found that in Cr_2O_3, ZnO and Zn-Cr (1:6) oxide catalysts, Lewis acid sites predominated, while Cr_2O_3 and Zn-Cr (1:6) oxide catalysts also had Brønsted acid sites. In addition, niobium oxides catalysts were found to possess both Brønsted and

Lewis acid sites. The acidity of niobium oxides increased as the calcination temperature increased from 100 to 300 °C.

3.10 References

1. S. J. Gregg and K. S. W. Sing, *Adsorption, Surface Area and Porosity, Academic Press,* London, 1982.
2. K. K. Unger, J. Roquerol, K. S. W. Sing and H. Kral (Eds.), *Characterisation of Porous Solids I, Elsevier,* Amsterdam, 1988.
3. J. Roquerol, F. Rodriguez-Reinoso, K. S. W. Sing and K. K. Unger, *Characterisation of Porous Solids III, in, Elsevier,* Amsterdam, 1994.
4. I. Siminiceanu, I. Lazau, Z. Ecsedi, L. Lupa and C. Burciag, *Chem. Bull*, 2008, 53, 1-2.
5. G. Leofanti, M. Padovan, G. Tozzola and B. Venturelli, *Catalysis Today*, 1998, **41**, 207-219.
6. I. Jasinska and W. Arabczyk, *Chemical Papers-Solvak Academy of Sciences*, 2005, **59**, 496-499.
7. E. P. Barrett, L. G. Joyner and P. P. Halenda, *Journal of the American Chemical Society*, 1951, **73**, 373-380.
8. Z. Wang, H. Ma, W. Zhu and G. Wang, *Reaction Kinetics and Catalysis Letters*, 2002, **76**, 271-279.
9. L. Chen, Y. Zhu, H. Zheng, C. Zhang and Y. Li, *Applied Catalysis A: General*, 2012, **411–412**, 95-104.
10. X.-J. Tang, J.-H. Fei, Z.-Y. Hou, H. Lou and X.-M. Zheng, *Reaction Kinetics and Catalysis Letters*, 2008, **94**, 3-9.
11. M. Fujiwara, H. Ando, M. Tanaka and Y. Souma, *Bulletin of the Chemical Society of Japan*, 1994, **67**, 546-550.

12. F. Simard, U. A. Sedran, J. Sepúlveda, N. S. Fígoli and H. I. de Lasa, *Applied Catalysis A, General*, 1995, **125**, 81-98.

13. E. F. Kozhevnikova and I. V. Kozhevnikov, *Journal of Catalysis*, 2006, **238**, 286-292.

14. M. Ohta, Y. Ikeda and A. Igarashi, *Applied Catalysis A: General*, 2004, **266**, 229-233.

15. M. C. J. Bradford, M. V. Konduru and D. X. Fuentes, *Fuel Processing Technology*, 2003, **83**, 11-25.

16. I. Díaz, E. Kokkoli, O. Terasaki and M. Tsapatsis, *Chemistry of materials*, 2004, **16**, 5226-5232.

17. E. E. Mallon, M. Y. Jeon, M. Navarro, A. Bhan and M. Tsapatsis, *Langmuir*, 2013, **29**, 6546-6555.

18. S. Bordiga, I. Roggero, P. Ugliengo, A. Zecchina, V. Bolis, G. Artioli, R. Buzzoni, G. Marra, F. Rivetti and G. Spanò, *Journal of the Chemical Society, Dalton Transactions*, 2000, 3921-3929.

19. K. A. Sashkina, N. A. Rudina, A. I. Lysikov, A. B. Ayupov and E. V. Parkhomchuk, *Journal of Materials Chemistry A*, 2014, **2**, 16061-16070.

20. C.-C. Chang, A. R. Teixeira, C. Li, P. J. Dauenhauer and W. Fan, *Langmuir*, 2013, **29**, 13943-13950.

21. J. Hua and Y. Han, *Chemistry of Materials*, 2009, **21**, 2344-2348.

22. G. P. Heitmann, G. Dahlhoff and W. F. Hölderich, *Journal of Catalysis*, 1999, **186**, 12-19.

23. H. Bayahia, E. Kozhevnikova and I. Kozhevnikov, *Chemical Communications*, 2013, **49**, 3842-3844.

24. B. Li and R. Gonzalez, *Catalysis Letters*, 1998, **54**, 5-8.

25. F. Al-Wadaani, E. F. Kozhevnikova and I. V. Kozhevnikov, *Applied Catalysis A: General*, 2009, **363**, 153-156.

26. A. M. Youssef, A. I. Ahmed, S. E. Samra, N. B. El-Assy and E. A. El-Sharkawy, *Adsorption Science & Technology*, 1998, **16**, 175-191.

27. M. delArco, V. Rives, R. Trujillano and P. Malet, *Journal of Materials Chemistry*, 1996, **6**, 1419-1428.

28. R. M. Gabr, M. M. Girgis, A. M. Elawad and B. M. Abouzeid, *Materials Chemistry and Physics*, 1994, **39**, 53-62.

29. V. V. Costa, H. Bayahia, E. F. Kozhevnikova, E. V. Gusevskaya and I. V. Kozhevnikov, *ChemCatChem*, 2014, **6**, 2134-2139.

30. E. V. Ramos-Fernández, J. Ruiz-Martínez, J. C. Serrano-Ruiz, J. Silvestre-Albero, A. Sepúlveda-Escribano and F. Rodríguez-Reinoso, *Applied Catalysis A: General*, 2011, **402**, 50-58.

31. S. Brunauer, P. H. Emmett and E. Teller, *Journal of the American Chemical Society*, 1938, **60**, 309-319.

32. M. Yang, Y. Men, S. Li and G. Chen, *Applied Catalysis A: General*, 2012, **433–434**, 26-34.

33. M. Paulis, M. Martın, D. Soria, A. Dıaz, J. Odriozola and M. Montes, *Applied Catalysis A: General*, 1999, **180**, 411-420.

34. Z.-C. Tang, D.-H. Yu, P. Sun, H. Li and H. Huang, *Bulletin of the Korean Chemical Society*, 2010, **31**, 3679.

35. J.-M. Jehng, A. M. Turek and I. E. Wachs, *Applied Catalysis A: General*, 1992, **83**, 179-200.

36. L. He, D. Li, K. Wang, A. K. Suresh, J. Bellare, T. Sridhar and H. Wang, *Nanoscale research letters*, 2011, **6**, 1-9.

37. R. M. Cavalcanti, I. d. C. L. Barros, J. A. Dias and S. C. L. Dias, *Journal of the Brazilian Chemical Society*, 2013, **24**, 40-50.

38. Z. F. Wang, J. Y. Xi, W. P. Wang and G. X. Lu, *Journal of Molecular Catalysis A: Chemical*, 2003, **191**, 123-134.

39. R. M. Gabr, M. M. Girgis and A. M. Elawad, *Materials Chemistry and Physics*, 1992, **30**, 169-177.

40. F. Al-Wadaani, E. F. Kozhevnikova and I. V. Kozhevnikov, *Journal of Catalysis*, 2008, **257**, 199-205.

41. A. M. Alsalme, P. V. Wiper, Y. Z. Khimyak, E. F. Kozhevnikova and I. V. Kozhevnikov, *Journal of Catalysis*, 2010, **276**, 181-189.

42. G. Sunita, B. M. Devassy, A. Vinu, D. P. Sawant, V. Balasubramanian and S. Halligudi, *Catalysis Communications*, 2008, **9**, 696-702.

43. A. Auroux, *Topics in Catalysis*, 1997, **4**, 71-89.

44. M. Ziolek, *Catalysis Today*, 2003, **78**, 47-64.

45. I. Nowak and M. Ziolek, *Chemical Reviews*, 1999, **99**, 3603-3624.

Chapter 4

Gas-phase ketonisation of propionic acid catalysed by silicalite

4.1 Introduction

Carboxylic acids readily available from natural resources are attractive as renewable raw materials for the production of value-added chemicals and bio-fuel components.[1, 2] For fuel applications, carboxylic acids require reduction in their oxygen content, i.e. deoxygenation. Therefore, much recent research has been focused on the deoxygenation of carboxylic acids using heterogeneous catalysis.[3, 4] Ketonisation of carboxylic acids (Equation 4.1) is widely used as a clean method for the synthesis of ketones.[5] It allows for partial deoxygenation of carboxylic acids to be achieved, accompanied by their carbon backbone upgrade. Ketonisation is catalysed by many basic and acidic metal oxide and mixed-oxide catalysts in the temperature range of 300-500 °C.[5-12] Chromium-zinc-manganese oxide has been used in the ketonisation of aliphatic acids in the gas phase at 300-400 °C and the optimum ketone yield was at 325 °C.[13] Additionally, many different metal oxides have been reported as active catalysts in the ketonisation of acids, including CeO_2-Mn_2O_3 in the ketonisation of propionic acid.[14] The ketonisation of carboxylic acids in both gas and liquid phases has also been catalysed by several metal oxides, including Cr_2O_3,[15] ZrO_2,[16-18] ZnO,[19] TiO_2[20] and iron oxide,[21] but the nature of catalytically active sites is not yet clear. It is generally thought that basic sites are favourable for ketonisation.[5] However, heteropoly acid $H_3PW_{12}O_{40}$ possessing very strong proton sites has also been found active in propionic acid ketonisation.[22] We now report that neutral metal-free silica materials, namely amorphous silica and, in

particular, crystalline silicalite (MFI structure[23]), are active and environmentally benign catalysts for the gas-phase ketonisation of propionic acid. Propionic acid was chosen as representative of carboxylic acids with the number of carbon atoms $n \leq 6$ derived from carbohydrate feedstocks.[10]

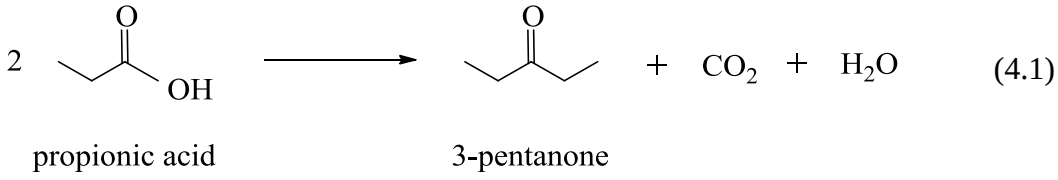

4.2 Blank reaction

Blank experiments in the absence of silica were done under optimal conditions: at 300-500 °C, 20 ml min^{-1} N_2 and 0.2 g of catalyst. First, at 400 °C, no ketonisation of propionic acid occurred. When the experiment was carried out at 500 °C (Table 4.2), homogeneous catalysis occurred to a small extent, as about 12% of propionic acid underwent pyrolysis, in agreement with a previous report.[24]

4.3 Ketonisation of propionic acid

The gas-phase ketonisation of propionic acid was performed in flowing N_2 at 300-550 °C under atmospheric pressure in a downflow quartz fixed-bed reactor. Typically, the reaction was carried out at a propionic acid concentration of 2 vol%, with 0.2 g of catalyst and an N_2 flow rate of 20 ml min^{-1} for six hours on stream. Prior to use, the catalysts were heated at the reaction temperature in N_2 flow for 1 h. The selectivity was defined as the percentage of carboxylic acid converted into a particular product taking into account the reaction stoichiometry; thus 100% ketone selectivity would mean 1 mole of carboxylic acid converted to form 0.5 mol of ketone. CO and CO_2 were not

quantified and not included in reaction selectivities. Table 4.1 shows the texture of catalysts used which has been presented in detail in section 3.2.2.

Table 4.1 Catalyst characterisation

Catalyst	S_{BET}[a] ($m^2 g^{-1}$)	Pore volume[b] ($cm^3 g^{-1}$)	Pore size[c] (Å)
Aerosil-300[d]	296	1.15	156
Silicalite	379	0.23	24
Silicalite modified by $NH_{3(aq)}/NH_4NO_3$	364	0.23	26

[a] BET surface area.

[b] Single point total pore volume.

[c] Average BET pore diameter.

[d]Aerosil-300 was wetted to form a gel then oven dried at 110°C and ground to a powder of 45-180 μm particle size.

4.3.1 The effect of temperature on the ketonisation of propionic acid

The reaction temperature has a significant effect on conversion, selectivity and overall yields of 3-pentanone, as reported in the literature.[18, 25-28] These ketonisation reactions were carried out over silica, ZSM-5 and silicalite in the temperature range of 300-550 °C, 1 bar pressure and 20 ml min^{-1} N_2 flow. The conversion of propionic acid and yields of 3-pentanone over silicalite catalyst increased with increasing temperature from 300 to 550 °C. At 550 °C, however, selectivity decreased to 65% and greater amounts of hydrocarbons and unknown products formed than at lower temperatures. The best yield of 3-pentanone was obtained at 500 °C over base-treated silicalite: conversion was 84% and the selectivity of 3-pentanone was 92%. Stonkus *et al.*[13] found that the yield of acetone in acetic acid ketonisation over chromium-zinc-manganese catalyst increased with increasing temperature from 300 to 325 °C. However, yield decreased when the

temperature was raised to 400 °C. In the ketonisation of propionic acid using the same chromium-zinc-manganese catalysts, the yield of 3-pentanone reached 90 % at 325 °C. Increasing the temperature to 400 °C increased conversion, but the yield of 3-pentanone decreased to 62%.

4.3.2 Ketonisation of propionic acid over amorphous silica

A wide range of amorphous silicas were tested for the ketonisation of propionic acid (Equation 4.1) in flowing N_2 at different temperatures and under atmospheric pressure using a fixed-bed continuous flow reactor.[4] These silicas were high purity powdered materials employed as catalyst supports and stationary phases in chromatography. They were active catalysts, but not selective for 3-pentanone.

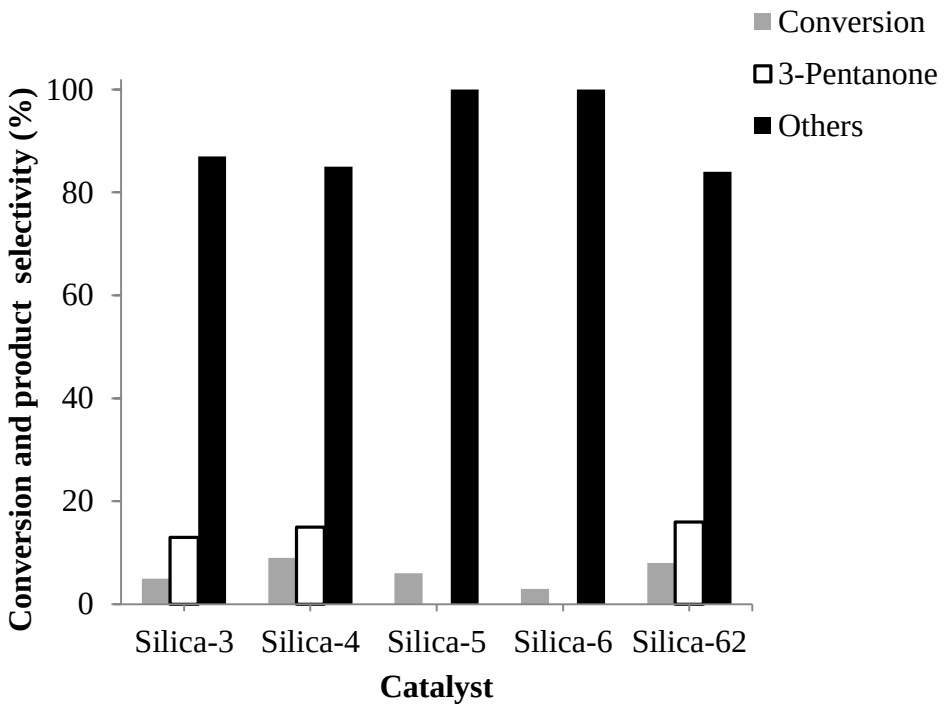

Figure 4.1 Propionic acid ketonisation over amorphous silica 0.2 g at 350 °C, 2 vol% propionic acid, 20 ml min^{-1} N_2, 4.0 h g mol^{-1} contact time.

At 350 °C, silica-5 and silica-6 were not selective for 3-pentanone, while other silicas such as silica-4 and silica-62 showed higher selectivity to 3-pentanone (Figure 4.1). Increasing the temperature to 400 and 450 °C (Table 4.2) increased the reactivity of the catalysts. Table 4.2 shows comparative results for commercial silica of high purity, amorphous Aerosil-300, consisting of nanosized nonporous spheres fumed in a high temperature flame (300 m^2 g^{-1} specific surface area). It was tested at 400-500 °C and exhibited a moderate to good catalytic activity in the formation of 3-pentanone, with some propionic anhydride also being formed. This was surprising, because silica is a practically neutral material. It lacks basicity and possesses very weak acidity due to its silanol groups, SiOH. The activity of Aerosil-300 increased when the reaction temperature was raised from 400 to 500 °C.

Table 4.2 Gas-phase ketonisation of propionic acid over amorphous silica[a]

Catalyst	Temperature (°C)	Conversion (%)	Selectivity (mol %)	
			3-pentanone	Others[b]
None	500	12	36	64
Silica-3	400	9	67	33
Silica-3	450	36	80	20
Silica-4	400	20	70	30
Silica-4	450	62	84	16
Silica-5	400	7	46	54
Silica-5	450	27	79	21
Silica-6	400	5	35	65
Silica-6	450	15	72	28
Silica-62	400	17	64	36
Silica-62	450	15	93	7
Aerosil-300	400	23	87	13
Aerosil-300	500	39	85	15

[a] 0.2 g catalyst, 2 vol% propionic acid in N_2 flow, 20 ml min^{-1} and 6 h time on stream.

[b] Other products included propionic anhydride, isopropanol and acetone, together with unidentified compounds.

Figures 4.2 and 4.3 show time courses for propionic acid ketonisation over Aerosil-300 at 400 and 500 °C respectively, demonstrating good catalyst stability over time on stream in both cases, as the reaction reached the steady state in the first hour.

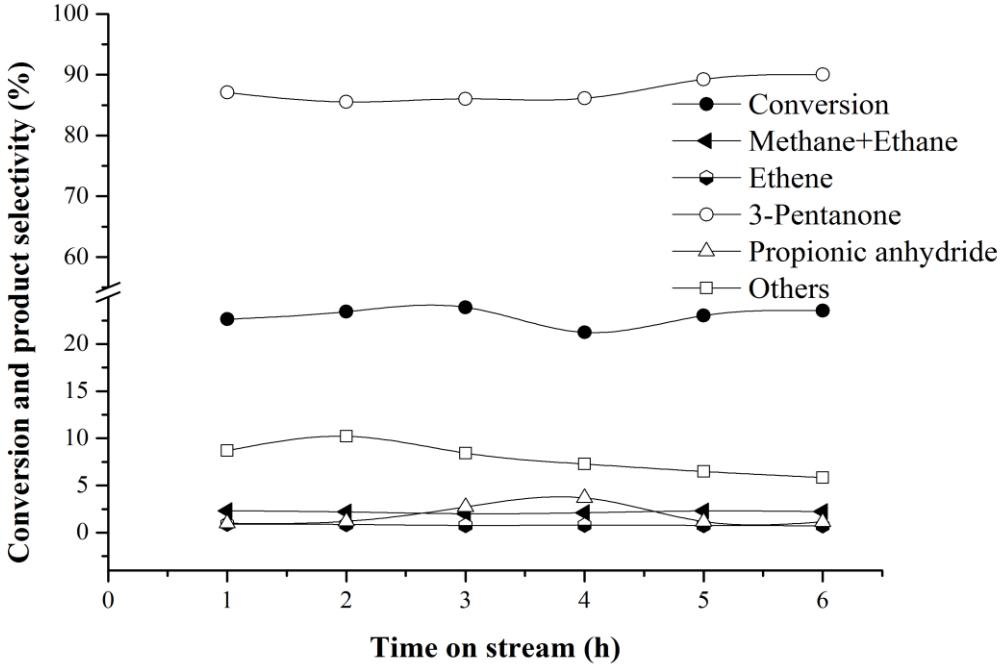

Figure 4.2 Time course for propionic acid ketonisation: 0.2 g Aerosil-300, 400 °C, 2 vol.% propionic acid, 20 ml min^{-1} N_2.

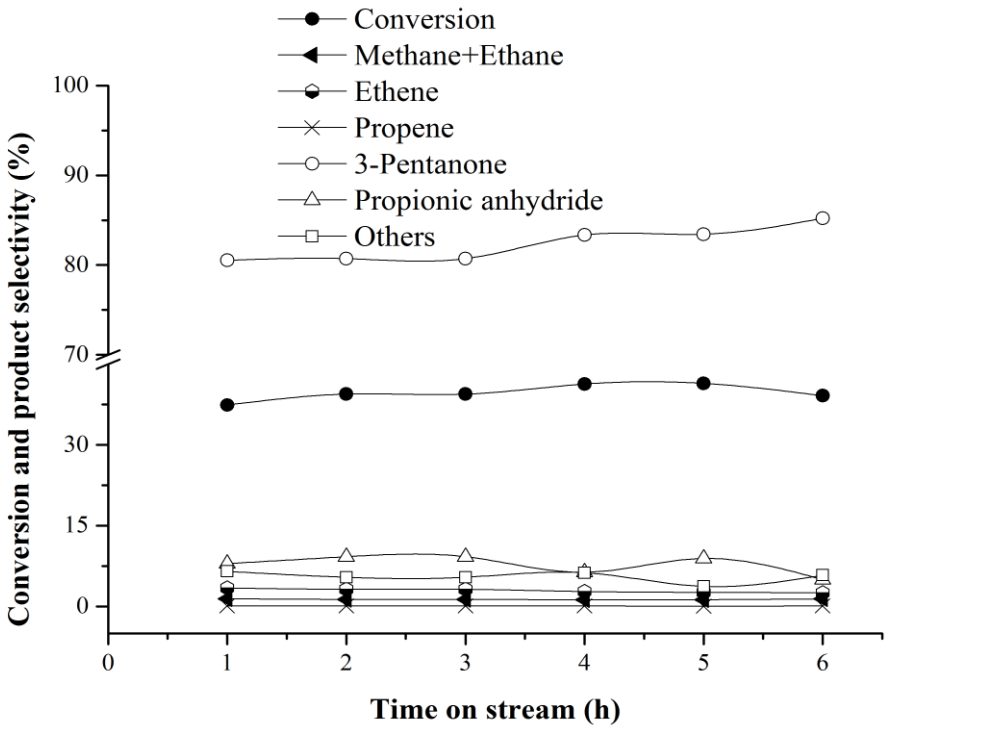

Figure 4.3 Time course for propionic acid ketonisation: 0.2 g Aerosil-300, 500 °C, 2 vol.% propionic acid, 20 ml min^{-1} N_2.

4.3.3 Ketonisation of propionic acid over crystalline silicalite

Crystalline materials, i.e. highly siliceous zeolites, were tested in the ketonisation of propionic acid. HZSM-5 zeolite (Si/Al = 180) possessing strong proton sites exhibited a small ketonisation activity at 300 °C but no such activity at 400-500 °C, mainly causing cracking of propionic acid to form light hydrocarbons, predominantly ethylene (Table 4.3). In contrast, purely siliceous silicalite (MFI structure) showed high catalytic activity in ketonisation, which peaked at 500 °C to afford a 50% 3-pentanone yield.

Table 4.3 Gas-phase ketonisation of propionic acid over silicalite[a]

Catalyst	Temperature (°C)	Conversion (%)	Selectivity (mol%)			
			3-pentanone	C1-C3 alkanes	C2-C3 alkenes	Others[b]
HZSM-5	300	43	30	1	6	63
HZSM-5	400	98	0	0	39	61
HZSM-5	500	99	0	0	97	3
Silicalite	400	23	76	3	0	21
Silicalite	450	42	72	5	18	5
Silicalite	500	95	53	15	28	4

[a] 0.2 g catalyst, 2 vol% propionic acid in N_2 flow, 20 ml min^{-1} and 6 h time on stream.
[b] Other products included propionic anhydride, isopropanol and acetone, together with unidentified compounds.

4.3.4 Ketonisation of propionic acid over chemically treated amorphous silica and crystalline silicalite

In search for better performance, the silicalite was chemically modified with aqueous acidic (0.01 M and 0.1 M HCl) or basic (3.7 M $NH_{3(aq)}$ and 3.7 M $NH_{3(aq)}$ + 0.7 M NH_4NO_3)[29] solutions, which enhanced the creation of silanol groups on the catalyst

surface. For silicalite, the acid treatment had little effect, the basic one, with ammonia and ammonium nitrate, significantly improved ketonisation selectivity (Table 4.4). It has been found that our base-modified silicalite samples have a much higher density of silanol nests compared to unmodified silicalite as found from DRIFT spectroscopy which discussed in section 3.6.1. A similar effect has been reported for the Beckmann rearrangement of cyclohexanone oxime to ε-caprolactam over silicalite, which has been attributed to the formation of framework defects (silanol nests) in silicalite acting as catalytically active sites.[29] Such nest occurs at silicon vacancies created by removing tetrahedral silicon atoms from the framework and termination the four loose oxygen atoms by hydrogen atoms (Scheme 4.1).[30, 31]

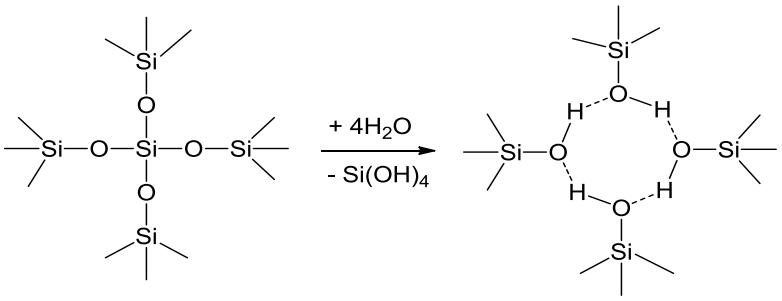

Scheme 4.1 Formation of a silanol nest.

DFT analysis shows[32] that the OH group in silanol nest, due to the extended H-bonding possess enhanced acidity compared to that of an isolated silanol group. This effect leads to increased reactivity of silanol nests. In contrast, the basic treatment had practically no effect on the performance of amorphous Aerosil-300 (Table 4.4). The conversion of propionic acid over silicalite increased with reaction temperature, but with some predictable loss in 3-pentanone selectivity. At 500 °C and a contact time of 4.0 h g mol^{-1}

the base-modified silicalite gave a very good 3-pentanone yield of 77% with 92% selectivity at 84% conversion (average for 6 h on stream). Increasing the contact time 2.5-fold to 10 g mol^{-1} raised the yield to 87%, which matches the performance of the best metal oxide catalysts.[5]

Table 4.4 Gas-phase ketonisation of propionic acid over silicalite[a]

Catalyst	Temperature (°C)	Conversion (%)	Selectivity (mol%)			
			3-pentanone	C1-C3 alkanes	C2-C3 alkenes	Others[b]
Silicalite[c]	500	57	95	2	2	1
Silicalite[d]	500	75	75	6	18	1
Aerosil-300[e]	500	40	81	2	3	14
Silicalite[e]	400	10	96	2	1	1
Silicalite[e]	450	46	93	2	1	4
Silicalite[e]	500	84	92	2	1	5
Silicalite[e]	550	92	65	3	5	27

[a] 0.2 g catalyst, 2 vol% propionic acid in N_2 flow, 20 ml min^{-1}, 6 h time on stream.

[b] Other products included propionic anhydride, isopropanol and acetone, together with unidentified compounds. CO and CO_2 not included.

[c] Modified by 0.1 M $HCl_{(aq)}$.

[d] Modified by 3.7 M $NH_{3(aq)}$.

[e] Modified by 3.7 M $NH_{3(aq)}$ + 0.7 M $NH_4NO_{3(aq)}$.

The Aerosil-300 catalyst showed a respectable 3-pentanone selectivity of 85% and 39% conversion at 500 °C, its performance was stable and no deactivation was observed for at least 28 h on stream. Figure 4.4 shows the catalysts was stable for 6 h time on stream.

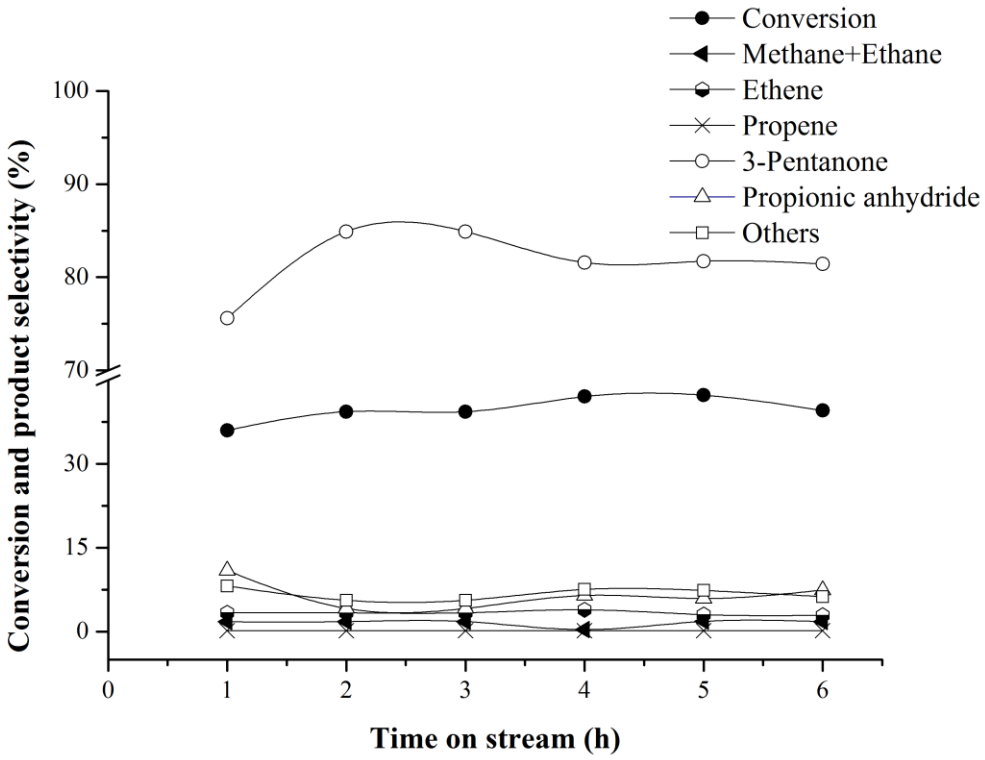

Figure 4.4 Time course for propionic acid ketonisation: 0.2 g Aerosil-300 modified with 3.7 (M NH_3+ 0.7 M $NH_4NO_3)_{(aq)}$, 500 °C, 2 vol% propionic acid, 20 ml min^{-1} N_2, 4.0 h g mol^{-1} contact time.

4.4 Stability of base-modified silicalite

The base-modified silicalite catalyst (3.7 M $NH_{3(aq)}$ + 0.7 M $NH_4NO_{3(aq)}$) showed a stable performance at 500 °C for at least 28 h with 84-92% 3-pentanone selectivity at 93-80% propionic acid conversion (Figure 4.5). A small decrease in catalyst activity over time on stream was probably caused by coke deposition on the catalyst, which amounted to 6.6 wt% as have been shown in section 3.8, Table 3.8. Coke could be removed by aerobic gasification at 450-500 °C, allowing full recovery of catalyst activity. The 3-pentanone product was quite stable under these reaction conditions, undergoing 3 and 8% conversion over base-treated silicalite at 450 and 500 °C respectively, to form a mixture of C1 – C3 alkanes and alkenes, as well as some heavier

products (section 4.5). Although silicalite requires a higher reaction temperature than the best metal oxide catalysts, e.g. CeO_2-MnO_2[8] and CeO_2-ZrO_2,[10] it has the important advantages of being an easily available nontoxic metal-free material, having perfect performance stability in ketonisation and allowing easy regeneration.

The possibility of catalysis by metal impurities in silicalite and Aerosil-300 can be ruled out because ICP analysis showed only traces of metals such as Al and Fe in these materials and because the results did not change when bi-distilled water was used for catalyst preparation and modification.

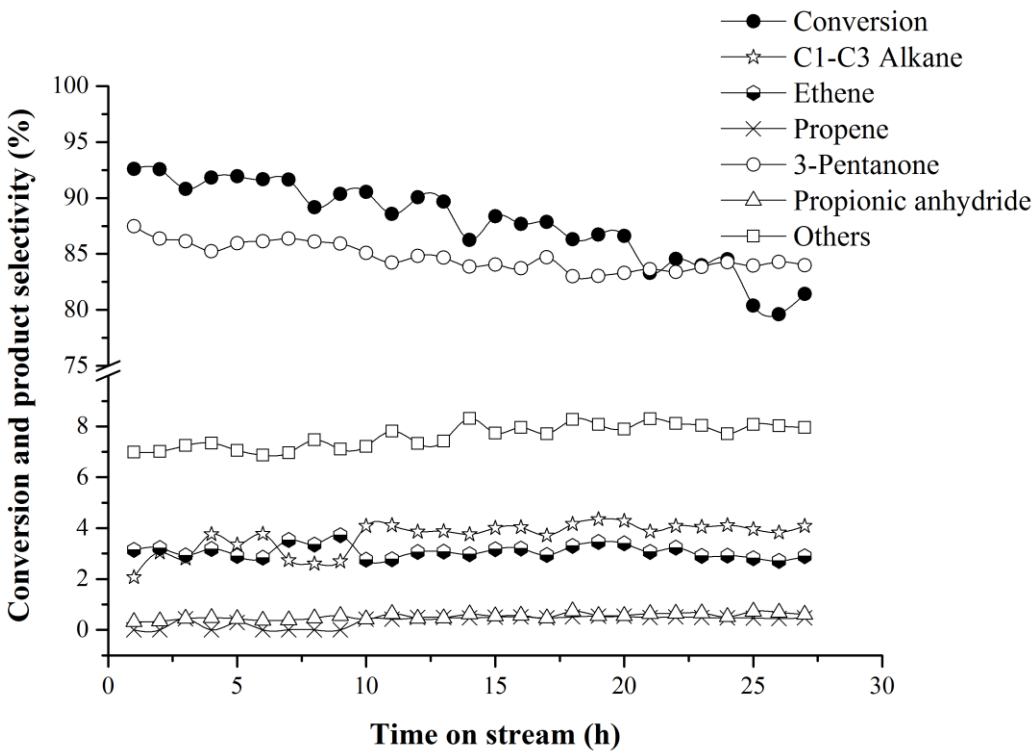

Figure 4.5 Time course for propionic acid ketonisation: 0.2 g silicalite modified with 3.7 M $NH_{3(aq)}$ + 0.7 M $NH_4NO_{3(aq)}$, 500 °C, 2 vol.% propionic acid, 20 ml min^{-1} N_2, 4.0 h g mol^{-1} contact time.

4.5 Conversion of 3-pentanone

3-Pentanone, the product of propionic acid ketonisation, was found to be quite stable under reaction conditions (Table 4.5). In this experiment, 0.2 g of silicalite catalyst modified by ammonia and ammonium nitrate was treated under reaction conditions with 1 vol% of 3-pentanone. It underwent 3 and 8% conversion over base-treated silicalite at 450 and 500 °C respectively, to form a mixture of C1 – C3 alkanes and alkenes, as well as some heavier products.

Table 4.5 Conversion of 3-pentanone over silicalite modified with 3.7 M $NH_{3(aq)}$ + 0.7 M $NH_4NO_{3(aq)}$.[a]

Temperature (°C)	Conversion (%)	Selectivity (mol%)			
		CH_4	C_2H_6	C_2H_4	Others
450	3	21	17	25	37
500	8	17	23	45	15

[a] 0.2 g catalyst, 6 h time on stream, 1 vol% 3-pentanone concentration in N_2, 20 ml min^{-1} N_2 flow, 6 h on stream.

4.6 Ketonisation mechanism

Ketonisation occurs with carboxylic acids possessing α-hydrogen atoms. Several mechanisms have been proposed for this reaction, including (i) decomposition of metal carboxylate, (ii) an acid anhydride intermediate route, (iii) a ketene intermediate route and (iv) a β-ketoacid intermediate route. The mechanism may depend on many factors, especially the type of catalyst used. Pestman *et al.*[33] suggest ketene intermediacy for the ketonisation of acetic acid over metal oxides (Figure 4.6). Ketonisation of propionic acid over heteropoly acid $H_3PW_{12}O_{40}$ may also occur via the ketene intermediate route.[22] Silica has been patented as a catalyst for the gas-phase production of ketenes

from carboxylic acids. This suggests that ketonisation of propionic acid over amorphous silica and silicalite may occur via ketene intermediacy as well.

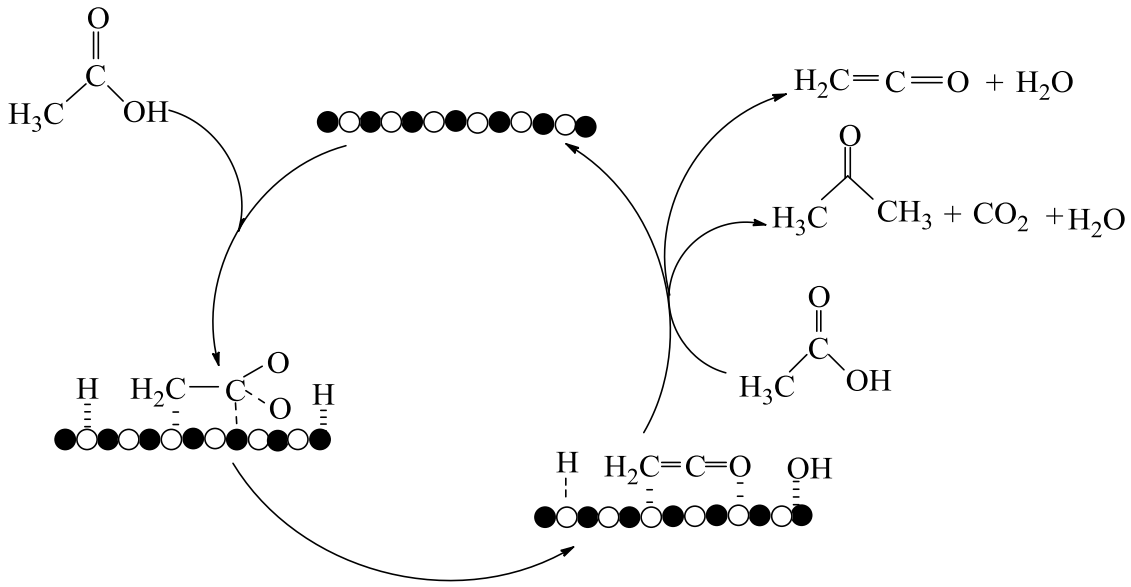

Figure 4.6 Ketene-based mechanism of acetic acid ketonisation.[34]

4.7 Conclusions

In this work, we tested a variety of amorphous silica catalysts with high purity in propionic acid ketonisation and they showed good and stable performance for six hours on stream. When tested in the range of 300-550 °C, they showed no activity at lower temperatures, but the activity increased with increasing temperature. Silicalite was prepared and tested in the ketonisation of propionic acid. It showed good activity and selectivity, with increased activity at higher temperatures. Amorphous silica and silicalite were chemically modified by acid and basic aqueous solutions (0.1 M hydrochloric acid or 3.7 M ammonia and 0.7 M ammonium nitrate). These treatments did not affect the activity of amorphous silica, but silicalite showed a very good improvement in catalyst activity. For silicalite, the base treatment with $NH_{3(aq)}$ +

$NH_4NO_{3(aq)}$ significantly improved propionic acid ketonisation selectivity. All catalysts showed very good stability for at least 6 hours on stream. In addition, base-treated silicalite showed excellent stability for at least 28 hours on stream with a small decrease in activity after 20 hours. It is concluded that neutral materials – amorphous silica and crystalline silicalite – are active and environmentally benign catalysts for propionic acid ketonisation at 450-500 °C to form 3-pentanone. Base-treated silicalite (MFI structure) is particularly efficient in ketonisation of propionic acid. DRIFTS indicates that silanol nests generated by basic modification of silicalite are responsible for its catalytic activity in the ketonisation of propionic acid.

4.8 References

1. A. Corma Canos, S. Iborra and A. Velty, *Chemical Reviews*, 2007, **107**, 2411-2502.
2. E. L. Kunkes, D. A. Simonetti, R. M. West, J. C. Serrano-Ruiz, C. A. Gärtner and J. A. Dumesic, *Science*, 2008, **322**, 417-421.
3. H. Bernas, K. Eränen, I. Simakova, A. R. Leino, K. Kordás, J. Myllyoja, P. Mäki-Arvela, T. Salmi and D. Y. Murzin, *Fuel*, 2010, **89**, 2033-2039.
4. M. Arend, T. Nonnen, W. F. Hoelderich, J. Fischer and J. Groos, *Applied Catalysis A: General*, 2011, **399**, 198-204.
5. M. Renz, *European Journal of Organic Chemistry*, 2005, 979-988.
6. C. A. Gaertner, J. C. Serrano-Ruiz, D. J. Braden and J. A. Dumesic, *Industrial and Engineering Chemistry Research*, 2010, **49**, 6027-6033.
7. T. Yokoyama and N. Yamagata, *Applied Catalysis A: General*, 2001, **221**, 227-239.
8. O. Nagashima, S. Sato, R. Takahashi and T. Sodesawa, *Journal of Molecular Catalysis A: Chemical*, 2005, **227**, 231-239.
9. A. D. Murkute, J. E. Jackson and D. J. Miller, *Journal of Catalysis*, 2011, **278**, 189-199.
10. C. A. Gaertner, J. C. Serrano-Ruiz, D. J. Braden and J. A. Dumesic, *Journal of Catalysis*, 2009, **266**, 71-78.
11. H. Benaissa, P. N. Davey, Y. Z. Khimyak and I. V. Kozhevnikov, *Journal of Catalysis*, 2008, **253**, 244-252.
12. H. Benaissa, P. N. Davey, E. F. Kozhevnikova and I. V. Kozhevnikov, *Applied Catalysis A: General*, 2008, **351**, 88-92.

13. W. Stonkus, J. Yuskovets, L. Leite, M. Fleisher, K. Edolfa, I. Liepina, A. Mishnev and A. Shmidlers, *Russian Journal of General Chemistry*, 2011, **81**, 1523-1528.

14. O. Nagashima, S. Sato, R. Takahashi and T. Sodesawa, *Journal of Molecular Catalysis A: Chemical*, 2005, **227**, 231-239.

15. J. C. Kuriacose and R. Swaminathan, *Journal of Catalysis*, 1969, **14**, 348-354.

16. R. Pestman, A. van Duijne, J. A. Z. Pieterse and V. Ponec, *Journal of Molecular Catalysis. A, Chemical*, 1995, **103**, 175-180.

17. K. Parida and H. K. Mishra, *Journal of Molecular Catalysis A: Chemical*, 1999, **139**, 73-80.

18. M. Gliński and J. Kijeński, *Applied Catalysis A: General*, 2000, **190**, 87-91.

19. R. Pestman, R. M. Koster, J. A. Z. Pieterse and V. Ponec, *Journal of Catalysis*, 1997, **168**, 255-264.

20. R. Martinez, M. C. Huff and M. A. Barteau, *Journal of Catalysis*, 2004, **222**, 404-409.

21. R. P. E.J. Grootendorst, R. M. Koster, V. Ponec, *Journal of Catalysis*, 1994, **148**, 261.

22. M. A. Alotaibi, E. F. Kozhevnikova and I. V. Kozhevnikov, *Applied Catalysis A: General*, 2012, **447-448**, 32-40.

23. I. Díaz, E. Kokkoli, O. Terasaki and M. Tsapatsis, *Chemistry of Materials*, 2004, **16**, 5226-5232.

24. P. G. Blake, and . K. J. Hole, *Journal of the Chemical Society B: Physical Organic*, 1966, 577-579.

25. M. Gliński, A. Kozioł, D. Łomot and Z. Kaszkur, *Applied Catalysis A: General*, 2007, **323**, 77-85.

26. M. Gliński, J. Kijeński and A. Jakubowski, *Applied Catalysis A, General*, 1995, **128**, 209-217.

27. R. W. Snell and B. H. Shanks, *Applied Catalysis A: General*, 2013, **451**, 86-93.

28. H. Bayahia, E. Kozhevnikova and I. Kozhevnikov, *Chemical Communications*, 2013, **49**, 3842-3844.

29. G. P. Heitmann, G. Dahlhoff and W. F. Hölderich, *Journal of Catalysis*, 1999, **186**, 12-19.

30. S. Bordiga, P. Ugliengo, A. Damin, C. Lamberti, G. Spoto, A. Zecchina, G. Spanò, R. Buzzoni, L. Dalloro and F. Rivetti, *Topics in Catalysis*, 2001, **15**, 43-52.

31. K. Barbera, F. Bonino, S. Bordiga, T. V. W. Janssens and P. Beato, *Journal of Catalysis*, 2011, **280**, 196-205.

32. T. Bucko, L. Benco and J. Hafner, Editon edn., 2005, vol. 158 A, pp. 601-608.

33. R. Pestman, R. M. Koster, A. van Duijne, J. A. Z. Pieterse and V. Ponec, *Journal of Catalysis*, 1997, **168**, 265-272.

34. T. N. Pham, T. Sooknoi, S. P. Crossley and D. E. Resasco, *ACS Catalysis*, 2013, **3**, 2456-2473.

Chapter 5

Ketonisation of carboxylic acids in the gas phase over Zn-Cr oxide catalyst

5.1 Introduction

The ketonisation of carboxylic acids plays an important role in the conversion of biomass by achieving partial deoxygenation, accompanied by carbon backbone upgrade.[1-6] Ketonisation of carboxylic acids, also known as ketonic decarboxylation, is a reaction which converts low carboxylic acid molecules into a ketone, carbon dioxide and water (Equation 5.1), is widely employed as a clean method for the synthesis of ketones, without any polluting by-products.[7, 8] This reaction has been known since 1858, when it was used to produce acetone by decomposing calcium acetate,[8] and in 1895 solid catalysts were used in the ketonisation of acetic acid as a direct reaction.[9] Recently, it has been catalysed by many basic and acidic metal oxides, mixed oxides[7, 9, 10] and zeolites,[11, 12] because it has promising applications in biomass conversion and in industrial processes.[8] Following its industrial application in the production of acetone, this reaction has gained increased interest for the upgrading of biomass-derived oxygenates, e.g. bio-oils obtained from fast pyrolysis of biomass containing lower carboxylic acids amongst other oxygenated molecules. Gas-phase ketonisation is catalysed by many oxides and mixed oxides, as well as zeolites and heteropoly acids in the temperature range of 250-500 °C,[7-10, 12-17] but the nature of catalytically active sites and reaction mechanism are not yet clear.

Among the oxides that have been used in the ketonisation of carboxylic acids are MnO_2,[18] Cr_2O_3,[19-22] ZrO_2, PbO_2, ZnO,[19] CeO_2,[14] TiO_2,[23] SiO_2[11, 18] and Al_2O_3.[19, 24]

Mn_2O_3-CeO_2 and ZrO_2-CeO_2 have also been found to have high activity at 350-450 °C.[25] Silicalite is an active catalyst at higher temperatures (Chapter 4). Pham *et al.*[26] reported that Ru/TiO_2 is a promising catalyst of the aqueous phase ketonisation of carboxylic acids, its activity being enhanced by reduction of the catalyst.

Here, we report that Zn^{II}-Cr^{III} mixed oxides prepared by co-precipitation of Zn^{II} and Cr^{III} hydroxides are highly active and durable catalysts of the ketonisation of carboxylic (acetic, propionic and pentanoic) acids in the gas phase to yield acetone and 3-pentanone, respectively, which are widely used as solvent and starting reagents for organic synthesis. Previously, Zn-Cr oxides have been used to catalyse various reactions such as the synthesis of methanol from the synthesis gas,[27] fluorination of hydrocarbons with HF, dehydrogenation of alcohols, hydrogenation of carboxylic acids and dehydroisomerisation of alpha-pinene to paracymene ([28, 29]and references therein). Pd/Zn-Cr has been reported as a bifunctional catalyst of the synthesis of methyl isobutyl ketone.[28] To our knowledge, Zn-Cr oxides have not so far been reported as catalysts of acid ketonisation so far.

$$2\ RCOOH \longrightarrow R_2CO + CO_2 + H_2O \qquad (5.1)$$

5.2 Catalyst testing

The gas-phase ketonisation of carboxylic acids was performed in flowing N_2 at 300-400 °C under atmospheric pressure in a downflow quartz fixed-bed reactor. The reactor was packed with 0.2 g catalyst powder of 45-180 μm particle size. Typically, the reaction was carried out at a carboxylic acid concentration of 2 vol% and an N_2 flow rate of 20 ml min^{-1}. Prior to reaction, the catalysts were heated at the reaction temperature in N_2 flow for 1 h. Once the reaction had started, the downstream gas flow was analysed by

the online GC to obtain reactant conversion and product selectivity as discussed in Chapter 2 section 2.5. The selectivity was defined as the percentage of carboxylic acid converted into a particular product taking into account the reaction stoichiometry; thus 100% ketene selectivity would mean 1 mol of carboxylic acid converted to form 0.5 mol of ketone. CO and CO_2 were not quantified and not included in reaction selectivities. The mean absolute percentage error in conversion and selectivity was ≤ 10% and the carbon balance was maintained within 95%.

5.3 Catalyst performance

5.3.1 Bulk Zn-Cr oxides

Bulk catalysts were tested in the ketonisation of acetic and propionic acids in the gas phase under the same conditions. In this case, the reaction was carried out in a range of temperatures and under N_2 flow, while the amount of catalyst was held constant at 0.2 g. The reaction was first tested for at least 4 h TOS, then the optimum catalyst was tested for a longer time under different temperature conditions. From the results it can be seen that both Zn-Cr ratio and temperature affected these ketonisation reactions. This section reports the selection of the best Zn-Cr ratio and the best catalytic activity at a suitable temperature for the long-term reaction, which was run for at least 18 h TOS.

The texture of the catalysts studied is summarised in Table 5.1. The Zn-Cr, ZnO and Cr_2O_3 oxides had Lewis acid sites. However, Zn-Cr (10:1) and Cr_2O_3 had also a small number of Brønsted acid sites. The acid strength of Zn-Cr oxide catalysts increased significantly with increasing the Cr content, with the ΔH values varying from -127 to -193 kJ mol^{-1}, which mostly represent strength of Lewis acid sites in Zn-Cr oxides. The Zn-Cr (1:10) oxide have an intermediate acid strength of ΔH = -150 kJ mol^{-1}. Catalyst characterisation results are presented in Chapter 3 in detail.

Table 5.1 Catalyst characterisation

Catalyst[a]	S_{BET}[b] ($m^2\ g^{-1}$)	Pore volume[c] ($cm^3\ g^{-1}$)	Pore size[d] (Å)
Cr_2O_3	243	0.26	42
Zn-Cr (1:6)	230	0.32	55
Zn-Cr (1:1)	136	0.11	32
Zn-Cr (3:1)	101	0.10	56
Zn-Cr (10:1)	43	0.10	90
Zn-Cr (20:1)	13	0.03	87
Zn-Cr (30:1)	10	0.02	86
ZnO	12	0.03	98

[a] Bulk oxides calcined at 300 ^oC under N_2 for 5 h.

[b] BET surface area.

[c] Single point total pore volume.

[d] Average BET pore diameter.

5.3.1.1 Gas-phase ketonisation of acetic acid

This subsection first reports experiments to test the effect of Zn-Cr ratio on the ketonisation of acetic acid, then the effect of temperature on both the conversion of acetic acid and the selectivity of acetone.

5.3.1.1.1 The effect of Zn-Cr ratio

Representative results obtained for the gas-phase ketonisation of acetic acid to acetone over bulk Zn-Cr oxides at 350 °C are shown in Table 5.2. It can be seen that catalyst performance depended crucially on the Zn/Cr atomic ratio. Most interestingly, Zn-Cr mixed oxides showed significantly higher catalytic activities than either of the pure parent ZnO and Cr_2O_3 oxides, with Zn-Cr (10:1) oxide being the most active one. The addition of Zn to Cr enhanced the activity of the catalyst.

Table 5.2 Ketonisation of acetic acid over bulk Zn-Cr oxide catalysts[a]

Catalyst	Temperature (°C)	Conversion (%)	Selectivity (%)	
			Acetone	Others[b]
ZnO	350	4	100	0
Zn-Cr (30:1)	350	11	100	0
Zn-Cr (20:1)	350	33	100	0
Zn-Cr (10:1)	350	86	100	0
Zn-Cr (3:1)	350	69	99	1
Zn-Cr (1:1)	350	50	99	1
Cr_2O_3	350	10	100	0

[a] 1 bar pressure, 0.2 g catalyst, 20 ml min^{-1} N_2 flow rate, 2 vol% acetic acid, 4 h time on stream.

[b] Other products: methane, ethane and ethene; CO and CO_2 not included.

At 350 °C the catalyst gave a very good acetone yield of 86% with 100% selectivity of acetone (average for 4 h TOS). This effect is similar to that observed with chromium-zinc-manganese oxide at 325 °C, modified zirconia at 355 °C and Mg/Al hydrotalcite catalysts which were tested at 275 to 425 °C, as reported by Stonkus *et al.*[30] and Parida *et al.*[31, 32] respectively.

5.3.1.1.2 The effect of temperature

Zn-Cr (10:1) was chosen as the optimum catalyst from the above results and the effect of temperature studied in the range of 300-400 °C. It was found that catalyst activity increased as the reaction temperature increased (Table 5.3). At 300 °C, only 16% of acetic acid was converted and selectivity was 100%. At 350 °C, conversion increased sharply to 86%, while selectivity remained at 100%. Conversion increased again to 99% at 380 °C, but selectivity now fell slightly to 95%. When the temperature was increased further to 400 °C, conversion reached 100% and selectivity again dropped slightly to

93%, with 7% of hydrocarbons (C_1 and C_2) formed. Thus, the results obtained at 380 °C were slightly better than at 400 °C.

At the optimum temperature of 380 °C, Zn-Cr (10:1) oxide gave 95% selectivity of acetone at 99% acetic acid conversion (i.e. 94% yield). Methane, ethane and ethene were formed as by-products, in addition to CO and CO_2, which were not monitored. A small decrease in selectivity was evident at 400 °C and may have resulted from coke deposition on the catalyst surface.[12]

Table 5.3 Ketonisation of acetic acid over bulk Zn-Cr (10:1) oxide catalyst[a]

Catalyst	Temperature (°C)	Conversion (%)	Selectivity (%)	
			Acetone	Others[b]
Zn-Cr (10:1)	300	16	100	0
Zn-Cr (10:1)	350	86	100	0
Zn-Cr (10:1)	380	99	95	4
Zn-Cr (10:1)	400	100	93	7

[a] 1 bar pressure, 0.2 g catalyst, 20 ml min^{-1} N_2 flow rate, 2 vol% acetic acid, 4 h TOS.

[b] Other products: methane, ethane and ethene; CO and CO_2 not included.

5.3.1.2 Gas-phase ketonisation of propionic acid

5.3.1.2.1 The effect of Zn-Cr ratio

Preliminary investigations with variable reaction parameters were carried out in order to obtain optimum conditions and the best Zn-Cr oxide catalyst for the ketonisation of propionic acid. The reaction was carried out at 330 °C under 20 ml min^{-1} N_2 for 4 h TOS, catalysed by pure zinc and pure chromium oxides and a series of Zn/Cr oxides (Table 5.4). The blank reaction was also tested and showed no pyrolysis of acid at 330 ^{o}C. The pure oxide catalysts were found to be highly selective, giving 100% selectivity for 3-pentanone, but much less reactive than mixed oxides; in other words, the conversion of

acid was enhanced by adding zinc to chromium. Zn-Cr (1:1) gave 48% conversion of propionic acid, but selectivity was only 81% and the yield 39%, whereas Zn-Cr (10:1) showed 45% of conversion and 98% 3-pentanone selectivity, i.e. a 44% yield. The finding that Zn-Cr (10:1) gave better results than pure zinc or chromium oxides and than Zn-Cr (20:1) or Zn-Cr (30:1) is consistent with the results reported by Nagashima *et al.*[14], who tested the performance of ceria mixed with other metal oxides such as Mg, Cr, Mn, Co, Ni, Cu, Zr, Fe and Al. The ketonisation of propionic acid to form 3-pentanone was carried out at 300-450 °C and 2.00 cm^3 h^{-1} flow rate of liquid feed, revealing that CeO_2-Mn_2O_3 was the most active catalyst.

Table 5.4 Gas phase ketonisation of propionic acid over zinc, chromium and mixed-oxide catalysts[a]

Catalyst	Conversion (%)	Selectivity (%)	
		3-Pentanone	Others[b]
none	0	0	0
ZnO	5	100	0
Zn-Cr (30:1)	21	100	0
Zn-Cr (20:1)	31	96	4
Zn-Cr (10:1)	45	98	2
Zn-Cr (1:1)	48	81	9
Zn-Cr (1:6)	6	89	11
Cr_2O_3	3	100	0

[a] 1 bar pressure, 330 ^oC, 0.2 g catalyst, 2 vol% propionic acid in N_2 flow, 20 ml min^{-1} flow rate, 4 h TOS.

[b] Other products: C_1-C_3 alkanes and alkenes, 2-propanol; CO and CO_2 not included.

5.3.1.2.2 The effect of temperature

As Zn-Cr (10:1) was found to be the optimum catalyst for the ketonisation of propionic acid in the gas phase, among those listed in Table 5.4, its performance was next tested

under the same conditions but at a range of reaction temperatures from 350 to 400 °C. For comparison, Zn-Cr (20:1) and Zn-Cr (30:1) were also tested at 350 °C and 400 °C (Table 5.5). Generally, the results show that increasing the temperature led to an increase in the conversion of propionic acid, but a reduction in the selectivity of 3-pentanone was observed, as previously reported. At 350 °C, Zn-Cr (10:1) showed 70% of acid conversion, compared with only 33% and 53% respectively for Zn-Cr (20:1) and Zn-Cr (30:1). Again, the performance of Zn-Cr (10:1) mixed oxide was best at 380 °C, where it gave 93% selectivity to 3-pentanone at 98% propionic acid conversion (i.e. 92% yield), with C_1-C_3 alkanes and alkenes and 2-propanol formed as by-products probably by decarbonylation and decarboxylation of propionic acid and acid-catalysed cracking of 3-pentanone. Table 5.5 shows clearly that conversion increased with temperature, reaching 97% at 400 °C over Zn-Cr (10:1), but selectivity decreased to 88% at this temperature. Similar results were obtained for Zn-Cr (30:1).

Table 5.5 Effect of temperature on the gas phase ketonisation of propionic acid over mixed zinc-chromium oxides[a]

Catalyst	Temp. (°C)	Conversion (%)	Selectivity (%)			
			3-Pentanone	C_1-C_3 alkane	C_2-C_3 alkene	Others[b]
Zn-Cr (10:1)	350	70	100	0	0	0
Zn-Cr (10:1)	380	98	94	0	0	6
Zn-Cr (10:1)	400	97	88	2	4	6
Zn-Cr (20:1)	350	33	100	0	0	0
Zn-Cr (20:1)	400	87	82	0	1	17
Zn-Cr (30:1)	350	53	97	0	0	3
Zn-Cr (30:1)	400	90	83	0	0	17

[a] 0.2 g catalyst, 2 vol% propionic acid in N_2 flow, 20 ml min^{-1} flow rate, 4 h TOS.

[b] Other products: C_1-C_3 alkanes and alkenes, 2-propanol; CO and CO_2 not included.

5.3.1.2.3 Stability of Zn-Cr (10:1) in the gas-phase ketonisation of propionic acid

Catalyst stability in propionic acid ketonisation was studied at the following reaction conditions: 2 vol% propionic acid, 0.2 g of bulk Zn-Cr (10:1) oxide, 20 ml min^{-1} N_2, 18 h TOS and 380 °C. The catalyst exhibited excellent stability in the formation of the main product, 3-pentanone, with the formation of some isopropanol, light hydrocarbons (C1-C3 alkanes and alkenes) as Figure 5.1 shows. These results show stable catalyst performance for at least 18 h TOS with only a small drift in conversion from 98 to 95% at a constant 3-pentanone selectivity 93-95%. The coke deposition on Zn-Cr (10:1) spent catalyst amounted to 4.10 wt% as have been presented in section 3.8, Table 3.8.

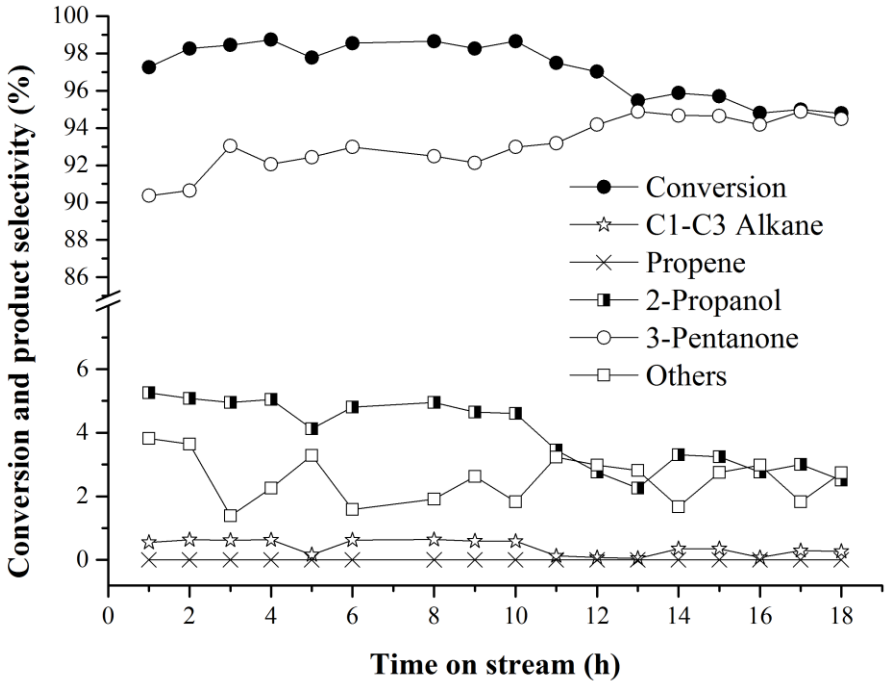

Figure 5.1 Propionic acid conversion and product selectivity over bulk Zn-Cr (10:1) versus time on stream (0.2 g of catalyst, 380 °C, 1 bar pressure, 20 mL min^{-1} N_2 flow rate, 2 vol% propionic acid).

5.3.1.3 Gas-phase ketonisation of pentanoic acid

Several authors report the production of 5-nonanone from both levulinic and pentanoic acids using heterogeneous catalysts such as Ru/C with Pd/Nb_2O_5, and supported metal oxides.[33-35] CeO_2/Al_2O_3 and MnO_2/Al_2O_3 were active catalysts in the ketonisation of pentanoic acid in the gas phase, achieving 80-94% conversion and ≥ 94% selectivity.[36] The ketone 5-nonanone has been found very useful in many applications, including the manufacture of detergents, paints and cosmetics.[35]

Here, in addition to acetic and propionic acids, the ketonisation of pentanoic acid was tested using 0.2 g of bulk Zn-Cr (10:1) oxide in the temperature range of 350-400 °C, at 20 ml min^{-1} of N_2 flow. Figure 5.2 shows that as the temperature increased, conversion also increased but selectivity decreased. At 350 °C, 5-nonanone selectivity was 66%, dropping sharply to 18% at 400 °C. By comparison, ZrO_2 calcined at 450-500 °C in air gave 66-65% 5-nonanone yields at 355 °C; when 10 wt% of CeO_2 was added to the ZrO_2 catalyst, then calcined at 450 °C, yield of 5-nonaone was found to improve to 73 % at 355 °C.[35]

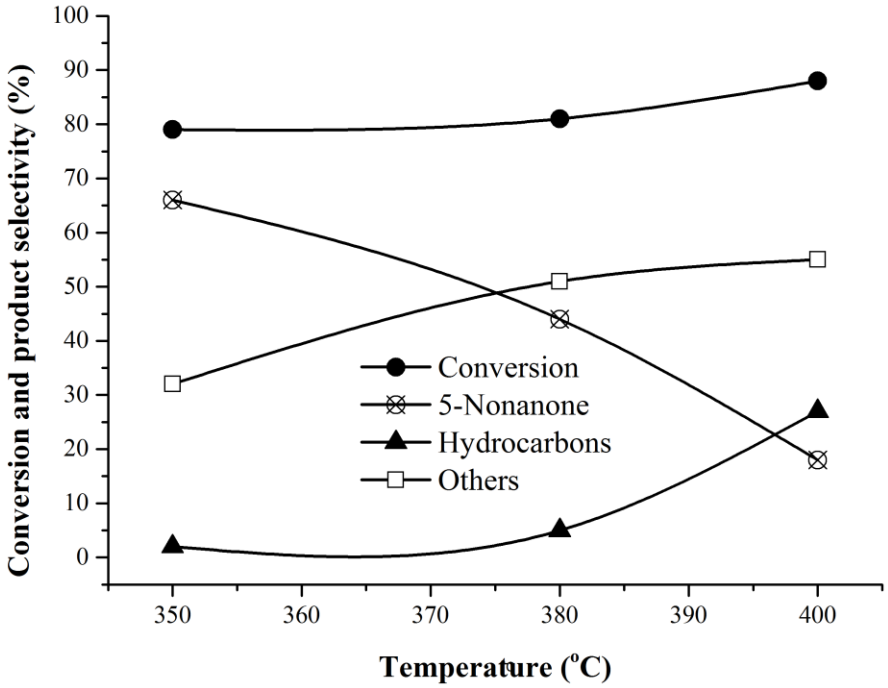

Figure 5.2 Ketonisation of pentanoic acid over 0.2 Zn-Cr (10:1), 2 vol%, 20 ml min^{-1} N_2.

5.3.2 Performance of supported catalysts

5.3.2.1 Ketonisation of propionic acid catalysed over SiO_2, Al_2O_3 and TiO_2

In the search for better catalytic performance, Zn-Cr (10:1), which showed the best results in the ketonisation reaction, was supported on SiO_2, Al_2O_3 and TiO_2. These supports possessing considerable Brønsted and Lewis acidity were themselves found active in this reaction and hence contributed to the catalyst activity observed. These materials were themselves first tested for their catalytic activity. The results in Table 5.6 show that they were all active as catalysts in the ketonisation of propionic acid. As the temperature was increased, conversion also increased. However, the selectivity of 3-pentanone decreased. SiO_2 gave no reaction at 350 or 380 °C, although it has been found active at higher temperatures (Chapter 4), while Al_2O_3 and TiO_2 showed good

catalytic activity at 380 and 400 °C. TiO_2 gave 99% of propionic acid conversion, but the selectivity of 3-pentanone dropped sharply to 40% at 400 °C.

TiO_2 catalyst showed moderate activity at higher temperatures 350-400 ^oC. However, this catalyst gave only 60% selectivity to 3-pentanone at 380 ^oC. In contrast, Zn-Cr (10:1) gave 94% 3-pentanone selectivity at 98 % conversion of propionic acid. At lower temperature 330 ^oC, Zn-Cr (10:1) was still active, whereas TiO_2 was practically inactive.

Table 5.6 Gas phase ketonisation of propionic acid over SiO_2, Al_2O_3 and TiO_2[a]

Catalyst	Temperature (°C)	Conversion (%)	Selectivity (%)	
			3-Pentanone	Others[b]
SiO_2	350	0	0	0
SiO_2	380	0	0	0
SiO_2	400	23	90	10
Al_2O_3	350	22	98	2
Al_2O_3	380	61	98	2
Al_2O_3	400	93	73	27
TiO_2	350	98	78	22
TiO_2	380	99	60	40
TiO_2	400	99	40	60

[a] 1 bar pressure, 0.2 g catalyst, 20 ml min^{-1} N_2 flow rate, 2 vol% propionic acid, 4 h time on stream. [b] Other products: C_1-C_3 alkanes and alkenes, 2-propanol; CO and CO_2 not included.

5.3.2.2 Gas-phase ketonisation of propionic acid over supported Zn-Cr (10:1)

Supporting Zn-Cr (10:1) oxide on γ-Al_2O_3 and TiO_2 was found to further improve its performance in propionic acid ketonisation (Table 5.7), whereas silica-supported Zn-Cr (10:1) oxide exhibited only a moderate ketonisation activity, consistent with the poor results for SiO_2 noted above. The best results were obtained with 20%Zn-Cr

(10:1)/Al_2O_3 at 380 °C: 97% 3-pentanone selectivity at 99% propionic acid conversion (96% yield). This performance is considerably better than that obtained for the 20:80 w/w physical mixture of Zn-Cr (10:1) and Al_2O_3. The latter showed a conversion of 63%, close to the weighted sum of activities of Zn-Cr (10:1) and Al_2O_3 (Table 5.7). The enhanced catalytic activity of supported catalyst may be attributed to a higher dispersion of Zn-Cr oxide on the alumina surface. This is supported by our powder XRD data Chapter 3 section 3.5.2, Bulk Zn-Cr(10:1) oxide and 20%Zn-Cr(10:1)/Al_2O_3 calcined at 380 ^oC/5 h were found to have a ZnO particle size of 52±6 and 37±1 nm, respectively, which indicates a higher dispersion of the ZnO phase in the supported catalyst compared to the bulk one.

Table 5.7 Gas phase ketonisation of propionic acid over supported Zn-Cr (10:1) oxide catalysts[a]

Catalyst[a]	Temperature (°C)	Conversion (%)	Selectivity (%)	
			3-Pentanone	Others[b]
20% Zn-Cr(10:1)/SiO_2	350	12	100	0
20% Zn-Cr(10:1)/SiO_2	380	51	94	6
20% Zn-Cr(10:1) / SiO_2	400	56	90	10
20% Zn-Cr(10:1)/Al_2O_3	350	48	100	0
20% Zn-Cr(10:1)/Al_2O_3	380	99	97	3
Zn-Cr(10:1)+Al_2O_3(20:80)[c]	380	63	97	3
20% Zn-Cr(10:1)/Al_2O_3	400	99	90	10
20% Zn-Cr(10:1)/TiO_2	350	65	97	3
20% Zn-Cr(10:1)/TiO_2	380	97	94	6
20% Zn-Cr(10:1)/TiO_2	400	100	88	12

[a] 1 bar pressure, 0.2 g catalyst, 20 ml min^{-1} N_2 flow rate, 2 vol% propionic acid, 4 h time on stream.

[b] Other products: C_1-C_3 alkanes and alkenes, 2-propanol; CO and CO_2 not included.

[c] Zn-Cr(10:1) + Al_2O_3 (20:80 w/w physical mixture).

5.3.2.3 Stability of supported Zn-Cr (10:1) oxide in the gas-phase ketonisation of propionic acid

The 20%Zn-Cr (10:1)/Al_2O_3 catalyst exhibited stable performance for at least 24 h time on stream practically without catalyst deactivation, with conversion slightly drifting from 99 to 97% at a constant 3-pentanone selectivity of 94-95% (Figure 5.3). This small drift in conversion may be caused by catalyst coking: a small amount of coke was indeed found in the catalyst after this run (1.4% carbon content).

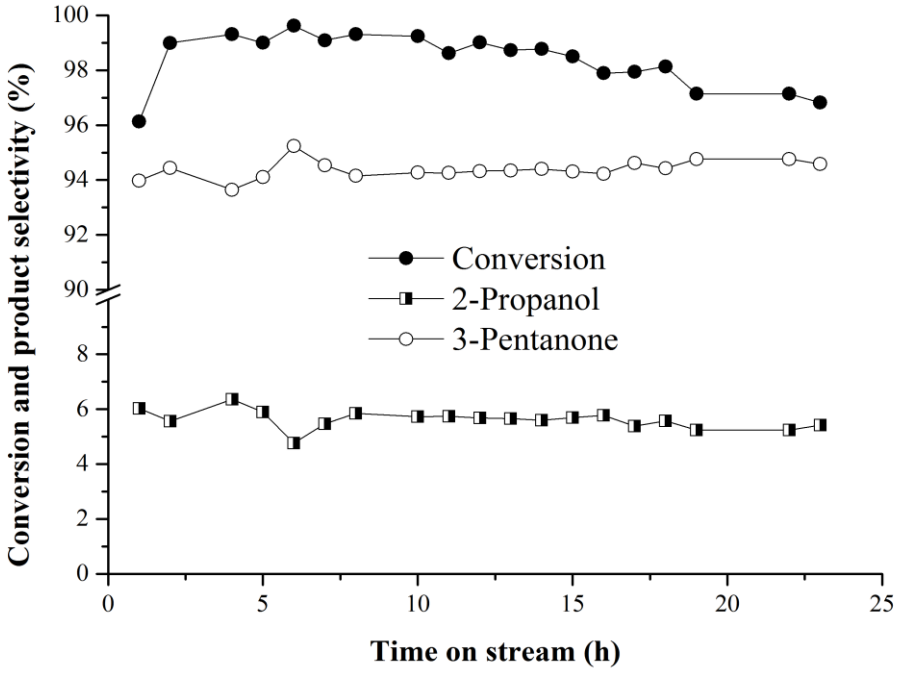

Figure 5.3 Propionic acid conversion and products selectivity versus time on stream (380 °C, 0.2 g of 20% Zn-Cr (10:1)/Al_2O_3, 20 ml min^{-1} N_2).

Both Bulk Zn-Cr (10:1) oxide and 20%Zn-Cr(10:1)/Al_2O_3 supported catalyst exhibited no any deactivation in the reaction at 350 ^oC at 72% and 44% conversion, respectively, and 100% 3-pentanone selectivity without any deactivation for at least 6 h on stream (Figure 5.4).

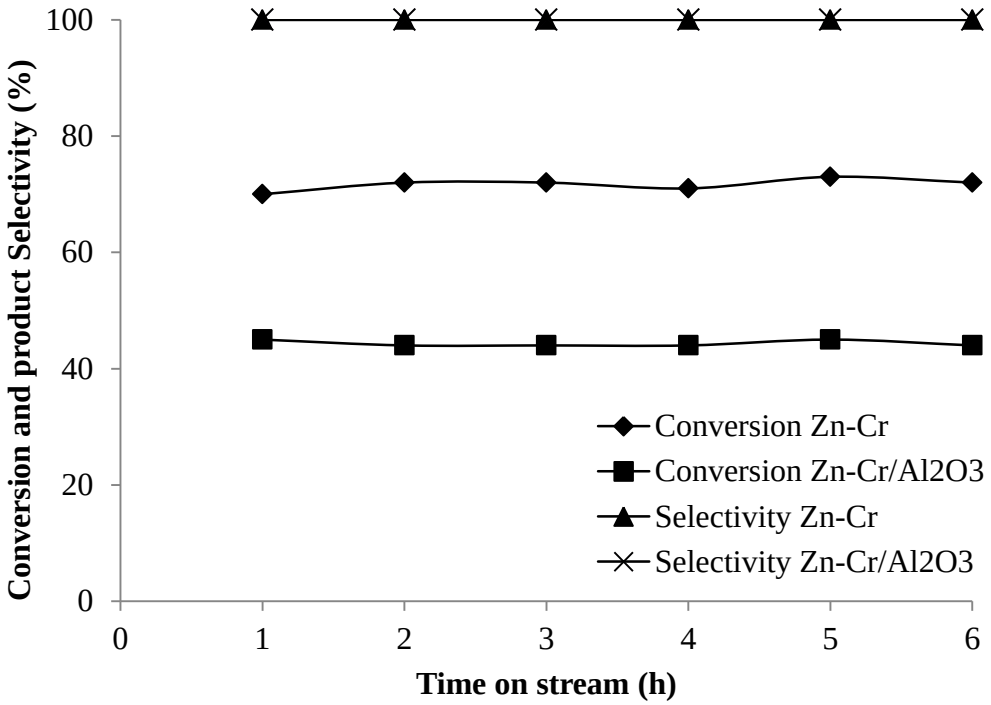

Figure 5.4 Time course for propionic acid ketonisation over bulk Zn-Cr(10:1) oxide and 20%Zn-Cr(10:1)/Al_2O_3 supported catalyst (350 ^oC, 1 bar pressure, 0.2 g catalyst, 20 mL min^{-1} N_2 flow rate, 2 vol% propionic acid).

It is generally difficult to compare the activity of catalysts reported by different groups due to different reaction conditions applied. Nevertheless, by the yield of 3-pentanone obtained, Zn-Cr (10:1) oxide is on a par with the best ketonisation catalysts reported so far,[7, 8] e.g., CeO_2-Mn_2O_3.[14] The CeO_2-Mn_2O_3 oxide has a higher catalytic activity than either of the parent CeO_2 and Mn_2O_3 oxides, with the highest activity at a Ce/Mn atomic ratio of 2:3 providing an average 3-pentanone yield of 84-90% over 5 h time on stream at 350-400 ^oC and W/F = 10 h g mol^{-1} for propionic acid.[14] The activity of CeO_2 and MnO_2 in ketonisation of acetic and propionic acids has been found to increase upon their loading (20%) on Al_2O_3,[18] similar to Zn-Cr oxide.

In related work reported in the literature, MnO_2/Al_2O_3 supported catalyst was studied in the ketonisation of heptanoic acid for 20 h TOS. Alumina was found to offer the most

pronounced augmentation of the catalytic activity, compared with other supports such as silica and zirconia.[37] In addition, when 20 wt% of CeO_2/SiO_2 was tested in the ketonisation of acetic acid for 15 h TOS, its performance was stable at 350 °C and 2 $cm^3\ g^{-1}\ h^{-1}$ of liquid hourly space velocity.[18] Mg catalyst supported on Al_2O_3 was tested in varying ratios and found to be active in the ketonisation of acetic acid in a gas phase fixed-bed reactor. The reaction was tested for 12.5 h TOS at 350 °C and the steady state was reached at 5 h TOS.[31]

5.4 Activation energy (E_a) for ketonisation of propionic acid

In this study, the activation energy of Zn-Cr(10:1) was calculated in the gas-phase ketonisation of propionic acid using a fixed-bed reactor, with 20 ml min^{-1} N_2 flow rate, 2 vol% concentration of propionic acid and 0.04 g of Zn-Cr (10:1) oxide catalyst diluted to 0.2 g by silica, Aerosil-300. The results are listed in Table 5.8 and the activation energy plot in Figure 5.5 shows that the apparent activation energy was 124 kJ mol^{-1} in the temperature range 300-320 °C (under differential conditions at propionic acid conversion $\leq$ 10%), which indicates that the reaction occurred under kinetic regime in this temperature range and probably above up to 380°C. This is also supported by the Weisz-Prater analysis[38] of the reaction system: Weisz-Prater criterion $C_{WP} = 1 \cdot 10^{-1} < 1$ indicating no internal diffusion limitations).

The conversion was kept below 10% to ensure differential conditions in the reactor. In differential mode, the reaction rate is proportional to the conversion, which allows conversion to be used instead of reaction rate in the Arrhenius equation. A conversion of less than 10% was achieved by reducing the amount of catalyst.

Table 5.8 Activation energy determination for gas-phase ketonisation of propionic acid to 3-pentanone over Zn-Cr (10:1)

Reaction temperature (ºC)	Propionic acid conversion (%)	1/T (K)	Ln (conversion)
300	2.91	0.001745	1.068
310	5.34	0.001715	1.675
320	6.99	0.001686	1.944

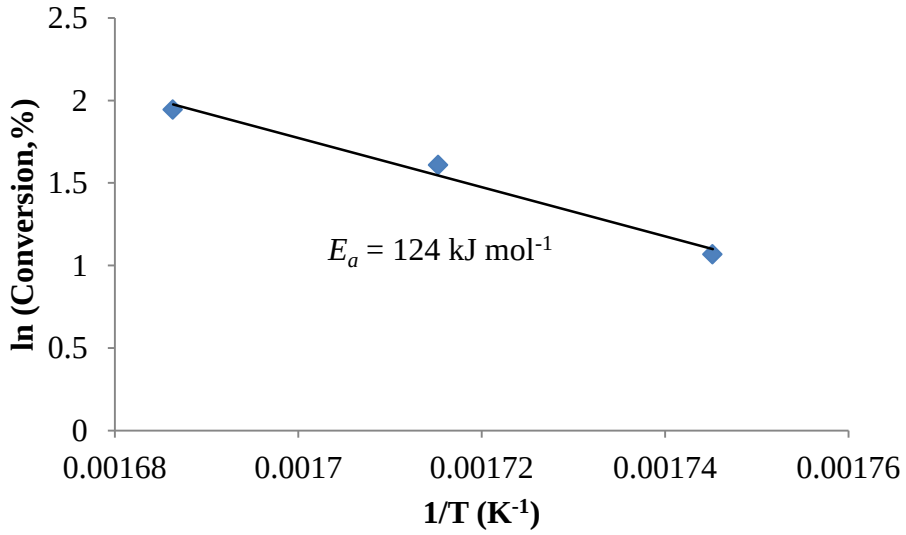

Figure 5.5 Arrhenius plot for ketonisation of propionic acid in the gas phase over Zn–Cr (10:1).

5.5 Ketonisation mechanism

Ketonisation occurs with carboxylic acids possessing α-hydrogen atoms at least in one of the reacting acid molecules.[7, 8] Several mechanisms have been proposed for this reaction.[7, 8] These include: (i) decomposition of metal carboxylate, (ii) via acid anhydride intermediate, (iii) via β-ketoacid intermediate and (iv) via ketene intermediate route (for a recent review, see[8]). It is thought that basic and amphoteric materials are favourable catalysts for ketonisation.[7, 8] However, heteropoly acid $H_3PW_{12}O_{40}$ possessing very strong proton sites and practically no bacisity has also been

found active in propionic acid ketonisation at 200-250 ^{o}C, probably occurring via the ketene intermediate route.[13] This suggests that the mechanism may depend on many factors, especially the type of catalyst used.

Numerous IR spectroscopic studies have dealt with carboxylic acid adsorption on metal oxides, e.g., TiO_2, Al_2O_3, CeO_2, SnO_2, and MgO.[39-42] There is compelling evidence that carboxylic acids adsorb dissociatively on a pair of the neighbouring Lewis acid and base sites on the metal oxide surface to form a metal carboxylate in monodentate, bidentate chelate or bidentate bridging bonding mode.

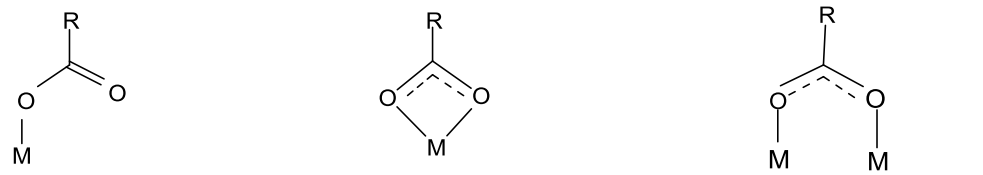

monodentate bidentate chelate bidentate bridging bonding

DFT analysis[40] shows that for adsorption of formic, acetic and propionic acids on metal oxides the bridging mode is more likely (Scheme 5.1), and such surface species have been suggested as possible intermediates for ketonisation of carboxylic acids.[39, 43]

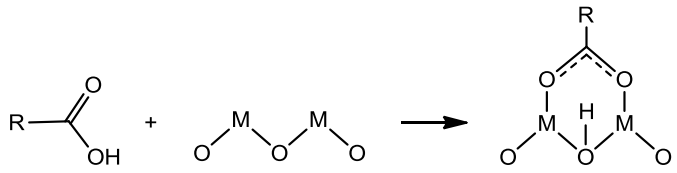

Scheme 5.1 Dissociative adsorption of carboxylic acid on a metal oxide.

Figure 5.6 shows the DRIFT spectrum of acetic acid adsorbed on Zn-Cr (10:1) oxide measured in the absence of acetic acid in the gas phase after evacuation at 160 ^{o}C. This spectrum is similar to those reported previously for other metal oxides.[39-42] The absence

of a peak characteristic of the C=O stretch in the region of 1690-1790 cm^{-1} clearly shows that there is no physisorbed acetic acid present. The peaks at 1424 and 1351 cm^{-1} can be assigned to C-H deformations. The bands at 1553 and 1462 cm^{-1} can be attributed to the antisymmetric and symmetric vibrations of the OCO group of acetate,[39-42] which indicates the bridging mode for acetate bonding (Scheme 5.1).[40]

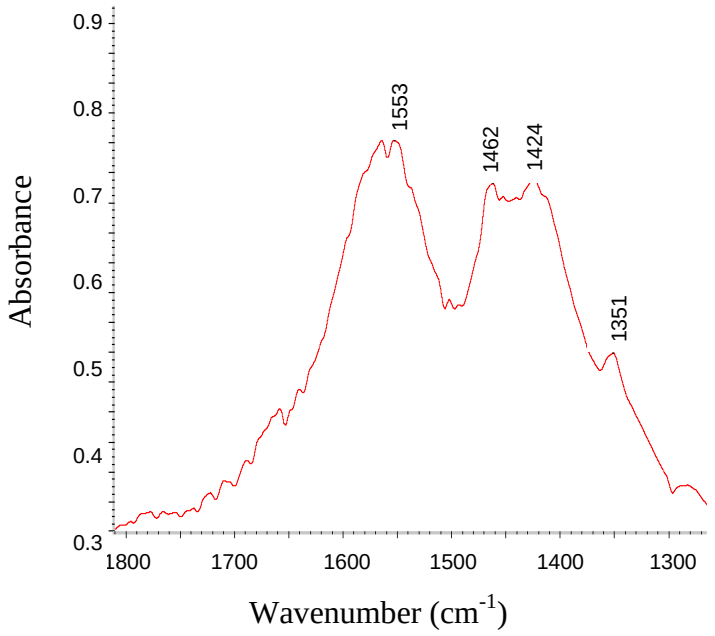

Figure 5.6 DRIFT spectrum of acetic acid adsorbed on Zn-Cr (10:1) oxide after evacuation at 160 $^{o}C/10^{-5}$ bar for 1 h.

It is conceivable that over Zn-Cr oxides ketonisation occurs via the β-ketoacid intermediate route (Scheme 5.2), which is considered favourable for amphoteric oxides.[8] This reaction pathway probably involves dissociative adsorption of a carboxylic acid molecule on the neighbouring Lewis acid and base sites of Zn-Cr oxide followed by non-dissociative adsorption of another acid molecule on adjacent Lewis acid site. Abstraction of α-hydrogen and C-C bond formation lead to the β-ketoacid intermediate. The latter is decarboxylated to yield ketone together with CO_2 and H_2O.

The formation of C-C bond may be the rate-limiting step, as found for ketonisation of acetic, propionic and butyric acids over Ru/TiO_2.[43] The higher catalytic activity of Zn-Cr oxide as compared to ZnO and Cr_2O_3 may be explained by more efficient activation of acid molecule when it bridges different metal sites.

Ketonisation over redox active CeO_2-Mn_2O_3 oxide has been proposed to occur via the β-ketoacid route involving a redox cycle.[14] This mechanism involves dissociative adsorption of acid molecules to form surface carboxylates, abstraction of α-hydrogen atom from surface carboxylate to form an anion radical and its addition to another carboxylate to produce β-ketoacid followed by decarboxylation to yield ketone. The surface metal in oxide may be reduced by the abstracted α-hydrogen atom and re-oxidised by the desorbed hydroxyl radical. Such redox cycle, however, is unlikely for the Zn-Cr oxide which lacks any significant redox ability.

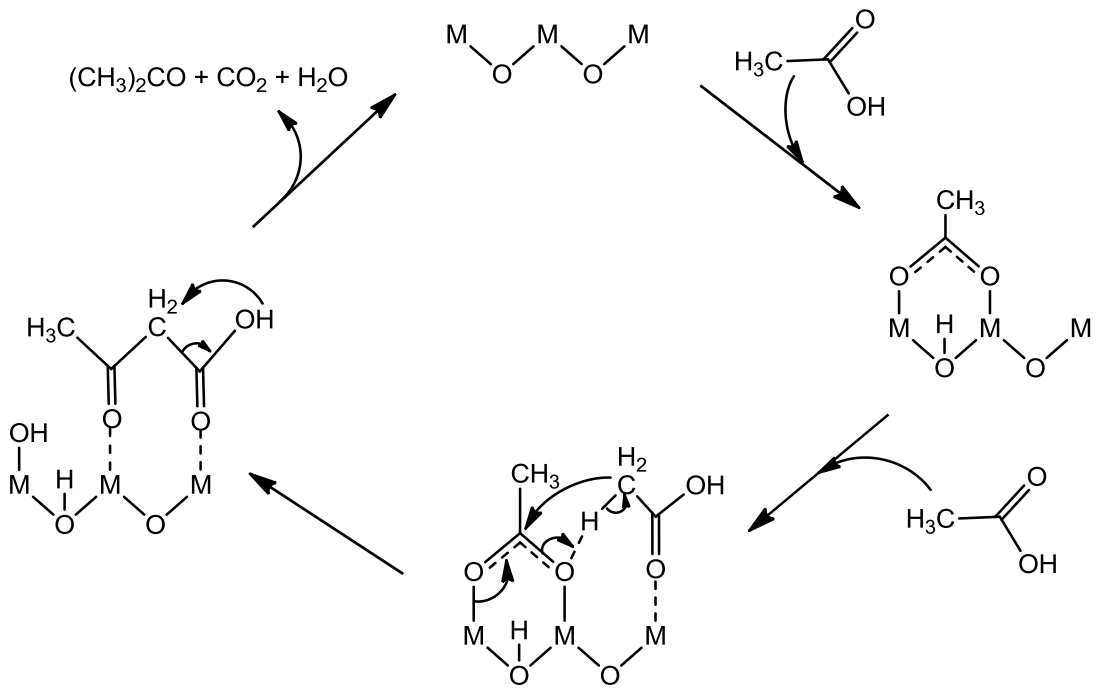

Scheme 5.2 Proposed mechanism for ketonisation of carboxylic acids via β-ketoacid intermediate route.

5.6 Conclusions

In this work, we have demonstrated that bulk Zn-Cr mixed oxides with a Zn/Cr atomic ratio of 1:1 to 20:1, prepared by co-precipitation of Zn^{II} and Cr^{III} hydroxides, are active and durable catalysts for the gas-phase ketonisation of carboxylic (acetic and propionic) acids at 300-400 °C and ambient pressure. Amongst them, Zn-Cr (10:1) oxide shows the best performance. In contrast, the parent oxides ZnO and Cr_2O_3 exhibit a poor ketonisation activity. Supporting the Zn-Cr oxide on TiO_2 or γ-Al_2O_3 enhances its catalytic activity. The 20%Zn-Cr/Al_2O_3 catalyst gives 97% selectivity to 3-pentanone at 99% conversion of propionic acid at 380 °C, without any observed catalyst deactivation during at least 24 h TOS. Zn-Cr oxides have been characterised by BET, XRD, DRIFTS of ammonia adsorption and microcalorimetry of ammonia adsorption. Zn-Cr (10:1) oxide possesses Brønsted and Lewis acidity with a ratio of acid site densities B/L = 0.07 and a differential enthalpy of ammonia adsorption ΔH = -150 kJ/mol. The high ketonisation efficiency of Zn-Cr (10:1) oxide may be ascribed to an appropriate combination of its acid-base properties.

5.7 References

1. A. Corma Canos, S. Iborra and A. Velty, *Chemical Reviews*, 2007, **107**, 2411-2502.
2. E. L. Kunkes, D. A. Simonetti, R. M. West, J. C. Serrano-Ruiz, C. A. Gärtner and J. A. Dumesic, *Science*, 2008, **322**, 417-421.
3. M. Snåre, I. Kubičková, P. Mäki-Arvela, K. Eränen and D. Y. Murzin, *Industrial and Engineering Chemistry Research*, 2006, **45**, 5708-5715.
4. H. Bernas, K. Eränen, I. Simakova, A. R. Leino, K. Kordás, J. Myllyoja, P. Mäki-Arvela, T. Salmi and D. Y. Murzin, *Fuel*, 2010, **89**, 2033-2039.
5. P. T. Do, M. Chiappero, L. L. Lobban and D. E. Resasco, *Catalysis letters*, 2009, **130**, 9-18.
6. J. G. Immer, M. J. Kelly and H. H. Lamb, *Applied Catalysis A: General*, 2010, **375**, 134-139.
7. M. Renz, *European Journal of Organic Chemistry*, 2005, 979-988.
8. T. N. Pham, T. Sooknoi, S. P. Crossley and D. E. Resasco, *ACS Catalysis*, 2013, **3**, 2456-2473.
9. A. D. Murkute, J. E. Jackson and D. J. Miller, *Journal of Catalysis*, 2011, **278**, 189-199.
10. T. Yokoyama and N. Yamagata, *Applied Catalysis A: General*, 2001, **221**, 227-239.
11. J. A. Martens, M. Wydoodt, P. Espeel and P. A. Jacobs, Editon edn., 1993, vol. 78, pp. 527-534.
12. H. Bayahia, E. Kozhevnikova and I. Kozhevnikov, *Chemical Communications*, 2013, **49**, 3842-3844.

13. M. A. Alotaibi, E. F. Kozhevnikova and I. V. Kozhevnikov, *Applied Catalysis A: General*, 2012, **447-448**, 32-40.

14. O. Nagashima, S. Sato, R. Takahashi and T. Sodesawa, *Journal of Molecular Catalysis A: Chemical*, 2005, **227**, 231-239.

15. C. A. Gaertner, J. C. Serrano-Ruiz, D. J. Braden and J. A. Dumesic, *Industrial and Engineering Chemistry Research*, 2010, **49**, 6027-6033.

16. H. Benaissa, P. N. Davey, Y. Z. Khimyak and I. V. Kozhevnikov, *Journal of Catalysis*, 2008, **253**, 244-252.

17. H. Benaissa, P. N. Davey, E. F. Kozhevnikova and I. V. Kozhevnikov, *Applied Catalysis A: General*, 2008, **351**, 88-92.

18. M. Gliński, J. Kijeński and A. Jakubowski, *Applied Catalysis A, General*, 1995, **128**, 209-217.

19. R. Pestman, R. M. Koster, A. van Duijne, J. A. Z. Pieterse and V. Ponec, *Journal of Catalysis*, 1997, **168**, 265-272.

20. R. Pestman, R. M. Koster, J. A. Z. Pieterse and V. Ponec, *Journal of Catalysis*, 1997, **168**, 255-264.

21. J. C. Kuriacose and R. Swaminathan, *Journal of Catalysis*, 1969, **14**, 348-354.

22. J. C. Kuriacose and R. Swaminathan, *Journal of Catalysis*, 1969, **14**, 348-354.

23. R. Martinez, M. C. Huff and M. A. Barteau, *Journal of Catalysis*, 2004, **222**, 404-409.

24. R. Pestman, A. van Duijne, J. A. Z. Pieterse and V. Ponec, *Journal of Molecular Catalysis. A, Chemical*, 1995, **103**, 175-180.

25. C. Liu, A. Karim, V. Lebarbier, D. Mei and Y. Wang, *Topics in Catalysis*, 2013, **56**, 1782-1789.

26. T. Pham, D. Shi and D. Resasco, *Topics in Catalysis*, 2014, **57**, 706-714.

27. M. C. J. Bradford, M. V. Konduru and D. X. Fuentes, *Fuel Processing Technology*, 2003, **83**, 11-25.

28. F. Al-Wadaani, E. F. Kozhevnikova and I. V. Kozhevnikov, *Journal of Catalysis*, 2008, **257**, 199-205.

29. F. Al-Wadaani, E. F. Kozhevnikova and I. V. Kozhevnikov, *Applied Catalysis A: General*, 2009, **363**, 153-156.

30. W. Stonkus, J. Yuskovets, L. Leite, M. Fleisher, K. Edolfa, I. Liepina, A. Mishnev and A. Shmidlers, *Russian Journal of General Chemistry*, 2011, **81**, 1523-1528.

31. K. Parida and J. Das, *Journal of Molecular Catalysis A: Chemical*, 2000, **151**, 185-192.

32. K. Parida and H. K. Mishra, *Journal of Molecular Catalysis A: Chemical*, 1999, **139**, 73-80.

33. A. D. Patel, J. C. Serrano-Ruiz, J. A. Dumesic and R. P. Anex, *Chemical Engineering Journal*, 2010, **160**, 311-321.

34. J. C. Serrano-Ruiz, D. Wang and J. A. Dumesic, *Green Chemistry*, 2010, **12**, 574-577.

35. A. A. Shutilov, M. N. Simonov, Y. A. Zaytseva, G. A. Zenkovets and I. L. Simakova, *Kinet Catal*, 2013, **54**, 184-192.

36. M. Gliński and J. Kijeński, *Reaction Kinetics and Catalysis Letters*, 2000, **69**, 123-128.

37. M. Gliński and J. Kijeński, *Applied Catalysis A: General*, 2000, **190**, 87-91.

38. P. B. Weisz and C. D. Prater, *Advances in Catalysis*, 6, 1954, 143-196.

39. M. A. Hasan, M. I. Zaki and L. Pasupulety, *Applied Catalysis A: General*, 2003, **243**, 81-92.

40. S. R. Tong, L. Y. Wu, M. F. Ge, W. G. Wang and Z. F. Pu, *Atmospheric Chemistry and Physics*, 2010, **10**, 7561-7574.

41. Z. F. Pei and V. Ponec, *Applied Surface Science*, 1996, **103**, 171-182.

42. L.-F. Liao, C.-F. Lien and J.-L. Lin, *Physical Chemistry Chemical Physics*, 2001, **3**, 3831-3837.

43. T. N. Pham, D. Shi and D. E. Resasco, *Journal of Catalysis*, 2014, **314**, 149-158.

Chapter 6

Metal oxide as active and recyclable catalysts for the synthesis of nopol by Prins condensation

6.1 Introduction

The development of sustainable chemical processes utilizing renewable raw materials is a major goal of academia and industry.[1, 2] In this context, terpenes are important feedstock for the perfumery, food and pharmaceutical industries.[3-5] Acid-catalysed transformations of terpenes, such as isomerisation, hydration, esterification and condensation, are widely employed for the industrial production of value-added terpenic compounds.[3-5] These reactions are often carried out as batch processes using large amounts of mineral acids as homogeneous catalysts, with moderate yields and an adverse impact on the environment. The challenge addressed in this chapter is the replacement of homogeneous acid catalysts with environmentally benign heterogeneous catalysts having the advantages of ease of recovery and suitability for continuous processing.

Nopol is an optically active bicyclic primary alcohol used in the agrochemical industry to produce pesticides and in soap fragrances, detergents and other household products due to its balsamic odour.[4] Nopol is generally produced by Prins condensation of β-pinene and paraformaldehyde (Equation 6.1) using homogeneous acid catalysts.[6] These methods, however, suffer from severe reaction conditions, low yields and unwanted side products. Several heterogeneous catalysts have been used to overcome these problems. These include mesoporous materials comprising Sn, Zn, Zr and Fe, zeolites, sulphated zirconia, Fe-Zn metal cyanides, $ZnCl_2$ supported on montmorillonite and Sn(OH)Cl ([7-12]

and references therein). Some of them provide high nopol yields and can be recycled, but are not easily available.

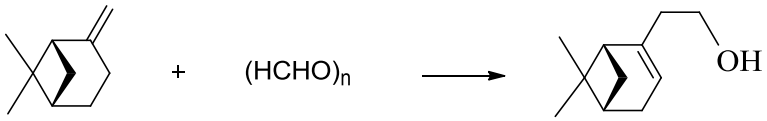

(6.1)

β-pinene paraformaldehyde nopol

In our group extensive search for efficient solid acid catalysts for terpene conversions,[13-18] we found that certain metal oxides were active heterogeneous catalysts for the synthesis of nopol. We now report that the readily available Zn(II)-Cr(III) mixed oxide is a highly efficient and recyclable catalyst for Prins condensation (Equation 6.1).* Previously, Zn-Cr oxide has been used to catalyse many reactions such as the synthesis of methanol, the fluorination of hydrocarbons with HF, dehydrogenation of alcohols, hydrogenation of carboxylic acids, dehydroisomerisation of α-pinene and synthesis of methyl isobutyl ketone ([19, 20] and references therein). To our knowledge, little research on the use of metal oxides as catalysts for the Prins reaction has been reported so far.[11]

6.2 Prins condensation by Zn-Cr mixed oxide catalysts

The Prins condensation reaction was carried out in a glass reactor equipped with a magnetic stirrer and reflux condenser. Typically, the reaction mixture contained 10 mmol paraformaldehyde, 5 mmol β-pinene, 5 ml acetonitrile solvent and 100 mg of catalyst, which was calcined at 300 °C under N_2 for 5 h and ground to 45-180 μm particle size.[19]

---

* This work was carried out in collaboration with Vinicius V. Costa, Federal Minas Gerais University, Brazil.

This mixture was placed in an oil bath preheated to the required temperature. After 6 h, when the reaction was complete, the mixture was cooled to room temperature.

The reaction products were then quantified by a GC equipped with flame ionisation detector, using the method detailed in Chapter 2.

The representative results of catalytic activity and the texture (surface area, pore volume and pore diameter) of Cr_2O_3, ZnO and Zn-Cr oxides catalysts studied are given in Table 6.1. The characterisation of theses catalysts has already been discussed in detail in section 3.2.3.

Table 6.1 Nopol synthesis catalysed by metal oxides at 80 °C[a]

Catalyst[b]	S_{BET}[c] (m^2g^{-1})	Pore vol[d] (cm^3g^{-1})	Pore size[e] (Å)	Conversion (%)	Selectivity (%)
Cr_2O_3	243	0.26	42.1	40	100
Zn-Cr(1:30)	223	0.16	29.0	23	100
Zn-Cr(1:10)	193	0.15	31.0	14	100
Zn-Cr(1:6)	230	0.32	55.3	42	100
Zn-Cr(1:1)	136	0.11	32.3	8	100
Zn-Cr(10:1)	43	0.10	90.3	3	100
Zn-Cr(20:1)	13	0.03	87.0	5	100
Zn-Cr(30:1)	10	0.02	86.1	2	100
ZnO	12	0.03	98.3	0	0

[a] Reaction conditions: 100 g catalyst, 10 mmol paraformaldehyde, 5 mmol β-pinene, 5 ml acetonitrile solvent, 6 h reaction time.

[b] Calcined at 300 °C under N_2 for 5 h and ground to 45-180 μm particle size.

[c] BET surface area.

[d] Single point total pore volume.

[e] Average BET pore diameter.

The reaction did not occur in the absence of catalyst. Four of the metal oxides tested, γ-Al_2O_3, ZrO_2, SiO_2 and TiO_2, showed only moderate catalytic activity (≤ 15% conversion), while Cr_2O_3 showed the best activity, with 100% nopol selectivity. The performance of this catalyst was improved by adding Zn(II) oxide to the Cr(III) oxide. Interestingly enough, the mixed Zn(II)-Cr(III) oxide with a Zn/Cr atomic ratio of 1:6 showed a better performance that pure Cr_2O_3, although Zn(II) oxide itself was practically inactive in reaction 6.1.

The synthetic protocol was further improved by increasing the amount of catalyst to 8 wt% of total reaction mixture and the paraformaldehyde/β-pinene molar ratio to 6:1, as well as by increasing the reaction time from 6 to 10 h. The Zn-Cr (1:6) mixed oxide that showed the best catalytic performance in nopol synthesis had surface area of 230 $m^2\ g^{-1}$, a pore volume of 0.32 cm^3g^{-1} and an average pore diameter of 55 Å. From XRD analysis, Zn-Cr (1:6) calcined at 300 ^oC was amorphous, but after calcination at 400 ^oC it exhibited the pattern of Cr_2O_3 phase, with a little of $ZnCr_2O_4$ spinel also presented. Zn-Cr (1:6) catalyst resulted in an excellent yield of nopol (97% β-pinene conversion at 100% nopol selectivity). It should be noted that pure Cr_2O_3 yielded 92% under the same conditions. For selective synthesis of nopol, the requirement of strong Lewis or weak Brønsted acid sites has been indicated.[21, 22] As demonstrated in Chapter 3, Zn-Cr (1:6), ZnO and Cr_2O_3 had Lewis acid sites. Zn-Cr (1:6) and Cr_2O_3 had also Brønsted acid sites. ZnO, however, did not show any Brønsted acid sites.

6.2.1 The effect of reaction temperature

Temperature has a significant effect on conversion and nopol selectivity in the Prins reaction, over a wide range of reported catalytic systems. Here, many catalysts were investigated in the liquid phase reaction, including pure chromium oxide, pure zinc

oxide and various mixtures of zinc and chromium oxides. However, to study the effect of temperature on catalyst performance, we concentrated on the best mixed-oxide catalyst, which was Zn-Cr (1:6). The Prins reaction was performed in the temperature range of 70-90 °C, using 100 mg catalyst, 10 mmol paraformaldehyde, 5 mmol β-pinene and 5 ml acetonitrile solvent, for a reaction time of 6 h.[7] Figure 6.1 shows the effect of temperature on the conversion of β-pinene and the selectivity of nopol as the main product. Increasing the temperature from 70 °C to 80 °C increased the conversion of β-pinene to 44% while the selectivity remained at 100%, but at 90 °C conversion fell to 35%, a possible reason being isomerisation and oligomerisation of β-pinene during the reaction. Since the best catalytic conversion was recorded at 80 °C,[23] the reaction was performed at this temperature in most of the work reported in this chapter.

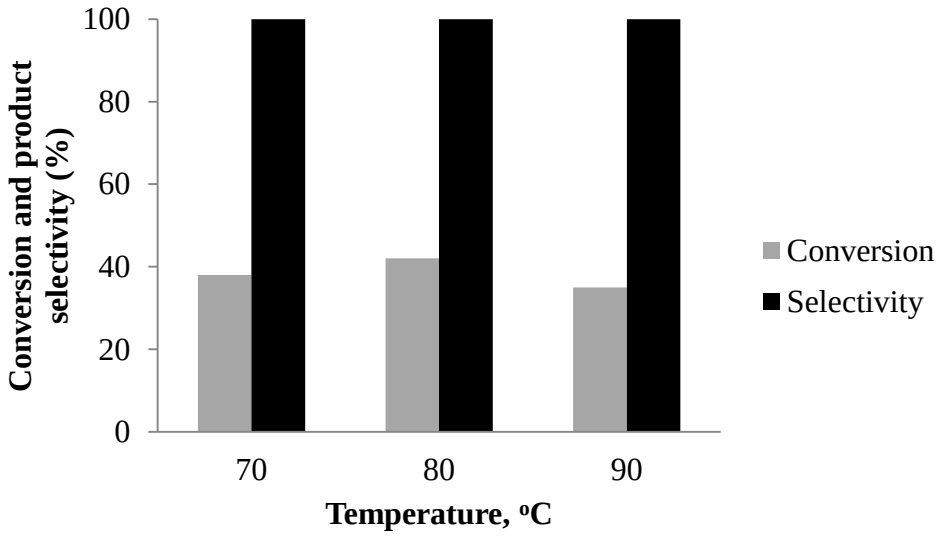

Figure 6.1 Effect of temperature in the Prins condensation of β-pinene and paraformaldehyde using 100 mg of Zn-Cr (1:6) catalyst, 10 mmol paraformaldehyde, 5 mmol β-pinene, 5 mL acetonitrile solvent, 6 h reaction time.

6.2.2 Effect of β-pinene/paraformaldehyde ratio

The effect of varying the ratio of β-pinene to paraformaldehyde in the Prins reaction to produce nopol was studied. The molar ratio was varied between 1:2 and 1:6, in acetonitrile at temperatures from 70 to 90 °C and 100 mg of catalyst Zn-Cr (1:6). Conversion increased as the molar ratio of substrates was increased up to 1:6, but at higher ratios than this, the mixture became viscous and no significant change in the conversion was noted. We therefore concentrated on the 1:6 molar ratio. The results of these experiments are presented in Figure 6.2.

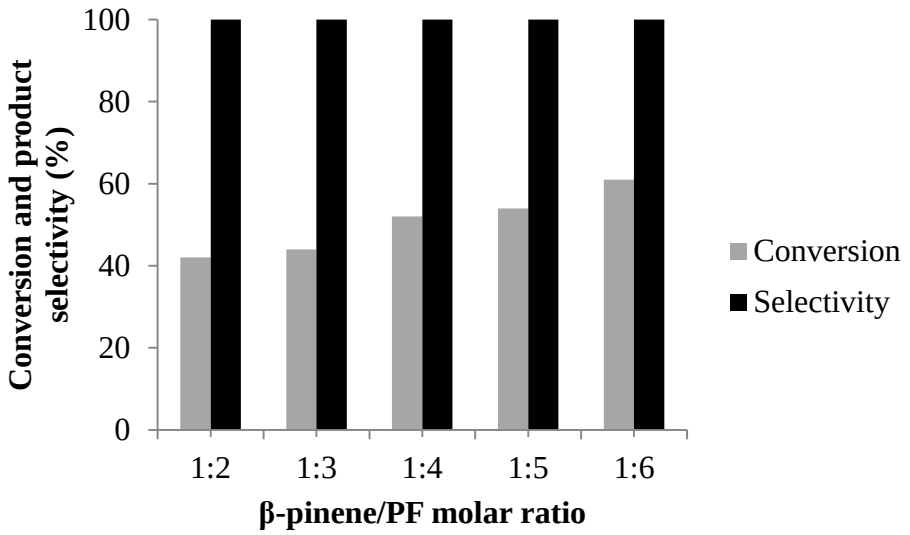

Figure 6.2 Effect of β-pinene to paraformaldehyde ratio in the Prins condensation reaction under the following conditions: 80 °C, 100 mg Zn-Cr (1:6) catalyst, 10-30 mmol paraformaldehyde, 5 mmol β-pinene, 5 mL acetonitrile solvent, 6 h reaction time.

6.2.3 Effect of Zn-Cr (1:6) amount

The effect of catalyst amount on conversion and selectivity was studied, using from 100 to 500 mg of catalyst, with different ratios of β-pinene to paraformaldehyde, 5 mL of acetonitrile as solvent and 6 h reaction time. Conversion of β-pinene reached 42% with

100% selectivity when using 100 mg of Zn-Cr (1:6). Increasing the amount of catalyst to 500 mg gave 80% conversion and a slightly lower selectivity of 98% (Figure 6.3). When 500 mg of catalyst was used with a higher ratio of 1:6 β-pinene to paraformaldehyde, the result was 95% conversion and 100% selectivity. Thus, the nopol yield increased with increasing the amount of catalyst.[24]

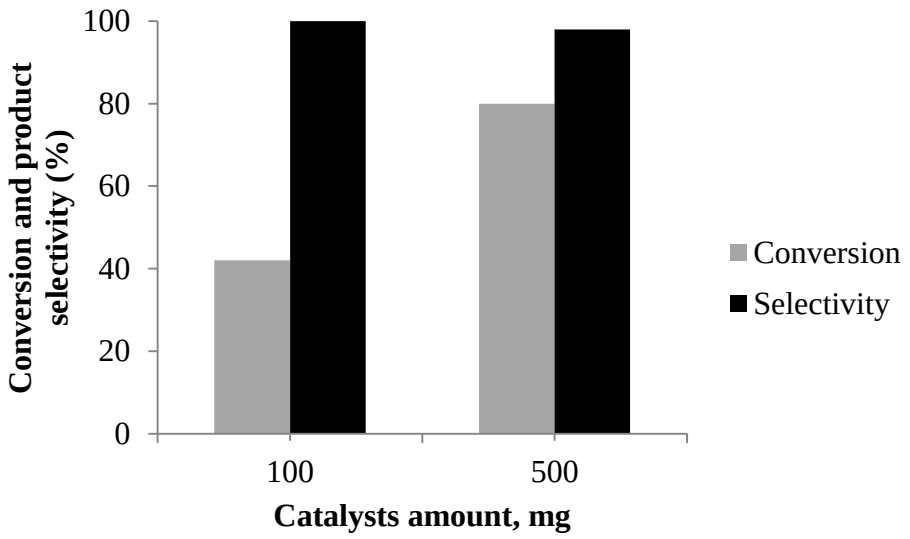

Figure 6.3 Effect of the amount of Zn-Cr (1:6) catalyst in Prins condensation under the following conditions: 100 and 500 mg catalyst, 10 mmol paraformaldehyde, 5 mmol β-pinene, 5 mL acetonitrile as solvent, 6 h reaction time.

6.2.4 Solvent effect

The next experiment tested the effect of two different solvents, acetonitrile and toluene, on the catalytic activity of Cr_2O_3 and Zn-Cr (1:6) in Prins condensation. Acetonitrile gave better activity than toluene, because the yield of nopol increases as the polarity of the solvent increases.[25] This probably results from the interaction between nitrogen lone pairs of electrons and positively charged intermediate species.[24] The effect of varying

the amount of solvent was tested by using 2.5 and 5 mL of acetonitrile. The molar ratio of β-pinene to paraformaldehyde was 1:2 and 100 mg of catalyst was used at 80 °C. The activity of the catalyst reached 42% when the amount of acetonitrile was 5 mL. Reducing the amount of acetonitrile to 2.5 mL, the conversion increased to 52% at a constant nopol selectivity of 100% as Figure 6.4 shows. These results are indicating that, increasing the amount of solvent reduced catalytic activity. A possible explanation is that the catalyst's active sites might be blocked.[24]

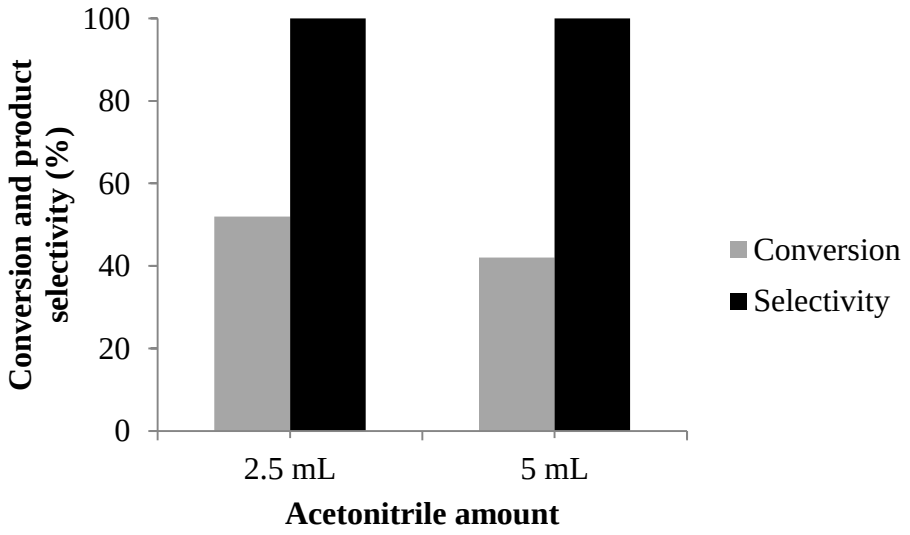

Figure 6.4 Effect of amount of acetonitrile solvent on conversion and selectivity in Prins condensation under the following conditions: 100 mg catalyst, 5 mmol β-pinene, 10 mmol paraformaldehyde, and 6 h reaction time.

6.2.5 Prins reaction over supported Zn-Cr catalysts

To examine the effect of catalyst supports, the pure supports Al_2O_3, SiO_2 (Aerosil-300 S_{BET}=300 m^2 g^{-1}) and TiO_2 were first tested under the following conditions: 100 and 500 mg of catalyst, 10 mmol of paraformaldehyde, 5 mmol of β-pinene, at 80 °C for 6 h.

The results listed in Table 6.2 show that both Al_2O_3 and TiO_2 were active at 100 mg catalyst amount, giving 100% selectivity and 15% conversion, while the silica support was practically inactive under the same conditions, with only 2% conversion.

Supporting Zn-Cr (1:6) oxide on silica gave significant improvement in activity when using 500 mg of catalyst. The 20% Zn-Cr (1:6)/SiO_2 catalyst, with a Zn-Cr oxide loading of 20 wt%, performed almost as well as the bulk Zn-Cr oxide per total catalyst weight, giving a 94% nopol yield at 80 °C, 500 mg of catalyst, a 1:6 ratio of β-pinene and paraformaldehyde and 6 h reaction time (Table 6.2).

Table 6.2 Effect of supported catalyst on Prins reaction[a]

Catalyst[b]	Catalyst weight (g)	Conversion (%)	Selectivity (%)
Al_2O_3	100	15	100
Al_2O_3	500	28	100
SiO_2	100	2	100
SiO_2	500	4	100
TiO_2	100	15	100
TiO_2	500	28	96
Zn-Cr (1:6)/SiO_2	500	69	100
Zn-Cr (1:6)/ Al_2O_3	500	77	96
Zn-Cr (1:6)/ TiO_2	500	62	98

[a] Reaction conditions: 10 mmol paraformaldehyde, 5 mmol β-pinene, 5 mL acetonitrile solvent, 6 h reaction time.

[b] Calcined at 300 °C under N_2 for 5 h and ground to 45-180 μm particle size.

6.3 Prins condensation using niobium oxide catalyst

Niobium oxide was studied as a catalyst of the Prins reaction to produce nopol, using 10 mmol paraformaldehyde, 5 mmol β-pinene and 5 mL acetonitrile solvent, for 6 h reaction time. Table 6.3 summarised the texture of niobium oxide catalysts studied in this reaction which have been discussed in detail in Chapter 3, section 3.2.4. The calcination temperature was varied and different quantities of catalyst were used to determine the effect of these parameters on catalytic activity. The reaction over niobium oxide was studied for at least 10 h reaction time.

Table 6.3 BET values for niobium oxide catalysts

Catalyst[a]	Calcination temperature (°C)	S_{BET}[b] (m^2g^{-1})	Pore volume[c] (cm^3g^{-1})	Pore size[d] (Å)
Nb_2O_5	110	243	0.25	41
Nb_2O_5	200	238	0.27	45
Nb_2O_5	300	226	0.27	47
Nb_2O_5	400	172	0.16	38
Nb_2O_5	500	90	0.18	82

[a] Calcined at 110-500 °C under air for 3 h and ground to 45-180 μm particle size.

[b] BET surface area.

[c] Single point total pore volume.

[d] Average BET pore diameter.

6.3.1 The effect of catalyst calcination temperature

To examine the effect of the calcination temperature of niobium oxide catalyst on the conversion of β-pinene and the selectivity of nopol, the reaction was carried out using 100 mg of catalyst, 10 mmol paraformaldehyde, 5 mmol β-pinene and 20 mmol acetonitrile as solvent, at 80 °C for 6 h. The catalyst was calcined at a range of temperatures from 110 to 500 °C. Nb_2O_5 exhibited high activity in the Prins reaction to

produce nopol, with 94-96% selectivity to nopol (β-pinene isomers pinocarveol and pinocarvone and nopol isomers myrtenal and myrtenol were formed as by-products). Table 6.4 shows that increasing the calcination temperature reduced the catalytic activity: niobium oxide calcined at 110 °C showed a higher conversion rate (50%) than the same catalyst calcined at higher temperatures. For example, at 500 °C, the conversion dropped to 31% with no significant change in selectivity. Nb_2O_5, calcined at 110-300 ^oC, possessing mainly Brønsted acidity, exhibited the ΔH values in the range of 115 to 129 kJ mol^{-1}, which are largely characteristic of the proton sites in niobia as it has been presented in Chapter 3 section 3.7. The reduction in activity with increasing calcination temperature can be explained by the decrease in the number of active sites available for the reaction as the catalyst is calcined at a higher temperature.

Table 6.4 Nopol synthesis catalysed by niobium oxide Nb_2O_5 at 80 °C[a]

Calcination temperature (°C)[b]	Conversion (%)	Selectivity (%)
110	50	95
200	49	96
300	36	95
400	33	95
500	31	94

[a] Reaction conditions: 100 mg catalyst, 10 mmol paraformaldehyde, 5 mmol β-pinene, 20 ml solvent acetonitrile, 6 h reaction time.

[b] Calcined under air for 5 h.

6.3.2 Effect of the amount of niobium oxide catalyst on Prins condensation

The effect of varying the content of Nb_2O_5 catalyst was studied in the Prins reaction to produce nopol using 20 mmol acetonitrile solvent, 5 mmol β-pinene and 10 mmol paraformaldehyde for 6 h at 80°C. Weights of 100 mg and 200 mg of catalyst calcined at 400 °C were used. Figure 6.5 shows that β-pinene conversion increased with increasing the amount of catalyst as expected. Similar result was observed when niobium oxide was calcined at 110 °C and used under the same conditions.

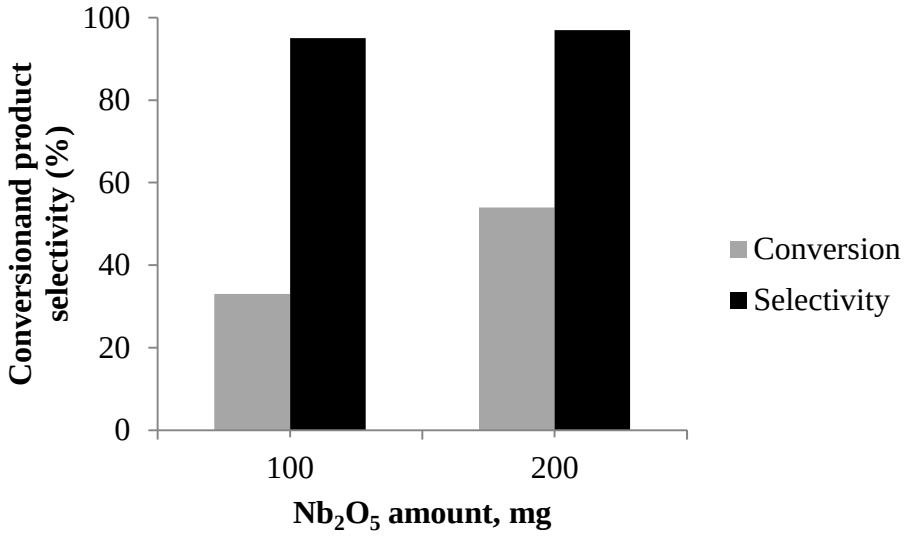

Figure 6.5 Effect of the amount of Nb_2O_5 catalyst calcined at 400 °C on Prins condensation, using 100 and 200 mg of catalyst, 10 mmol paraformaldehyde, 5 mmol β-pinene, 5 mL acetonitrile solvent, 6 h reaction time.

6.4 The effect of reaction time

Figure 6.6 shows the time course for Prins condensation of β-pinene in the presence of the supported 20% Zn-Cr (1:6)/SiO_2 catalyst and the bulk Cr_2O_3 and Zn-Cr (1:6) oxides using 500 mg of catalyst, 5 mmol β-pinene, 30 mmol paraformaldehyde and 5 ml acetonitrile at 80 °C. It can be seen that the reaction was almost complete in 2 h, followed by a rather slow increase in conversion afterwards. Nb_2O_5 was the most active

amongst these catalysts giving 100% β-pinene conversion in 4 h. However, it was less selective than Cr_2O_3 and Zn-Cr.

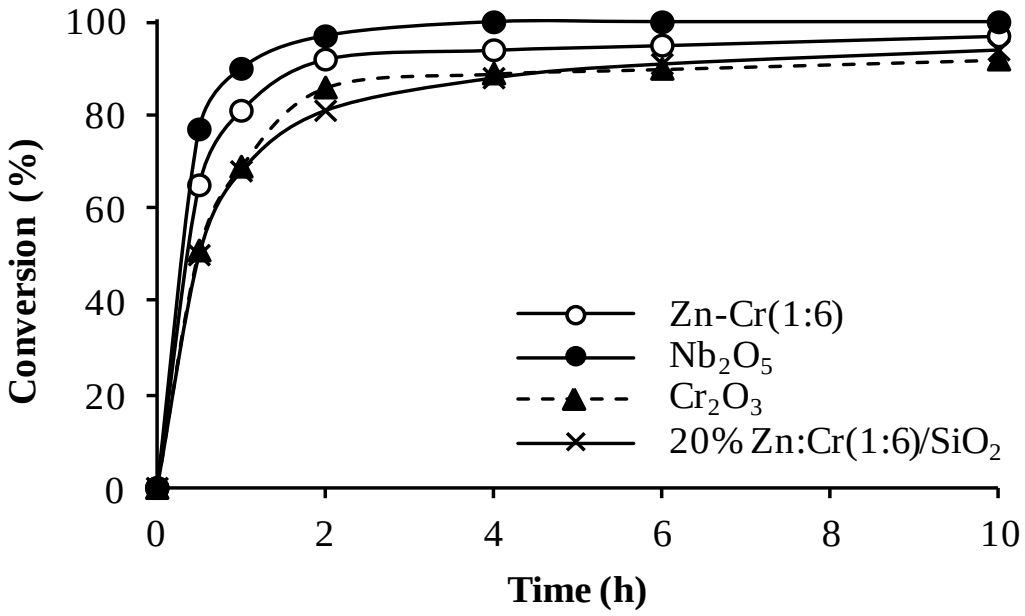

Fig 6.6 Conversion of β-pinene versus time (80 °C, 500 mg catalyst, 5 mmol β-pinene, 30 mmol paraformaldehyde, 5 mL acetonitrile). Catalyst pre-treatment: Cr_2O_3 and Zn-Cr (1:6) were calcined at 300 °C in N_2 for 5 h, 20% Zn-Cr (1:6)/SiO_2 at 400 °C in N_2 for 5 h and Nb_2O_5 at 110 °C in air for 3 h.

In terms of the nopol yield Zn-Cr (1:6) was best (97%), followed by 20%Zn-Cr (1:6)/SiO_2 (94%), Cr_2O_3 (92%) and Nb_2O_5 (88%) in 10 h reaction time. The Zn-Cr oxide is on a par with the best heterogeneous catalysts reported so far.[7-12] On top of that, it has the advantage of being an inexpensive robust material which is easy to prepare and handle. Zn-Cr (1:6) oxide showed higher activity than either supported catalyst or pure chromium oxide. It achieved 97% of conversion and 100% of selectivity.

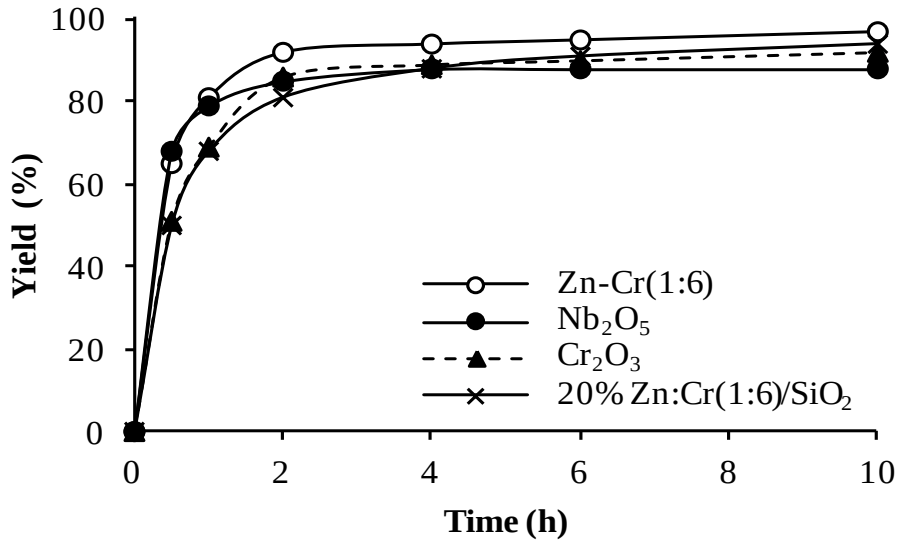

Fig 6.7 Yield of nopol versus time (80 °C, 500 mg catalyst, 5 mmol β-pinene, 30 mmol paraformaldehyde, 5 ml acetonitrile). Catalyst pre-treatment: Cr_2O_3 and Zn-Cr (1:6) were calcined at 300 °C in N_2 for 5 h, 20% Zn-Cr (1:6)/SiO_2 at 400 °C in N_2 for 5 h and Nb_2O_5 at 110 °C in air for 3 h.

6.5 Reusability study

After the completion of the reaction, the oxide catalysts were easy to recover by filtration and reused. Their performance upon reuse depended on catalyst treatment. Even a minor treatment of the recovered Zn-Cr (1:6) oxide by washing with warm ethanol and drying in an oven at 110 ^oC for 4 h allowed sufficient catalyst recycling, with a decrease in conversion from 93 to 61% at constant nopol selectivity of 100% in four successive reaction runs (Figure 6.8). Washing the catalyst with acetonitrile followed by heating at 300 ^oC under N_2 flow for 5 h led to better catalyst recyling, with a small decrease in nopol yield from 93 to 75% in four runs (Figure 6.9). The decrease in yield was probably due to catalyst loss during filtration. Catalyst leaching during nopol synthesis was negligible as determined from the inductively coupled plasma analysis (0.003% loss of Cr and 0.07% Zn in the filtrate). Further improvement in the

catalyst recycling may be possible. Unreacted paraformaldehyde could also be recovered and recycled.

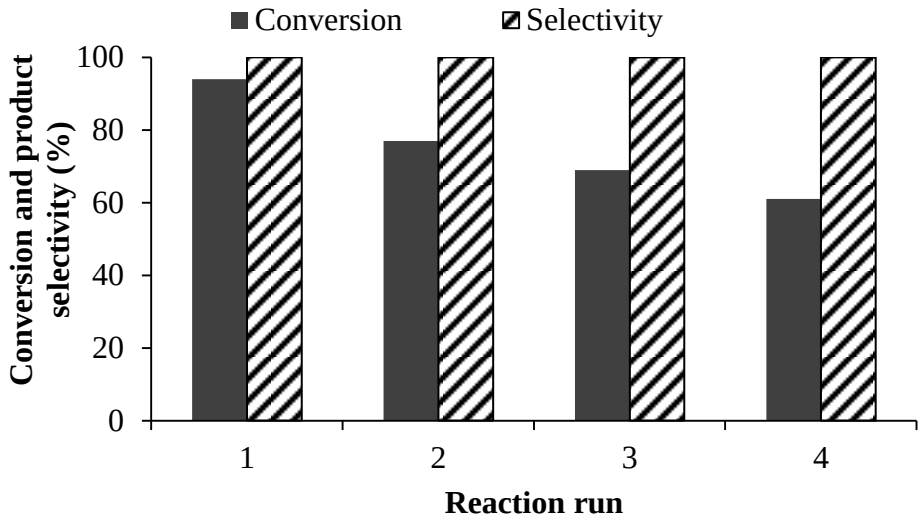

Fig 6.8 Reuse of Zn-Cr (1:6) catalyst in the synthesis of nopol (80 °C, 0.50 g catalyst, 5.0 mmol β-pinene, 30 mmol paraformaldehyde, 5.0 ml acetonitrile, 4 h reaction time), with used catalyst washed in warm ethanol and dried in an oven at 110 °C for 4 h.

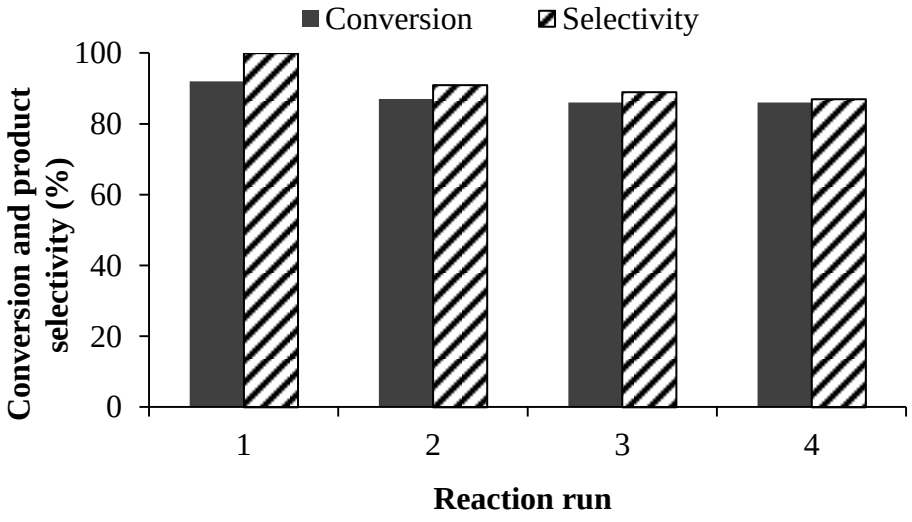

Fig 6.9 Reuse of Zn-Cr (1:6) catalyst in the synthesis of nopol (80 °C, 0.50 g catalyst, 5 mmol β-pinene, 30 mmol paraformaldehyde, 5 ml acetonitrile, 4 h reaction time), with used catalyst washed in acetonitrile followed by heating at 300 °C under N_2 for 5 h.

6.6 Reaction mechanism

A plausible mechanism of nopol synthesis through Prins condensation (Equation 6.1) is shown in Scheme 6.1.[26] This mechanism involves protonation of the aldehyde followed by attack on the methylene group of β-pinene, which forms a β-hydroxyl carbocation intermediate. In the absence of a competing nucleophile, which is the case in our system, this carbocation undergoes proton elimination to yield nopol. With excess of aldehyde in a homogeneous system, the β-hydroxyl carbocation would add another aldehyde molecule to form 1,3-dioxane.[26] No such product was observed in our case even with a sixfold excess of paraformaldehyde over β-pinene, which indicates that the formation of 1,3-dioxane on the surface of solid acid catalysts is not feasible, probably owing to steric constraints. The reaction therefore involves both protonation and deprotonation and is thus subject to acid and base catalysis. This reaction can be performed effectively with certain metal oxides possessing both acid (Brønsted and Lewis) sites and base sites and can thus act as bifunctional acid–base catalysts.[27] Zn-Cr mixed oxide possesses the required acid–base properties (Chapter 3, Table 3.6 and Figure 3.29). The high catalytic activity of Zn-Cr oxide in nopol synthesis is related to an appropriate combination of its Brønsted and Lewis acidity and basicity. It can be hypothesised that strong Lewis acid sites in Zn-Cr oxide act as adsorption centres for the reactants whereas relatively mild neighbouring Brønsted acid sites and base sites selectively affect Prins condensation (Equation 6.1) in a concerted way by protonating the aldehyde and deprotonating the β-hydroxyl carbocation, respectively (Scheme 6.1). In this regard, the addition of Zn^{II} to Cr_2O_3 could increase the basicity of the catalyst, which would enhance proton elimination from the β-hydroxyl carbocation. Zn^{II} oxide is practically inactive in the reaction owing to the lack of Brønsted acidity in it (Figure 3.29). In contrast, Nb_2O_5 has predominantly Brønsted acidity, which appears to be quite

strong (Table 3.6). This property could increase its catalytic activity but could also lead to side reactions (e.g., isomerisation and oligomerisation of β-pinene and nopol), which impairs its selectivity towards nopol (Table 6.4). Similarly, the use of zeolites possessing strong Brønsted acidity for the synthesis of nopol has resulted in the formation of isomerised products.[28] However, the acid properties of the catalysts were measured at the gas–solid interface (by using the DRIFT spectroscopy of adsorbed pyridine and ammonia adsorption calorimetry) whereas the reaction was performed in the liquid phase in a polar and slightly basic acetonitrile, which levelled off the acidity of the catalysts. Therefore, in the reaction system, the difference in the acidity of the catalysts is likely to be less than that in the gas–solid system and thus the small effect of catalyst acidity on the reaction, as can be observed from Tables 6.1 and 6.4 and Figures 6.6 and 6.7.

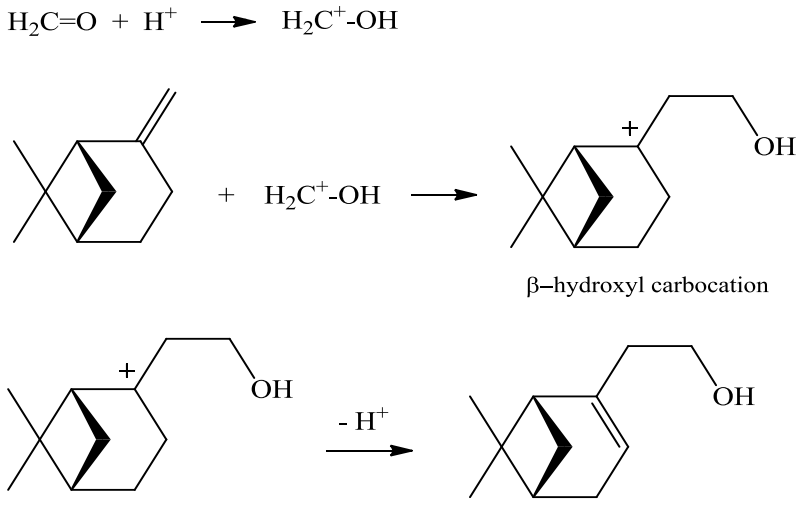

Scheme 6.1 Proposed mechanism of the synthesis of nopol by Prins condensation of β-pinene and formaldehyde.

6.7 Conclusions

In this study, the Prins reaction was catalysed by Cr_2O_3, ZnO and a series of Zn-Cr mixed oxides with varying Zn/Cr atomic ratios prepared by co-precipitation of Zn^{II} and Cr^{III} hydroxides. The Zn-Cr (1:6) catalyst was supported on Al_2O_3, TiO_2 and SiO_2 using the impregnation method. Cr-rich catalysts showed good activity in the Prins reaction to obtain nopol. The most active catalyst was Zn-Cr (1:6), which showed very high conversion and 100% selectivity. Reaction conditions varied in this study included temperature, amount of solvent and the ratio between substrates. Increasing the temperature and the β-pinene/paraformaldehyde molar ratio led to increase catalyst activity, while selectivity remained constant. The nopol yield also increased with reaction time and the amount of catalyst. With a 6:1 molar ratio of paraformaldehyde to β-pinene, the Zn-Cr (1:6) catalyst gave 97% β-pinene conversion at 100% nopol selectivity. Pure Al_2O_3 and TiO_2 oxides were active in the reaction, but silica was not. The Zn-Cr (1:6) catalyst supported on silica had excellent performance as well as bulk catalyst oxide per total catalyst weight, giving a 94 % nopol yield. After reaction, the catalyst was recoverable by washing with ethanol or acetonitrile solvents and heat treatment. Zn-Cr (1:6) can be reused at least four times.

Niobium oxide was also used to catalyse the Prins reaction. This catalyst has been found to possess stronger Brønsted acidity than Zn-Cr oxide which decreased with increasing the calcination temperature. The catalysts were calcined at different temperatures at 110 to 500 ^{o}C. The catalyst calcined at 110 °C gave the best results for conversion of β-pinene and nopol selectivity. Niobium oxide gave 88% of nopol selectivity at 100% conversation for 6 h reaction time.

We have demonstrated that the readily available and easy-to-handle Zn-Cr (1:6) mixed oxide is a highly active and recyclable heterogeneous catalyst for the clean, high-yielding synthesis of nopol by Prins condensation of β-pinene with paraformaldehyde. An appropriate combination of acid-base properties of the Zn-Cr oxide is thought to be responsible for its effectiveness. Catalysts were characterised by DRIFT spectroscopy of adsorbed pyridine and ammonia adsorption microcalorimetry. The results show that ZnO, Cr_2O_3 and Zn-Cr (1:6) oxides had Lewis acid sites, and Zn-Cr (1:6) and Cr_2O_3 had also Brønsted acid sites which are required for the synthesis of nopol.

6.8 References

1. G. W. Huber, S. Iborra and A. Corma, *Chemical Reviews*, 2006, **106**, 4044-4098.
2. A. Corma Canos, S. Iborra and A. Velty, *Chemical Reviews*, 2007, **107**, 2411-2502.
3. W. E. Erman, *Chemistry of Monoterpenes*, New York, 1985.
4. K. Bauer, D. Garbe and H. Surburg, *Common Fragrance and Flavour Materials. Preparation, Properties and Uses, VCH*, 1990.
5. C. Sell, *in The Chemistry of Fragrances: from Perfumer to Consumer, ed*, C. Sell, RSC Publishing, Dorset, UK, 2nd edn, 2006.
6. J. P. Brain, 1946, *Journal of American Society*, **68**, 638-641.
7. S. V. Jadhav, K. M. Jinka and H. C. Bajaj, *Catalysis Today*, 2012, **198**, 98-105.
8. U. R. Pillai and E. Sahle-Demessie, *Chemical Communications*, 2004, **10**, 826-827.
9. A. L. Villa de P, E. Alarcón and C. M. De Correa, *Chemical Communications*, 2002, 2654-2655.
10. M. V. Patil, M. K. Yadav and R. V. Jasra, *Journal of Molecular Catalysis A: Chemical*, 2007, **273**, 39-47.
11. S. V. Jadhav, K. M. Jinka and H. C. Bajaj, *Applied Catalysis A: General*, 2010, **390**, 158-165.
12. V. S. Marakatti, G. V. Shanbhag and A. B. Halgeri, *RSC Advances*, 2013, **3**, 10795-10800.
13. K. A. da Silva Rocha, J. L. Hoehne and E. V. Gusevskaya, *Chemistry - A European Journal*, 2008, **14**, 6166-6172.

14. K. A. da Silva Rocha, P. A. Robles-Dutenhefner, I. V. Kozhevnikov and E. V. Gusevskaya, *Applied Catalysis A: General*, 2009, **352**, 188-192.

15. K. A. da Silva Rocha, N. V. S. Rodrigues, I. V. Kozhevnikov and E. V. Gusevskaya, *Applied Catalysis A: General*, 2010, **374**, 87-94.

16. A. L. P. de Meireles, K. A. Da Silva Rocha, I. V. Kozhevnikov and E. V. Gusevskaya, *Applied Catalysis A: General*, 2011, **409-410**, 82-86.

17. V. V. Costa, K. A. Da Silva Rocha, L. F. De Sousa, P. A. Robles-Dutenhefner and E. V. Gusevskaya, *Journal of Molecular Catalysis A: Chemical*, 2011, **345**, 69-74.

18. V. V. Costa, K. A. Da Silva Rocha, I. V. Kozhevnikov, E. F. Kozhevnikova and E. V. Gusevskaya, *Catalysis Science and Technology*, 2013, **3**, 244-250.

19. F. Al-Wadaani, E. F. Kozhevnikova and I. V. Kozhevnikov, *Journal of Catalysis*, 2008, **257**, 199-205.

20. F. Al-Wadaani, E. F. Kozhevnikova and I. V. Kozhevnikov, *Applied Catalysis A: General*, 2009, **363**, 153-156.

21. A. Corma, S. Iborra, M. Mifsud and M. Renz, *Arkivoc*, 2005, **9**, 124-132.

22. D. Esquivel, A. J. Cruz-Cabeza, C. Jiménez-Sanchidrián and F. J. Romero-Salguero, *Microporous and Mesoporous Materials*, 2013, **179**, 30-39.

23. D. M. Do, S. Jaenicke and G. K. Chuah, *Catalysis Science and Technology*, 2012, **2**, 1417-1424.

24. S. V. Jadhav, K. M. Jinka and H. C. Bajaj, *Catalysis Today*, 2012, **198**, 98-105.

25. M. Opanasenko, A. Dhakshinamoorthy, Y. K. Hwang, J. S. Chang, H. Garcia and J. Čejka, *ChemSusChem*, 2013, **6**, 865-871.

26. J. J. Li, *Name Reactions: A Collection of Detailed Mechanisms and Synthetic Applications*, 4th ed., Springer, 2009.

27. K. Tanabe in Catalysis by Acids and Bases (Eds.: B. Imelik, C. Naccache, G. coudurier, Y. Ben Taarrit, J. C, Vedrine), Elsevier, Amsterdam, 1985, p. 1-14.

28. J. Wang, S. Jaenicke, G. K. Chuah, W. Hua, Y. Yue and Z. Gao, *Catalysis Communications*, 2011, **12**, 1131-1135.

Chapter 7

Conclusions

The conversion of biomass has been known for several decades, having begun with the production of fuels and chemicals from wood biomass in the mid-1970s. This process is important economically, environmentally, academically and industrially, allowing the sustainable and renewable production of energy from biomass sources and the derivation of high-valued products from natural feedstock. One such method of obtaining fuels and chemicals is the fast pyrolysis of biomass material.

Thus, a modern equivalent of the traditional use of fossil fuels is the increasingly feasible sourcing of heat, power and liquid fuels from the process of biomass conversion. For example, biofuels produced in this way have been shown to emit far less harmful greenhouse gases into the Earth's atmosphere than conventional fossil fuels. The energy sourced from biomass is based on sustainable carbon with many environmental and socioeconomic benefits. To utilise a biomass-derived energy supply as a fuel, compounds are formed by fast pyrolysis, bio-oil, containing a mixture of oxygenated compounds, must first be upgraded or reformed in a ketonisation (or ketonic decarboxylation) reaction.

Oil is the world's primary source of energy and chemicals with a current demand of about 12 million tonnes per day (84 million barrels a day) with a projection to increase to 16 million tonnes per day (116 million barrels a day) by 2030. While 30% of the global oil consumption accounts for transportation fuels at present, it is strikingly expected to increase to 60% by 2030.

Renewable biofuels are needed to displace petroleum derived transportation fuels, which contribute to global warming and are of limited availability. Biodiesel and bioethanol are the two potential renewable fuels that have attracted the most attention. However, biodiesel and bioethanol produced from agricultural crops using existing methods cannot sustainably replace fossil-based transportation fuels. In general, increased demand for biofuels has caused the prices of agricultural commodities used as feedstocks and other competing crops to increase because of the direct impact of biofuels production on agricultural commodities and markets, with implications for food prices and allocations of rural agricultural land. There is an alternative, however, which is biodiesel from microalgae. This biodiesel seems to be the only renewable biofuel that has the potential to completely displace petroleum-derived transport fuels without adversely affecting supply of food and other crop products. Most productive oil crops, such as oil palm, do not come close to microalgae in being able to sustainably provide the necessary amounts of biodiesel. Similarly, bioethanol from sugarcane is no match for microalgal biodiesel.

First generation biodiesel is currently the most common biofuel in Europe. It remains in the political and economic arena and is playing a part in the biofuels expanding process as the awareness of alternative fuel spreads among the general public. In 2007, 19 biodiesel plants started operations or were under construction/planning in the new EU member states. Relatively large plants can be found in Lithuania, Poland and Romania, with capacities of 100 000 tonnes/year.

Europe has been involved in direct production of liquid fuels from biomass for over two decades. Prior to 1989, the only European plant was a conventional slow pyrolysis demonstration plant of 500 kg/h operating in Italy for liquid and char production to yield approximately 25% of each. Also Bio-Alternative in Switzerland was operating a

fixed bed carbonisation pilot plant fed with wood and waste for charcoal production yielding 20% of secondary liquids as a by-product. Tests carried out on combustion of these oils served to foster interest in direct production of liquids from biomass in atmospheric processes. This also revealed a poor liquid quality and low product yields. In 1993, a 200 kg/h fast pyrolysis pilot plant based on the University of Waterloo (Canada) process was launched in Spain by Union Fenosa. In 1991 – 1992, Egemin (Belgium) designed and operated a 200 kg/h capacity entrained down bio-oil pilot plant. ENEL purchased a 15 t/d Ensyn RTP3 pilot plant to produce bio-oils for testing which was installed in Italy in 1996. The inclusion of fast pyrolysis in the 4th Non Fossil Fuel Obligation (NFFO) tranche in the UK in 1996 served to strengthen awareness of this technology and boosted interest in it Europe.

In North America a number of commercial and demonstration plants for fast pyrolysis have been operating at a scale of up to 2000 kg/h. Ensyn (Canada) are marketing commercial fast pyrolysis plants of up to 10 t/h throughput. Two plants of around 1 t/h capacity are operated in the USA for food edditives production which is still the only commercial application for fast pyrolysis. Castle Capital have acquired the Continuous Ablative Reaction (CAR) process and were operating a 1-2 t/h plant in Canada until 1996. The second generation 1360 kg/h Interchem demonstration plant in Kansas is based on the NREL vortex ablative pyrolysis process.

The UK currently has a total biofuel production capacity of over 1,500 million litres per year. Figure 1 shows the larger scale commercial biofuel plants in the UK, indicating both operational and planned plants. Bioethanol projects have been slower to develop with the UK’s first bioethanol plant being commissioned by British Sugar in 2007. This plant remained the UK’s only bioethanol plant for three years until had been complemented by two very large bioethanol plants (Ensus in 2010 and Vivergo in

2013), significantly increasing the overall bioethanol capacity in the UK, with a third plant (Vireol) planned for 2016. Therefore, bioethanol capacity represents the larger share in the UK biofuel industry.

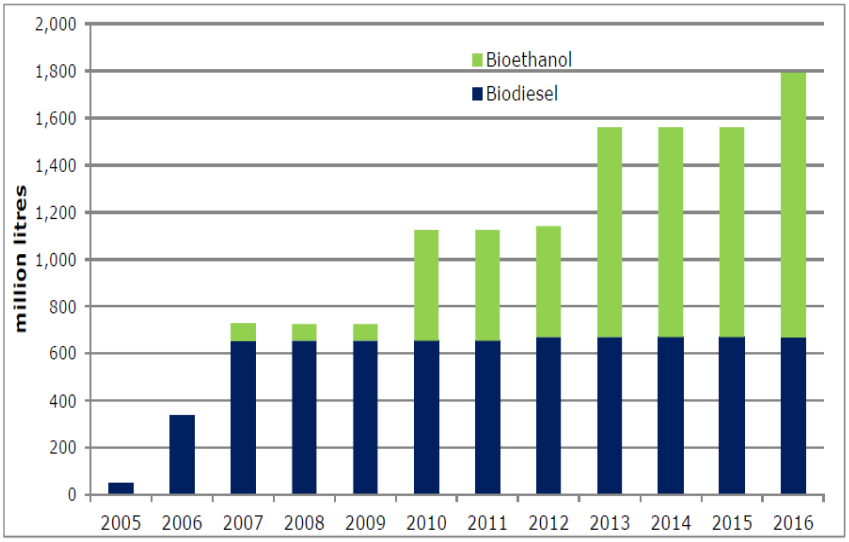

Figure 7.1 Commercial-scale bioethanol and biodiesel production in the United Kingdom.

Several biodiesel initiatives were planned in the UK in recent years, but did not result in actual projects. These include a 255 million litre plant in South West England proposed by ABS Biodiesel running on virgin and waste oils and a 204 million litre plant in North Tyneside proposed by Goes on Green running on yellow grease (both planned for 2011). UK bioethanol production has also been significantly lower than production capacity since 2009, particularly in 2011 and 2012 when utilisation was only 6% and 17% respectively.

The upgrading of bio-oil is thus a crucial step in the derivation of hydrocarbon fuels from biomass. Notably, highly reactive and corrosive small-chain carboxylic acids are

removed during the process, halting detrimental side reactions and complications during the transportation and storage of the mixture. Among the products obtained are ketones possessing an increased length of carbon chain, useful, for instance, as chemical building blocks to produce hydrocarbons for transportation fuels from C–C coupling and hydrodeoxygenation reactions. Among the compounds widely used in chemical synthesis are acetic, propionic and pentanoic acids, which can be seen as model bio-oil compounds. These undergo the aforementioned ketonisation reaction to produce the symmetrical ketones acetone, 3-pentanone and 5-nonanone, as shown in the following equation.

$$2\ RCOOH \longrightarrow R_2CO + H_2O + CO_2$$

Recently, the process of producing fuels and chemicals from renewable biomass feedstocks in both gas and liquid phases has become a major challenge across the world. In the conversion of vegetable oils, wood oils, waste cooking oils and animal fats to produce biofuels, it is necessary to reduce the viscosity of the liquid biomass and enhance its stability using catalysed deoxygenation reactions. This process reduces or removes the effective oxygen atoms in these organic compounds in the form of carbon monoxide or carbon dioxide.

Organic acids are important as platform molecules in such biomass transformation processes. Carboxylic acids are readily available from natural sources and are attractive as renewable raw materials for the production of value-added chemicals and biofuel components. For fuel applications, carboxylic acids require reduction in their oxygen content. Therefore, much recent research has focused on their deoxygenation using heterogeneous catalysis. In this study, acetic, propionic and pentanoic acids were chosen as representative of carboxylic acids with six or fewer carbon atoms, derived from carbohydrate feedstock.

Nopol is an optically active bicyclic primary alcohol used in the agrochemical industry to produce pesticides and also in soap fragrances, detergents and other household products, due to its balsamic odour. It is generally produced by the Prins condensation of β-pinene and paraformaldehyde using homogeneous acid catalysts. Recently, catalysts of many kinds, such as metal oxides and zeolites, have been found to produce good yields of nopol in the liquid phase reaction.

The aim of this study was to investigate the gas phase ketonisation of carboxylic acids to form ketones in a fixed-bed continuous flow reactor and the liquid phase Prins condensation reaction using heterogeneous catalysts. The project achieved the following three main objectives:

1. Amorphous silica and crystalline silicalite were used to catalyse the ketonisation of propionic acid in the temperature range of 300-550 °C.
2. Others catalysts, such as pure zinc and chromium oxides, a series of mixtures of zinc and chromium oxides and their supported catalysts, were tested in the ketonisation of carboxylic acids at temperatures from 350 to 450 °C.
3. The liquid phase condensation of β-pinene to produce nopol as the main product using metal oxide catalysts such as Zn-Cr and Nb_2O_5 was investigated under a variety of conditions. The parameters which were varied included temperature, amount of catalyst, substrate ratio and type of solvent.

The catalysts used included commercial silica. Silicalite was prepared and calcined according to procedures described in the literature. It was modified by acid and base aqueous solutions and characterised by various techniques. The surface area and porosity of fresh and spent catalysts were characterised by the N_2 physisorption method and the results showed that the chemical treatment did not affect the texture of the

catalysts, i.e. their surface area, pore diameter or pore volume. The XRD pattern of our silicalite sample was measured and found to match the authentic materials. We also noted no change in the catalyst patterns after modification by acid or base treatments.

In order to investigate their active sites, silica and silicalite catalysts were characterised by DRIFT spectroscopy. The results gave important information about active sites in the ketonisation of propionic acid in the gas phase. It can be concluded that basic modification generated silanol nests in the silicalite catalysts and enhanced their performance in the ketonisation reaction, but that the treatment had no effect on the silica. In other words, silanol nests were created on the crystalline silicalite but not on the amorphous silica.

The reaction was first carried out using a wide range of amorphous silica catalysts. At 500 °C, these showed very good (85%) selectivity of 3-pentanone at 39% conversion of propionic acid. However, their modification by acid and base solutions had no impact on their activity or selectivity, so research continued in an attempt to improve catalytic performance and reactivity.

Crystalline materials such as HZSM-5 and silicalite were next tested in the ketonisation of propionic acid. HZSM-5 was found to have very low ketonisation activity at low temperature. Increasing the temperature increased the conversion of acid, but the main products were hydrocarbons, predominantly ethene. Better results were obtained with silicalite, which showed excellent catalytic activity in the ketonisation of propionic acid. When the silicalite catalyst was chemically treated using different concentrations of hydrochloric acid, ammonia and ammonium nitrate, it was found that the acidic treatment had little effect on activity and selectivity, whereas basic treatment strongly affected ketonisation selectivity. The selectivity of 3-pentanone was 92% with 84% conversion at 500 °C, while increasing the temperature to 550 °C reduced

selectivity to 65% with 92% conversion. Silicalite catalysts were stable for at least 28 hours time on stream at 500 °C, but activity was slightly reduced at 20 h TOS. This slight deactivation may have been caused by the deposition of coke on the catalyst surface during the reaction.

A number of other catalysts were tested in the ketonisation of propionic and acetic acids. The catalysts used in this part of the project were pure zinc and chromium oxides, various mixtures of zinc and chromium oxides, and zinc and chromium mixed oxides supported on Al_2O_3, SiO_2 and TiO_2. The co-precipitation method was used to prepare the bulk metal and mixed metal oxide catalysts, while the supported catalysts were prepared by co-impregnation.

Preliminary experiments in the ketonisation of acetic, propionic and pentanoic acids were conducted to test the effects on catalyst performance of using pure zinc and chromium oxides and of varying the Zn/Cr atomic ratio. Zn-Cr (10:1) oxide with 43 m^2 g^{-1} surface area and 90.3 Å pore size showed the best performance, significantly exceeding that of the parent oxides ZnO and Cr_2O_3. At 330 °C and 20 ml min^{-1} of N_2 flow, the yield of 3-pentanone was 44 % achieved by using Zn-Cr (10:1) oxide as a catalyst. The 3-pentanone yield was increased to 70% at 350 ^oC. Pure oxide was found to be less active, while conversion decreased as the zinc or chromium content of the mixed oxide catalysts was increased. The results also showed the profound effect of temperature on catalysed reactions: propionic acid conversion increased with increasing temperature at 350 and 400 °C. At 380 °C, Zn-Cr (10:1) showed good activity: 98% conversion and 94% selectivity to 3-pentanone, which was a higher yield than any other catalyst. It also showed excellent stability for at least 18 h TOS with no deactivation being observed. Conversion of propionic acid increased with reaction temperature,

reaching 100% at 450 °C, but at this temperature the selectivity of 3-pentanone dropped to 78%.

Catalysts comprising 20 wt% of mixed oxides supported on SiO_2, Al_2O_3 and TiO_2 were tested in the ketonisation of propionic acid in the range of temperatures between 350 and 400 °C. Pure supports were active and the order of activity was $TiO_2 > Al_2O_3 > SiO_2$, in agreement with published reports. The Zn-Cr mixed oxide catalyst supported on Al_2O_3 and TiO_2 had enhanced activity compared with SiO_2, which had a higher surface area. The reason for this is that when the oxides are deposited on the supports, their dispersion increases and their acidic functions are incorporated into the interface of the oxides' basic sites. 20% Zn-Cr (10:1)/Al_2O_3 had the highest yield of 3-pentanone at 380 °C. Its performance was also stable at this temperature for at least 24 h TOS with no reduction in the conversion of propionic acid or 3-pentanone selectivity during the reaction.

TiO_2 catalyst showed moderate activity at higher temperatures 350-400 ^oC. However, this catalyst gave only 60% selectivity to 3-pentanone at 380 ^oC. In contrast, Zn-Cr (10:1) gave 94% 3-pentanone selectivity at 98 % conversion of propionic acid. At lower temperature 330 ^oC, Zn-Cr (10:1) was still active, whereas TiO_2 was practically inactive.

Mixed zinc-chromium oxides were also found to be active catalysts of the ketonisation of acetic acid to form acetone as the main product, at temperatures of 300, 350, 380 and 400 °C. Zn-Cr (10:1) was again the most active and selective catalyst, yielding 86% of acetone (100% selectivity of acetone at 86% conversion of acetic acid) after an average of 4 h TOS at 350 °C. The selectivity of acetone decreased slightly with increasing temperature between 380 and 400 °C.

The ketonisation of pentanoic acid was studied over Zn-Cr (10:1) in the temperature range of 350-400 °C, using 0.2 g of catalyst at 20 ml min^{-1} of N_2 flow and 2 vol% of acid. As temperature increased, pentanoic acid conversion also increased, but selectivity decreased. At 350 °C, 5-nonanone selectivity was 66%, dropping sharply to 18% at 400 °C.

The texture of Zn-Cr oxides was characterised by N_2 physisorption. The BET surface areas of fresh Cr-rich oxides increased significantly as the Cr content increased. The amorphous Cr-rich oxides had larger surface areas and pore volumes, but smaller average pore diameters than the crystalline Zn-rich oxides.

X-ray diffraction pattern of the catalysts showed that their crystallinity depended on the calcination temperature and the Zn/Cr ratio: Cr-rich catalysts such as Cr_2O_3, Zn-Cr (1:1) and Zn-Cr (1:6) were amorphous, whereas ZnO and Zn-rich mixed oxides, Zn-Cr (10:1), (20:1) and (30:1), were crystalline. When the Zn-Cr (1:6) catalyst was calcined at 400 ºC, a clear pattern of chromium oxide as a crystalline phase and zinc chromate spinel was observed. It was also found that with increasing calcination temperature the catalyst became crystalline and the peaks of intensity became stronger, consistent with reports in the literature.

The Brønsted or Lewis nature of acid sites was determined by FTIR spectroscopy of adsorbed pyridine. All chromium oxide, zinc oxide and mixed Zn-Cr oxide catalysts had Lewis acid sites as indicated by the band at 1450 cm^{-1} in their FTIR spectra, while Cr_2O_3 and Zn-Cr (1:6) oxide possessed both Brønsted and Lewis acid sites, as evidenced by FTIR bands at 1540 cm^{-1}. The strength of acid sites was measured by ammonia adsorption microcalorimetry to determine the differential enthalpy of ammonia adsorption at zero coverage. The acid strength of Zn-Cr oxide catalysts, possessing mainly Lewis acid sites, increased significantly with increasing Cr content

and the ΔH values were found to be -127 to -193 kJ mol^{-1}, representing the strength of Lewis acid sites in Zn-Cr oxides. Zn-Cr (10:1) oxide had a ratio of acid site densities B/L = 0.07 and a differential enthalpy of ammonia adsorption ΔH = -150 kJ mol^{-1}. The high ketonisation efficiency of Zn-Cr (10:1) oxide may be ascribed to an appropriate combination of its acid-base properties.

Finally, Zn-Cr mixed oxides and niobium oxides were studied as catalysts of the Prins condensation of β-pinene to form nopol as the main product. When the reaction conditions were varied, the amount of solvent, the amount of catalyst, the temperature and the ratio of paraformaldehyde to β-pinene were all found to affect catalyst performance. 100 mg of Zn-Cr (1:6) gave 100% of nopol selectivity at 42% of β-pinene conversion at 80 °C, with molar ratio of β-pinene to paraformaldehyde of 1:2, using acetonitrile as solvent, and 6 h reaction time.

Further significant improvements were obtained by supporting 20% Zn-Cr (1:6) oxide on silica: the supported catalyst showed 100% selectivity of nopol at 94% β-pinene conversion at 80 °C, 500 mg of catalyst, a 1:6 ratio of β-pinene and paraformaldehyde and 6 h reaction time. The catalyst was also easy to recover and recycle, by filtration and washing in warm ethanol, acetonitrile or water. The reuse performance depended on the treatment, with the best result being obtained when the catalyst was washed in acetonitrile and dried at 300 °C under N_2 for 5 h.

Niobium oxide catalyst was prepared and characterised by various techniques. They were calcined at temperatures from 110 to 500 °C and their surface area was found to decrease with increasing calcination temperature. All of the catalysts had both Brønsted and Lewis acid sites, with the amount of proton sites decreasing as calcination temperature increased. Ammonia adsorption microcalorimetry revealed ΔH values in the range -115 to -129 kJ mol^{-1}. When the niobium oxide catalysts calcined at different

temperatures were tested in the Prins condensation reaction under the same conditions as the Zn-Cr (1:6) oxide catalyst, the selectivity of nopol was found to be stable, but conversion decreased with increasing calcination temperature. The conversion of β-pinene decreased in the order Nb_2O_5 (110 °C) > Nb_2O_5 (200 °C) > Nb_2O_5 (300 °C) > Nb_2O_5 (400 °C) > Nb_2O_5 (500 °C).

Future work on acid ketonisation over Zn-Cr oxide catalysts may be focussed on the following issues:

1. Further characterisation of bulk and supported Zn-Cr oxide catalysts, especially the characterisation of their acid and base properties.
2. Kinetics and mechanism of ketonisation reaction.
3. Modification of Zn-Cr oxide by adding a third component (e.g. Ce(IV), Mn(III), etc.).
4. Ketonisation of longer-chain fatty acids in the liquid phase.

7.1 References

1. T. N. Pham, D. Shi and D. E. Resasco, *Applied Catalysis B: Environmental*, 2014, **145**, 10-23.
2. R. Luque, L. Herrero-Davila, J. M. Campelo, J. H. Clark, J. M. Hidalgo, D. Luna, J. M. Marinas and A. A. Romero, *Energy & Environmental Science*, 2008, **1**, 542-564.
3. Y. Chisti, *Trends in biotechnology*, 2008, **26**, 126-131.
4. A. V. Bridgwater and G. V. C. Peacocke, *Renewable and Sustainable Energy Reviews*, 2000, **4**, 1-73.
5. Sacha Alberici, Gemma Toop, ECOFYS, 2013, 1-33.
6. D. M. Alonso, J. Q. Bond and J. A. Dumesic, *Green Chemistry*, 2010, **12**, 1493-1513.
7. A. Pandey, C. Larroche, S. C. Ricke, C. G. Dussap and E. Gnansounou, *Biofuels: Alternative Feedstocks and Conversion Processes*, Elsevier Science, 2011.
8. T. P. Vispute, H. Zhang, A. Sanna, R. Xiao and G. W. Huber, *Science*, 2010, **330**, 1222-1227.
9. F. Al-Wadaani, E. F. Kozhevnikova and I. V. Kozhevnikov, *Applied Catalysis A: General*, 2009, **363**, 153-156.
10. H. Bayahia, E. Kozhevnikova and I. Kozhevnikov, Chemical Communications, 2013, 49, 3842-3844.
11. V. V. Costa, H. Bayahia, E. F. Kozhevnikova, E. V. Gusevskaya and I. V. Kozhevnikov, ChemCatChem, 2014, 6, 2134-2139.
12. H. Bayahia, E. F. Kozhevnikova and I. V. Kozhevnikov, *Applied Catalysis B: Environmental*, 2015, **165**, 253-259.